

THESIS FOR THE DEGREE OF DOCTOR OF PHILOSOPHY



Smart Knives: Controlled Cutting Schemes to Enable Advanced Endoscopic Surgery

Towards Dye-Mediated Laser Ablation

Ifung Lu

Department of Medical Physics and Bioengineering
University College London (UCL)
London, England / 2011

Supervisors:
Tim N. Mills, PhD & C. Alexander Mosse, PhD

I, Ifung Lu, confirm that the work presented in this thesis is my own.

Where information has been derived from other sources,

I confirm that this has been indicated in the thesis.

.....
Ifung Lu

Abstract

With the backdrop of the rapidly developing research in Natural Orifice Transluminal Endoscopic Surgery (NOTES), analysis of the literature supported the view that inventing new, controlled tissue dissection methods for flexible endoscopic surgery may be necessary. The literature also confirmed that white space exists for research into and the development of new cutting tools.

The strategy of “deconstructing dissection” proposed in this thesis may provide dissection control benefits, which may help address the unique manoeuvring challenges for tissue dissection at flexible endoscopy.

This assertion was supported by investigating six embodiments of the strategy which provided varying degrees of enhanced tissue dissection control. Seven additional concepts employing the strategy which were not prototyped also were offered as potential solutions that eventually might contribute evidence in defence of the strategy.

One concept for selective ablation — dye-mediated laser ablation — was explored in-depth by theoretical analysis, experimentation and computation. The ablation process was found to behave relatively similar to unmediated laser ablation, but also to depend on cyclic carbonisation for sustained ablation once the dye had disappeared.

An Arrhenius model of carbonisation based on the pyrolysis and combustion of wood cellulose was used in a tissue ablation model, which produced reasonable results.

Qualitative results from four methods for dye application and speculation on three methods for dye removal complete the framework by which dye-mediated laser ablation might deliver on the promise offered by “deconstructing dissection”.

Overall, this work provided the “deconstructing dissection” strategic framework for controlled cutting schemes and offered plausible evidence that the strategy could work by investigating embodiments of the scheme.

In particular, dye-mediated laser ablation can provide selective ablation of tissue, and a theoretical model for the method of operation was offered. However, some practical hurdles need to be overcome before it can be useful in a clinical setting.

*This work is dedicated to my parents
Tsinpoa and Leepha
who dreamed and strived and sacrificed
so that I could be here today.*

Lots of love and many thanks.

Table of Contents

Abstract	3
List of Figures	12
List of Tables.....	24
Chapter 1: Surgery and the case for new cutting tools	26
1.1. Chapter Overview	26
1.2. Surgery – always towards the cutting edge.....	26
1.3. A history of intervention	29
1.3.1. Surgery through the ages.....	29
1.3.2. Preventing bacterial infection.....	32
1.3.3. Dulling the pain	32
1.3.4. Medicine to treat infections	32
1.3.5. Cutting tissue with electricity	33
1.4. To peer within – the development of endoscopy.....	34
1.4.1. Rigid endoscopy	34
1.4.2. Semi-flexible and flexible endoscopy.....	38
1.5. The anatomy of the modern endoscope	40
1.5.1. The modern rigid laparoscope	40
1.5.2. The modern flexible endoscope	42
1.5.3. Future endoscopes.....	46
1.6. The anatomy of human gastrointestinal tract	52
1.7. Minimizing the invasiveness of surgery with rigid endoscopy	62
1.7.1. From open surgery to “keyhole” surgery.....	62
1.7.2. Laparoscopy and the case for adding to surgical complexity	65
1.7.3. Cholecystectomy – the king of laparoscopic procedures	68
1.7.4. Bariatric surgery for obesity.....	70

1.7.5.	Transanal endoscopic microsurgery (TEM).....	72
1.7.6.	“Less-invasive” laparoscopy.....	74
1.7.7.	Laparoscopic / flexible endoscopic “rendezvous” procedures.....	76
1.8.	Advanced intraluminal surgery with flexible endoscopes.....	77
1.8.1.	From diagnostics to advanced intervention	77
1.8.2.	Endoscopic retrograde cholangiopancreatography (ERCP)	78
1.8.3.	Mucosal resections – polypectomy, endoscopic mucosal resection (EMR) and endoscopic submucosal dissection (ESD)	80
1.8.4.	Tissue remodelling for management of gastro-oesophageal reflux disease	86
1.8.5.	EUS guided fine needle aspiration (FNA) and pseudocyst drainage.....	88
1.9.	Natural Orifice Transluminal Endoscopic Surgery (NOTES)	88
1.10.	The need for new endoscopic cutting methods	93
1.11.	Chapter Conclusions	97
1.12.	Recent developments as of 2010.....	98
Chapter 2:	Existing endoscopic cutting methods	101
2.1.	Chapter Overview	101
2.2.	Literature survey methodology	101
2.3.	Tissue cutting instruments in open and minimally invasive surgery	102
2.3.1.	Mechanical shearing of tissue.....	102
2.3.2.	Waterjet cutting of tissue	107
2.3.3.	Gas dissection of tissue.....	108
2.3.4.	Radiofrequency electrosurgery.....	108
2.3.5.	Ultrasonic / harmonic cutters	114
2.3.6.	Laser ablation.....	115
2.3.7.	Chemically assisted mechanical dissection of tissue	119
2.4.	Directing where the cut occurs.....	119

2.4.1.	Sensitizing tissues with chemicals.....	119
2.4.2.	Feedback control.....	121
2.4.3.	Articulation.....	121
2.4.4.	Diathermy dissection control by electrode geometry.....	123
2.5.	Chapter Conclusions	124

Chapter 3: Deconstructing dissection and an exploration of concepts 127

3.1.	Chapter Overview	127
3.2.	Dissection, deconstructed.....	128
3.2.1.	Dissection as simultaneous targeting and cutting tasks	128
3.2.2.	Breaking apart dissection into sequential tasks.....	129
3.2.3.	The sensitization tactic.....	131
3.2.4.	The protection tactic.....	132
3.2.5.	Other concepts.....	133
3.3.	Overview of concepts	133
3.4.	Dye-mediated laser ablation.....	134
3.4.1.	Using dyes to sensitize tissue.....	134
3.4.2.	Dye potentiation of low-power lasers for laser ablation.....	135
3.4.3.	Selectivity of tissue ablation due to the presence of dye	143
3.4.4.	Dependence of ablation on tissue type	147
3.4.5.	The potential for dye-erasure	150
3.4.6.	Carbonisation to sustain laser ablation	156
3.4.7.	Overall conclusions for dye-mediated laser ablation	162
3.5.	Selective tissue stiffening prior to mechanical shearing with scissors	163
3.5.1.	The problem with endoscopic scissors	163
3.5.2.	Deployable polymer stiffeners (glue) to mediate cutting with scissors	165
3.5.3.	Proof-of-concept in <i>ex vivo</i> tissue.....	166

3.5.4.	A physical basis for enhanced cutting.....	169
3.5.5.	Overall conclusions for selective tissue stiffening	174
3.6.	Blunt dissection by gas-evolving chemical reaction	175
3.6.1.	A “volcanic” reaction.....	175
3.6.2.	Proof-of-concept in post-mortem tissue	176
3.6.3.	Overall conclusions for dissection by gas-evolving chemistry.....	181
3.7.	Non-Newtonian fluid barrier.....	182
3.7.1.	Protection from liquid “force fields”	182
3.7.2.	Evaluating corn flour and water to protect against needle penetration.....	183
3.7.3.	Overall conclusions for protective shear-thickening liquid barriers.....	190
3.8.	Monopolar and bipolar electrofulguration.....	191
3.8.1.	Improvements to electrosurgical diathermy	191
3.8.2.	Proof-of-concept experiments with electrofulguration	192
3.8.3.	Overall conclusions for electrofulguration	198
3.9.	Conductive or insulating masks for directing RF energy.....	199
3.9.1.	Rubber tires and lightning rods.....	199
3.9.2.	Computer modelling of conductive and insulating masks.....	199
3.9.3.	Overall conclusions on conductive or insulating masks.....	205
3.10.	Miscellaneous Ideas	206
3.10.1.	Endoscopic scissors with local-tensioning	206
3.10.2.	Cheesewire cutter with tissue-depth stop.....	206
3.10.3.	Tissue differentiation by acoustic fingerprinting	207
3.10.4.	Circular and rotary saw cutter	208
3.10.5.	RF-vaporisation or hydrogen peroxide decomposition for waterjet cutting and rotary steam engine.....	210
3.10.6.	Vibrating blade.....	211
3.10.7.	Shear-thickening fluids for transmitting ultrasonic vibrations	212

3.11.	Summary of concepts, selection criteria and selection results	213
3.12.	Chapter Conclusions	214
Chapter 4: Dye-mediated laser ablation		215
4.1.	Chapter Overview	215
4.2.	The concept.....	215
4.3.	Lasers	217
4.3.1.	Light amplification by stimulated emission of radiation.....	217
4.3.2.	The Diomed 805 nm semiconductor laser	217
4.3.3.	Laser output power measurements.....	218
4.3.4.	Beam profile and divergence	219
4.3.5.	Wavelength	226
4.4.	Absorbers	228
4.4.1.	Indocyanine green dye.....	228
4.4.2.	Absorption spectrum of ICG solutions	229
4.4.3.	Diffusion into tissue	234
4.4.4.	Lateral spread on the surface of porcine muscle.....	239
4.5.	Feasibility of dye-mediated ablation <i>in vivo</i>	242
4.6.	Theoretical model of laser ablation	245
4.6.1.	Modelling laser ablation in tissue	245
4.6.2.	The McKenzie model.....	247
4.6.3.	The importance of carbonisation.....	252
4.7.	Ablation tissue effects revealed by histology	256
4.8.	Ablation sequence of events revealed by high speed videography	262
4.9.	Growth of the ablation crater assessed by <i>en face</i> videography	268
4.10.	Growth of the ablation crater from cross-section photography	277
4.11.	Statistical analysis of ablation response due to power, time, dye	288

4.12.	Modification to the theory for dye-mediated laser ablation.....	297
4.13.	An Arrhenius-based model for carbonisation.....	299
4.14.	Multiphysics computer model	299
4.14.1.	Light transport model	300
4.14.2.	Heat diffusion model.....	302
4.14.3.	Tissue model	303
4.14.4.	Model geometry	309
4.14.5.	Results.....	309
4.14.6.	Discussion.....	313
4.15.	Dye-mediated ablation compared with existing techniques.....	315
4.16.	Other factors for consideration	316
4.16.1.	Methods for dye application.....	316
4.16.2.	Potential methods for dye removal	321
4.17.	Chapter Conclusions	323
Chapter 5: Overall conclusions and future work.....		324
5.1.	Overall summary of work.....	324
5.2.	Main findings and conclusions.....	325
5.3.	Recommendations for future work	325
5.4.	Closing thoughts.....	326
Appendix A: Histology slide preparation techniques.....		327
Appendix B: Alternative light transport models		332
Appendix C: Thermal and optical coefficients		335
Overview of coefficients used in the model		335
Thermal properties		336
Specific heat capacity.....		336
Thermal conductivity		336

Tissue constituents	336
Dependency of thermal properties on water content.....	336
Optical properties	337
Absorption coefficient for porcine muscle	337
Normalised absorption coefficient	338
Extinction coefficient of soot	338
References.....	339

List of Figures

Figure 1-1. 'Vitruvian Man' by Leonardo da Vinci, ca.1492, Gallerie dell'Accademia in Venice. (Reproduced from Wikipedia, http://en.wikipedia.org/wiki/Vitruvian_Man)	27
Figure 1-2. A metastasizing breast cancer cell. (Reproduced from http://www.allthingsbeautiful.com/all_things_beautiful/images/metastasizing_cancer.jpg) .	27
Figure 1-3. An Egyptian circumcision scene, drawn from a tomb carving in Sakkara cemetary at Memphis, Egypt, c. 2400-3000 BC. (Reproduced from Ellis. [9]).....	30
Figure 1-4. Chinese surgeon Hua Tuo performs a surgical procedure on the war lord general Kuan Yun as he plays a board game (left), and a 19 th century drawing of a woman having a cataract procedure done as described by Indian surgeon Susruta (right). (Reproduced from Ellis. [9]).....	31
Figure 1-5. Bozzini's lichtleiter, or "light conductor" – the first endoscope. (Reproduced from Edmonson. [12]).....	35
Figure 1-6. Desormeaux's endoscope. (Reproduced from Berci and Ford. [14])	36
Figure 1-7. Kussmaul's gastroscope (a) and its introduction into the throat of a sword swallower (b). (Reproduced from Edmonson. [12])	37
Figure 1-8. The Nitze optical system (left), and intubation of a patient in a deep head-down (Trendelenberg) position (right). (Reproduced from Berci and Ford. [14]).....	38
Figure 1-9. A selection of Karl Storz rigid endoscopes (and one flexible endoscope). (Reproduced from the Surgical Optics website.)	41
Figure 1-10. A laparoscopic surgery performed with a rigid endoscope and a laparoscopic instrument inserted through two cannula. (Reproduced from Laparoscopic Surgery Complications website. [20])	42
Figure 1-11. Schematics of a modern flexible endoscope. (Reproduced from Ginsberg, et. al. [17]) A. Endoscope controls and serviceable parts. B. Schematic of light, air and water conduits from the control unit to the scope tip. C. Breakaway view of all the conduits that are contained inside the scope shaft. D. Cross-section view of the distal end, including the objective lenses and the CCD that make up the video camera.....	45
Figure 1-12. The Olympus R-Scope gastroscope for endoscopic mucosal dissection. (a) Additional controls on the handle to manage new degrees-of-freedom. (b) Dual-bending articulating segments allows for an S-shaped bend. (c) Dual accessory channels each with elevator / accessory articulators to allow independent motion control of two endoscopic	

devices, typically a tissue grasper and electrosurgical cutter. (Reproduced from Reavis and Melvin. [21]).....	47
Figure 1-13. A small calibre transnasal esophagoscope can be used for sedation-less examination of the upper GI tract. (Reproduced from Reavis and Melvin. [21]).....	48
Figure 1-14. The SpyGlass direct visualization fibre optic probe for direct visualization in ERCP. The delivery catheter is passed through the working channel of a duodenoscope (left) and cannulated into the common bile duct. The fibre optic probe (right) then is passed through the delivery catheter tip (centre). (Reproduced from Reavis and Melvin. [21]).....	48
Figure 1-15. The Transport endosurgical operating platform featuring ShapeLock technology from USGI. (Reproduced from Reavis and Melvin. [21])	49
Figure 1-16. The USGI Cobra experimental endoscope, which uses ShapeLock technology to freeze the scope shape on demand, features one visualization and two accessory cannulae that can be articulated independently. (Reproduced from Richards et. al. [27])	49
Figure 1-17. The da Vinci surgical system. (Reproduced from Intuitive Surgical website. [28])	50
Figure 1-18. The da Vinci surgical robot is dexterous enough to fold a miniature origami paper crane. (Reproduced from Ishikawa et. al. [29])	50
Figure 1-19. Two experimental <i>in vivo</i> endoscopes. (Reproduced from Rentschler and Oleynikov. [32]).....	51
Figure 1-20. A schematic of the electro-stimulation concept – using pulses of electricity to induce the muscles in the gut to peristaltically move a device within its lumen. (Reproduced from Mosse et al. [36])	52
Figure 1-21. The Olympus Guidance System. The concept employs magnets to move and rotate a capsule endoscope within the lumen of the gastrointestinal tract. (Reproduced from Menciassi, Quirini and Dario. [37])	52
Figure 1-22. The oesophagus. Nearby anatomy accessible by a trans-oesophageal approach include the oesophagus, thyroid gland, thoracic cavity, trachea, lungs, aorta, heart, and the cervical and thoracic spinal column. (Reproduced from Netter. [38])	55
Figure 1-23. The stomach. Nearby anatomy accessible by a transgastric approach include the peritoneal cavity, stomach, liver, gallbladder, spleen, small intestine, large intestine, kidneys, ureters, bladder, uterus, ovaries, fallopian tubes, and the lumbar spinal column. (Reproduced from Netter. [38])	56
Figure 1-24. The duodenum (the proximal part of the small intestine) which is connected to the stomach. (Reproduced from Netter. [38])	57

Figure 1-25. The small intestine (duodenum, jejunum and ileum). (Reproduced from Netter. [38]).....	58
Figure 1-26. The connection between the ileum (the distal part of the small intestine) and the caecum (the proximal part of the large intestine). (Reproduced from Netter. [38])	59
Figure 1-27. The large intestine (ascending colon, transverse colon, descending colon, sigmoid colon and the rectum). Nearby anatomy accessible by a transcolonic or a transanal approach include the peritoneal cavity, stomach, liver, gallbladder, spleen, small intestine, large intestine, kidneys, ureters, bladder, prostate, uterus, ovaries, fallopian tubes, and the lumbar and sacral spinal column. (Reproduced from Netter. [38])	60
Figure 1-28. A cross-sectional view of the layers composing the tissues in the gastrointestinal tract. (Reproduced from Netter. [38])	61
Figure 1-29. Laparoscopic cholecystectomy. (Reproduced from [74].).....	70
Figure 1-30. Options for bariatric surgery. (1) Adjustable gastric banding, (2) vertical banded gastroplasty, (3) Roux-en-Y gastric bypass, and (4) biliopancreatic diversion. (Reproduced from Gentileschi et al. [78]).....	72
Figure 1-31. Instruments for transanal endoscopic microsurgery. (Reproduced from Buess et al. [97]).....	74
Figure 1-32. A laparoscopic / endoscopic "rendezvous" procedure. (Reproduced from Saccomani et al. [115]).....	77
Figure 1-33. A Billroth II sphincterotomy (Cook Inc; Bloomington, IN, USA). (Reproduced from Cook website. [118])	79
Figure 1-34. Polypectomy of a pedunculated polyp performed with an endoscopic snare. (Reproduced from Baron. [120]).....	80
Figure 1-35. Experimental caps with electrosurgical blades embedded in them for performing widespread EMR. (Reproduced from Rajan et al. [126])	83
Figure 1-36. A. Hook knife. B. Triangle tip (TT) knife. C. Insulated tip (IT) knife. (Reproduced from Chiu et al. [139]).....	85
Figure 1-37. Flex knife. (Reproduced from Fujishiro et al. [138])	85
Figure 1-38. An ESD performed using the R-Scope (Olympus; Tokyo, Japan). (a) The R-Scope has two independently controlled elevators to articulate two instruments. (b) The defect remaining in the tissue after ESD has been completed. (c) The resected tissue has been removed <i>en bloc</i> in one piece. (Reproduced from Reavis & Melvin. [21])	86

Figure 1-39. Manipulation of the porcine liver to reveal the gallbladder in a NOTES experiment. (Personal photograph.)	93
Figure 2-1. Olympus biopsy forceps. (Reproduced from Olympus website. [225]).....	104
Figure 2-2. The Olympus EMR scissors. (Reproduced from Miyashita. [224])	104
Figure 2-3. An electrosurgical generator by ERBE Elektromedizin GmbH. (Reproduced form MDA Electrosurgical Devices Review 2002. [239])	112
Figure 2-4. Many electrosurgical generators can operate in two modes: (1) a bipolar mode (left) in which both leads of the electrical circuit are connected to the electrosurgical instrument, and (2) a monopolar mode (right) in which the active lead is connected to the electrosurgical instrument, and the return electrode takes the form of a grounding pad or plate that is affixed to the patient's thigh or buttocks. (Reproduced from MDA Electrosurgical Devices Review 2002. [239]).....	112
Figure 2-5. Common lasers and their wavelengths. (Reproduced from [249].)	116
Figure 2-6. A number of articulating devices for flexible endoscopy that were designed by the author from 2004 to 2006. (Personal photographs.).....	123
Figure 2-7. A 3.2mm diameter articulating grasper with an "intuitive" control interface. (Personal photograph.)	123
Figure 2-8. Research opportunity based on the literature.	126
Figure 3-1. An overview of concepts explored for deconstructing dissection. Sections 3.4-3.10 explain and discuss each concept in depth, and section 3.11 compares the concepts against each other.	134
Figure 3-2. Extinction coefficient vs. wavelength for ICG, MB and fluorescein (also oxy- and deoxy-hemoglobin for comparison).	136
Figure 3-3. A linear incision by made an 805 nm Diomed laser in chicken tissue stained with ICG. Features of the ablation crater are typical of ICG-mediated ablation.....	139
Figure 3-4. Tissue stained with the higher concentration (11 mg/ml) MB was ablated when exposed to the laser.....	139
Figure 3-5. Tissue stained with the lower concentration (1 mg/ml) MB typically was coagulated when exposed to the laser (right arrow), although occasionally ablation was observed (left arrow). However, when ablation was observed, the process took tens of seconds to occur, which is above the 9.9 s exposure time limit set in these experiments.....	140
Figure 3-6. MB-stained tissue ablated by an 805 nm Diomed laser.....	140
Figure 3-7. Ablation with the carbon dioxide laser.....	141

Figure 3-8. Ablation is confined laterally above sub-surface injection of ICG.....	145
Figure 3-9. Islands of ablation are confined to where “HI” (outlined in white) was painted in ICG on the tissue surface.	145
Figure 3-10. ICG-mediated laser ablation of liver, kidney, muscle.....	148
Figure 3-11. (1) Subsurface injection of ICG into chicken muscle could mediate laser ablation. Ablation occurred where the tissue was stained green by the ICG (top arrow), while ICG-free regions were not ablated (bottom arrow). (2) Subsurface injection of ICG followed by injection of hydrogen peroxide resulted in a whitening of tissue. Whitened areas of tissue were not ablated by the laser (bottom arrow), while areas that remained green were able to be ablated (top arrow).	153
Figure 3-12. Cross-sectional view of the control bleb cut through the laser path. Tissue with green ICG beneath could be ablated by the laser (right arrow). Tissue without ICG could not be ablated (left arrow).....	154
Figure 3-13. Cross-sectional view of the test bleb cut through the laser path. Tissue with green ICG that had been whitened with the hydrogen peroxide injection did not ablate (left arrow). ICG marked tissue that had not been whitened could be ablated (right arrow).	154
Figure 3-14. Schematic of the experimental laser setup (top). Photograph of the setup (bottom).....	157
Figure 3-15. (Left image) (A) ICG-mediated laser ablation resulted in ablation. (B) Two 9.9 s prolonged exposures in tissue with no dye both resulted in ablation. (C) Two 2 s exposures in tissue with no dye did not result in ablation. (Right image) Cross-section through the tissue at (B).....	158
Figure 3-16. Ablation of unstained tissue by a 9.9s pulse of 805nm laser light at 25W. Subsequent pulses result immediately in the generation of smoke and continued ablation. Typical ablation craters are shown (left) and in cross-section (right).	159
Figure 3-17. Laser ablation of unstained tissue by an 805nm diode laser. Each test location with the run number. Arrows denote crater formation and carbonisation indicative of tissue ablation.	160
Figure 3-18. Cyanoacrylate adhesive (Loctite SuperGlue brand) applied to chicken skin in order to increase mechanical stiffness.....	167
Figure 3-19. Chicken skin tissue stiffened with cyanoacrylate adhesive (solid rectangle), and untreated tissue (dotted rectangle). Scissor cuts in the glue-stiffened region were sharp and	

easy to make (solid arrows), while the cuts in the control region were jagged and hard to make in the soft, floppy and shrivelled tissue (dotted arrows).....	168
Figure 3-20. The CA glue-tissue composite could be cut with great precision. A ~0.5 mm wide piece cut from the sample is shown at the arrow.	168
Figure 3-21. Geometry of scissors cutting a swatch of material of thickness h . (Reproduced from Mahvash et al. [284])	170
Figure 3-22. Stages of cutting by scissors. θ is the angle between the centreline of the scissors blades, and τ is the torque required at the scissors handle. From 0 to 1, the closing scissors blades have not yet engaged the material. From 1 to 2, the material is being deformed until a fracture occurs at 2. From 2 to 3, the material is being cut. From 3 to 4, the material is relaxing as the scissors are opened. (Reproduced from Mahvash et al. [284])	170
Figure 3-23. The bending of a cantilever beam.	171
Figure 3-24. A common failure mode when cutting with scissors – the material bends, stretches and gets stuck between the scissor blades instead of being cut.	172
Figure 3-25. Schematic (left) and photograph (right) of the experimental setup.	184
Figure 3-26. 3D scatterplot of layers of foil penetration versus initial needle height versus depth of liquid barrier. Composition “0” is water, “2” is the corn flour/water liquid and “4” is the corn flour/water “mud”.....	185
Figure 3-27. 2D scatterplot of foil penetration versus initial needle height for each liquid barrier composition. Composition “0” is water, “2” is the corn flour/water fluid and “4” is the corn flour/water “mud”.	186
Figure 3-28. The main effects plot for penetration based on data means.	186
Figure 3-29. A model for the mechanism for shear thinning and shear thickening in non-Newtonian fluids. (Reproduced from Wetzel et al. [296]).....	188
Figure 3-30. A spark can be made to jump a small air gap by using the high voltage spray coagulation mode to induce electrical breakdown.	192
Figure 3-31. Comparison of incisions in chicken thigh made by electrofulguration, electrosurgical diathermy and scalpel.	195
Figure 3-32. Tissue dissection by bipolar electrofulguration.	195
Figure 3-33. Electrosurgical dissection through the serosa of the small intestine.....	196
Figure 3-34. Tissue dissection by monopolar electrofulguration.	197
Figure 3-35. Axis-symmetric geometry of the model.	200
Figure 3-36. 2D cross-section of the 3D axis-symmetric model geometry.....	201

Figure 3-37. The meshed 2D geometry.	201
Figure 3-38. Results FEM simulation of monopolar electrosurgical diathermy with no implant (top), an implanted insulator (middle) and an implanted conductor (bottom). Surface colours represent the magnitude of total current density and the red lines are streamlines for total current density.....	203
Figure 3-39. Mechanical, vacuum-based and electro-stimulation concepts for tissue stiffening.	206
Figure 3-40. The Cheesewire cutting concept. (1) The metal wire is placed at depth into tissue with a curved needle and regrasped with the device. (2) Cheesewiring effect used to cut tissue by sliding the wire and cinching it against the captured tissue t the same time. (3) When the wire is fully retracted back into the device, it can be reset to make another incision.....	207
Figure 3-41. Acoustic "fingerprinting" experimental setup with CO ₂ laser, tissue, and needle hydrophone submersed in a water bath.	208
Figure 3-42. Rotary grinding and drilling tools used with a high speed rotary instrument.....	209
Figure 3-43. Of the cutting tools in the Dremel kit, the circular cut-off disk was the most effective at cutting the slippery, mucus coated porcine gastric tissue.	210
Figure 3-44. One embodiment of a miniature hydrogen peroxide steam engine to generate rotary motion <i>in situ</i> . (Reproduced from author's personal design notebook.)	211
Figure 3-45. A crude attempt at a vibrating blade using a commercial vibrating shaving razor handle.	212
Figure 4-1 - Calibration of the set power vs. measured output power for the Diomed 25 laser (n=28). Error bars are standard errors. The overall laser system with the fibre and mode scrambler has an output efficiency of ~66%.....	219
Figure 4-2. The visible red aiming annulus circumscribes the targeting area of the invisible NIR treatment beam.....	220
Figure 4-3. An electoviewer is used to visualize the near-infrared radiation from the Diomed laser.....	221
Figure 4-4 – At low power settings, the beam profile from the Diomed 25 laser set to a constant power, projected onto a white screen and viewed through an electoviewer varied from one activation to the next. At high power settings, the profile was relatively consistent between activations.....	221
Figure 4-5. Mode scrambling fixture.....	222
Figure 4-6. Experimental setup for the beam profile measurement experiments.....	222

Figure 4-7. The photodiode fixtured into a block of wood (left). It was used in photovoltaic mode and the generated current was measured with a digital multimeter (right).	223
Figure 4-8. Beam profile of the Diomed 25 laser at 25 W, 20 W and 15 W set power. Error bars represent 95% CI. Red areas represent where the aiming annulus would be located. The aiming beam was disabled for the experiments.	224
Figure 4-9. Variation in the beam profile in three sequential firings of the Diomed 25 laser at 15 W set power. The data in the dotted profile are data means at each radial position, and error bars represent 95% CI. Red areas represent where the aiming annulus would be located. The aiming beam was disabled for these experiments.	224
Figure 4-10. Measurements and linear regression of beam radius v the separation height between the tip of the optic fibre and the projection surface.....	225
Figure 4-11. Spectral measurements of a HeNe laser with wavelength of 632.8 nm confirmed the spectrometer's poor spectral resolution.....	226
Figure 4-12. Wavelength spectra of Diomed laser at power settings from 1 W to 25 W.	227
Figure 4-13. The wavelength corresponding to peak intensity for each power Diomed power setting. Dotted lines correspond to the wavelength spread at half maximum intensity.....	228
Figure 4-14. The molecular structure of indocyanine green sodium iodide.....	228
Figure 4-15. Absorption spectra of ICG in water and plasma for different concentration solutions. (Reproduced from Landsman. [305])	230
Figure 4-16. The dependence of optical density at $\lambda=805$ nm on concentration of ICG in human plasma. Concentrations for data points denoted by triangles should be multiplied by 0.1 as this data represents concentrations of 0-20 mg/l. (Reproduced from Landsman. [305]).....	230
Figure 4-17. Absorption spectra of ICG in plasma at various high concentrations. Experimental data (solid) were combined with literature data (dashed, dotted).....	231
Figure 4-18. Absorption spectra of ICG in water at various high concentrations. Experimental data (solid) were combined with literature data (dashed, dotted).....	232
Figure 4-19. The dependence of the absorption coefficient at 805 nm on the concentration of ICG in plasma. Experimental data (solid) and literature data (dashed, dotted) have been combined.	232
Figure 4-20. The dependence of the absorption coefficient at 805 nm on the concentration of ICG in water. Experimental data (solid) and literature data (dashed, dotted) have been combined.	233

Figure 4-21. Cross section through tissue samples after immersion in ICG/water and ICG/DMSO for 24 hours.....	235
Figure 4-22. Image of the tissue digitally split into hue (left), saturation (middle) and brightness (right) channels. The hue channel provided the best visual contrast for detecting the green colour of ICG.	236
Figure 4-23. The thickness of the thresholded regions are measured in ImageJ. ICG/water (left) and ICG/DMSO (right).....	236
Figure 4-24. Box-and-whisker plot of the data.....	237
Figure 4-25. Outlines traced around dyed muscle in ImageJ.....	240
Figure 4-26. Dotplot and data means for surface coverage data vs. dye volume. Error bars represent standard error.	241
Figure 4-27. Craters, charring and tissue whitening on the surface of an ICG/H ₂ O filled subsurface bleb.....	244
Figure 4-28. McKenzie's three zone model of laser ablation. (Reproduced from McKenzie. [317])	249
Figure 4-29. Cyclical waves of carbonisation and ablation as revealed by videography. (Reproduced from Verdaasdonk, Borst and van Gemert. [319]).....	253
Figure 4-30. Absorbance spectra of denatured myoglobin from 450-700 nm. (Reproduced from Trout. [321])	255
Figure 4-31. Measurement of the absorbance spectrum of char. (Reproduced from Jacques. [320]).....	256
Figure 4-32. Three frozen histology section of ICG-mediated laser ablation in pork muscle tissue. The red arrows indicate the location of the laser beam. In region (1),.....	259
Figure 4-33. A frozen section that subsequently has undergone H&E staining. As can be seen when compared with slides not stained with H&E, much of the tissue at (1) and (2) has been lost.....	260
Figure 4-34. Gömöri trichrome staining of ICG-mediated laser ablation of tissue — control (left) and test (right).	260
Figure 4-35. Staining for NADH reductase in ICG-mediated laser ablation of tissue — control (left) and test (right).....	260
Figure 4-36. The Vision Research Phantom MIRO4 (left) and the Photron Fastcam SA1 (right) shown to approximate scale.....	263
Figure 4-37. Experimental setup for producing the <i>en face</i> ablation videos.....	263

Figure 4-38. Dye-mediated laser ablation of pork muscle captured with the Phantom SA1...	265
Figure 4-39. Dye-mediated laser ablation of pork muscle captured with the Phantom MIRO4.
	266
Figure 4-40. Plot of the pixels in a vertical line through the centre of the ablation crater (y-axis) versus time (x-axis). (Top) Photron SA1 filmed at 20,000 fps for 4.3658 s; (Bottom) Phantom MIRO4 filmed at 4000 fps for 7.8303 s. Time axes (horizontal) were scaled and aligned. The space axes (vertical) were scaled to maintain the aspect ratio.....	267
Figure 4-41. A typical ablation crater and regions of interest are marked in ImageJ.....	269
Figure 4-42. The diameter growth of regions denoted as black, white and coag at three laser irradiances. (n=255, x- and y- error bars represent 95% CI)	270
Figure 4-43. Linear regression of the “black” region growth over time at three irradiances. Error bars represent 95% CI.....	271
Figure 4-44. Diameter growth of the “black” region increased with larger laser irradiances..	272
Figure 4-45. The growth of the “white” region over time at three irradiances. Error bars represent 95% CI.....	273
Figure 4-46. Average thickness of the coagulated region at three irradiances over time. Error bars represent 95% CI.....	274
Figure 4-47. Experimental setup for cross-section laser ablation videography.	279
Figure 4-48. Porcine muscle tissue target after laser ablation run.....	279
Figure 4-49. Cross-section view of laser ablation. The laser is active from t=0 to 9.9 s.....	280
Figure 4-50. The vertical pixels through the centre of the crater section in each frame (y-axis) are plotted against frame / time (x-axis).	281
Figure 4-51. Computer segmentation of regions of black corresponding to the ablation crater and carbonisation (top) and regions of white corresponding to coagulation (bottom).	281
Figure 4-52. Average boundary location at three laser irradiances (orange = high, green = mid, blue = low) for the maximum depth in pixels of the black region (top) and the thickness of the white region (bottom).	282
Figure 4-53. Linear regression of average distance from top of image to the bottom of black region.	283
Figure 4-54. Positive correlation between the growth rate of the black region and the irradiance.	284
Figure 4-55. Linear regression of the thickness of the white region.	285

Figure 4-56. Negative correlation between the growth rate of the thickness of the white region and irradiance.....	286
Figure 4-57. An <i>en face</i> view of an ablation crater after ROI annotation.....	290
Figure 4-58. A cross-section view of an ablation crater after ROI annotation.....	290
Figure 4-59. RSM regression for the <i>en face</i> data. The thickness of the white region (top) and the diameter of the black region (bottom) as reaction to set power, time and dye volume... ..	292
Figure 4-60. RSM regression for the cross-section data. The thickness of the white region (top) and the diameter of the black region (bottom) as reaction to set power, time and dye volume.	293
Figure 4-61. Growth of the black region depth at the high power setting.....	296
Figure 4-62. The FEM model consists of three sub-models that are linked to each other — the light transport model, the heat transfer model, and the tissue model.....	300
Figure 4-63. Model geometry and mesh.	309
Figure 4-64. Results of FEM model over 2.5 seconds of simulation time.....	311
Figure 4-65. En face results. Growth of the crater radius and thicknesses of damage zones at z=0.....	312
Figure 4-66. Cross-section results. Growth of the crater depth and thicknesses of damage zones at r=0.....	312
Figure 4-67. Absorption (top), irradiance (middle) and the spatial heat source (bottom) one second into the ablation simulation after replacing the frequency factor in the Arrhenius equation for carbonisation with a higher coefficient.	314
Figure 4-68. Droplets of ICG applied to the surface of tissue tends to seep into and follow fissures and cracks.	317
Figure 4-69. ICG injected into tissue is contained within tissue planes.....	318
Figure 4-70. ICG lines formed by dragging soaked thread across the tissue surface (1). ICG soaked thread implanted into tissue using a curved needle (2).....	320
Figure 4-71. A concept “chalk”-line dye applicator. A forceps-like endoscopic device is deployed by opening the jaws to a 180° angle and placing the device in contact with tissue. Dye-saturated thread then is dragged across the tissue, guided by the jaw structure of the open forceps-like device.	320
Figure C-1. Specific heat capacity of muscle tissue [J/(g K)]. (Reproduced from Duck. [279]).	336
Figure C-2. Temperature and thermal conductivity of muscle tissue [W/(m K)]. (Reproduced from Duck. [279])	336

Figure C-3. Composition of human cardiac and skeletal muscle tissue. (Reproduced from Duck. [279]).....	336
Figure C-4. The thermal conductivities of biological fluids depending on water content (at near body temperatures). (Reproduced from Spells. [350]).....	337
Figure C-5. Scatter and absorption coefficients for pork muscle at 632 and 800 nm. (Reproduced from Birth et al. [351])	337
Figure C-6. Normalised absorption coefficient of rat prostate during coagulation. (Reproduced from Skinner et al. [333])	338
Figure C-7. Extinction coefficient, k , of soot from propane combustion [$1/\mu\text{m}$]. (Reproduced from Köylü and Faeth. [336] Logarithmic grid overlay added.)	338

List of Tables

Table 1-1 – Representative thicknesses of GI tissues from individual studies in the literature. Figures do not capture the large biological variance within the population.....	54
Table 1-2. A brief timeline of the development of laparoscopy, compiled from Birkett's review article. [3]	63
Table 1-3. Summary of developments in natural-orifice, transluminal and transvisceral endoscopic surgery.....	90
Table 1-4. Barriers to NOTES, according to the 2006 NOTES working group white paper. [8] ..	95
Table 3-1. Outcomes matrix of success / failure of cutting and control capability during endoscopic cutting.....	128
Table 3-2. Results of dye-mediated laser ablation.....	138
Table 3-3. Percentage constituents of adult human tissues. (Selected data compiled from Duck [279].) Overall ranges given except when in square brackets, which represent ± 1 SD.	149
Table 3-4. Exposure times and outcomes for 805nm laser ablation of unstained pork tissue.	160
Table 3-5. Selected material properties for chicken skin and cyanoacrylate.....	173
Table 3-6. DOE model coefficients.....	187
Table 3-7. Concept selection Pugh chart.....	214
Table 4-1. Summary of Mann-Whitney rank sum test.....	237
Table 4-2. Mean dye coverage areas vs. volume and time.....	240
Table 4-3. Summary of ANOVA analysis.....	241
Table 4-4. Thickness of the dye layer.....	242
Table 4-5. Summary of "black" region growth assuming a linear model.....	271
Table 4-6. Summary of the black region growth rate, assuming a linear model.....	283
Table 4-7. Summary of the white region growth rate, assuming a linear model.....	285
Table 4-8. Low, mid and high levels for irradiance, exposure time and dye volume.....	289
Table 4-9. RSM regression coefficients for the <i>en face</i> data relating the input factors to the output responses.....	291
Table 4-10. RSM regression coefficients for the cross-section data relating the input factors to the output responses.....	291
Table 4-11. Summary of changes in thermal coefficients.....	308
Table 4-12. Summary of changes in optical coefficients.....	308
Table 4-13. Summary of how state changes are modelled.	309

Table 4-14. Depth of coagulation necrosis from various cutting instruments using “normal operating settings” for different surgical procedures. Various power settings used on different tissue types. Data provided for qualitative comparision only.....	316
Table C-1. Summary of changes in thermal coefficients.	335
Table C-2. Summary of changes in optical coefficients.	335
Table C-3. Summary of how state changes are modelled.	335

Chapter 1: Surgery and the case for new cutting tools

The journey of a thousand leagues began with what was under the feet.

Lao Tzu

Tao Te Ching

1.1. Chapter Overview

This chapter provides a general introduction to surgery – the development of the surgical practice through history, details on the instruments used in rigid and flexible endoscopy, a general review of the anatomy and physiology in the human abdomen, and a brief description of some of the procedures that doctors wish to re-envision for surgery at flexible endoscopy.

This information serves as necessary background for discussing natural orifice transluminal endoscopic surgery (NOTES) and other advanced endoscopic surgical approaches, their goals and requirements, and how selective and controlled cutting tools with haemostasis, or bleeding management capabilities, may be important and contribute to the success of NOTES and other advanced endoscopic procedures.

It also provides evidence that demand exists for the development for more advanced minimally invasive surgical procedures, and that existing instrumentation for performing these new procedures at flexible endoscopy is lacking.

1.2. Surgery – always towards the cutting edge

Surgery – derived from the Greek *cheir*, meaning hand, and *ergon*, meaning work. [1] The word and all it represents evokes in many people a very strong emotional response. To some, even the mere mention of the word strikes a chord of terror within them, invoking dire images of amputations, notions of extensive pain and long convalescences, even fears of death.

For many others, however, surgery offers them the chance and the hope for healing, when lifestyle changes, medication and other treatments have been ineffective, or when the nature of the injury or disease can be addressed adequately only by nothing less than full-blown surgical intervention.

Scholars and philosophers of past often have had idealized notions about the form and function of the human body. For example, in the sketch of the “Vitruvian Man,” Leonardo da Vinci highlighted the symmetry and proportions of the human form as a symbol of the perfect symmetry in the universe itself (see Figure 1-1). [2]

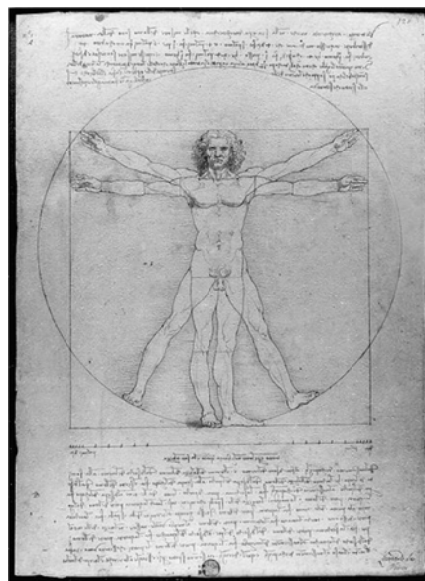


Figure 1-1. 'Vitruvian Man' by Leonardo da Vinci, ca.1492, Gallerie dell'Accademia in Venice.
(Reproduced from Wikipedia, http://en.wikipedia.org/wiki/Vitruvian_Man)

Yet while the human body as a product of millions of years of evolution is indeed quite a marvel of biological engineering, we know from modern biology and medical science that it is far from perfect, and that things can and often do go wrong, for example when one of myriad forms of cancer starts to grow uncontrollably and invade inside the body (see Figure 1-2). In many cases when things do go wrong, surgery is the best and sometimes only option available.

Copyrighted material

Figure 1-2. A metastasizing breast cancer cell.
(Reproduced from http://www.allthingsbeautiful.com/all_things_beautiful/images/metastasizing_cancer.jpg)

In the last two centuries, medical knowledge, technology and procedure development in surgery have advanced quite rapidly. During this time, some of the most important surgical advances have occurred, including the introduction of antiseptic techniques, anaesthesia, antibiotics, and later fibre optic and video endoscopic technology. [3]

For some medical procedures, the advances in endoscopy have led to the introduction, adoption and promotion as the current gold standard, minimally invasive techniques which depend on the use of rigid and flexible endoscopes to visualize surgical fields that are outside of direct line-of-sight, and that can be far and deep within the human body.

Laparoscopy, sometimes called keyhole surgery because of the small “keyhole” incisions made in the abdominal wall as part of the technique, is considered to be the gold standard for cholecystectomy, or the surgical removal of the gall-bladder. [4] Colonoscopy, utilizing a flexible endoscope that is inserted through the anus to examine the large intestine, is the most common and the most effective method to detect and remove abnormal growths or polyps found within the human colon. [5]

In recent years, starting from around the turn of the twenty-first century, gastroenterologists, who are experienced wielding flexible endoscopes to provide therapy, and colorectal surgeons, who perform many surgical procedures using rigid laparoscopes, have joined together in proposing natural orifice transluminal endoscopic surgery (NOTES) as a potentially revolutionary approach to performing minimally invasive surgery (MIS). [6] These concepts, which involve the use of flexible endoscopes that traditionally have fallen within the expertise of gastroenterologists, aspire to improve upon advanced surgical procedures that typically are performed by colorectal surgeons.

This alliance of physicians and surgeons desires to combine their respective skills and expertise to create a new minimally invasive surgical approach performed by teams of surgeons and gastroenterologists, or perhaps by a new hybrid specialty with the skills and expertise of both. [7][8] But, like with many medical paradigm shifts, this potential revolution might also require a corresponding technological revolution, and new controlled cutting tools may be needed in order to realize the doctors and surgeons’ dreams of a surgical procedure free of abdominal incisions.

Before we delve into the details and rationale for NOTES and other advanced endoscopic surgical approaches as argued by the thought leaders in the medical community, and why some at the forefront of the field have publicly called for the development of new technology, in the next few sections of this chapter we'll take a step back and review briefly the history of surgery, get acquainted with the technologies used for rigid and flexible endoscopy, and revisit the anatomy of the human gastrointestinal system. Historical developments might help us to predict trends for the future, and general familiarity with anatomy, and the tools and procedures doctors currently use will serve as useful background for discussing hypothetical and experimental future techniques.

1.3. A history of intervention

1.3.1. Surgery through the ages

There is no reason to doubt that whenever it was physiologically and technologically possible to do so, human beings throughout written history have endeavoured to repair injuries and heal maladies in fellow human beings through the practice of surgery. Across continents in every civilization and culture, people who have demonstrated an aptitude to heal have taken it upon themselves to care for the injured and for the sick.

Through the efforts of professional healers constantly refining their medical practice, and through the innovation of the scientists and engineers who support them, clinical outcomes have improved dramatically alongside the increase in our knowledge of medicine, and great leaps forward often have corresponded with the introduction of a new technology.

Harold Ellis compiled a fantastic and intriguing review of the development of surgery through history in his book “A History of Surgery,” (which incidentally is a wonderful read outside of any research context) and much of the following is summarized from his text.

Although there probably is evidence of prehistoric attempts at surgery, the earliest written record, according to Ellis, dates back some 6000 years to Mesopotamia and to ancient Egypt. [9]

In Mesopotamia, one translated section of the Code of King Hammurabi described the legal consequences for an unsuccessful clinical procedure:

If a doctor has treated a man for a severe wound with a bronze instrument and the man dies and if he has opened the spot in the man's eye with the instrument of bronze but destroys the man's eye, his hands are to be cut off. [9]

It is fascinating, perhaps, that the only known written record of surgery in Mesopotamia existed within the text of a code of law, and is about the legal consequences of an unsuccessful procedure.

In ancient Egypt, tomb drawings in a Sakkara cemetery in Memphis Egypt depicted men undergoing circumcision by means of some sort of bladed cutting instrument circa 2400-3000 BC (see Figure 1-3). [9] In ancient China, surgeon Hua Tuo (? AD 190-265), is depicted performing a surgical procedure (probably draining an abscess) on the warlord Kuan Yun; [9] and in ancient India, the renowned Indian surgeon and author Susruta compiled many surgical texts documenting numerous medical procedures, including the reconstruction of an amputated nose as well as an early cataract surgery (see Figure 1-4). [9]

Copyrighted material

Figure 1-3. An Egyptian circumcision scene, drawn from a tomb carving in Sakkara cemetery at Memphis, Egypt, c. 2400-3000 BC. (Reproduced from Ellis. [9])

Figure 1-4. Chinese surgeon Hua Tuo performs a surgical procedure on the war lord general Kuan Yun as he plays a board game (left), and a 19th century drawing of a woman having a cataract procedure done as described by Indian surgeon Susruta (right). (Reproduced from Ellis. [9])

The ancient Greeks also made significant contributions to medicine. Hippocrates (? 460-437 BC), who often is referred to as the “Father of Medicine,” probably is one of the most recognizable names in medicine. Although the specifics of what Hippocrates and his fellow Greeks thought to be the causes of diseases – imbalances in the body of the four humours or fluids: black bile, yellow bile, blood and phlegm – we know to be untrue, their greatest contribution to medicine perhaps was their rational, observation-based approach to explaining phenomena in medicine and science. [9]

The ancient Romans, who were strongly influenced by the Greeks, also made significant contributions to medical knowledge. Probably the most famous Roman physician was Galen (? AD 131-201), who is well known for the vast numbers of texts on anatomy, physiology and pathology that he authored based on his dissections and experiments on animals (human dissections were not allowed). [9]

His texts subsequently would become the basis of some great arguments by European doctors later in history, many of whom took as sacrosanct his work on animal physiology and inappropriately applied it to human medicine – a warning from history about the dangers involved with extrapolating results from animal models to humans.

However, what we consider to be modern medicine really did not come into being until after the introduction of three key discoveries — antiseptic techniques, anaesthesia, and antibiotics.

1.3.2. Preventing bacterial infection

Perhaps the greatest single discovery in medical history, Joseph Lister (1827-1912) proposed the link between micro-organisms, which Louis Pasteur (1822-1895) demonstrated were responsible for the decay and decomposition of organic materials, and the infection of open wounds. [9]

Quite unorthodox at the time, Lister expanded upon this idea and proposed killing these micro-organisms by applying carbolic acid to wounds, thus disinfecting them and allowing the wounds to heal with a much reduced bacterial load. In 1865, he completed his first successful surgical case using antiseptic techniques on an 11 year-old Glaswegian boy with a compound leg fracture. [9]

Antiseptic technique later would be augmented by our modern concept of maintaining an aseptic, or germ free surgical environment through meticulously maintaining sterile fields and disinfecting everything from instruments to surgical theatres to the surgeons themselves.

1.3.3. Dulling the pain

The earliest attempts at anaesthesia typically involved the ingestion of large amounts of alcohol, opiates or herbals before surgery to dull the pain. But it was William Thomas Green Morton (1819-1868) who introduced and popularized the use of inhaled diethyl ether as an effective form of anaesthesia, earning him popular recognition as the father of modern anaesthetics. [9]

The first public demonstration of anaesthesia was performed by Morton in 1846 in Boston, Massachusetts (United States) on a 20 year-old male with a benign vascular tumour of the neck. John Collins Warren (1778-1856), the surgeon who operated on the anesthetised boy to remove the tumour, is said to have turned to the audience after the successful surgical procedure to say, "Gentlemen, this is no humbug." [9]

1.3.4. Medicine to treat infections

The third cornerstone of modern medicine, antibiotics, was discovered by Alexander Fleming (1881-1955), a Scottish biologist and pharmacologist. The famous story of his accidental discovery of penicillin due to his messy laboratory technique is well known in scientific and medical circles. Of course, this initial discovery was only the first in a chain of discoveries that has led us to our use of modern antibiotics like amoxicillin (the drug of choice in the beta-lactam class of antibiotics) and ciprofloxacin (which became a part of popular culture in the

United States after the anthrax attacks in 2001), and biocides like triclosan (an antibiotic and antifungal that is found in numerous consumer products).

However, some scientists are concerned that the overuse of antibiotics has forced the evolution of antibiotic resistant strains of bacteria like multiple-resistant *Staphylococcus aureus* (MRSA) and *Clostridium difficile* (C. diff). Still, new drugs are being researched in this arms war between the scientists and corporations that develop them and the micro-organisms that evolve to survive and resist these drugs.

1.3.5. Cutting tissue with electricity

While the history and details of the access and viewing instruments used in rigid and flexible endoscopy will be reserved for the next section, one final historic development that is important to this thesis will be reviewed.

This development is the invention of the Bovie electrosurgical knife by physicist William T. Bovie (1882-1958) and neurosurgeon Harvey Cushing (1869-1939).

Bovie, with the financial assistance of the Liebel-Flarsheim Company of Cincinnati (United States), built a surgical device based on the flow of electric currents into the tissue that was capable of both cutting and coagulating tissue, and Cushing demonstrated the use of the device clinically for the first time in a procedure he performed in 1926. [10]

Up until this time, tissue incisions had been made primarily with bladed instruments, although a number of scientists and engineers had been experimenting with the use of electricity and other physical phenomena to cut and coagulate tissue. [10] The introduction and popularization of the Bovie electrosurgical knife, directly or indirectly, led to a chain of other tissue cutting inventions through the years, including other electrosurgical devices, powered mechanical cutters, ultrasonics (which cut with vibrations) and lasers (which cut with focused light) that would come to augment, and in some medical specialties replace the simple scalpel.

It is appropriate to stress at this juncture the importance of the dual capability of the Bovie electrosurgical knife to both cut and coagulate simultaneously. Surgical dissection of tissue can and often does result in bleeding from unintended transection of blood vessels and capillaries, and the ability to control bleeding through the application of timely haemostasis often can mean life or death for the patient. The ability to perform both tasks either simultaneously or

without a significant time delay will be very relevant to surgical procedures performed at flexible endoscopy.

Attention will be paid later to the armamentarium of existing cutting tools and their advantages and disadvantages as applicable to NOTES, and to advanced intraluminal procedures like endoscopic submucosal dissection (ESD). In response, “deconstructing dissection” will be proposed to deal with the tissue cutting challenges when performed through a flexible endoscope.

One final note about Bovie – although the electrosurgical knife would become quite popular and the word “Bovie” would become almost synonymous with electrosurgical instruments, Bovie himself did not profit from his invention. He apparently had sold his patents to the company that had financed its development for one US dollar, and it is said that he died a poor man. [10]

1.4. To peer within – the development of endoscopy

1.4.1. Rigid endoscopy

Human curiosity and the desire to explore the unknown, the unreachable and the unfathomable probably have been responsible for the majority of our advances in knowledge throughout history. This probably also drove our deep desire to peer inside the human body with viewing devices of our own invention, through naturally existing orifices, or through surgical incisions or “-otomies.”

Early viewing instruments were very basic – nothing like the modern flexible video-endoscopes we have today. According to Milne, the earliest written reference to an instrument for viewing inside the body was made by Hippocrates in ancient Greece, referring to a rectal speculum in his treatise on fistulae. [11] The Roman physician Galen also wrote about the similarities and differences between anal and vaginal specula in his *Lexicon*. [11] Of course, as people probed deeper and further into the human body, more sophisticated and complex instruments would have to be invented.

The history of endoscopy is nicely reviewed in two articles – in Edmonson’s “History of the instruments for gastrointestinal endoscopy” and in Berci and Forde’s “History of endoscopy.” Much of the following is summarized from these two articles.

Most agree that the era of endoscopy did not begin until the invention by Philipp Bozzini (1773 – 1809) in 1805 of the first “true” endoscope, which he called the lichtleiter, or “light conductor” (see Figure 1-5). [12] This early contraption combined various tubular specula for accessing different anatomy, with a candle housed inside a vase-shaped body to provide illumination. However, design flaws and perhaps professional rivalries with his contemporaries led to the instrument’s failure in practical use. Unfortunately, Bozzini died in 1809 of typhoid without ever being able to realize the success of his invention.

Copyrighted material

Figure 1-5. Bozzini’s lichtleiter, or “light conductor” – the first endoscope. (Reproduced from Edmonson. [12])

The next devices to be introduced were incremental improvements to Bozzini’s design that came from contemporaries Pierre Salomon Segalas (1792 – 1875) in Paris (France) and John D. Fischer (1797 – 1850) in America. Segalas used his device, the “speculum urethra-cystique” to view and crush stones in the bladder. [12] Fischer employed his instrument in gynaecology, in order to examine a woman of great modesty – “so great were her feelings of delicacy that I could not prevail upon her to suffer me to make an examination with a common speculum”. [13] Fischer’s greatest improvement to the Bozzini design was to include a lens to focus and enlarge the viewed image. [12]

Although groundbreaking at the time, Bozzini, Segalas and Fischer’s inventions did not attain popular clinical use. It was not until the introduction of an improved endoscope by Antonin

Jean Desormeaux (1815-1881) along with his medical text *De l'endoscopie* that marked the beginning of popular endoscopy. [12] His instrument, primarily used in women to examine the urinary bladder, improved upon Segalas' design by using a condenser lens to concentrate the light provided by an alcohol and turpentine burning lamp (see Figure 1-6). [14]

Copyrighted material

Figure 1-6. Desormeaux's endoscope. (Reproduced from Berci and Ford. [14])

It is generally agreed that 1868 marked the coming of age of rigid endoscopy when Adolf Kussmaul successfully performed gastroscopy, or examination of the stomach, with a rigid device inserted down the throat of a cooperative sword swallower (see Figure 1-7). [15] Although this clinical achievement proved that endoscopy to view internal cavities and structures such as the stomach that were deep within the body was technically feasible, albeit only with the cooperation of a highly motivated and anatomically accommodating patient, it was far from practical for normal clinical use on a typical patient.

Figure 1-7. Kussmaul's gastroscope (a) and its introduction into the throat of a sword swallower (b).
(Reproduced from Edmonson. [12])

Furthermore, Kussmaul's early gastroscope suffered from dim illumination because light had to be transported from the exterior of the body through the long length of the device into the stomach. This problem was solved by Josef Leiter (1830-1892) and Maximilian Nitze (1848-1906) in 1877, originally collaborators who turned into bitter rivals after the success of their cystoscope enticed them each to claim personal credit for the device. [12]

Their design solution was to place the illumination source at the distal tip, or far end of the device, which is inserted into the stomach. Their first embodiment used an electrified platinum wire in a glass jacket cooled by water. After the invention by Edison of the carbon filament bulb in 1879, Nitze refitted the cystoscope with a miniature Edison bulb. [14]

Leiter would find a new partner in surgeon Johann von Mikulicz (1850-1905), with whom he would introduce in 1881 both an oesophagoscope and a gastroscope. Although their gastroscope was not a success, the oesophagoscope, which also used an Edison's incandescent lamp in the model introduced in 1886, was the first truly usable endoscope to explore the oesophagus (see Figure 1-8). [12]

Figure 1-8. The Nitze optical system (left), and intubation of a patient in a deep head-down (Trendelenberg) position (right). (Reproduced from Berci and Ford. [14])

One can see that already these early endoscopes bear a remarkable resemblance to the modern rigid endoscopes used in laparoscopy today. Further improvements in optics (the use of a series of lenses along the length of the device as in a telescope, and the subsequent use of gradient index lenses), advances in miniaturized video technology, enhancements in illumination with brighter and cooler light sources, and innovation in therapeutic access with the introduction of a working channel all were important advances that led to the emergence of the modern rigid endoscope.

1.4.2. Semi-flexible and flexible endoscopy

The development of semi-rigid and eventually fully flexible endoscopes from the original rigid devices most likely came about in part as a response by physicians and instrument makers to make the endoscope a more practical and less risky instrument for insertion into flexible, fleshy and fragile structures like the oesophagus and the colon.

So much of the innovation in the development of semi-flexible scopes came from the German-American gastroenterologist Rudolf Schindler that the era between 1932 and 1957 is referred to as the Schindler era. Schindler's development of the semi-flexible gastroscope in 1932 with instrument maker Georg Wolf (1873 – 1938), along with his proselytizing of the "gospel of gastroscopy" – mainly in America after he escaped detention in Nazi Germany and emigrated to the United States – transformed endoscopy from a novel, but risk-prone and seldom performed procedure into a routine and essential part of gastroenterology. [12]

Two notable developments that occurred during the Schindler era were (1) the introduction of the biopsy gastroscope by Edward B. Benedict in 1948, which allowed physicians not only to see diseased tissues but also to retrieve a sample for later histopathology, and (2) the improvement of endoscopic photography to a clinically useable state by Harry L. Segal and James S. Watson, who received great technical assistance and cooperation from the Carl Zeiss Company, the Eastman Kodak Company, and the Bausch & Lomb Optical Company. [12]

However, the most crucial developments in fully flexible endoscopes came about after the incorporation of fibre optic technology into endoscopy. Bundles of fibres could be used to transmit light around bends in the instruments, providing bright illumination while keeping the sometimes bulky and usually extremely hot illumination bulbs away from the business end of the scopes.

Transmitting images required fibre bundles that were spatially organized, or coherent. Although the resolution of the viewed images was limited inherently by the spatial density of the coherent fibre bundles, the use of fibre optics resulted in a truly flexible device that could transmit images from the inserted, distal end to the doctors' eye at the proximal end, replacing the segmented, semi-flexible devices with their complicated arrays of convex and rod lenses.

The first practical prototype of a fiberscope was introduced by Basil Hirschowitz in 1957 at a meeting of the American Gastroscopic Society. [12] Hirschowitz, who then worked with American Cystoscopic Makers Inc. (ACMI) on commercializing of a more advanced version of his gastroscope, received his first working production sample in 1960.

The device was marketed as ACMI's Hirschowitz FO-4990 flexible gastroduodenoscope. However, ironically, the most frequent complaint was that the device was too flexible. Robert Kemp commented in Lancet in 1962 that "excessive flexibility means that one cannot control the position of the fiberscope head or push it directly forward ... pressure from above is as likely to increase the length of the bend as to advance the tip." This led ACMI and other companies to incorporate an articulatable tip that could be manoeuvred to help with seeing the pathology and travelling to specific anatomical landmarks.

Interestingly enough, although instrument flexibility is required to navigate tortuous enclosed structures, issues of too much flexibility and formation of loops in the endoscope are still problems today in colonoscopy. These issues may continue to play an important role in

shaping how intraluminal and transluminal surgeries are performed as physicians and engineers devise innovative ways to obtain instrument stiffness and flexibility on-demand.

Fibre optic scopes really came of age in the late 1960s and early 1970s when American companies (mainly ACMI) and Japanese corporations Olympus and Machida released products that continuously leapfrogged each other, incorporating such features and improvements to their endoscopes as altering the angle of vision, incorporating a suction channel, and fitting a mechanism for cleaning the lens with air or water. [12]

The final technological addition that completes the modern flexible endoscope is the incorporation of a miniaturized video charged coupled device (CCD) into the distal end of the instrument, replacing the coherent optic fibre bundle and the eyepiece with electrical wires. Flexible endoscopists finally were freed from having to stoop down over the eyepiece in the vicinity of the splash and contamination zone near the instrument channel opening, and instead were able to stand upright in front of a monitor screen with improved ergonomics and sanitation. [16][17]

1.5. The anatomy of the modern endoscope

1.5.1. The modern rigid laparoscope

The modern rigid laparoscope bears a remarkable resemblance to the rigid endoscopes of the past, retaining their overall shape and functions, although modern materials, optics and construction methods have made them smaller. A number of rigid scopes from Karl Storz Endoskope, a leading manufacturer of rigid endoscopes and surgical devices for laparoscopic surgery, are shown in Figure 1-9. They can be attached to a removable video camera for viewing of the operative field on a television monitor.

Figure 1-9. A selection of Karl Storz rigid endoscopes (and one flexible endoscope).
(Reproduced from the Surgical Optics website.)

The typical initial steps of a laparoscopic surgical procedure are described by Kaban et al. [18] The first step is to create a working space in the abdominal cavity and establish pneumoperitoneum, typically by blind insertion of a Veress needle – invented by János Veres, it is a sharp, hollow needle with a spring-loaded inner obturator that slides forwards once the tip has penetrated the abdominal wall to protect the underlying viscera [19] – into the abdomen and gas insufflation through the needle with carbon dioxide gas to lift the abdominal wall and create a working space.

Once pneumoperitoneum has been achieved, a number of openings through the abdominal wall – the position and number of “ports” necessary determined by the type of procedure being performed – are made typically with a trocar-cannula system. This system consists of a tissue cutting trocar, which may have pyramidal or conical blades or may function by blunt dissection, which is inserted into a pneumoperitoneum-preserving cannula that has flaps or gaskets to allow for instrument exchange while minimizing gas leakage. The trocar and cannula are inserted through the abdominal wall together, and the trocar is removed leaving the cannula in the abdominal wall once correct placement has been verified (see Figure 1-10).

After the correct number of cannulae has been placed and the endoscope and laparoscopic instruments inserted through the cannulae, the laparoscopic procedure can begin in earnest.

Figure 1-10. A laparoscopic surgery performed with a rigid endoscope and a laparoscopic instrument inserted through two cannula. (Reproduced from Laparoscopic Surgery Complications website. [20])

1.5.2. The modern flexible endoscope

Modern flexible endoscopes are truly marvellous little packages of technology, as they pack within the slender confines of their sleek profiles not only conduits for illumination light, electronic video signals, lens cleaning water and lumen insufflating air, clot and debris busting waterjets, articulation wires and therapeutic instruments, but also decades of miniaturization and manufacturing know-how to produce robust, reliable and reusable instruments (see Figure 1-11).

The majority of the modern flexible endoscopes in use in gastrointestinal clinics around the world are manufactured by the Japanese conglomerates Olympus, Pentax and Fujinon. Scopes made by Karl Storz of Germany and other manufacturers also can be found in clinical use, although the market share enjoyed by these companies is much smaller than that of the big three.

Regardless of the make and model, all video-endoscopes share some key features. The video-endoscope system generally consists of a detachable, reusable and cleanable endoscope

portion that is inserted into the patient, and an instrument “tower” that consists of a video screen, light source and video processor, in either separate or combined boxes.

The endoscope portion typically has a handle-shaped control portion with two coaxial angulation knobs to control the deflection of the distal tip, two valves to control vacuum suction, lens cleaning and air insufflation, one or more accessory channels for passing endoscopic accessories and remote switches to capture images and perform other tasks (see Figure 1-11).

Although there are minor performance, ergonomic and industrial design differences between different makes and models, the generally shared user interface allows trained endoscopists to be proficient operators of all endoscopes of a particular class.

Endoscopes typically are classified based on the anatomy to be targeted. Gastroscopes typically are shorter and more slender than other types, typically long enough to allow for examination of the upper gastrointestinal tract – the oesophagus, the stomach, and the duodenum. Colonoscopes typically are longer and thicker and are used to examine the lower GI tract – the anus, sigmoid colon, left descending colon, transverse colon, the right ascending colon and the caecum. Newer Olympus models also feature a variable-stiffness control to decrease the probability of the scope “looping” on itself once the scope has been intubated past the more tortuous sigmoid colon.

Paediatric variants of gastroscopes and colonoscopes are thinner to allow for easier intubation of children and patients of smaller stature. Therapeutic variants typically are larger in diameter to accommodate a second accessory channel so that two endoscopic instruments can be used in tandem.

Specialty endoscopes include side-viewing duodenoscopes and ultrasound-capable echoendoscopes for ERCP, fine needle aspiration (FNA) and other advanced endoscopic procedures (briefly reviewed later in this chapter), and enteroscopes (with or without double balloons) for examining the small bowel from the duodenum to the caecum. These classes of scopes also feature specialized controls to control elevators for articulating accessories and to control the endoscopic ultrasound.

Copyrighted material

Copyrighted material

Figure 1-11. Schematics of a modern flexible endoscope. (Reproduced from Ginsberg, et. al. [17])
A. Endoscope controls and serviceable parts. B. Schematic of light, air and water conduits from the control unit to the scope tip. C. Breakaway view of all the conduits that are contained inside the scope shaft. D. Cross-section view of the distal end, including the objective lenses and the CCD that make up the video camera.

1.5.3. Future endoscopes

Nature abhors a vacuum, and free markets abhor commercial vacuums absolutely. Where there is an unmet commercial need, companies rush in with their solutions for how to meet the demand. In recent years, large corporations, small start-ups and individual inventors have answered the call for new technology by testing and commercializing a number of new endoscopes that may provide endoscopists with the tools needed to perform a new generation of therapeutic procedures. Revis and Melvin reviewed in 2008 the current state of technology in flexible endoscopy, some of which is summarized here. [21]

Important developments in diagnostic imaging such as high definition and high magnification video, multi-colour and narrow band imaging, and new features that may improve scope capabilities and ergonomics have been adopted by major scope manufacturers in their state-of-the-art endoscopes.

For example, Olympus has upgraded their flexible endoscopes with new advanced features such as high definition video for “clearer observation of fine capillaries and intricate mucosal structures,” close focus for “detailed observation without electronic magnification,” narrow band imaging for “enhanced observation of the mucosa,” a 170 degree field of view wide angle optics, larger 3.7 mm diameter accessory channels, an auxiliary water jet to remove colonic mucus and debris, variable stiffness capability “for adjustment of insertion tube flexibility,” a smaller diameter insertion tube and “wide-ranging 4-way angulation,” according to marketing material for the top model Olympus CF-H180AL/I colonoscope. [22]

A more revolutionary device is the Olympus R-Scope advanced gastroscope for performing endoscopic submucosal dissection (ESD), which is popular in Japan (see Figure 1-12). [21] Designed with the procedural challenges of ESD in mind, the endoscope features a dual-bending distal section that is capable of entering into an S-shaped articulated position, and two independently articulatable accessory channels to allow two devices – typically a grasper and an electrosurgical cutter – to be converged and diverged as desired by the endoscopist.

Figure 1-12. The Olympus R-Scope gastroscope for endoscopic mucosal dissection. (a) Additional controls on the handle to manage new degrees-of-freedom. (b) Dual-bending articulating segments allows for an S-shaped bend. (c) Dual accessory channels each with elevator / accessory articulators to allow independent motion control of two endoscopic devices, typically a tissue grasper and electrosurgical cutter. (Reproduced from Reavis and Melvin. [21])

New small calibre scopes are being used for easier and direct visualization of difficult anatomy. The Olympus EndoEye flexible video transnasal esophagoscope PEF-V is a new 5.3 mm diameter CCD-based videoendoscope that allows for transnasal visualization of the upper GI tract (see Figure 1-13). [23] Because of its small calibre size, the scope can be used without patient sedation, potentially reducing procedure time and cost and increasing patient comfort.

The SpyGlass direct visualization system from Boston Scientific (see Figure 1-14), consists of a 0.77 mm diameter fibre optic probe for direct visualization of the common bile duct, and a 10 Fr (3.3 mm diameter), four channel delivery catheter with a channel for the visualization probe, an accessory channel and two smaller, independent irrigation channels. According to the product website, the system allows “the physician the ability to directly see the site of interest, whether it be a stricture, stones or areas of concerns, vs. the traditional non-direct visualization techniques such as x-ray.” [24]

It is not too hard to imagine either the EndoEye or the SpyGlass used in conjunction with a primary scope or a blind access device to assist in visualizing the surgical field in a yet to be determined advanced intraluminal or transluminal procedure. As new tools are developed or re-tasked for new indications, the scope of what's possible is limited only by the physician's imagination.

Copyrighted material

Figure 1-13. A small calibre transnasal esophagoscope can be used for sedation-less examination of the upper GI tract. (Reproduced from Reavis and Melvin. [21])

Copyrighted material

Figure 1-14. The SpyGlass direct visualization fibre optic probe for direct visualization in ERCP. The delivery catheter is passed through the working channel of a duodenoscope (left) and cannulated into the common bile duct. The fibre optic probe (right) then is passed through the delivery catheter tip (centre). (Reproduced from Reavis and Melvin. [21])

Some modern-day devices for flexible endoscopy can change their flexibility on demand. While the Olympus variable-stiffness colonoscopes can vary their stiffness, the TransPort endosurgical operating platform introduced by USGI Medical Inc. takes this to a new level by using its ShapeLock technology to freeze the shape of the flexible, multi-lumen catheter at will (see Figure 1-15). [25] The USGI Cobra, an experimental therapeutic scope based on the ShapeLock technology that features three independently articulatable cannulae for camera

probes and therapeutic accessories, has been sighted in experimental procedure development arenas for its potential use in transluminal surgery (see Figure 1-16). [26][27]

Copyrighted material

Figure 1-15. The Transport endosurgical operating platform featuring ShapeLock technology from USGI.
(Reproduced from Reavis and Melvin. [21])

Copyrighted material

Figure 1-16. The USGI Cobra experimental endoscope, which uses ShapeLock technology to freeze the scope shape on demand, features one visualization and two accessory cannulae that can be articulated independently.
(Reproduced from Richards et. al. [27])

When discussing future technology, the topic of robotics invariably comes up. Today's best in robotics-assisted technology probably is best represented by the da Vinci surgical system by Intuitive Surgical, which allows a surgeon to control the stereoscopic camera and multiple laparoscopic instruments simultaneously from the surgeon's control console (see Figure 1-17). According to the product website, the system can scale and filter hand motions in controlling the robotic EndoWrist instruments to provide "an intuitive interface with breakthrough surgical capabilities" [28] – one has far more dexterity and capability available with the robotic system than with standard laparoscopic instruments. One surgeon has even managed to fold miniature origami paper cranes with da Vinci (see Figure 1-18)! [29]

Copyrighted material

Figure 1-17. The da Vinci surgical system. (Reproduced from Intuitive Surgical website. [28])

Copyrighted material

Figure 1-18. The da Vinci surgical robot is dexterous enough to fold a miniature origami paper crane.
(Reproduced from Ishikawa et. al. [29])

The da Vinci system also is quite intuitive and easy to learn, as this author, with no surgical training and only about fifteen minutes of practice time on the system, was able to successfully tie surgical knots in suture on a practice trainer. The overall impression left with this author after the time spent with the machine was one of awe and wonderment and hope for the future of technology in medicine. However, probably the biggest drawback to the system is the high cost, which in 2004 was about 1.4 million US dollars per da Vinci system. [30] Many institutions find it hard to justify the high cost of the system.

Currently, there are no robotics systems for flexible endoscopy that are approved for clinical use for gastroenterology; however, there are both published and unpublished reports of an experimental endoscopic system called the ViaCath by EndoVia Medical, now Hansen Medical.

This system consists of computer controlled flexible instruments that are passed through cannulae attached alongside a flexible endoscope; the physician can control the instruments from an operator's console, similar to the da Vinci system. Rothstein reported in 2004 a successful endoscopic mucosal resection procedure performed in an *ex vivo* porcine stomach using the system. [31]

Other robots that have been described in the literature include two experimental devices designed by Rentschler and Oleynikov in 2007 (see Figure 1-19). [32][33] These miniature robots were designed to be placed within the peritoneal cavity and can move about by various ingenious means.

Copyrighted material

Figure 1-19. Two experimental *in vivo* endoscopes. (Reproduced from Rentschler and Oleynikov. [32])

In the commercial realm, the most well-known “autonomous” *in vivo* endoscope is PillCam from Given Imaging. It is a passive device that follows the natural peristaltic motion of the gastrointestinal tract (it has no locomotion capability of its own) to navigate and visualize the interior of the oesophagus, the small bowel and soon, the large intestine (the device to view the latter anatomy is not commercially available yet as of 2008). [34]

These imaging devices could be combined with a locomotion scheme like electro-stimulation as described by Mosse [35] and Mosse et al. [36] (see Figure 1-20) or magnetic guidance as proposed by Olympus Corporation for their Olympus Guidance System (see Figure 1-21), [37] and then coupled with onboard therapeutic tools. With such devices, one could imagine futuristic surgical procedures in which the surgeon could use *in vivo* robots to take a “Fantastic Voyage” into the body to repair anatomical defects and cure diseases, reminiscent of the 1966 science fiction film written by Harry Kleiner.

Future devices currently being developed and others yet to be imagined set the background for future procedure development in advanced intraluminal and transluminal surgeries. And dreams of future procedures likewise call for new devices to be dreamed up and physically realized.

Copyrighted material

Figure 1-20. A schematic of the electro-stimulation concept – using pulses of electricity to induce the muscles in the gut to peristaltically move a device within its lumen. (Reproduced from Mosse et al. [36])

Copyrighted material

Figure 1-21. The Olympus Guidance System. The concept employs magnets to move and rotate a capsule endoscope within the lumen of the gastrointestinal tract. (Reproduced from Menciassi, Quirini and Dario. [37])

1.6. The anatomy of human gastrointestinal tract

The gastrointestinal tract is part of the digestive system, which is responsible for taking in ingested food, converting it into a usable form of energy for the body, and disposing of solid wastes. Topologically part of the exterior of the body, the alimentary tract is a long, hollow, mostly tubular structure that enlarges at portions into sacs that allows for temporary retention of solid materials, e.g. the stomach which holds partially digested food and the rectum which consolidates solid wastes before it is expelled from out the anus. Clear illustrations of the

anatomy of the digestive system are reproduced below from Netter's excellent Atlas of Human Anatomy. [38]

Solid material enter the GI tract at the mouth and then passes down the oesophagus (see Figure 1-22), through the gastro-oesophageal junction into the stomach (see Figure 1-23), through the pylorus into the small intestine – the duodenum (see Figure 1-24), the jejunum (see Figure 1-25), and the ileum (see Figure 1-26) – through the ilial-cecal valve into the large intestine – the caecum, ascending colon, transverse colon, descending colon, sigmoid colon and the rectum – and out the anus (see Figure 1-27).

Although the biology, morphology and function vary between organs of the gastrointestinal tract, the general structure of the tissues is consistent.

The tissues of the GI tract normally consist of three layers, which are, in order from the inner lumen towards the outside surfaces, (1) the mucus-producing mucosa layer which also contains a thin muscle layer called the *muscularis mucosae*, (2) the matrix of connective tissue called the submucosa that contains glands and vasculature, and (3) the *muscularis propria*, or muscle layer, which contains a layer of circular muscles with fibres that run along the circumference of the structure, surrounded by a layer of longitudinal muscles with fibres that run in the direction along the length of the structure (see Figure 1-28).

Approximate thicknesses of each layer are provided in Table 1-1 to get a sense of the general scale of the anatomy, although actual anatomy can vary quite a bit depending on the pathology and measurement technique.

The organs are covered by and separated from other tissues by a layer of connective tissue called the serosa.

Table 1-1 – Representative thicknesses of GI tissues from individual studies in the literature. Figures do not capture the large biological variance within the population.

Alimentary Tract Layer (measurement method)	Thickness
Oesophagus (endoscopic ultrasound) mucosa (histology) submucosa (histology)	2.4±0.6(SD) mm [39]
	0.581±0.0163(SD) mm [40]
	0.432±0.0243(SD) mm [40]
Stomach (abdominal ultrasound)	5.107±1.100(SD) mm [41]
Jejunum (abdominal ultrasound)	3 mm [42]
Colon (histology) mucosa (histology) submucosa (histology)	1.080±0.239(SD) mm [43]
	0.499±0.104(SD) mm [43]
	0.519±0.234(SD) mm [43]

As can be seen from the illustrations of the anatomy, the GI tract passes by and potentially allows access to virtually every organ and structure in the body – access to organs in the thoracic cavity via a trans-oesophageal approach, and to organs in the peritoneal cavity through a transgastric, transcolonic or transanal approach.

Copyrighted material

Figure 1-22. The oesophagus.

Nearby anatomy accessible by a trans-oesophageal approach include the oesophagus, thyroid gland, thoracic cavity, trachea, lungs, aorta, heart, and the cervical and thoracic spinal column. (Reproduced from Netter. [38])

Copyrighted material

Figure 1-23. The stomach.

Nearby anatomy accessible by a transgastric approach include the peritoneal cavity, stomach, liver, gallbladder, spleen, small intestine, large intestine, kidneys, ureters, bladder, uterus, ovaries, fallopian tubes, and the lumbar spinal column. (Reproduced from Netter. [38])

Copyrighted material

Figure 1-24. The duodenum (the proximal part of the small intestine) which is connected to the stomach.
(Reproduced from Netter. [38])

Copyrighted material

Figure 1-25. The small intestine (duodenum, jejunum and ileum). (Reproduced from Netter. [38])

Copyrighted material

Figure 1-26. The connection between the ileum (the distal part of the small intestine) and the caecum (the proximal part of the large intestine). (Reproduced from Netter. [38])

Copyrighted material

Figure 1-27. The large intestine

(ascending colon, transverse colon, descending colon, sigmoid colon and the rectum).

Nearby anatomy accessible by a transcolonic or a transanal approach include the peritoneal cavity, stomach, liver, gallbladder, spleen, small intestine, large intestine, kidneys, ureters, bladder, prostate, uterus, ovaries, fallopian tubes, and the lumbar and sacral spinal column. (Reproduced from Netter. [38])

Copyrighted material

Figure 1-28. A cross-sectional view of the layers composing the tissues in the gastrointestinal tract.
(Reproduced from Netter. [38])

1.7. Minimizing the invasiveness of surgery with rigid endoscopy

1.7.1. From open surgery to “keyhole” surgery

Upon initiation into their professions, physicians and surgeons swear to uphold the ethical standards of the Hippocratic Oath, including the famous prohibition which Michael North of the National Library of Medicine in the United States translated in 2002 as “I will do no harm or injustice to them [the patients]”. [44]

However, oftentimes some harm must be done to the body in order to reach the diseased or malfunctioning anatomy and correct the condition. Chests must be split and hearts must be stopped in order to restore blood circulation to dying cardiac muscle after a heart attack. The abdomen must be opened and the inflamed appendix or gallbladder removed in order to save the patient from infection, blood poisoning (sepsis) and likely death if left untreated. Pre-cancerous tissues and deadly cancers must be cut out with a reassuring amount of adjoining healthy tissue to be confident that the no traces of the cancer remain to spread and consume the patient alive.

Doing some harm to the patient is tolerated if the benefits in doing so outweigh the explicit harm done. Still, physicians and surgeons continue to explore and develop new ways to minimize access and collateral damage done while performing their treatments on the patients. The popular and successful migration from open to laparoscopy as the standard of care for many types of surgical procedures was motivated by this desire to “do less harm,” and this, in part, also motivates current trends towards surgery at flexible endoscopy.

Furthermore, many laparoscopic procedures are associated with a significant overall financial saving to healthcare systems when compared with open surgery despite typically higher equipment costs because the less invasive procedures result in much shorter hospital-based convalescence for the patients. Some procedures like cholecystectomy can be performed on an ambulatory or outpatient basis, negating costly overnight or longer hospital stays required for convalescence from traditional open surgery.

In the adoption of new techniques and new products, one must maintain a careful balance between the enthusiasm to promote the idea, and the steady and measured approach necessary to prove efficacy, ensure patient safety and educate doctors on benefits and correct

use of the product. The goals of clinical efficacy and patient safety must remain paramount throughout the concept and product development cycle, and ultimately be supported by data.

At the same time, it also is important to understand that results from early controlled studies necessarily reflect only the state of a specific embodiment at a particular point in time rather than evaluate the overall idea or concept itself. Early results do not convey the potential improvement and benefits that could come with further development and training.

A brief timeline of the development of minimally invasive laparoscopic surgery with important milestones follows in Table 1, as compiled from Birkett's review article.

Table 1-2. A brief timeline of the development of laparoscopy, compiled from Birkett's review article. [3]

1901	Georg Kelling inserted a cystoscope into the peritoneal cavity as part of his Lufttamponade research to control gastrointestinal bleeding.
1910	Hans Christian Jacobaeus used a cystoscope to perform the first laparoscopy and thoracoscopy in seventy-two patients. Kelling performed forty-five peritoneoscopies with a cystoscope.
1910's	Bernheim performed the first laparoscopy in the United States on two patients. Nordentoft described using gravity to retract organs for better laparoscopic visualization (Trendelenburg position).
1920	Orndoff introduced the use of pyramidal-shaped trocars to access the peritoneal cavity.
1921	Goetze introduced the first manual insufflator to provide pneumoperitoneum.
1924	Zollikofer described switching from air to carbon dioxide for insuflation.
1920's	Stone improved on trocar design by incorporating a rubber gasket to prevent gas leakage from the inflated abdomen. Kalb designed both forward-viewing and angled rigid endoscopes. Kalb describes a two-puncture laparoscopic technique.
1933	Fervers describes his experiences with using electrocautery and laparoscopy to cut adhesions.
1936	Boesch reported the first tubal ligation with electrocoagulation.
1937	Boesch used laparoscopy to diagnose an ectopic pregnancy.
1938	Veress introduced his spring-loaded safety needle that later would become one of the standard methods for initial access to the peritoneal cavity.

1952	Forestier introduces the “cold light” for illuminating the surgical field through the laparoscope with minimal heat.
1953	Hopkins introduces the rod lens system.
1960's	Kurt Semm introduces the automatic insufflator.
& 70's	
	Cuschieri and Berci advocate using laparoscopy for diagnosing liver pathology.
1983	Semm performs the first laparoscopic appendectomy (also first lap procedure on the gastrointestinal tract).
1985	Introduction of the charged-couple device (CCD) camera to laparoscopy. Erich Muhe performs the first laparoscopic cholecystectomy.
1987	Philippe More, Francois Dubois and Jacques Persist each performed laparoscopic cholecystectomies in quick succession, which catapulted therapeutic laparoscopy to general acclaim. Muhe had performed 97 laparoscopic cholecystectomies by March, 1987.
1988	Barry McKenna and William Say perform the first laparoscopic cholecystectomy in the United States.
1989	Harry Reich reported the first laparoscopic hysterectomy.
1990's	Laparoscopic cholecystectomy quickly becomes the “gold standard” for treatment of cholelithiasis, replacing more traditional open surgery as the standard of care.
1991	Berci describes laparoscopic intraoperative cholangiography. Stoker performed a choledochotomy with the placement of a T-tube. Dallemagne performed the first Nissen fundoplication for the treatment of gastic-oesophageal reflux disease.
	Katkouda and Mouiel performed a lap vagotomy for the treatment of duodenal ulcer disease. Jacobs and Sclinkert both independently perform a lap-assisted colectomy.
	Delaitre performed the first lap splenectomy. Ger reported inguinal hernia repair.
	Oenchain reported laparoscopic discectomy of the lumbar spine. Clayman et al. reported on the first laparoscopic nephrectomy for benign disease.
	Schuessler performed a laparoscopic pelvic lymphadenectomy for prostate disease staging.

1992 Brune et al. and Mouiel reported successful lap gastrojejunostomy.

Gagner reported laparoscopic adrenalectomy for Cushing syndrome and pheochromocytoma.

Kozminski and Partamian performed laparoscopically assisted ileal conduit urinary diversion.

Schuessler performed laparoscopic radical prostatectomy.

1993 Belachew and Legrand performed the first lap-band placement for bariatrics.

Clark and Wittgrove performed the first laparoscopic Roux-en-Y gastric bypass for bariatrics.

1995 Zuckerman and Zdeblick performed the first laparoscopic spinal fusion.

2001 700,000 to 800,000 laparoscopic cholecystectomies are performed annually in the United States.

2002 30,000 laparoscopic colectomies are performed annually in the United States.

1.7.2. Laparoscopy and the case for adding to surgical complexity

Performing laparoscopic surgery – viewing the operative field with a video endoscope and indirectly manipulating tissue with long instruments inserted into the body – increases the physical workload and “is significantly more stressful for the surgeon than open surgery,” according to a study by Berguer, Smith and Chung in 2000. [45]

One would expect physical manipulations such as cutting, manipulating and coagulating tissue, knot tying, sewing and stapling to be easier when one can directly touch, feel and manipulate them with one’s hands, rather than using long, instrumented “chopsticks” inserted to the patient’s body through small abdominal incisions.

However, data accumulated over the last fifteen years or so have demonstrated at least clinical equivalence, if not advantages for patients who undergo laparoscopic procedures instead of corresponding open procedures, as well as important physiological, immunological and cosmetic benefits. It is hoped that these advantages and additional ones will be transferred to surgery at flexible endoscopy.

Laparoscopic surgery often is associated with decreased pain, increased patient comfort and a faster convalescence than conventional open surgery. These outcomes often are revealed in qualitative verbal rating scales of post-procedure surveys of patients; however Stumpf *et. al.* in 2001 attempted to quantify this in an objective way by employing three-dimensional

stereoscopy to measure abdominal motility in patients during the convalescence period after laparoscopic and open surgery.

They found a significant difference in the time to the return of abdominal motility, with the laparoscopic group regaining motility approaching the levels of the healthy control group after seven days, while the open group still had significant motility deficiencies twelve days after the surgical procedure. [46]

Novitsky, Litwin and Callery reviewed in 2004 the “physiologic and immunologic alterations” that surgery may provoke “an exaggerated response [that] may result in immunosuppression and lead to significant postoperative morbidity and mortality.” [47] In other words, the systemic inflammatory response of the body to invasive surgical trauma, which is believed to be proportional to the initial injury, may, through “a complex interaction between neuroendocrine, metabolic and immune systems,” paradoxically cause immunosuppression by negative feedback loops the body employs to resolve the hyper-inflammatory state. [47]

From their review of the literature, they conclude that “in summary, most investigators have demonstrated that laparoscopic surgery better preserves peritoneal macrophage numbers and viability, improves bacterial clearance, and stimulates cytokine production in a manner similar to that of control subjects that have not undergone surgery. As a result, the laparoscopic approach appears to be advantageous to peritoneal host defences, as compared with open surgery.” [47]

Laparoscopic surgery also helps to preserve the cosmetic appearance of the patient, post-procedure by the nature of the smaller, but oftentimes more numerous incisions in laparoscopy (compared with one large incision in open surgery). However, Peetz cautioned in an editorial in 2004 that the desire for a positive clinical outcome should never be trumped by the desire for cosmesis alone:

“[Laparoscopic] cholecystectomy, appendectomy, fundoplication, adrenalectomy, and VATS are all well established as the standard of care, not just because they are more cosmetic, but also because, in most cases, we can see the operative areas better. These approaches are less invasive to the abdominal wall and thus result in fewer postoperative complications. They are safer. ... Increasing the length or depth of anaesthesia [sic] to approach an

organ from a distant site is of questionable value. Sacrificing anything, be it visibility, vessel coagulation, security of anastomotic closure, or extent of resection margins, for cosmetic purposes is of questionable value and, as always, each of us, patient and surgeon alike, must weigh the risks of surgery vs. the benefits, and we must live with our choices.” [48]

It has taken time for the laparoscopic approach to become accepted widely in the medical community. Because the lives of patients often are on the line, clinical evidence and scientific data often are required for a new technique to go from being an interesting concept to becoming the standard of care.

Still, laparoscopy is mature enough now that there are numerous comparative studies, prospective and retrospective, acute and long-term demonstrating equivalent or better outcomes between the laparoscopic and the corresponding open procedures. These studies have been conducted for but are not limited to the following (listed alphabetically):

Adrenalectomy, [49][50] appendectomy, [51][52] cholecystectomy, [53] colectomy, [54][55][56][57][58] diverticular disease treatment, [59] esophagectomy, [60] excision of submucosal tumours of the oesophagus, [61] gastrectomy, [62][63] groin hernia repair, [64] lumbar hernia repairs, [65] nephrectomy, [66] Nissen fundoplication, [67] gastric stromal tumour excision, [68] rectal cancer resection [69] [70][71] and thorascopic surgery [72].

Similar scientific and clinical proof probably will be required to justify performing surgery at flexible endoscopy, and it could be many years before the justifications for doing so are widely accepted.

This would parallel the almost two decades between when the modern laparoscopic approach was first utilized in humans in the early eighties, to the current acceptance of laparoscopic colectomy as a legitimate procedure only after publication of ten-year post-operative survival data.

Still, when one reviews that explosion of recently published research in transluminal surgery from researchers around the world, one cannot help but sense the excitement and creativity from researchers around the world, as well as the words of caution and the wait-and-see

sentiments of some trusted physicians and surgeons who had made their marks on medicine during the laparoscopic revolution.

In many ways, the eruption of new ideas and the emergence of counterpoint arguments for restraint, clinical justification and scientific data are reminiscent of the initial development and eventual acceptance of laparoscopy. And probably as it did with laparoscopy, the interplay between the voices for change and the calls for restraint will serve as a useful vetting process to filter these new ideas through the collective common sense and wisdom of the medical community.

The following are common laparoscopic procedures that are potential targets for re-envisioning as advanced intraluminal or transluminal surgery performed at flexible endoscopy.

1.7.3. Cholecystectomy – the king of laparoscopic procedures

Cholecystectomy is the surgical removal of the gallbladder, or cholecyst. Laparoscopic cholecystectomy is considered to be the “gold standard” for management of symptomatic cholelithiasis, or the presence of gallstones in the gallbladder or bile ducts, and it is by far the most common procedure performed laparoscopically.

The gallbladder stores and concentrates bile, which is used to emulsify fats and neutralize acids in partially digested food. When partially digested fatty foods enter the duodenum, the gallbladder contracts, releasing a bolus of bile that aids in their digestion.

In the diseased gallbladder, the concentrated bile crystallizes and forms stones that can accumulate in the gallbladder and block the bile duct, disrupting the functioning of the gallbladder and causing pain and infection. Untreated, the gallbladder can burst, leading to peritonitis, or infection of the abdominal cavity, sepsis (blood poisoning) and death.

After the removal of the gallbladder, the liver continues to produce bile, although this is available now only as a trickle rather than a bolus concentrated in the gallbladder, reducing the body's ability to digest fat. Ingestion of foods high in fat content after cholecystectomy can lead to diarrhoea and other digestive discomfort.

Procedurally, the surgery involves (1) dissecting tissue to clear Calot's Triangle to mobilize the cystic duct and the cystic artery, (2) clipping, suturing or stapling the duct and the artery

before transecting them, (3) dissecting the gallbladder to free it from the liver bed, and (4) removing the organ from the body (see Figure 1-29).

This laproscopic procedure appears to be high on the priority list for procedure development for transgastric, transcolonic or transvaginal surgery at flexible endoscopy, with numerous physicians reporting some successes in pre-clinical animal models, and at least one team reporting a successful transgastric cholecystectomy in human patients in India. More will be said about transluminal cholecystectomy in the section on Natural Orifice Transluminal Endoscopic Surgery or NOTES.

It perhaps is interesting that Ethicon Endo-Surgery, Inc, a leading producer of surgical equipment for laparoscopic cholecystectomy, has contributed nearly one million US dollars towards NOTES research, according to the Natural Orifice Surgery Consortium for Assessment and Research (NOSCAR) website. [68] NOSCAR is a joint initiative sponsored by the leading gastrointestinal society, the American Society for Gastrointestinal Endoscopy (ASGE), and the by the leading laparoscopic surgery society, the Society of American Gastrointestinal and Endoscopic Surgeons (SAGES).

Other major contributors to the NOSCAR research initiative include healthcare product manufacturer Covidien (500,000 USD), flexible endoscope manufacturer Olympus Medical (500,000 USD), and laparoscope and flexible endoscope manufacturer Karl Storz Endoscopy (250,000 USD). [73]

Figure 1-29. Laparoscopic cholecystectomy. (Reproduced from [74].)

1.7.4. Bariatric surgery for obesity

Obesity has become an increasing problem in Western societies with our high calorie, high fat diets and our increasingly sedentary lifestyles. In the US, nearly a third of the population is considered to be obese, based on National Institutes of Health (NIH) metrics (body mass index>30). [75] Similarly, in England approximately a quarter of the population are obese according to the National Health Service (NHS) in 2008. [76] Overall obesity rates in the rest of the Western world are lower, at about 10-15 percent. [77]

As the availability and popularity of effective bariatric surgery (surgical intervention to treat obesity) has increased, there has been a corresponding six fold increase in the prevalence of the procedure in the US from 1990 to 2000, from 2.4 to 14.1 procedures per 100,000 adults. [75] Much of this procedural growth in the US has been in gastric bypass, which has experienced a nine-fold increase in the same time period to make up 93% of bariatric procedures performed in 2000. Other bariatric procedures also have seen growth, with the gastric banding procedure being very popular in Europe.

Bariatric surgery generally involves employing surgical methods to restrict the food intake into the body (restriction), reduce absorption of the nutrients into the body (malabsorption), or both. The menu of available bariatric procedures includes Roux-en-Y gastric bypass (RYGB), biliopancreatic diversion (BPD), adjustable gastric banding and vertical banded gastroplasty (see Figure 1-30). [77][78][79]

Both RYGB and BPD involve radical surgical re-plumbing of the digestive system to reduce the size of the stomach and to bypass a portion of the small-intestine to induce malabsorption. While RYGB works mostly by restricting food intake with some supplementary malabsorption from a bypassed length of small bowel, BPD functions primarily by malabsorption as a much longer length of the small intestine is bypassed and digestive juices do not come into contact with the food until at the ileum. In terms of efficacy, BPD induces the greatest weight loss; however it also is complicated by a higher occurrence of nutritional problems.

Gastric banding involves the implantation of a saline-inflatable, belt-like device to reduce the size of the proximal part of the stomach, slowing the passage of food into the stomach and creating a sense of fullness in the patient. Vertical banded gastroplasty works in a similar way by using a band in addition to a line of sutures or staples to create a reduced-volume proximal pouch, restricting food intake by the patient. Vertical banded gastroplasty has very much been replaced by the gastric banding procedure as the latter procedure has similar effectiveness [80] while having a simpler operative procedure. Both restrictive procedures tend to result in less weight loss than combination malabsorption / restriction procedures like RYGB and BPD. [77]

Although the first open bariatric procedures were introduced in the 1960s, the introduction of laparoscopic RYGB and gastric banding approaches in the early 1990s is mainly responsible for the rising popularity of bariatric surgery in recent years, according to Cottom et al. [81] Schirmer and Watts agree, but also point out the increasing size of the patient pool (and of the patients themselves) as well as increased media coverage as contributing factors as well. [82]

Fernandez, et al concluded after reviewing over 3000 gastric bypass procedures that laparoscopic RYGB is “technically demanding” and may result in an increased occurrence of internal leaks. [83] Marema, Perez and Buffington found that although laparoscopic RYGB had the disadvantages of “a longer operative time and a higher incidence of fistulas, internal hernias and small bowel obstruction,” the advantages included a “shorter hospital stay, lower

incidence of wound infections, and fewer incisional hernias." They found that both laparoscopic and open RYGB were equivalent in terms of efficacy in inducing weight loss. [84]

For those who are trying to re-envision bariatric surgery in a transluminal surgery context, these procedures have a special appeal to them as violating the wall of the GI tract is a fundamental part of the procedures themselves. Attempts at endoscopic gastroplasty for stomach volume reduction, gastrojejunostomy, gastric pacing of the vagus nerve and vagotomy will be reviewed in more detail in the NOTES section.

Copyrighted material

Figure 1-30. Options for bariatric surgery. (1) Adjustable gastric banding, (2) vertical banded gastroplasty, (3) Roux-en-Y gastric bypass, and (4) biliopancreatic diversion. (Reproduced from Gentileschi et al. [78])

1.7.5. Transanal endoscopic microsurgery (TEM)

Transanal endoscopic microsurgery (TEM) was first introduced by Buess et al. in 1983, and has become a popular procedure to treat early rectal cancers that have advanced too far for successful endoscopic mucosal resection at flexible endoscopy but for which classical radical surgery such as colectomy and lower abdominal resection (which has significant morbidity and mortality risks as well as a high occurrence of pelvic nerve injury leading to urinary and sexual dysfunction) is overtreatment. [85][86]

Studies have demonstrated that TEM is a safe, effective, minimally invasive treatment for the removal of rectal adenomas (pre-cancers) and carcinomas (cancers). When paired with adjunct cancer therapy such as chemotherapy or radiation therapy for treatment of later-stage cancers, TEM is equivalent in long-term curative rates to laparoscopic resection and lower anterior resection without the associated mortality and lower morbidity rates. [87][88][89][90][91][92][93][94][95]

TEM is an endoscopic technique that “combines an endoscopic view of the rectum under gas insufflation via a stereoscopic telescope” with specialized rigid instruments that are inserted into the scope (see Figure 1-31). [96] The retraction, cutting and suturing instruments that allow for large area, full-thickness, *en bloc* resections are similar to their laparoscopic equivalents, and the surgical technique in many ways is akin to performing laparoscopy with all the instruments inserted through one single, specialized trans-anal “trocar”.

The TEM procedure potentially is interesting for researchers working on advanced intraluminal and transluminal procedure development because it is transluminal surgery being performed in humans now. Although the instruments are rigid, like they are in laparoscopy, they exit from the end of a relatively small diameter tube as they would in flexible endoscopy. Problems solved and lessons learned in TEM may be applicable to the development of tools for and procedures in surgery at flexible endoscopy.

Figure 1-31. Instruments for transanal endoscopic microsurgery. (Reproduced from Buess et al. [97])

1.7.6. “Less-invasive” laparoscopy

Surgeons and scientists in the laparoscopy community have been collaborating to reduce the amount of trans-abdominal trauma caused by access ports required for laparoscopic surgery. Their efforts have been in three main areas – (1) using smaller diameter trocars, laparoscopes and instruments that require smaller abdominal incisions, (2) reducing the number of trocars and incisions necessary for the procedures, and (3) moving the location of the incisions and trocars.

The exact definition of what constitutes “minilaparoscopic,” “microlaparoscopic,” “microendoscopic,” “needlescopic,” or “microinvasive” varies widely, although all the terms generally refer to laparoscopic surgery using instruments that are smaller in diameter than 5 mm. However, authors sometimes are a bit generous in their nomenclature, for example making exceptions for the conversion of one or more of the trocars to a larger diameter port to remove large amounts of tissue from the body, or to introduce large calibre instruments such as a laparoscopic stapler into the surgical field.

Santoro et al. reported 161 laparoscopic colon resections between 2001 and 2006 using mini-laparoscopic instruments that all were less than 5mm in diameter. [98] However, one 5 mm port was converted to a 10 or 12 mm port for introduction of a stapler and the removal of the resected colon.

Lee, Lai and Yu performed 1,009 minilaparoscopic cholecystectomies between 1997 to 2002 using 2 mm diameter instruments, but they used a standard laparoscope which was inserted through a larger 10 mm port. [99] Other groups also have reported successes using reduced diameter instruments for cholecystectomy. [100][101][102][103]

Mamazza et al. performed a retrospective study comparing 101 minilaparoscopic procedures with procedures using standard sized instruments – these procedures included cholecystectomy, Nissen fundoplication, bilateral sympathectomy, splenectomy, Heller myotomy, adrenalectomy, and colon resection – and found no significant differences in conversion rates, morbidity or mortality. [104]

Other surgeons have endeavoured to reduce the total entry wound size made in the abdomen by reducing the number of ports / trocars used.

Leggett et al. described successes with a three-port microlaparoscopic cholecystectomy procedure in 159 patients (as opposed to the standard four-port procedure). [105] Mori et al. reported a technique for a two-trocar laparoscopic cholecystectomy in 2001, although technically it was still a four puncture technique with one trocar replaced by direct insertion of a 2 mm grasper forceps through the abdominal wall, and the second substituted with a 16-gauge needle cannula to accommodate the passage of a retraction suture. [106]

Still other surgeons have experimented with moving the location of trocars.

Ghezzi et al. reported in 2002 trans-vaginal extraction of pelvic masses in 63 patients following a laparoscopic surgical procedure using only 5mm ports. [107] The large 10 mm port necessary to extract the pelvic mass was made trans-vaginally with a colpotomy. Zanetti-Dällenbrach et al. described a combined vaginal-laparoscopic-abdominal approach for treating rectovaginal endometriosis that allowed for confirmation of bowel infiltration before potentially unnecessary colectomy. [108]

Schardey et al. reported the first endoscopic thyroidectomy (surgical removal of the thyroid gland located in the neck) by a dorsal approach from the scalp rather than from a ventral or lateral approach in the neck. They commented that one of the advantages of endoscopic surgery is that unlike in convention surgery in which “it makes sense to choose the shortest route to the organ to be treated ... endoscopic surgery enables the positions of the wounds to be far removed from the target organ, which may be reached by using safe pre-existing anatomic planes of dissection.” [109]

Cuesta, Berends and Veenhof described in 2008 an interesting approach to “invisible cholecystectomy” in ten patients using two 5mm trocars both inserted through the umbilicus. [110] A 1 mm Kirschner wire bent into the shape of a hook is inserted at the subcostal line to help with retraction of the gallbladder. Although rigid mini-instruments were used in this study, Cuesta, Berends and Veenhof discuss the potential use of the umbilicus as a potential access point for the introduction of a flexible endoscope that would avoid “possible added complications produced by [creating] the opening in the stomach or colon” that is associated with NOTES as currently proposed. [110]

1.7.7. Laparoscopic / flexible endoscopic “rendezvous” procedures

For some procedures, both rigid and flexible devices are being used. Sometimes, flexible endoscopy is used for pre-procedure reconnaissance and disease or anatomy staging, or for post-procedure follow-up or endoscopic revision procedures.

Yamaner et al. studied retrospectively the records and outcomes of 418 patients who underwent endoscopic retrograde cholangio-pancreatography (ERCP) follow-up after open and laparoscopic cholecystectomy, and found that ERCP is “a reasonable method for treating papillary stenosis and some post-cholecystectomy pain or symptoms”. [111] Champion, Hunt and DeLisle recommended in 2002 routine intraoperative flexible endoscopy after laparoscopic bariatric surgery to identify and repair errors to reduce postoperative morbidity. [112]

In other instances, flexible endoscopy has become an integral part of the clinical procedure.

Kalimi et al. reported in 2000 combined cholecystectomy and ERCP procedures in 29 patients to treat simultaneously stones in the gallbladder and in the common bile duct in one treatment setting. [113] X-ray cholangiography was performed to determine the presence and

location of stones, and the on-call flexible endoscopists were notified to prep the patient for ERCP while surgeons performed the laparoscopic cholecystectomy.

Morino et al. recommended in 2003 endoscopic ablation of intestinal metaplasia in the oesophagus after laparoscopic Nissen fundoplication to control acid reflux disease as combination therapy to treat Barrett's oesophagus. [114]

Saccomani et al. reported in 2005 their experiences with 28 patients who underwent routine intraoperative cholangiography followed by peroperative ERCP (a procedure to remove stones in the common bile duct using a flexible duodenoscope) in a one step rendezvous procedure, and 24 patients who had a transcystic drain followed by postoperative ERCP. [115]

In the "rendezvous" cases, the laparoscopists and flexible endoscopists demonstrated sort of a medical *glasnost* – the gastroenterologist intubating the Vater papilla in the duodenum with a duodenoscope was assisted by the trans-cystic guidewire placed by the surgeon at laparoscopy after completing cholecystectomy.

Also, in many of the experimental studies being conducted for NOTES research, the laparoscope has been an essential visualization tool, aiding surgical procedures at flexible endoscopy by providing an additional, bird's eye perspective of the procedure.

Copyrighted material

Figure 1-32. A laparoscopic / endoscopic "rendezvous" procedure. (Reproduced from Saccomani et al. [115])

1.8. Advanced intraluminal surgery with flexible endoscopes

1.8.1. From diagnostics to advanced intervention

A number of therapeutic procedures – some routine and others experimental – are currently performed at flexible endoscopy. These advanced procedures include intraluminal resection of oesophageal, gastric or colonic tissues in endoscopic mucosal resections (EMR) and endoscopic

submucosal dissections (ESD), management of stones in the common bile duct in endoscopic retrograde cholangiopancreatography (ERCP) and transluminal drainage and biopsy through the gastric wall in fine needle aspiration (FNA).

Also, flexible endoscopists have to be creative in resolving more unusual conditions such as retrieving foreign objects that have been ingested and lodged in the gastrointestinal tract, providing palliative relief for late-stage cancer patients, and treating patients with unusual anatomies.

Physicians constantly are pushing the limits of what can be targeted and what can be achieved with these existing therapeutic procedures. Because many of the proposed surgical approaches have some basis in existing therapeutic procedures, they are briefly reviewed here.

1.8.2. Endoscopic retrograde cholangiopancreatography (ERCP)

Endoscopic retrograde cholangiopancreatography, or ERCP, is a procedure performed at flexible endoscopy — typically using a side-viewing flexible duodenoscope — for diagnostic procedures to view the biliary tree and the pancreatic ductal system and for therapeutic procedures such as stone removal, brush cytology and duct stenting. [17] Oftentimes it is performed with the assistance of a secondary visualization method such as X-ray fluoroscopy or endoscopic ultrasound to see through the walls of the duodenum. New systems like the SpyGlass (Boston Scientific Corp; Natick, MA, USA) miniature endoscope have been introduced to the marketplace for direct optical visualization.

Probably the most difficult part of the procedure involves the cannulation of the papilla, which is a small sphincter at the distal end of the common bile duct that opens into the duodenum. A small 5 French diameter cannula may be used for cannulation, although a guidewire followed by an instrument exchange over the guidewire may be used for more difficult cannulations. [17] These guidewires, which are flexible metal monofilament wires possibly with an outer spiral coil wire and a low-friction polymer coating like polytetrafluoroethylene (PTFE), help to establish and maintain access to lumens such as the common bile duct and function as the “railroad” down which other devices and instruments such as sphincterotomes and biliary balloons can be delivered. They are an essential tool for ERCP and other GI procedures. [116]

If the opening in the papilla needs to be enlarged, either for improved access to the duct or to allow stones to exit from the duct, a sphincterotome can be used to make the incision (see

Figure 1-33). This device, which consists of a flexible plastic shaft with a metal wire bowstring that can be foreshortened to bend the plastic shaft and expose the wire, is inserted deep into the papilla so that part of the wire lies within the duct. By foreshortening the wire and simultaneously applying current through it with an electrosurgical generator, the wire becomes a hot knife that is capable of slicing through the sphincter and other tissues with ease.

For lithotripsy, or breaking apart stones that may be in the common bile duct, a variety of technologies are used including mechanical, electrohydraulic or laser devices. [117] These devices are used typically under direct visualization, although alternatively they are used with a centring balloon while visualized with X-ray fluoroscopy. Although these powerful stones shattering technologies can occasionally cause accidental perforation of the bile duct, they are not designed specifically for use as a tissue dissector.

ERCP may be interesting to researchers of advanced intraluminal surgery and NOTES because of a number of reasons.

First, many physicians consider it to be one of the most difficult endoscopic procedures to perform. Techniques that help in driving the scope and positioning instruments in ERCP may be applicable to advanced intraluminal surgery and NOTES.

Second, the techniques of cannulating small openings, guidewire exchanges, balloon dilation and sphincterotome dissection of tissue translate well to the NOTES realm and already have been used in some NOTES procedures. More about this will be discussed later in the NOTES section.

Copyrighted material

Figure 1-33. A Billroth II sphincterotome (**Cook Inc; Bloomington, IN, USA**). (Reproduced from Cook website. [118])

1.8.3. Mucosal resections – polypectomy, endoscopic mucosal resection (EMR) and endoscopic submucosal dissection (ESD)

Polypectomy, endoscopic mucosal resection (EMR) and endoscopic submucosal dissection (ESD) are endoscopic procedures to cut out areas of mucosa and underlying submucosa in the linings of the oesophagus, stomach and large colon. Polypectomy and EMR are more commonly performed than ESD, which is performed in a clinical setting on a regular basis only in Japan. These techniques provide patients with a minimally invasive, out-patient alternative to major surgery for the removal of diseased tissue in the GI tract.

Polypectomy is an endoscopic procedure in which a lesions or growths are removed typically by using biopsy forceps or endoscopic snares (see Figure 1-34). These neoplasms, or new growths, can be small, focal lesions on the mucosa or pedunculated, mushroom-shaped polyps protruding from the tissue surface. How they present themselves to the physician determines which tools and techniques should be used for their removal.

According to Sivak (2004), colonoscopic polypectomy as it is practiced today is the result of a collaboration between Hiromi Shinya, then a young surgical resident, and Hiroshi Ichikawa, the junior engineer at Olympus Medical who is credited with inventing the endoscopic snare. [119] This collaboration resulted in the first electrosurgical snare polypectomy by Shinya in a 70-year old male patient in 1969. Although, at the time, the whole concept of the electrosurgical snare was considered by Olympus to be “very dangerous,” snare polypectomy has since become the most commonplace endoscopic therapeutic procedure performed in terms of numbers, according to Sivak. [119]

Copyrighted material

Figure 1-34. Polypectomy of a pedunculated polyp performed with an endoscopic snare.
(Reproduced from Baron. [120])

EMR generally refers to procedures performed endoscopically in which pedunculated or sessile (flat) polyps smaller than 2 cm cut out and removed for examination by histology. [121] EMR

typically involves injecting a fluid into the submucosa under and around the lesion to lift it and provide a safety cushion, followed by some method to encapsulate or isolate the lesion (needle-knife dissection of the boundary, band ligation or suction into a cap) and subsequent resection with an endoscopic snare.

The injection fluid typically is a mixture of saline, epinephrine, a dye such as methylene blue or indigo carmine, and sometimes dextrose. Other fluids like sodium hyaluronate, hydroxypropyl methylcellulose, glycerol and fibrinogen have been used because their higher viscosity tends to result in a longer lasting submucosal fluid cushion. [122]

A number of EMR techniques have been reported in the literature, including (1) inject and cut, (2) inject, lift and cut / strip biopsy, (3) EMR with ligation (EMRL), and (4) cap-assisted EMR (EMR-C). [17]

Also, a number of new experimental EMR techniques, such as widespread EMR (W-EMR) and percutaneous traction-assisted EMR can be found in the literature.

The goal of all these EMR techniques is to remove the complete lesion *en bloc* in one resection. The alternative, removing tissue in piecemeal resections, produces specimens that are harder to evaluate pathologically for invasion depth and clear margins, and also is associated with a higher risk of local recurrence. [123]

Incidentally, many practicing physicians, including Fleicher (2000) consider saline-assisted snare polypectomy also to be an EMR procedure, although some clinicians do make this distinction. They separate out colonic polypectomies from oesophageal and gastric EMR procedures, despite polypectomies technically being endoscopic resections of mucosa. [124] For this reason, we will discuss these two procedures separately.

The “inject and cut technique” and the “strip biopsy” method are similar EMR procedures that both begin with the creation of a fluid cushion by injection of a liquid under and around the lesion with an endoscopic injection needle. With the inject and cut technique, the fluid injection lifts the lesion high enough so that a snare can adequately be positioned around the lesion to resect it.

In the strip biopsy technique, grasping forceps and a snare are passed through the two channels of a therapeutic scope (standard endoscopes have only one working channel), the

snare is positioned around the lesion, and the forceps are used to grab and pull the lesion into the snare. The snare then is closed with application of electrosurgical current resulting in the excision of the lesion.

“EMR with ligation” (EMRL) and “cap-assisted EMR” are related techniques. Both require the use of special transparent caps that are attached to the distal end of the endoscope, which is inserted into the patient. Like all EMR techniques, the procedure begins with the injection of a fluid to form a submucosal fluid cushion that elevates the lesion.

In the EMRL technique, which is performed using a special band-applying cap provided in Duette Multi-Band Mucosectomy system (Cook Inc; Bloomington, IN, USA), the cap is positioned over the lesion, vacuum is applied to suck the lesion into the cap, and a polymer band is deployed off the end of the cap around the base of the lesion. This results in the formation of an artificial pedunculated polyp with the band around the base of the “stalk,” and can quickly be removed by snare polypectomy.

Multiple lesions can be banded and resected without having to withdraw the scope for reloading. Pouw et al. (2008) found that the EMRL technique was faster and cheaper than cap-assisted EMR; however the resections made were smaller and less deep, perhaps making EMRL less suitable for lesions with a higher risk of submucosal invasion. [125]

The cap-assisted EMR technique (EMR-C) can be performed using a special cap provided in the Olympus EMR kit (Olympus; Tokyo, Japan). In this technique, the cap, which has a snare preloaded at the distal end, is positioned over the lesion. Vacuum is applied to suck the lesion into the cap, and the snare is closed part-way to form an artificial pedunculated polyp with the snare at its base. The snare then can be fully closed with application of diathermy current and the lesion resected. After each deployment of the snare, the scope and cap need to be withdrawn from the patient so that a new snare can be reloaded into the cap.

A more labour-intensive EMR technique involves the use of an electrosurgical needle-knife to score a path around the periphery of the lesion after submucosal injection, to create a lip onto which the snare can lodge and grasp. Once the snare is in position, it once again is closed with the application of electrosurgical current to resect the tissue *en bloc*.

Widespread EMR was described by Rajan et al. (2004) as a new cap-based EMR technique for resecting lesions larger than 2 cm. [126] Using two prototype “hood knives” (see Figure 1-35),

one to make longitudinal cuts and the other to make circumferential cuts, the investigators were able to resect in six pigs 5 cm lengths of porcine oesophagus that included 50% of the oesophageal circumference.

Copyrighted material

Figure 1-35. Experimental caps with electrosurgical blades embedded in them for performing widespread EMR.
(Reproduced from Rajan et al. [126])

Percutaneous traction-assisted EMR was reported by Kondo et al. in 2004. [127] In this technique, a snare was inserted percutaneously through a 2 mm port through the abdominal and gastric walls into the stomach to retract the gastric tissue containing a lesion with an early cancer. The experimental EMR was conducted successfully and safely in 8 patients in Japan.

Endoscopic submucosal dissection (ESD) describes the surgical removal at flexible endoscopy of large pre-cancerous or cancerous growths in the alimentary tract.

While standard EMR techniques, which are indicated by the Japanese Gastric Cancer Society for excision of lesions smaller than 10 mm diameter, [128] can be used to remove larger swatches of diseased tissue through multiple and piecemeal resections, this can lead to incomplete removal of the lesion, and potentially bury remnants left behind in scar tissue. Argon plasma coagulation (APC), a non-contact method for delivering high-frequency monopolar electrical current through ionized argon gas to superficially coagulate and destroy tissue, commonly is used to “clean-up” residual tissue after piecemeal polypectomy or EMR. [129]

However, with ESD the goal is to remove the entire lesion with a surrounding margin of healthy tissue in one continuous piece *en bloc* to ensure a high degree of confidence for complete resection and a high probability that the procedure is curative. Also, *en bloc*

resection allows for good histopathology to accurately stage the disease and evaluate the completeness of the resection, unlike with piecemeal resection.

The procedure requires a high degree of skill and patience. The doctor cuts around the periphery of the resection after submucosal fluid injection, and then meticulously dissects and peels off the diseased layer of tissue, being careful not to puncture through underlying layers in the process (see Figure 1-38).

Doctors with the talent and skills to perform ESD successfully perhaps are the superstars of the gastroenterological world, but for the vast majority of physicians and surgeons, the high costs and long procedure times associated with ESD cannot be justified within the context of their healthcare systems.

While EMR procedures can be performed in the gastroenterologists' clinic on patients with no or minimal anaesthesia (conscious sedation) and take on the order of minutes to perform, ESD procedures currently are performed in a hospital setting with patients under full sedation and require hours to complete.

Oka et al. found in their comparative study of EMR vs. ESD that ESD procedures requires significantly more time to complete than EMR – 3.5 minutes vs. 58.5 minutes for lesions smaller than 10 mm in diameter, and 12.6 minutes vs. 84.4 minutes for lesions larger than 21 mm in diameter. [128] Furthermore, ESD was associated with a higher rate of complication than EMR. However, Oka et al. also presented data highlighting the benefits of ESD including a higher complete resection rate and a lower risk of recurrence than EMR, regardless of how large the lesion was and where it was located.

Because of differences in healthcare systems and cost structures, ESD is performed clinically in only a few countries worldwide such as in Japan and Korea in which the healthcare system will pay for the time consuming but minimally invasive procedures. In the US, for example, there is no reimbursement code for ESD, and patients who perhaps might be good candidates for the procedure instead are referred to the colorectal surgeon for open or laparoscopic removal of the diseased tissue.

Despite popularity only in limited locales, ESD has many proponents, many of whom are colorectal surgeons that perform ESD in Japan, who have published numerous reports in the

literature of successful and sometimes heroic ESD procedures performed in the oesophagus, [130][131][132] stomach, [133][134][135] colon [136] and sigmoid/rectum. [137][138]

New technology has been introduced by Olympus Corporation (Olympus; Tokyo, Japan) to assist with performing ESD. These include new electrosurgical cutting tools like the hook knife, [139] triangle tip (TT) knife, [139] insulated tip (IT) knife, [139] and the flexknife [138][140] (see Figure 1-36, Figure 1-37), and new flexible videoendoscopes like the R-Scope (see Figure 1-38). [21]

Other new experimental ESD instruments and techniques include the electrocautery incision forceps with a flat-ended transparent hood described by Yamamoto et al., [141] and the twin-endoscope scissors resection described by Brooker et al. [142]

Copyrighted material

Figure 1-36. A. Hook knife. B. Triangle tip (TT) knife. C. Insulated tip (IT) knife.
(Reproduced from Chiu et al. [139])

Copyrighted material

Figure 1-37. Flex knife.
(Reproduced from Fujishiro et al. [138])

Figure 1-38. An ESD performed using the R-Scope (Olympus; Tokyo, Japan). (a) The R-Scope has two independently controlled elevators to articulate two instruments. (b) The defect remaining in the tissue after ESD has been completed. (c) The resected tissue has been removed *en bloc* in one piece. (Reproduced from Reavis & Melvin. [21])

1.8.4. Tissue remodelling for management of gastro-oesophageal reflux disease

Gastro-oesophageal reflux disease (GORD) is a chronic condition in which the corrosive liquids from the stomach abnormally reflux into the oesophagus causing damage to the mucosal lining; typical symptoms include heartburn and regurgitation, but also can manifest as laryngeal inflammation, chronic cough and asthma. [17]

Drug therapies to treat GORD include over-the-counter and prescription proton pump inhibitors (PPI's) that reduce the acid secretions in the stomach, but many, unfortunately, require daily dosing and a lifetime of medication.

Surgical interventions typically work by narrowing or tightening the gastro-oesophageal junction by some physical means to prevent acid reflux. The laparoscopic Nissen fundoplication is the current gold standard therapy and relieves symptoms in 85% of patients, but is considered to be major surgery associated with a not insignificant rate of morbidity and mortality, and can result in serious side effects like dysphagia, or difficulty swallowing, in about 5% of patients. [143]

Endoscopic therapies are available and include the use of suturing devices like the EndoCinch plication device (CR Bard, Inc; Murray Hill, NY, USA) [144] and the NDO Endoscopic Plication System (NDO Surgical, Inc; Mansfield, MA, USA), [145] implantable bulking agents like polymethylmethacrylate (PMMA) beads, [146] polyacrylonitrile (PAN) hydrogels in the Gatekeeper Reflux Repair System (Medtronic Inc; Minneapolis, MN, USA) [17] and the

ethylene vinyl alcohol (EVA) polymer Enteryx (Boston Scientific Corp; Natick, MA, USA), [17] and radiofrequency energy methods like the Stretta (Curon Medical Inc; Sunnyvale, CA, USA) procedure. [147][148][149]

An experimental technique reported by Fritscher-Ravens et al. (2004) uses a tag-based sewing system deployed from a EUS-guided 19-gauge FNA needle to perform gastropexy, or surgical fixation of the posterior stomach to the median arcuate ligament (MAL). This procedure significantly increased pressure at the lower oesophageal sphincter in pigs, and may be effective independently or in combination with other GORD therapies in controlling reflux. [150]

Two commercial products, the Gatekeeper and Enteryx, were voluntarily withdrawn from the marketplace by their manufacturers due to safety concerns from significant complications. In the case of Enteryx, one death was reported due to a mistaken injection of the polymer through the oesophagus into the aorta and subsequent embolism.

According to Pearl and Marks, of the remaining procedures, Stretta and the NDO Plicator show the most promise, although the manufacturer of Stretta has since declared bankruptcy as of 2007. [143] Torquati and Richards (2007) in an evidence-based medicine (EBM) analysis of the literature found that only the NDO Plicator was effective in symptom reduction and acid exposure in the distal oesophagus. [151]

Endoscopic therapies for GORD, in the opinion of Pearl and Marks (2007), are being “scrutinized closely” and perhaps “held to a higher standard than either medical or surgical management” because their introduction “preceded sound clinical data supporting their use ... [some devices] were either ineffective or caused an inordinate number of complications.” [143] Mellinger (2007), in an editorial, draws a number of lessons learned from the experience with GORD therapy including these three maxims:

“The marketing pressure (on both physicians and manufacturer) to cash in on a product’s potential value remains a real patient safety concern to be reckoned with, and dictates that expert-derived data be available before the product is detailed, promoted or embraced by practitioners on a widespread basis.”

"Aiming low (e.g., symptoms vs. acid control, excluding patients normally deemed most appropriate for invasive therapy) does not ensure the success of a new technique, and may in fact highlight its shortcomings."

"We [doctors] are accountable to our patients first and foremost." [152]

Whatever eventually happens with endoscopic GORD therapies, concepts and devices developed for GORD may be directly applicable to NOTES. The various plication devices are essentially sewing machines that could be used for repairing perforations, closing defects and sewing organs together. Biocompatible bulking implants may be interesting for protecting tissues.

1.8.5. EUS guided fine needle aspiration (FNA) and pseudocyst drainage

Fine needle aspiration involves the use of hollow needles to reach pathology that lie beyond the walls of the gastrointestinal tract.

Typically guided by endoscopic ultrasound to "see through the walls," although computed tomography (CT) fluoroscopy and less commonly magnetic resonance imaging (MRI) also have been used, FNA has been used to biopsy liver, pancreas, sentinel lymph nodes and other tissues, and to drain liquid filled sacs. [153][154]

FNA also is used to deliver chemicals to targeted locations and there are reports in the literature of transgastric injection by an endoscopic needle to deliver alcohol or chemotherapeutic drugs into tumours. [155][156][157]

Mango et al. reported the use of FNA under EUS guidance to inject contrast agent through the stomach wall into various veins and arteries in a live porcine model for fluoroscopic angiography. [158]

1.9. Natural Orifice Transluminal Endoscopic Surgery (NOTES)

In 1991, Swain and Mills published a seminal paper in *Gastrointestinal Endoscopy* detailing their work on spring compression buttons or magnets for gastrojejunostomy (joining the stomach to the small intestine) in pigs using a flexible endoscopic approach. [159] Although not purely endoscopic because a mini-laparotomy was used to access and bring the jejunum to the stomach before the -ostomy, the study was the first published attempt using a per-oral, flexible endoscopic approach.

Nine years later, Seifert et. al in 2000 performed one transgastric splenectomy and three pancreatic debridements in three human patients. [160] Four years after that in 2004, Kalloo et al. rekindled interest with a report of flexible transgastric peritonoscopy (examination of the peritoneal cavity) in pigs. [161]

Since then, interest and research in transluminal surgery have expanded at what seems like an exponential rate. Almost every organ in the abdominal cavity now has been viewed, poked, cauterized, resected at endoscopy and then described in detail in peer-reviewed journals. Some doctors even are examining the use of NOTES techniques for accessing the thoracic cavity.

Although most of the literature is centred on procedures taking the transgastric approach to access, there are reports of transesophageal, transcolonic, transvaginal, transvesical and transumbilical procedures being attempted by resourceful doctors as they examine access by every natural orifice possible. Table 1-3 summarizes developments in natural orifice surgery from published literature.

The formation of the natural orifice transluminal endoscopic surgery (NOTES) working group in 2005, the publication of their white paper in 2006, [8] and the first congress in the same year of the Natural Orifice Surgery Consortium for Assessment and Research (NOSCAR), a collaboration between the American Society for Gastrointestinal Endoscopy (ASGE) and the Society of American Gastrointestinal Endoscopic Surgeons (SAGES), has only added the sense of excitement in the field.

Thought leaders in NOSCAR have helped to organize development efforts by focusing research on how to perform a few key tasks necessary for endoscopic surgery. Also, explicit cooperation between the two leading societies ASGE and SAGES has lent tremendous credibility to the NOTES movement.

Early infusion of grant money to the research coffers of NOSCAR by large corporations such as Ethicon Endo-Surgery (a Johnson & Johnson company), Olympus Medical, Covidian (formally Tyco Healthcare) and Karl Storz Endoscopy has reinforced the notion that commercial entities are interested in and willing to support NOTES development.

Table 1-3. Summary of developments in natural-orifice, transluminal and transvisceral endoscopic surgery.

- 1991** Swain & Mills performed button gastrojejunostomy at flexible endoscopy with access to the jejunum via a mini-laparotomy in pigs. [159]
- 2000** Seifert et al. performed transgastric pancreatic debridement and splenectomy. [160]
- 2004** Kalloo et al. performed flexible transgastric peritonoscopy in pigs. [161]
- 2005** Jagganath et al. performed transgastric ligation of the fallopian tubes in pigs. [162]
Kantsevoy et al. performed transgastric gastrojejunostomy at flexible endoscopy without laparoscopic manipulation of the jejunum. [163]
- Park et al. performed transgastric cholecystectomy using a two scope approach. [164]
- 2006** Bergstrom et al. performed transgastric gastrojejunostomy using a FNA needle / metal tag based suturing system. [165]
Kantsevoy et al. performed transgastric splenectomy. [163]
Wagh et al. performed transgastric oophorectomy and tubectomy. [166]
- Fong et al. performed transcolonic hepatic wedge resection. [167]
- Merrifield et al. performed transgastric partial hysterectomy. [168]
- Rao & Reddy reported on transgastric appendectomy performed in humans. [169]
Sumiyama et al. explored the use of the uterine horn as a model for transgastric appendectomy. [170]
- 2007** Kantsevoy et al. described a PEG-like approach to peritoneal cavity access from the stomach. [171]
Sumiyama et al. described submucosal tunnelling gastrotomy approach to peritoneal cavity access from the stomach. Submucosal dissection is achieved through high pressure CO₂ injection and balloon dissection. [172]
Meireles et al. compared the intra-abdominal insufflation pressures between on-demand endoscopic insufflation through the endoscope and the auto-regulated pressures from a laparoscopic insufflator. Concluded that wide pressure variations in on-demand insufflation may lead to risk of hemodynamic and respiratory compromise. [173]
Sumiyama et al. used their SEMF submucosal tunnelling technique and the new R-Scope to perform transgastric cholecystectomy. [174]
Park et al. perform pyloroplasty with transgastric and transduodenal myotomy. [175]

Matthes et al. performed transgastric pancreatectomy. [176]

Shih et al. performed hybrid transgastric cholecystectomy using a 10 mm laparoscopic port to provide tissue traction. [177]

Hondo et al. described an access system consisting of an overtube with a balloon used to access the peritoneal cavity in a canine model. [178]

Zhu performed transumbilical liver cyst fenestration and appendectomy in humans using a 12 mm port at the umbilicus and a flexible endoscope. [179]

Rolanda et al. performed transgastric cholecystectomy by a combined transgastric and transvesical approach in pigs. The port made across the bladder allowed for the introduction of forceps to countertraction tissue. [180]

Bessler et al. performed a hybrid transvaginal / laparoscopic cholecystectomy in a human patient. The laparoscopic ports were used for tissue countertraction, clip application and video documentation. [181]

McGee et al. studied endoscopic measurement of intraabdominal pressure. [182]

Ryou et al. evaluated various gastric closure methods. [183]

Kantsevoy et al. performed endoscopic gastric reduction in pigs. [184]

Filho et al. performed a hybrid transvaginal / laparoscopic cholecystectomy in a human patient. The laparoscopic port at the umbilicus was used for mobilizing the gallbladder. [185]

Scott et al. performed a transvaginal cholecystectomy in pigs using magnetically anchored instruments. [186]

Lima et al. performed a transvesical thoracoscopy in pigs. Starting with the entry port in the bladder, they performed peritonoscopy and inspection of the diaphragm. This was followed by introduction through the left diaphragmatic dome into the left thoracic cavity. [187]

Whiteford et al. reported on a transanal sigmoid colectomy using rigid TEMS instrumentation. [188]

Fong et al. reported on transcolonic peritonoscopy. [189]

2008 Hazey et al. reported on a 10-patient human trial for transgastric peritonoscopy. [190]

Peretta et al. performed transgastric cholecystectomy in survival porcine model. [191]

Devière et al. reported on a 21-patient human study of endoscopic gastroplasty for weight loss. [192]

Zornig et al. reported on a 20-patient human trial of a combined transvaginal and transumbilicalcholecystectomy. The transvaginal port was used for retraction and the transumbilical port was used for dissection. Only rigid instruments were used. [193]

Palanivelu et al. reported on a 6-patient human trial of transvaginal appendectomy. [194]

Zorron et. al. reported on a 4-patient human trial of hybrid transvaginal / laparoscopic cholecystectomy. The laparoscopic port was used for retraction of the gallbladder. [195]

Sumiyama et al. reported transoesophageal epicardial coagulation in pigs. [196]

Willingham et al. reported transoesophageal mediastinoscopy, thoracoscopy and lymph node resection in pigs. [197]

Ever since Rao and Reddy, in 2006 at the SAGES conference in Dallas, TX, USA, publicly revealed their experiences performing the first endoscopic transgastric appendectomy in a human patient in India, [169] there has been a dramatic increase in transluminal studies being performed in humans.

Many of these procedures employed a transvaginal access approach that is based on existing and proven culdoscopy techniques using rigid endoscopes. However, it must be noted that a transvaginal approach by definition rules out use in about half the human population.

These transvaginal reports along with other reports of transumbilical laparoscopic or hybrid approaches in human patients demonstrate the increasing competition to NOTES from modified or evolved laparoscopic procedures.

That many competing approaches exist and that there are no definite answers to a constantly changing set of questions in NOTES research is a testament to how dynamic and in flux everything is. Researchers in the field have the opportunity to explore novel and interesting techniques, technology and science as the white space in this nascent field is vast.



Figure 1-39. Manipulation of the porcine liver to reveal the gallbladder in a NOTES experiment.
(Personal photograph.)

1.10. The need for new endoscopic cutting methods

As clinicians, scientists and engineers work on new procedures and new devices for NOTES, thought leaders in gastroenterology and colorectal surgery also have weighed in with their thoughts in support of NOTES or with cautionary words, speculation on what's needed and how to proceed, and prognostications on what the future holds.

In an editorial in 2005, [6] Hocheberger and Lamadé offered cautious support of the NOTES movement, comparing talk by some of NOTES as being “crazy” to similar dismissals of ERCP procedures thirty years ago, which now are commonplace in gastroenterology. They optimistically agreed that NOTES might provide advantages in treatment of the morbidly obese or palliative relief for the deathly ill. They also speculate that it might result in reduced pain and lower overall costs when compared with laparoscopy.

However, they noted that these perceived advantages have to be proven with data, and discussions of success and recurrence rates, morbidity and mortality, and comparisons to competitive procedures must be discussed with the ultimate goal of patient benefit in mind.

Swain in a 2007 editorial [198] echoed many of these same rationales for justifying NOTES. He added that a NOTES approach might improve ease of surgical access to anatomy such as the lower oesophageal sphincter and upper stomach for some bariatric procedures.

Swain also optimistically suggests that through “human ingenuity and invention” and striving to improve, new procedures and new tools might be invented that could enable NOTES or perhaps improve laparoscopic and endoscopic surgery.

Valdivieso et al. summed up their opinion [199] of the inevitability of NOTES by responding to the question of “what is the future of NOTES?” with a quote from a German philosopher Arthur Schopenhauer:

“There are three steps in the revelation on any truth: In the first, it is ridiculed; in the second, resisted; in the third, it is considered self-evident.”

Contrary or cautionary opinions of NOTES are harder to find amongst all the enthusiasm for NOTES. However, a number of senior surgeons have advised taking a more measured approach.

Buess and Cuschieri offered a dissenting opinion in a 2007 editorial, [200] expressing a number of criticisms of NOTES but essentially focusing on how it increased patient risk without offering any clear patient rewards. Furthermore, they criticized the concept of violating one internal organ just to access another, and questioned the use of such a large number of animals for experimental procedures when “its future application for humans [might not] be performed with clinically acceptable safety.”

Agarwal and Agarwal expressed similar opinions in their 2007 editorial – “Let us focus our mindset and humanize our skill set so as not to be seen as innovators at the cost of basic human values. Otherwise the trend of NOTES will not help in making us a hero but surely make us a proverbial Nero”. [201]

And Pomp noted in his 2008 editorial entitled “Notes on NOTES: The emperor is not wearing any clothes” [202] that “there seems to be some urgency to present some sort of practical applicability to these procedures and be the first to do something in patients. This leads to meetings where undue emphasis and expectation is placed on a technology that is really not quite ready for prime time.”

These cautionary editorials are a useful reminder to the clinician and scientist alike not to put the proverbial cart before the horse and to temper scientific enthusiasm and external commercial pressures with good old-fashioned science. Keeping the patients’ interest above all is paramount.

So what is necessary to enable NOTES?

New tools and technology seems to be a common answer. Swain alluded to the creation of an endoscopic toolset in his editorial, and then called for new “deconstructed endoscopes” in an opinion piece co-written with Kochman. [26]

Swanstrom, in a 2007 editorial, [203] stated that “there is a massive effort to develop enabling technologies for NOTES” and that “the technology will eventually be created,” acknowledging current research efforts in technology and emphasizing its importance in enabling NOTES.

Swanstrom et al., in a 2007 paper entitled “Developing essential tools to enable transgastric surgery”, [204] described the process by which technology is developed as a collaboration between clinicians and technicians and reviewed instruments in development that try to address various issues including instrument triangulation.

Nakao, in his 2007 editorial, explained the need for tissue retraction and instrument triangulation, and proceeded to describe his technical embodiments for how to solve these problems. [205]

Hawes et al. in a 2008 NOSCAR white paper, reviewed the barriers to NOTES (see Table 1-4) identified in the previous white paper of 2006 and updated the progress of work to resolve the eight identified issues.

Table 1-4. Barriers to NOTES, according to the 2006 NOTES working group white paper. [8]

Access to peritoneal cavity
Gastric (intestinal) closure
Prevention of infection
Development of suturing / anastomotic device
Maintenance of special orientation
Development of a multitasking platform
Management of iatrogenic intraperitoneal complications
Identifying physiologic untoward events

Three particular items of note from this paper are highlighted below:

- (1) “intraperitoneal contamination and infection appears to be less of a problem than originally feared,”

- (2) NOTES can be performed at very low pressure pneumoperitoneum casting anecdotal support for the original vision that “NOTES procedures might one day be performed with patients under conscious sedation in an outpatient setting,” and
- (3) Although no published control data is available, there is a “uniform reporting [from investigators in three continents] of the dramatic lack of post-operative pain in patients undergoing NOTES cholecystectomies.”

In particular, the first point on the adverse effects of intraperitoneal contamination and infection was unexpectedly good news to the author.

Given that such effort is taken in modern surgery to maintaining an antiseptic surgical field, the prospects of leakage into the peritoneal cavity through holes made during NOTES procedures seemed frighteningly real. Infection leading to sepsis and potentially death seemed to be an urgent consideration that needed to be addressed.

Still, if initial evidence seem to indicate that infection from leakage is less of a problem than initially feared, this helps greatly to mitigate negative arguments against NOTES. Research to understand why this is the case might also help in this regard.

While new methods for controlling the cutting of tissue in a flexible endoscopic environment is not specifically identified in the NOTES / NOSCAR white papers as a barrier to NOTES, the author believes that the difficulty in controlling endoscopic cutting often is unstated and the recognition of the problem is taken for granted.

For example, Peretta et al. expressed their frustration in a 2008 report of transgastric cholecystectomy in pigs: [191]

“The standard endoscopic dissecting and grasping tools used were partially if not totally responsible for the gallbladder perforations. The enormous dependence of surgeons on instrument manufacturers for progress in NOTES is apparent. There is an urgent need for more effective flexible endosurgical tools, which frankly are poor currently.” [emphasis added]

Inui expressed a similar need in a 2007 paper: [206]

"Improvement of instruments and procedures is needed for successful clinical implementation of NOTES. ... Improvements of procedures is needed to optimize ... incision making (by using a needle knife, then extending the incision with a sphincterotome or dilating with a balloon), ..."

However, the method by which physicians and surgeons frame the problem, in the author's opinion, assumes the solution. One barrier to NOTES described in the 2006 & 2008 white papers is the "development of a multitasking platform" that allows for instrument access, stability and triangulation.

The author believes that this statement implicitly suggests that the preferred solution is a mechanism for providing stability and triangulation, most likely in the form of articulating instruments or cannulae. However, articulation is but one possible solution to the controlled cutting problem.

Indeed, if one considers the number of instances in which stability, triangulation or articulation are mentioned as part of a wish list of enabling NOTES technologies, and for arguments sake, that perhaps each instance is an appeal for better controlled cutting, then this is quite a problem indeed! To the author, this is confirmed by personal communication with surgeons and physicians in NOTES research, as well as personal experiences developing articulating instruments for NOTES.

1.11. Chapter Conclusions

Surgery, and in particular, therapeutic endoscopy, has come a long way – from its humble beginnings with crude tubes and specula, to current medical procedures utilizing modern rigid laparoscopes and modern flexible endoscopes. Advancements in the field often times has been the result of a collaborative (although sometimes cantankerous) relationship between thought-leading doctors who push the boundaries of their practice, and the engineers and medical corporations who co-invent, co-develop and co-market the tools that the doctors use.

The gastrointestinal tract is quite extensive in physical reach and touches upon or is within easy reach of almost all of the major organs in the abdominal and thoracic cavities, potentially allowing for access to a large portion of the internal human anatomy if the boundaries of the alimentary tract are allowed to be penetrated to access other organs.

Currently a large number of procedures are performed to correct conditions in organs in the gastrointestinal tract using open, laparoscopic or flexible endoscopic approaches. While historically gastroenterology and colorectal surgery have been two very distinct medical specialties, advancements in both fields have blurred these lines. Some procedures that once used to be performed with major surgery by colorectal surgeons can now be performed as an outpatient procedure by gastroenterologists at flexible endoscopy.

Advanced endoluminal procedures like ESD and transluminal or transvisceral procedures like NOTES, TEMS, hybrid endo-lap procedures and modified laparoscopic procedures that place the ports at natural orifices further blur the distinctions between the two specialties. However, recent collaborations between the two major societies for American gastroenterologists and colorectal surgeons hopefully will ensure mutually beneficial procedure and technology development rather than destructive competition and turf wars.

Although controlled cutting schemes for endoscopic surgery is not explicitly stated as a problem to be solved, the author believes that this problem is under-represented based on implicit desires in the literature, on personal communication with surgeons and physicians in NOTES research, and on personal experiences developing articulating instruments for NOTES.

These new controlled cutting schemes also might be relevant in other surgical arenas including laparoscopic and open surgery.

1.12. Recent developments as of 2010

From even before this PhD project began in 2006, NOTES development has stormed ahead with seemingly boundless enthusiasm only to have slowed down in recent years. Now, some physicians even have questioned whether or not NOTES is dead!

According to an editorial by Rattner in 2010, the dissipation of some of the initial excitement since Rao and Reddy's first transgastric human cholecystectomy was due to (1) the inherently difficult technical challenges of NOTES instrumentation development, (2) US government regulatory scrutiny of the medical / commercial partnership, and (3) new developments in single-port laparoscopic, transvaginal and TEM procedures. [207]

Arguably, recent global economic difficulties also may have contributed to the perceived cooling of enthusiasm for developing brand-new technologies and procedures for NOTES.

But Rattner argues in his editorial that NOTES development is continuing in earnest in the slow, methodical manner necessary for evidence-based medicine. The problems laid out in the original ASGE/SAGES NOTES white paper in 2006 are being addressed methodically and holistically as the unknown and the uncertain are being explored and dealt with step by step.

He also makes an impassioned plea to move away from purist definitions of NOTES towards more expansive ones that include procedures beyond the narrow description of a transgastric approach using a flexible endoscope.

His arguments closely echo the approach and positions taken in this thesis. As has been explained in great detail, there are many ways, including NOTES, to perform surgery in a less invasive manner. New technology and techniques developed for any of these approaches can help move forward the overall goal of improving minimally invasive surgery.

Some of the ideas and trends speculated and highlighted in this thesis now have been tried by clinicians in a clinical setting.

In 2008, Denk, Swanström and Whiteford demonstrated the feasibility of a transanal approach by TEM to access to the peritoneal cavity. [208] In 2009, Salinas et al described their early experiences in hybrid transgastric / transvaginal endoscopic cholecystectomy in humans. [209]

And Romanelli and Earle reviewed in 2009 new technologies combining some of the best aspects of laparoscopic surgery and NOTES for new experimental procedures alternatively named “single-port access”, “single-incision laparoscopic surgery” and “single-site laparoscopy”. [210]

The review also cited recent reports of human cholecystectomies performed using single-site multiport trocars as well as with hybrid rigid / flexible instruments. [210][211]

Furthermore, new technologies for “pure” NOTES have been introduced.

Akahoshi et al reported in 2008 on a new diathermy grasping-type scissors forceps for ESD at flexible endoscopy. [212] Moran, Gostout and Bingener reported in 2009 on a new flexible cap and catheter-based endoscopic suturing system. [213] And Park et al reported in 2010 on flexible bipolar haemostasis forceps that can seal blood vessels in a porcine model at flexible endoscopy as well as a commercially available laparoscopic system. [214]

Incremental improvements have been made to articulation platforms in 2009 as reported by Mullady, Lautz and Thompson [215] and Thompson et al. [216]. And in 2009 a new method for affecting weight loss using a duodenojejunal bypass liner placed endoscopically to affect weight loss has added a potential new indication for flexible endoscopy.

New developments within NOTES and in rigid endoscopy are not to be feared as battles in a turf war between gastroenterologist and laparoscopic surgeons, between NOTES and new incarnations of laparoscopy. Within a united effort for MIS, there are many opportunities for new ways to cut tissue.

Chapter 2:

Existing endoscopic cutting methods

*Your work is to discover your world
and then with all your heart give yourself to it.*

Buddha

2.1. Chapter Overview

This chapter reviews the literature for existing methods and devices for cutting tissue at endoscopy, and for schemes to control the tissue dissection.

The survey methodology is described and followed by a review of existing surgical cutting devices. Cutting methods described in the literature and an examination of published schemes to control the cutting including feedback control, articulation and robotics also are presented.

From the literature review, the overall conclusion that a good deal of intellectual “white space” is available for scientific research is drawn.

2.2. Literature survey methodology

The literature survey was conducted in two phases.

The first phase consisted of keyword searches in Google (general search), Google Scholar (scientific journal search) and Google Patents (patent search) for various known cutting devices and cutting methods.

These searches were supplemented by additional searches in eUCLid (the UCL Libraries search engine), Scopus (a search engine for scholarly journal articles owned by the publishing company Elsevier) and PubMed (a free database run by the National Institutes of Health and the National Library of Medicine that accesses the MEDLINE database).

The second phase was composed of in-depth review of every abstracts between 2000 and 2010 in two major American clinical journals – *Gastrointestinal Endoscopy* and *Surgical Endoscopy* – and every abstract between 2007 to 2010 from leading optics journals — *Lasers in Surgery Medicine*, *Lasers in Medical Science* and *Optics and Laser Technology*.

2.3. Tissue cutting instruments in open and minimally invasive surgery

Cutting tissue is one of three fundamental surgical tasks that a surgeon needs to perform during surgery. These tasks are (1) tissue dissection, (2) haemostasis and (3) reconnecting or sealing tissues.

Over the years, many cutting instruments have been invented and are available to the surgeon for cutting tissue. These devices, in general, can be categorized by how they work into two groups – (1) devices that exert direct mechanical forces to load and shear tissues past their material yield strengths, and (2) devices that impart energy to the inter- and intracellular water to cause explosive vaporization for the division of tissues.

For example, tools such as scalpels, scissors, powered bone saws, debriders and dissecting balloons fall into the first category of devices that cut by mechanical means. Radiofrequency (RF) electrosurgical knives, laser scalpels and ultrasonic cutters belong to the second group of devices that cut by nonmechanical means.

2.3.1. Mechanical shearing of tissue

Using simple physical machines like wedges and levers to focus mechanical forces causing material to yield and separate is a simple and age-old method. Surgical devices like scalpels, scissors and saws are very efficient and effective at using these physics to cut tissues at will.

Perhaps due to their simplicity and effectiveness, mechanical cutting tools are ubiquitous in surgery across such varied medical specialties as emergency triage, colorectal surgery and ocular surgery.

For example, miniature ocular scissors are used for epiretinal membrane dissection and for small vessel incision for the treatment of retinal angiomatic proliferation. [217][218] Elongated scissors used through trocars are essential tools for the laparoscopic surgeon.

Other mechanical tools like surgical stapler devices simultaneously lay down multiple staple lines and cut between them to seal and divide hollow organs into two halves. These tools are staples of modern open and laparoscopic surgery, so much so that some thought leaders in NOTES have expressed their desires to replicate stapling capabilities for use at flexible endoscopy. [219]

Reports exist of experimental full-thickness gastric resection procedures performed in animals using flexible linear staplers like the SurgASSIST (Power Medical Interventions Deutschland GmbH; Hamburg, Germany) [220][221] and flexible semi-circular staplers like the experimental, full-thickness resection device (Boston Scientific Corp; Natick, MA, USA). [222] However, these devices tend to be large and cumbersome due to the high forces involved with reliably forming metal staple lines.

Power-assisted mechanical cutting tools like surgical drills and grinders, circular bone saws and cartilage debriders have made it easier for surgeons to perform normally physically taxing tasks. Power tools often are used at arthroscopy to cut and reshape bone and cartilage for orthopaedic hip and knee replacements.

Powered cutting tools also can provide precision cutting in a repeatable manner. Microkeratomes use oscillating blades to cut corneal flaps of precise thicknesses in the eye in preparation for corrective laser eye surgery. Liposhavers – vacuum-assisted tissue shaver with an oscillating blade – are used in plastic and reconstructive surgery to precisely shave and contour fat in order to improve cosmetic appearance. [223]

In the world of flexible endoscopy, devices that cut tissues by purely mechanical means are few and far between. Instead, most devices, like needle-knives, snares and sphincterotomes, pass electrosurgical current through the tissue to cut tissue by nonmechanical means. Endoscopic instruments that do cut primarily by mechanical means may also use electrical current to cauterize tissue to help control bleeding.

In the literature, only three manual, flexible, endoscopic instruments could be found that cut tissue mechanically – the “cold” biopsy forceps (see Figure 2-1), the endoscopic snare (see Figure 1-34), and endoscopic scissors (see Figure 2-2). [224]

Copyrighted material

Figure 2-1. Olympus biopsy forceps. (Reproduced from Olympus website. [225])

Copyrighted material

Figure 2-2. The Olympus EMR scissors. (Reproduced from Miyashita. [224])

“Cold” or non-cautery biopsy forceps rely on two sharp cup-shaped jaws that close to “bite” off tissue. They are available from a number of manufacturers in a variety of sizes, jaw configurations, with or without stabilizing features like a central barb between the jaws. “Hot” biopsy forceps that uses electricity to help with tissue cutting and haemostasis also are available.

Biopsy forceps are used at flexible endoscopy quite routinely for a variety of diagnostic and therapeutic procedures — for example, biopsy for diagnostic monitoring of Barrett’s oesophagus and therapeutic biopsy to rip out a focal lesion occur with regular frequency in gastroenterology.

Overall, they allow the gastroenterologist to cut off very small volumes of tissue safely. According to the ASGE technology status report on polypectomy devices in 1997, biopsies with "cold" forceps are perceived to be very safe.

However, the report also expressed concerns about adequate polyp removal or destruction, citing a study in which 29% of patients had residual neoplastic tissue three weeks after treatment by cold biopsy forceps, and a second study in which 17% had residual tissue two weeks after treatment by hot biopsy forceps. [129]

Endoscopic snares are lasso-like devices that are used for cutting tissue at flexible endoscopy. Consisting of a conductive metal loop inside a hollow, insulating polymer sheath, they function by first encircling the tissue and then cut by a "cheese-wire" effect when the loop is cinched down around the tissue.

Snares are available from a number of manufacturers in a variety of sizes, configurations and designs. Available choices include thick vs. thin wire, monofilament vs. braided wire, circular vs. polygonal or D-shaped loops.

Many snares are designed to be used with electrosurgical current. These "hot" snares can be used either with or without cautery at the physician's discretion, although cheaper "cold" snares that lack the electrical connector usually are used when it is known in advance that cautery is not necessary.

Other features that aid in correct placement of the snare on the target tissue include barbed or needle-tips at the distal end of the loop to act as an anchor, and rotation features to assist with the initial "snaring" of the tissue.

Cold snaring of small sessile polyps ($\leq 6-7$ mm) is becoming popular as an alternative to hot biopsies because it is associated with a low rate of bleeding. [120] Also, cold snares are more compatible with patients implanted with pacemakers and implanted defibrillators in which the use of electrosurgical diathermy is contraindicated.

Endoscopic scissors are a relatively rare device that is available from Olympus Inc. exclusively. They look and function like miniaturized scissors attached at the end of a long flexible actuator. Suture cutters designed to cut polymer and braided thread rather than tissue also are available, have a similar appearance and also have been used experimentally to cut tissue.

Unfortunately, praise from doctors for the cutting performance of the scissors is equally rare. Past informal questioning of gastroenterologists by the author about the scissors had evoked responses ranging from “it doesn’t work” to a more scathing “it’s a piece of [expletive removed].”

From personal observation of physician interaction with both the Olympus scissors and a larger prototype of flexible endoscopic scissors, much of the frustration came from two areas – the inability of the scissors to get a proper purchase onto the tissue, pushing the tissue out upon closure, and the slippage of tissue between the two blades on closure instead of cutting.

Still, Miyashita et al. reported in 2003 a successful clinical experience using endoscopic scissors developed in collaboration with Olympus Optical Co. Ltd. (Tokyo, Japan) to cut out a superficial gastric cancer. [224] They described the use of a two channel gastroscope during the procedure to grasp tissue with forceps in one channel to provide countertraction, and cut with the endoscopic scissors in the second channel.

Also, Beilstein and Kochman in 2005, used endoscopic suture cutters model FS-3L-1 (Olympus America Corp; Melville, NY, USA) to cut through oesophageal scar tissue in a human patient. [226] They were able to cut through the fibrous tissue with “small, repetitive snips” despite the device being designed to cut suture rather than tissue.

Incidentally, Beilstein and Kochman chose to use the suture scissors “off-label” instead of using a more traditional electrosurgical needle knife because “of an inability to hold the endoscope in position while visualizing the band and controlling the incision”. Needle knives sometimes can cut farther and deeper than intended even with direct visualization.

Although the use of countertraction while cutting with scissors is standard surgical technique, it is rare and uncommon at flexible endoscopy due to the simple fact that most endoscopes have only one accessory channel and allow for using only one tool through the endoscope at a time. Tissue countertraction simply cannot be performed using standard endoscopic equipment in a standard procedure, which may help to explain why the endoscopic scissors have such a poor reputation in gastroenterology.

Blunt dissection devices use relativelyatraumatic wedge shapes to stretch, rip and tear tissues along tissue boundaries or at tissue planes. They have become popular in such surgical

procedures as harvesting the saphenous vein graft in cardiac bypass surgery, and in liposuction procedures for cosmetic surgery.

Blunt dissection also is commonly used at laparoscopy as a surgical technique; it is achieved by tunnelling into connective tissue with closed laparoscopic forceps or scissors and then opening the forceps jaws or the scissors blades to stretch and rip tissues apart.

In experimental NOTES procedures, the author has witnessed attempts by some investigators to perform similar actions with flexible endoscopic forceps. However, much more difficulty usually is observed with the endoscopic forceps than with their laparoscopic counterparts.

The primary difficulty seen has been in opening the jaws or blades once they have been tunnelled into connective tissue. This is a technical challenge due to the current construction of endoscopic forceps and scissors, which are strong in closing the jaws or blades but are weak in opening.

2.3.2. Waterjet cutting of tissue

Waterjet cutting is a technology that uses small diameter, high-pressure, ultra-coherent streams of water to cut materials like a knife. A key advantage is the inherent cooling of the cut material by the water stream itself, which is beneficial if high temperatures generated from an alternate cutting process might introduce thermal stresses leading to thermal damage.

The technology has been used successfully in industrial applications to cut plastics, soft metals and non-hardened steels, typically with the assistance of fine, abrasive particles added to the water stream to increase the cutting ability of the high-pressure jet of liquid.

Medical waterjets have been used to cut soft tissues and debride (remove necrotic tissue from healthy tissue) damaged organs using a high pressure stream of isotonic salt water without any added particulates. They also can selectively cut parenchyma, or the functional parts of soft organs, while leaving structural and connective tissues such as blood vessels intact. Research by de Boorder et al. showed that cavitation effects were involved in tissue dissection by water jets. [227]

For example, a commercial waterjet system, the Müritz 1000 (Euromed Medizintechnik; Schwerin, Germany), was used for the blunt dissection of brain tumours in nine human patients, as described in a 1998 report by Piek et al. Shekarriz et al. reported in 2000 the use of

the Müritz 1000 for partial nephrectomy in pigs. And Granick et al. published in 2006 a retrospective study of 40 patients who had their wounds debrided using a high-powered parallel water jet (Versajet, Smith-Nephew; Hull, UK). [228][229][230]

Sold et al. reported in 2007 an interesting effect in which the liquid jet from a commercial waterjet system (Helix Hydrojet, ERBE Elektromedizin GmbH; Tübingen, Germany) was directed at *in vivo* gastric mucosa in pigs. The jet of liquid was selectively deposited through the mucosa into the submucosa, resulting formation of a submucosal fluid cushion and mucosal lift. The German group successfully deposited saline, gelatin, hydroxyethyl starch (HES), dextran and 50% glucose solution into the submucosa using their waterjet method. [231]

A number of groups have experimented with waterjets created at the distal end of catheters by laser vaporization. These devices work by using the laser to vaporise water into gas, creating a jet of water that is ejected out of the exit nozzle in a controlled fashion.

Eversole et al. reported in 1997 the use of a pulsed erbium, chromium:yttrium-scandium-gallium-garnet (ER, CR: YSGG) laser to vaporize water to cut dental hard tissues in rabbits and dogs. [232] Nakagawa et al. in 2002 used a pulsed holmium yttrium-aluminum-garnet (Ho: YAG) laser to create a controllable micro-jet of water fired from a micro-nozzle that they used to dissect brain tissue in rabbits. [233][234][235]

Fletcher and Palanker in 2001 reported the use of a tungsten filament heating element powered by a high voltage electrical discharge to vaporize water and create a controllable micro-jet of water from a micro-nozzle. [236]

2.3.3. Gas dissection of tissue

High-pressure carbon dioxide (CO_2) gas has been used for blunt dissection to separate tissue layers. Sumiyama et al. reported the use of gas blunt dissection to create a submucosal tunnel for gastrotomy and oesophagotomy for transgastric and transoesophageal access in pigs. [237][172][174][196] The gas dissection was followed by injection of hydroxypropylmethylcellulose (HPMC) and subsequent blunt dissection “cleanup” by a 15 mm biliary retrieval balloon.

2.3.4. Radiofrequency electrosurgery

Radiofrequency electrosurgery, also called surgical diathermy or endothermy, is the most commonly used cutting method after cutting with bladed instruments.

Electrosurgery, which is used in open surgery, laparoscopy and flexible endoscopy, is quite versatile, being able both to cut and to coagulate tissue. Electrosurgery plays a crucial role at flexible endoscopy because most endoscopic cutting and coagulating tools are electrosurgical in nature.

Electrosurgery is different from electrocautery. Although both methods use electricity to generate heat, the terms describe two technically different processes. Confusingly, the two terms often are used interchangeably by clinicians in practice.

In electrocautery, electrical current is used to heat a heating element like a tungsten filament. This hot instrument then is brought into physical contact with the tissue to burn through or to coagulate the tissue.

In electrosurgery, high frequency electrical current travels through the tissue between electrodes to produce rapid resistive heating directly in the tissue. While the high current density in this tissue volume rapidly heats it up, vaporizing water and tissue in the process, the electrodes themselves stay relatively cool.

An electrosurgical generator like the ERBE ICC 200 shown in Figure 2-3 produces various electrical waveforms optimized to cut or coagulate tissue. The specific characteristics of the waveforms depend greatly on the make and model of the generators as well as the functional mode used — whether it is optimized for cutting, coagulation, spray coagulation / fulguration or a blend between modes.

In general for tissue cutting, peak voltage usually needs to be high enough — on the order of a few hundred volts — to develop the required cutting arc in tissue, [238] but low enough to prevent charring and direct arcing between active electrodes.

For contact coagulation, peak voltage can vary between hundreds of volts to kilovolts. For non-contact spray coagulation peak voltage may range from kilovolts to ten kilovolts — high enough to cause electrical breakdown in air and direct arcing between the active electrode and the grounded tissue for non-contact tissue coagulation or fulguration. [239]

The frequency of the electrical current typically ranges between 200 kHz and 5 MHz. This is well above the 100 kHz threshold below which involuntary stimulation of skeletal and cardiac muscle can lead to unwanted complications.

Whether the high-frequency electrical current functions to cut, to coagulate or both depends on the power setting, the electrode geometry and the current waveform.

Typically cut waveforms usually are pure sinusoids, although in reality, the actual waveforms can be more complicated due to optimization strategies by the manufacturers and equipment limitations due to cost.

Pure coagulation waveforms typically are damped sinusoids which often are modulated as pulse trains, but again the actual waveform delivered depends greatly on the generator make and model. Coagulation waveforms usually have a higher crest factors (the ratio between peak voltage and root-mean-square voltage) than cut waveforms. [239]

Electrosurgical tools are designed for monopolar or bipolar operation, depending on the configuration of electrodes used (see Figure 2-4). All electrosurgical instruments require a closed electrical circuit in order to function. However, variations in relative sizes of electrodes and their placement on the body determine how they function in practice.

Bipolar devices use two electrodes of similar size positioned relatively close to each other. Electrical current flows through the tissue between the two electrodes and the heating effect generally is well controlled and confined intra-electrode volume of tissue. Advantages of the bipolar electrodes configuration compared to monopolar electrodes include typically lower power requirements with less heat conduction, and a relatively predictable current path between the two electrodes. [240]

An example of a common bipolar endoscopic device is the Gold Probe (Boston Scientific Corp; Natick, MA, USA) haemostatic probe, which typically is used to control non-variceal bleeding in the upper GI tract.

Other bipolar coagulation devices also are available in the marketplace, but bipolar cutting devices are rare, probably because generating high enough current densities to cut tissue is more difficult with bipolar electrodes. Also, the high voltage needed for cutting might cause electrical breakdown between the electrode leads.

Electrosurgical generators that work with bipolar devices usually have a separate bipolar mode of operation. The output impedance of the generator in bipolar mode typically is about 50 ohms compared with about 400 ohms when in monopolar mode.

Monopolar devices typically use two electrodes of very different sizes positioned relatively great distances away from each other. The small, active electrode is used for cutting and coagulation under direct control by the doctor and can take the form of a needle, paddle, scissors, etc.

The large, stationary, grounding electrode is placed at some distance from the surgical site (typically on the thigh or buttocks in human patients) to act as the return electrode.

The electrical current travels between the active and grounding electrodes through the body. At the contact point between the small active electrode and the tissue, the current density in the tissue is very high which results in rapid tissue heating and cutting or coagulation.

Away from the contact point, the current density falls rapidly as multiple electrical paths are available for the current to travel through the body to the grounding electrode.

Because the grounding pad is so much larger than the active electrode, current densities in tissue in contact with it never get high enough to result in significant heating. However, an improperly affixed or partially detached grounding pad can result in serious burns due to the reduced contact surface area and the resultant higher current densities.

Also caution must be taken when working with monopolar devices on pedicle-like organs with narrow connective stalks. Narrowing of conductive geometry can “focus” currents potentially increasing current densities to damaging levels. Similarly, areas of high tissue impedance with large electrolyte-filled blood vessels can “route” currents to the vessels, potentially damaging them in the process.

Despite the potential hazards with monopolar diathermy, its main advantage is that monopolar devices are simple and easy to manufacture and most monopolar devices can be used with a standard electrosurgical generator and grounding pad.

Needle knives, snares, sphincterotomes — almost all cutting devices used at flexible endoscopy are monopolar devices.

Copyrighted material

Figure 2-3. An electrosurgical generator by ERBE Elektromedizin GmbH.
(Reproduced from MDA Electrosurgical Devices Review 2002. [239])

Copyrighted material

Figure 2-4. Many electrosurgical generators can operate in two modes: (1) a bipolar mode (left) in which both leads of the electrical circuit are connected to the electrosurgical instrument, and (2) a monopolar mode (right) in which the active lead is connected to the electrosurgical instrument, and the return electrode takes the form of a grounding pad or plate that is affixed to the patient's thigh or buttocks.
(Reproduced from MDA Electrosurgical Devices Review 2002. [239])

The electrosurgical generator market is relatively mature, with most units providing similar and competitive feature sets. Higher-end products have differentiated themselves by optimizing the electrical waveforms and power regulation to improve the cutting and coagulation capability of their devices and by providing different "blend" modes that combine cut and coagulate waveforms. However, some devices have been introduced that employ new ways to use electrical energy to cut tissue.

Ion or argon plasma coagulation (APC) is a monopolar, non-contact coagulation method that uses compatible electrosurgical generators and ionized argon gas to conduct electrical current to the tissue in a safer, more gentle manner than contact coagulation.

Theoretically, the APC method limits the depth of tissue coagulation by allowing current to arc through the ionized gas to lower impedance, less-desiccated tissues adjacent to coagulated tissue. In practice this is generally true, although Goulet et al. reported in a 2007 study in swine that the safety features of APC are not foolproof. At higher power settings and longer treatment durations, deeper-layer tissues like the *muscularis propria* in gastrointestinal tissues can still be damaged with APC when using a broad range of clinical APC settings. [241]

Monopolar fulguration to cut tissue is used in a commercial device that recently has been introduced to the marketplace as the PlasmaBlade (Peak Surgical Inc; Palo Alto, CA, USA). According to the product website, the device uses “pulsed waveforms that produce short plasma-mediated electrical discharges ... heat diffusion and associated heat damage to surrounding tissue is limited, resulting in less collateral damage and more precise tissue dissection.” [242]

Gyrus ACMI, now a part of Olympus Medical, is the manufacturer of the plasma kinetics (PK) technology (Gyrus ACMI / Olympus Corp; Southborough, MA, USA) that uses bipolar fulguration to vaporize tissue. Bipolar fulguration is similar to bipolar electrosurgery in that the two necessary electrodes are in relatively close physical proximity when compared with monopolar fulguration or monopolar electrosurgery.

The Plasma Trisector device of the PK line also has the capability to seal vessels. Botto et al. published in 2004, their experiences using the device in prostate surgery, [243] and Abouljoud published their experiences with laparoscopic liver resection in 2008. [244]

Also, electrosurgical devices exist that use the heat generated by electrical currents passing through tissue to form a coagulum to seal tissues.

The Ligasure vessel sealing system (ValleyLab / Covidien PLC; Boulder, CO, USA) uses “an optimized combination of pressure and energy [to create] the seal by melting the collagen and elastin in the vessel walls and reforming it into a permanent, plastic-like seal,” according to the product website. [245]

Although the Ligasure was designed primarily for vessel sealing, one could imagine this technology leading to an electrosurgical super-tool that combined the capabilities to cut, coagulate and seal tissues.

2.3.5. Ultrasonic / harmonic cutters

Ultrasonic cutters and welders cut and seal plastics by concentrating ultrasonic vibrations by specially designed “horns” into these materials. They are used quite extensively in industrial plants for product and packaging manufacturing.

In the medical world, ultrasonic cutters are used to cut and coagulate tissue. The two most popular laparoscopic ultrasonic dissectors are the Ultracision Harmonic Scalpel (Ethicon Endo-Surgery, Inc / Johnson & Johnson Inc; Cincinnati, OH, USA) and the AutoSonic System (AutoSuture / Covidien PLC; Norwalk, CT, USA). Some of the newer ultrasonic devices from these two companies also have the ability to seal small blood vessels in addition to cutting and coagulating tissue.

These devices use small piezoelectric elements to vibrate cutting surfaces at ultrasonic frequencies to cut, coagulate and seal tissues. [246] According to a 1999 technology review by Cuschieri, low power ultrasonic dissectors operate at around 25 kHz and cleave cells with high water content through cavitation. High power ultrasonic dissectors operate at 55.5 kHz and function mainly through “tissue sawing [high speed frictional deformation] coupled with linear compression of the tissue [by the surgeon].” [247]

Some advantages of ultrasonic cutters over electrosurgery, according to the website of one manufacturer, include minimal charring and smoke, no electrical currents passing through the patient, and fewer instrument exchanges. [248]

From personal communication with a number of surgeons in NOTES research, the development of ultrasonic devices at flexible endoscopy is highly desirable. However, no ultrasonic devices for flexible endoscopy currently exist, and there are no discernable indications that companies are actively pursuing a viable product either from the literature or from personal communication with industry sources.

This might be due to physical limitations with miniaturizing ultrasonic transducers capable of generating enough force and displacement, and to problems with efficient ultrasonic power transmission through a long, flexible shaft that can take on various geometries.

However, one probably wouldn't be wrong to speculate that given how secretive industry can be, someone somewhere could be hard at work trying to solve these problems.

2.3.6. Laser ablation

The laser, which stands for light amplification by stimulated emission of radiation, is an optical device that emits light by a process called stimulated emission. The light emitted typically is coherent, low-divergence, and narrow bandwidth.

Many types of lasers have been conceived of, functioning by various physical means to cause stimulated emission of light. These lasers include the traditional gas, dye, metal-vapour, solid-state and semiconductor lasers used in medical, industrial and consumer applications (see Figure 2-5).

More exotic free electron lasers that use relativistic electron beams as the lasing medium exist, and theoretical lasers like the gamma laser pumped by positronium annihilations and the x-ray laser powered by nuclear explosions also are possible.

In medicine, lasers are used to coagulate tissues and there is ongoing research on using lasers to close wounds and seal tissues. However, only a handful of lasers can be used to cut tissue clinically.

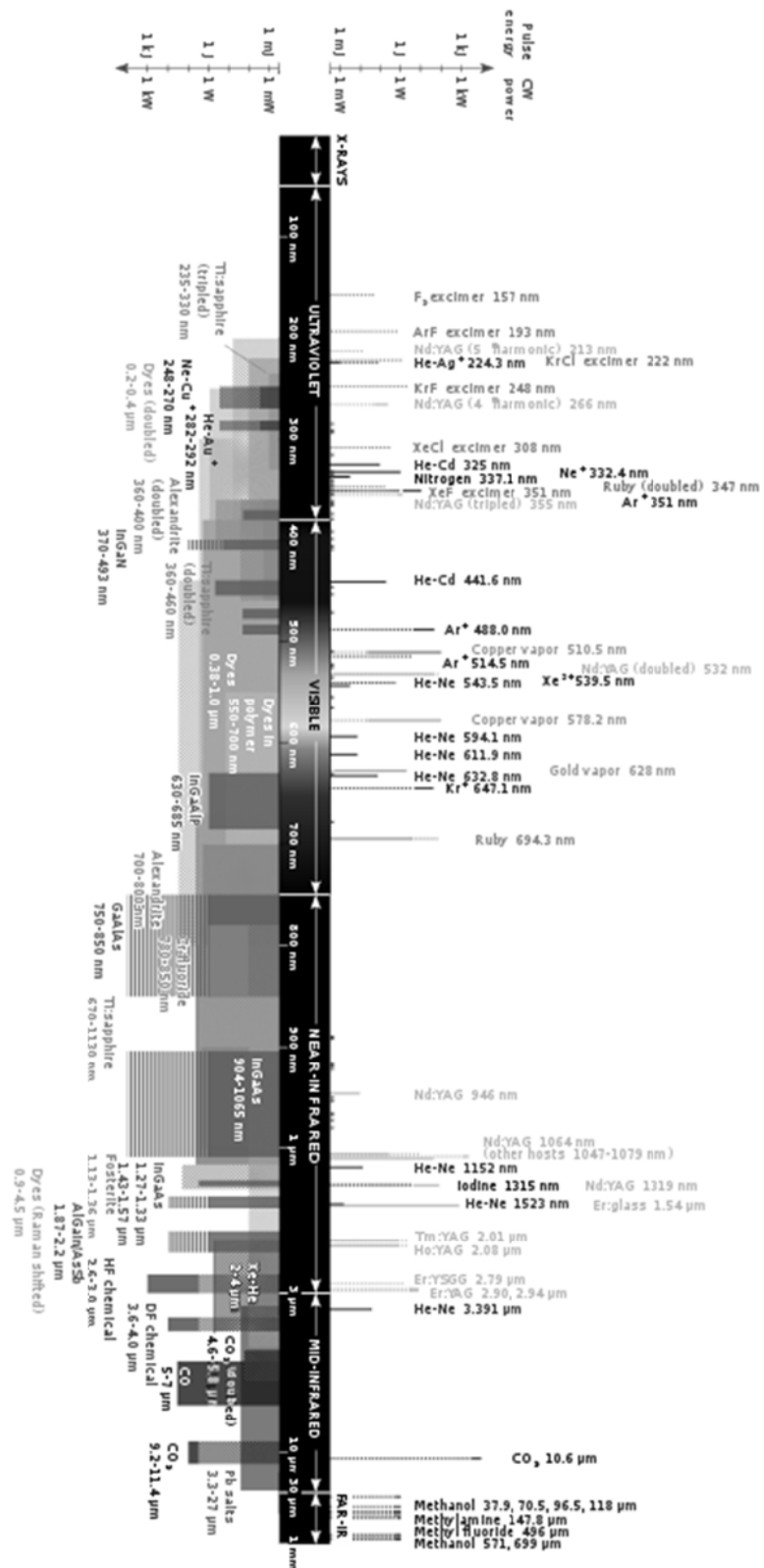


Figure 2-5. Common lasers and their wavelengths. (Reproduced from [249].)

Excimer lasers emit light in the ultraviolet (UV) region of the spectrum and are well known for their use in laser eye surgery to resurface corneal tissue. These “excited dimer” gas lasers interact with tissue photochemically (except for longer wavelength excimers at 248, 308 and 351 nm which interact photothermally), [250] imparting energy directly to breaking chemical bonds and causing tissue to disintegrate into the air. Because cutting is achieved through the photochemical effect, very little heat is generated that could thermally damage tissue.

The argon fluoride laser (which has a wavelength of 193 nm) is used for corneal surgery whilst the krypton fluoride and various other excimer lasers have been used for laser angioplasty.

Excimer lasers also can cut tissue by the photomechanical effect, although this usually is an unwanted side-effect.

In excimer laser angioplasty, rapid absorption of the laser light by blood can form vapour bubbles which subsequently collapse and cause acoustomechanical cavitation damage to the blood vessel walls. This can lead to accidental dissection of blood vessels leading to haemorrhage and worse. To mitigate this problem, Deckelbaum et al. reported in 1995 on the use of saline infusion to dilute the blood and lower the risk of accidental tissue dissection. [251]

Although the holmium:YAG laser (which has a wavelength of 2.1 μm) used for shattering gallstones commonly is thought to function by the photomechanical effect, there is evidence to suggest that this is secondary to a dominant photothermal effect. [252] Some experiences with this laser were reported by Teichman et al. in 2001 after they delivered 0.6-1.0 J of laser energy to the gallstone surface at 6-10Hz using an optic fibre to shatter them. [253]

Direct laser cutting of tissue in a form that more resembles the laser scalpels of science fiction typically is performed using three lasers —the CO₂ laser (10.6 μm), the Er:YAG laser (2.94 μm) and Ho:YAG laser (2.1 μm).

These lasers emit light in the infrared region of the spectrum which is highly absorbed by water, the major component of soft tissues. Infrared radiation also is well absorbed by hydroxylapatite, a calcium-based mineral that is found in bone, allowing these lasers to be effective for cutting bone and dental enamel as well. Deppe and Horch reviewed the use of CO₂ and Er:YAG laser in oral surgery in 2007. [254]

Although the CO₂ laser is the ubiquitous medical laser for cutting in open and laparoscopic surgery, there are problems with this laser at endoscopy because few suitable methods exist to transmit the laser through a flexible endoscope.

Normal fused silica-based optic fibres have high absorption at 10.6 microns and are unsuitable for transmitting and directing CO₂ laser light. Typically, CO₂ lasers are used together with articulated arms housing gold mirrors to direct the 10.6 μm light to the target. However, these can be awkward to use, even at open surgery. All are far too large and cumbersome to be passed down the operating channel of a clinical endoscope.

Hollow fibre optics has been used, and Raanani et al. reported in 1997 their experiences with a hollow fibre and a CO₂ laser to harvest the internal mammary artery for cardiac bypass surgery. [255] However, most of these fibres readily available are too large and too inflexible to fit down even the largest working channel of a flexible endoscope.

In 2002, Temelkuran et al. described their fabrication of a thin, hollow fibre optic lined with an interior omni-directional dielectric mirror that could efficiently guide light at the CO₂ laser 10.6 μm. [256] OmniGuide (OmniGuide; Cambridge, MA, USA) has commercialized the technology produces the BeamPath flexible photonic band-gap fibres.

The Nd:YAG solid state laser (1064 nm) also has been used for tissue ablation, although this laser struggles more to cut tissue because absorption by intrinsic tissue chromophores is much less than at the wavelengths of the other YAG lasers mentioned above or by the CO₂ laser.

Typically, the low absorption is compensated for by increasing overall power or using high intensity, high repetition rate pulses.

Price et al. reported in 2007 Nd:YAG laser ablation of a lesion on a patient's vocal cords with 30 W of laser power. [257]

Sato et al. reported in 2001 the use of nanosecond, high intensity pulsed ablation by using a Q-switched Nd:YAG laser to cut porcine myocardium tissue. [258] Based on optical and acoustic emissions as well as histological data, they concluded that laser ablation at 1064 nm predominantly was due to photodisruption.

In general, the tissue effects of short duration nano, pico and femto-second pulsed lasers appears to be a popular research area and is represented by the large number of published articles in the literature.

The KTP / frequency doubled Nd:YAG laser (532 nm) is another popular laser, with its distinctive green light output. Saito et al. reported in 1999 the use of the KTP laser for tonsillectomy in human patients. [259] They cited as the benefits of the KTP laser the faster cutting speed compared to the YAG laser and better coagulation capabilities compared to a CO₂ laser.

The Er:YAG laser transmitted by ZrF fibres also has been used for tissue ablation. Although ZrF exhibits high optical transparency at mid-infrared wavelengths, it is expensive, fragile, and not very forgiving of bending in tight curves.

2.3.7. Chemically assisted mechanical dissection of tissue

In an isolated study, Sumiyama et al. reported in 2008 the use of mesna (sodium-2-mercaptoethanesulfonate) to chemically assist mechanical dissection of submucosal gastric tissue in pigs. [260] This mucolytic drug normally is used to reduce mucus viscosity and as an uroprotective in oncology.

Although the chemical injection was not directly responsible for separating the tissue layers, the investigators reported that it significantly enhanced the technical ease by which submucosal dissection was performed with a blunt dissection balloon.

2.4. Directing where the cut occurs

While a lot has been written in the literature describing various methods to cut tissue (although many of these schemes didn't appear to be readily compatible with flexible endoscopy), the search for ways to control where the cut occurred was much more difficult and yielded fewer results. Key methodologies found in the literature for controlling dissection are presented.

2.4.1. Sensitizing tissues with chemicals

Chemicals and drugs have been used in clinical practice that target specific cell types as well as enhance ablation in schemes that require multiple factors to be present to function.

Some methods depend on the increased uptake of chemical substances by targeted cells to “direct” the treatment to desired locations in the body.

For example, photodynamic therapy can use light-sensitizing porphyrin drugs, carbon nanotubes or gold nanoparticles that preferentially accumulate in cancer cells to effectively tag them for treatment. When these photosensitized cancer cells subsequently are exposed to laser light, they are destroyed in larger numbers than normal cells due to the higher concentration of the photosensitizing drugs inside them. PDT techniques have been described abundantly in the literature.

One interesting paper by Roy et al. from 2006 described laser-illuminating gold nanoparticles placed into target cells to nucleate photoacoustic cavitation. It is not too far a stretch to imagine a technique for particle-mediated tissue cutting based on photodisruption. Of course, the devil would be in the details in order to move the idea towards a clinically viable technique.

Chemicals also can be injected directly into tissue for direct targeting of pathology.

Chen et al. in 1996 injected indocyanine green (ICG) dye into mouse mammary tissue to increase the photothermal interaction with an 808 nm diode laser. [261] Hino et al. in 2001 injected ICG into tissue surrounding varices at the oesophagogastric junction to coagulate tissue in human patients. [262]

A number of other groups have used ICG to enhance laser ablation of tissue.

Mills and Laufer from the Medical Lasers and Endoscopy group at UCL and Essenpreis from Roche Diagnostics GmbH in unpublished work, used ICG to enhance 805 nm laser drilling through the *stratum corneum* layer in the skin for blood sugar monitoring.

Arai et al. published four papers in 1997 – 2001 describing their use of ICG to enhance 805 nm laser ablation in harvested canine and porcine stomach, percutaneous lumbar disc decompression in canine model, as well as a feedback-controlled system that monitored the presence of ICG dye to control laser activation. [263][264][265][266]

In these papers, they proposed that ICG had two main effects on the tissue — it sensitized the tissue by increasing light absorption and enhancing the photothermal effect for ablation, and it shielded underlying tissues from the laser.

Because a large part of the work in this thesis is focused on dye-mediated laser ablation, the author contacted Professor Arai to inquire about more recent work in this area. It was revealed through the correspondence, however, that no further work had been conducted beyond the published papers after his graduate student, Dr. Hayashi, had completed medical school.

Yamashita et al. also reported in 1999 ICG-mediated laser EMR in canine model at laparoscopy and human patients at transanal endoscopic microscopy (TEM). [267]

2.4.2. Feedback control

Some schemes for feedback control to guide electrosurgical dissection were found in the literature. Found patents describe controlling cutting using tissue impedance (EP1810633), using probe motion as measured by accelerometers (US7235072), and using tissue temperature (US7297143) as signals for feedback control. As typical of most patents, while broad and general concepts were claimed, specific details on implementation were lacking and empirical data justifying the claims were scarcer still.

On a more speculative note, one could imagine coupling various existing technologies for diagnostic visualization with feedback mechanisms to control cutting. Techniques such as reflectance spectroscopy, electrical impedance tomography and endoscopic ultrasound conceivably could be used to control and direct cutting tools.

However, the value proposition of adding such complexity to the system in order to control dissection tools might not be very good when considering the alternatives that are available in open and laparoscopic surgery. Surgeons are quite adept at directly controlling cuts with their bare hands in these surgical domains.

However, when one considers how hard it is to cut accurately at flexible endoscopy, the value proposition becomes much more interesting and the added complexity becomes perhaps more compelling.

2.4.3. Articulation

Much of the current ESD and NOTES research to control how and where tissue dissection occurs has been invested in designing articulation platforms that provide triangulation and stability to existing endoscopic cutting tools.

New devices such as the R-Scope from Olympus Medical, the Transport Surgical System from USGI and the Direct Drive Endoscopic System from Boston Scientific feature much greater scope and instrument articulation capabilities that go far beyond that of the current generation of endoscopes.

The R-Scope incorporates two elevators to allow instruments in the two working channels to be deflected independently. Also, a second bending section in the scope has been added to allow the distal end to double bend into an 'S' shape configuration.

The Transport Surgical System features three cannula at its the distal end that are independently steerable, and a proximal section that uses ShapeLock technology to freeze the scope into any shape. Being able to toggle between flexible and rigid states allows the device to be flexible for intubation and rigid for device stability and force transmission through the cannulae. [215]

The Direct Drive Endoscopic System is similar to the Transport Surgical System in that it also has three ports to accommodate two instruments and a scope. It also has accessory rails to support the attachment of interchangeable instruments controlled by ergonomic drive handles. [216]

It probably is not inappropriate to speculate that more next-generation articulation platforms and more capable endoscopes may be in development pipelines, being incubated, further developed and patented before they are revealed to the general public.

The author spent two years previous to the PhD research developing miniaturized mechanical systems for manually controlled articulating instruments that are compatible with the current generation of flexible endoscopes (see Figure 2-6).

The research was focused on developing a number of core technology platforms for articulating generic end-effectors, and as such could be mated with cutting end-effectors – electrosurgical needle-knives, mechanical scissors, laser apertures or ultrasonic dissectors – or any of a number of other instruments like as graspers, retractors or cameras. Much of this work is accessible in published US patent applications which can be found online. [268][269][270][271][272][273][274]



Figure 2-6. A number of articulating devices for flexible endoscopy that were designed by the author from 2004 to 2006. (Personal photographs.)



Figure 2-7. A 3.2mm diameter articulating grasper with an “intuitive” control interface. (Personal photograph.)

Based on the author’s experience, a number of technical issues possibly constrain the potential solution space and potentially limit the performance envelopes of these devices. These issues include problems with volume and size limitations, material performance and cost constraints, force transmission problems and mechanical issues such as cable stretch, wire twisting and gear backlash.

Still, scientists and engineers are renowned for innovating their way past technical constraints, and no doubt these articulating instruments will one day be as dexterous as the human hand.

2.4.4. Diathermy dissection control by electrode geometry

Another strategy for cutting control has been to incorporate safety features in the cutting devices themselves to help limit where the cutting action can occur. Innovations employing this strategy can be seen in the design of tools for endoscopic submucosal dissection (ESD).

The IT knife incorporates a ceramic ball at its tip to reduce the chance of an accidental plunge cut through tissue with electrosurgical current. The TT and hook knives recreate at flexible endoscopy the retract-and-cut strategy used in open and laparoscopic surgery to limit cuts to tissue that has been hooked and pulled back by the probe. The FlexKnife uses an insulating polymer sheath to control the depth of cut by limiting the length of the exposed electrode.

2.5. Chapter Conclusions

Through the years, many instruments have been devised for cutting tissue in an endoscopic environment, and these devices have been described and documented thoroughly in the literature. Keyword searches for cutting instruments and modalities as well as an in-depth review of major clinical and scientific journals were conducted to survey the breadth and status of cutting instruments and control system in surgery.

In general, cutting implements in medicine function either by mechanical means or by nonmechanical means. Mechanical cutters cut through the shearing and abrasion of tissue, e.g. scalpels, scissors, powered debriders, dissecting balloons and waterjets. Nonmechanical based methods impart energy of various forms that eventually disrupt the tissue with shockwaves or explosive vaporization of water in the tissue, e.g., radiofrequency electrosurgery, laser ablation and ultrasonic / harmonic cutting.

Different devices that employ different methods to cut tissue have different performance capabilities and characteristics.

Currently, at flexible endoscopy, the most common cutting devices are mechanical or electrosurgical in nature. Of these two categories of devices, the less capable mechanical cutting devices are more common. Mechanical devices typically are used for simple biopsies and snaring of tissue or for grabbing and positioning tissues in more complicated procedures.

While scissors, essential cutting instruments in open and laparoscopic surgery, do exist for flexible endoscopes, they perform poorly and are widely disregarded in the clinical community.

Other modalities for cutting that have been reported in the literature typically exist outside of flexible endoscopy at open or laparoscopic surgery or in a research environment in experimental preclinical or clinical work. Example modalities include waterjet cutting, laser ablation, dye-mediated laser ablation and feedback-controlled electrosurgical cutting.

However, the literature search did not reveal any new developments in non-electrosurgical tissue cutting methods at flexible endoscopy between 2003 and 2010.

The bulk of electrosurgical instruments consist of pure diathermy devices like needle-knives and sphincterotomes, and electrically-assisted mechanical devices such as hot forceps and hot snares. A number of innovations have been made to the needle-knife to increase safety and improve cut control when used for ESD procedures.

Other strategies to control tissue cutting at flexible endoscopy generally have come in the form of improving the articulation range of motion by providing more degrees-of-freedom in the devices or the scopes. However, the increased range of motion usually comes at the expense of more difficult ergonomics and usability as more capable devices usually are harder to control.

Robotics has been proposed as a method to improve control of the cutting instruments at flexible endoscopy, and have been implemented in at least one commercial system – the EndoVia endoscopic robot (Hansen Medical). However, robotic solutions increase device complexity tremendously and usually come at a huge cost as well.

A few reports have been found in the literature of chemicals to sensitize tissue for enhanced laser ablation. However, it appears that the main research group in this area has been dissolved and have not continued any further research.

Patents have been found on the topic of feedback control of electrosurgical diathermy systems, but details and data on actual embodiments and practice are not readily available.

Overall, based on a review of the literature, there appears to be ample white space available for research into new methods for the control of tissue cutting at flexible endoscopy.

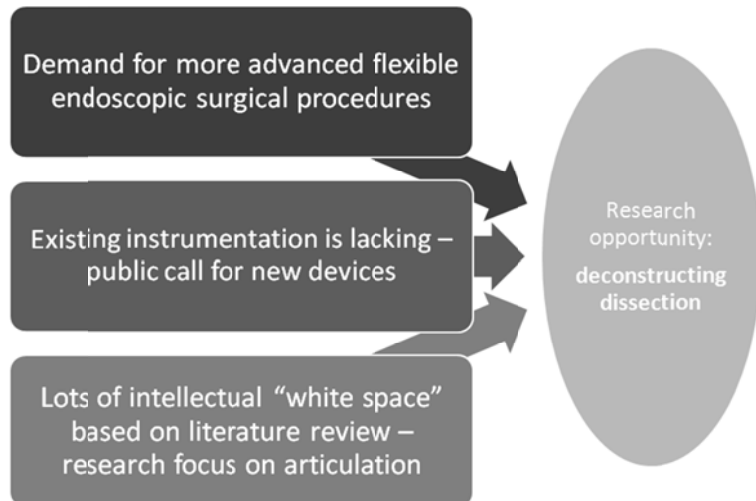


Figure 2-8. Research opportunity based on the literature.

Chapter 3: Deconstructing dissection and an exploration of concepts

Give us the tools, and we will finish the job.

Sir Winston Churchill

3.1. Chapter Overview

Based on the expressed physician desires and unmet needs for endoscopic surgery presented in Chapter 1, and the literature survey of available tissue dissection methods and control schemes reviewed in Chapter 2, we concluded that new approaches to cutting tissue at flexible endoscopy are desirable and possibly necessary in order to enable advanced intraluminal surgery and NOTES.

This chapter introduces a new strategy called “deconstructing dissection” and two tactics for achieving controlled cutting of tissue — sensitization and protection.

An exploration of the solution space was performed through thoughtful brainstorming and exploratory experimentation, and the majority of concepts studied could be classified as either sensitization or protection. A third, miscellaneous category is used as a catchall for all other brainstormed ideas that didn’t fit into the first two categories.

The most promising ideas for achieving controlled cutting by deconstructing dissection are presented along with preliminary experimental data and thoughtful discussion to examine the feasibility of each idea.

These data, along with educated guesses on the availability of research equipment and materials, predictions for biocompatibility, thoughts on patient safety and an evaluation of available advisory expertise, taken together with subjective metrics for the level of scientific content and the author’s own personal research desires form the basis by which one method was chosen for further study.

Based on these metrics, the dye-mediated laser ablation approach to controlled tissue dissection was chosen as the main concept to pursue in depth. This research towards dye-mediated laser ablation is presented in subsequent chapters.

3.2. Dissection, deconstructed

3.2.1. Dissection as simultaneous targeting and cutting tasks

Endoscopic surgery is hard! As surgeons attempt to perform more complicated surgeries through smaller incisions, the actual techniques needed become harder and harder and more technology is required that is interposed in between the surgeons and their patients.

In minimally invasive surgery, surgeons simply aren't able to perform procedures directly with their hands, but instead must do so through technological proxies. Unfortunately, these technologies oftentimes have complicated user interfaces coupled to limited mobility and articulation capabilities.

Present efforts to improve technology for advanced endoscopic surgery and NOTES are focused mainly on inventing more capable articulation platforms that recreate at flexible endoscopy the capabilities of a skilled pair of surgeon's hands.

While this approach is a perfectly reasonable one, it perpetuates the existing conceptual construct that considers cutting to be the simultaneous performance of targeting and cutting tasks.

In other words, successful cutting can be thought of as requiring simultaneous application of a means for positioning and a means for tissue dissection, and both processes must work together correctly, effectively and concurrently. If either or both processes fail, the result at best is no incision, and at worst, a misplaced incision (see Table 3-1).

Table 3-1. Outcomes matrix of success / failure of cutting and control capability during endoscopic cutting.

Outcomes matrix		Cutting means (e.g., mechanical, diathermy, laser)	
		Successful cut	Failed cut
Control means (e.g. hands, articulation, robotics)	Successful control	Successful incision	<i>No incision</i>
	Failed control	Misplaced incision	<i>No incision</i>

While no incision is the better of the two failure outcomes, this can be very frustrating for the surgeon or physician. Repeated failures might subconsciously entice the doctor to take more risks in order to successfully make an incision, or alternatively to give up the procedure

altogether. Both of these fight-or-flight responses have been witnessed by the author while observing veteran doctors working in pre-clinical experiments in porcine models.

3.2.2. Breaking apart dissection into sequential tasks

In this thesis, what is proposed is a new way to think about dissection, to deconstruct it into a control task and a cutting task that instead of being performed simultaneously are completed sequentially, one after the other.

By doing so, this strategy of deconstructing dissection potentially affords us the capability to optimize the ease, efficacy and safety of the targeting and cutting tasks separately. By decoupling targeting from cutting, new opportunities are exposed for doing each task better, faster and safer.

On the other hand, the biggest potential cost probably comes from increased procedure time and complexity, as sub-tasks previously performed simultaneously surely must take longer when performed sequentially.

However, it could be argued that any increases in procedure time and complexity incurred in a technique that successfully cuts most of the time might still be faster than combined time needed for multiple attempts at cutting with a less controllable, less reliable method.

If with current technology it is almost impossible to target and cut at the same time at flexible endoscopy, perhaps it is worthwhile to consider doing them separately.

Slow and steady might trump fast and careless, but hypothetical comparisons are meaningless unless specific clinical procedures are compared. Still, the potential benefits are attractive enough to justify further investigation.

Could a separate and distinct targeting task in deconstructing dissection allow for new ideas to be useful at flexible endoscopy? For example, does a separate targeting task allow for new ways to demark *en bloc* areas of tissue to be cut?

Snap lines that lay down chalk allow for quick one-dimensional marking in building construction. Rubber stamps for marking the date and photolithography techniques in microchip fabrication enable fast two-dimensional imprinting of predetermined patterns onto substrates. Could similar ideas from other disciplines be employed to demark areas to be cut or protected at flexible endoscopy?

Alternatively, methods to draw pre-defined shapes like lines, curves, circles and rectangles potentially could be used to make up a basic vocabulary by which more complicated patterns could be derived. As one would do in art and architecture with stencils and French curve templates, could one potentially build up complex cutting paths from very simple building blocks?

On the cutting side of the equation, an important prerequisite of the cutting technique for the deconstructing dissection strategy to work would be an inherent cutting selectivity that followed or avoided paths and areas pre-specified by the targeting task.

Some sort of physical interaction that gated whether cutting would occur would be crucial so that precision control during the cutting task would not be necessary. This may be obvious, but it is important to mention. Otherwise, application of the deconstructing dissection strategy would simply result in precisely tracing the desired cutting path twice!

(Although from personal observation of many clinical and experimental procedures at flexible endoscopy, doctors currently do exactly this — they practice tracing the path they want to take with the endoscope a couple times before actually cutting the tissue.)

In the best case, a strong interaction between targeting and cutting could allow the cutting task to be completely untargeted.

For example, an interaction akin to photodynamic therapy in which a diffuse light source activates light-sensitizing drugs that have been preferentially absorbed by diseased tissue would be fantastic. Although the degree of selective uptake by cancer cells of PDT drugs is rarely useful clinically, if this could be greatly enhanced, then there would be no need to steer the laser light during treatment.

Likewise, if a cutting technique employed a similar interaction conceptually, then once the marking drug has been laid down, theoretically there would be no need to steer the cutting laser for tissue dissection.

Also consider the following interaction between targeting and cutting:

The targeting task could consist of laying down “railroad tracks” which then guide the cutting task. Like the steam engine, which blindly follows where the tracks go, no directional controls would be necessary for a cutting technique that did this.

After the targeting task has been completed, the only controls necessary for the cutting task would be an accelerator and emergency brakes.

Specific ideas for how to realize the deconstructing dissection strategy will be discussed later in the chapter. However, in the process of brainstorming ideas, a natural division organically appeared for how the ideas achieved the results.

From a conceptual standpoint, the ideas seem to cluster around two tactics for how they achieve selective cutting — either (1) sensitizing where the cut should be or (2) protecting areas of tissue from being cut.

3.2.3. The sensitization tactic

The sensitization tactic is all about finding ways to make tissue cutting a multi-factor process that can occur only when all factors are present.

Whatever factor is reserved for the cutting task cannot function successfully without the presence of the other factors that are deployed during the targeting task. Conversely, the factors placed during the targeting task cannot cut the tissue without the addition of the final factor introduced in the cutting task.

For example, again consider PDT. It is not a method for cutting tissue, but what is interesting to us is how it functions through the interaction of the drug and the laser. The technique depends on the presence of both factors to work. Each, on its own, is relatively harmless. Only the combination of the two results in the desired effect.

Now consider a cutting technique that used a similar interaction to function — similar not in the actual physics of creating singlet oxygen to destroy cells, but in the co-dependency of the drug and laser to get the desired effect. One could imagine deploying the drug with a rubber stamp like device in the targeting phase, and then blanketing the tissue with laser light in the cutting phase.

This tactic confers several potential advantages.

Because the demarcation task is performed separately from the cutting task, errors made during the demarcation task do not pose an immediate threat to the patient. Also, the cutting task is made more robust because the dissection paths have already been defined previously in

the demarcation task and it is less dependent on (and ideally independent of) control issues encountered during the cutting task.

Also, by splitting up dissection into targeting and cutting, this affords us the opportunity to optimize these subtasks independently in new ways that may not be possible otherwise.

For the demarcation task, a potential area for optimization is the ability to draw *en bloc* predefined geometries like ellipses and rectangles of various sizes by using rubber stamps, silk screening, photolithography or a tattooing technique.

For the cutting task, increasing the potency of the “gating” factors deployed in the targeting phase to a great level could enable cutting to occur completely un-aimed.

3.2.4. The protection tactic

The protection tactic is all about setting boundaries and protecting tissues from being cut. While the sensitization tactic involves identifying and sensitizing paths and areas of tissue to be cut, the protection tactic involves isolating and protecting areas of tissue where cuts are not to occur.

This primarily is accomplished by erecting a barrier, which denies the cutting means some factor crucial to how they can cut.

This could involve something as simple as deploying a physical barrier that impedes the movement of a cutting blade. Something like a stencil bonded onto tissue could be used to limit the motions of a scalpel-like device similar to how a metal stencil constraints the possible motions of a pencil.

Another form of protection could be liquid injections into the tissue that solidify to act as physical barriers and block cutting beyond a predetermined depth.

Or conductive or insulating materials could provide electrical protection, shaping how electrical currents from an electrosurgical generator flow through tissue and directing it away from areas to be protected.

One potential advantage of the protection tactic is that because it is inherently a tactic to disrupt and disable factors necessary for a cutting technique, this technique that could be an existing, clinically proven cutting method such as diathermy or bladed cutting.

Being able to augment and adapt an existing cutting method could give the protection tactic a time and developmental advantage.

3.2.5. Other concepts

Ideas that didn't quite fit into either the sensitization or the protection groups were lumped together in a catchall bucket. These include ideas for new mechanical cutting devices and concepts for feedback control using a variety of sensing methods. They are presented in this thesis for completeness, as the author felt that all ideas and experiences shared could inspire and assist future investigators in developing new procedures and technology for minimally invasive surgery.

3.3. Overview of concepts

What follows next are descriptions, experiments and discussions of the concepts investigated for deconstructing dissection. The main goal was to select one scientifically interesting concept for further study.

The experiments described in this chapter are not meant to provide conclusive evidence as to their viability, but rather to help filter ideas and guide the selection of one for further study.

An overview of the concepts described in the next sections is given in Figure 3-1.

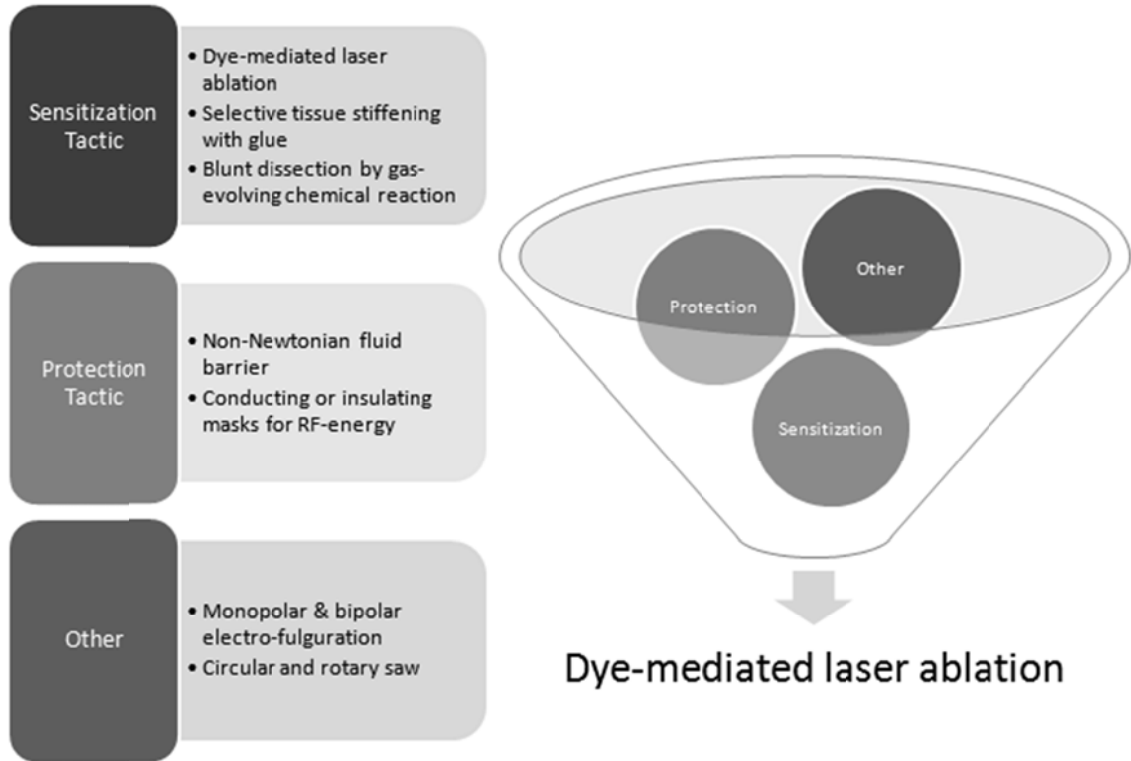


Figure 3-1. An overview of concepts explored for deconstructing dissection. Sections 3.4-3.10 explain and discuss each concept in depth, and section 3.11 compares the concepts against each other.

3.4. Dye-mediated laser ablation

3.4.1. Using dyes to sensitize tissue

Chemicals have been used in medicine in the past to sensitize tissues to laser light, although specific reports on dye-mediated ablation were scarce and rather hard to find.

A literature search revealed that indocyanine green (ICG) dye has been used to increase absorption of 805nm laser light and enhance the photothermal effect to allow low-power semiconductor infrared lasers to ablate stained tissues. [263][264][265][266][267]

The majority of these reports were authored by members of a Japanese research group lead by Prof. Tsunenori Arai, currently of Keio University in Tokyo, Japan. Personal correspondence with Prof. Arai revealed that they stopped research in this area after his graduate student at the time, Dr. Hayashi, graduated from medical school.

The method of ICG sensitization used is similar in all these reports. Typically, the researchers injected dye into tissue with a needle to sensitize it, and then the tissue is irradiated with laser light to induce either tissue coagulation or ablation. Delivery of the laser light is by a fibre optic

either placed interstitially inside the tissue or positioned outside of the injection site for non-contact irradiation.

These papers focused on the clinical aspects of the procedure feasibility and not on the physical mechanism for how the laser ablation occurred. Arai et al. also investigated feedback control based on laser light backscattered from the tissue.

All of the groups described whole-scale staining of tissue with the dye injection rather than precise deployment to control the location of cuts. And there was no discussion of whether dye erasure was possible in case of mis-deployment.

These factors taken together made it appealing to investigate dye-mediated laser ablation for deconstructing dissection.

3.4.2. Dye potentiation of low-power lasers for laser ablation

A series of proof-of-concept experiments were conducted to confirm that dye-mediated laser ablation was possible.

The general concept is to introduce an extrinsic dye to tissue in locations where cutting is desirable in order to greatly enhance heat generation from absorbed laser light. If the light absorption and heat generation could be increased sufficiently by the dye, explosive vaporization of inter- and intra-cellular water would occur resulting in tissue ablation. Areas without the dye ideally would not be affected by the laser.

Three commonly used medical dyes already approved for human use for a variety of medical procedures were considered — indocyanine green (ICG), methylene blue (MB) and fluorescein. Absorption spectra for the three dyes (with oxy- and deoxy-hemoglobin spectra for comparison) are shown in Figure 3-2.

The ICG, MB and Hb data were compiled by Dr. Scott Prahl from the Oregon Medical Laser Centre, [275][276][277] and the fluorescein data are from PhotochemCAD. [278]

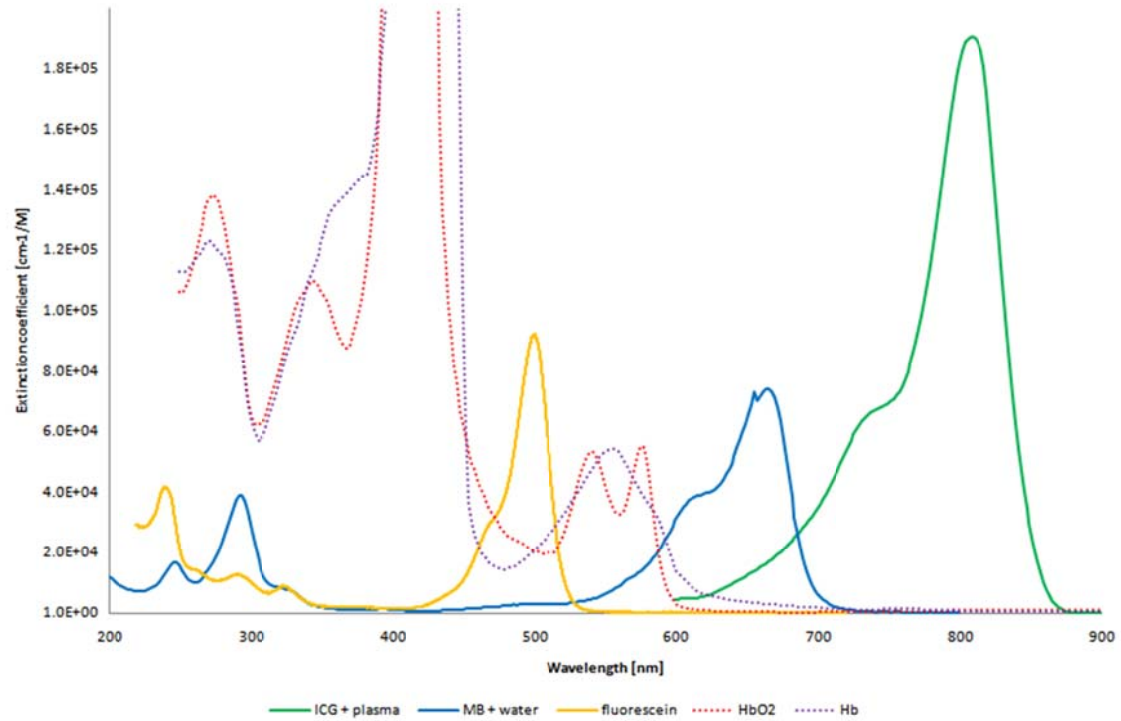


Figure 3-2. Extinction coefficient vs. wavelength for ICG, MB and fluorescein (also oxy- and deoxy-hemoglobin for comparison).

Medical lasers were sought that output light at wavelengths near the absorption peaks of these three dyes. Matching dye absorption peaks with laser wavelengths maximized the impact the addition of dyes to tissue would have on potentiating light absorption and increasing the likelihood of ablation.

Unfortunately, only two lasers were available to the author for research use — an 805 nm Diomed laser (25 W maximum) (Angiodynamics Co; Queensbury, NY, USA) and a 10.6 μm Shanning carbon dioxide laser (30 W maximum) (Shanning / Visual Investments, Ltd; London, UK). Very limited access to a 652 nm Diomed PDT laser (2 W maximum) (Angiodynamics Co; Queensbury, NY, USA) also was obtained.

For these experiments, the 805 nm Diomed laser was paired with ICG which has a corresponding absorption peak at 805 nm, and the 652 nm PDT laser was used with MB which has a peak absorption wavelength of 668 nm. The carbon dioxide laser could be used as an ablation reference standard.

Unfortunately, the lack of an available blue-green laser to match the 500 nm absorption peak of fluorescein meant that we had to rule out any serious work with this dye.

Methods

These experiments were designed to determine whether or not dye-mediated laser ablation was possible with ICG and MB dyes. The maximum available power from each clinical laser was used. Dwell time allowed was the time it took for the onset of ablation up to a maximum of 9.9 s, whichever came first.

9.9 s was chosen because it was the maximum exposure time possible with the particular operating mode we used on the Diomed 805 nm laser. But more importantly, it was felt that a dwell time longer than 10 second in any particular spot would be too long and not competitive with other existing dissection methods.

Fresh chicken thighs obtained from the local supermarket were used as the tissue model. Store-bought meat was inexpensive and readily available providing us with a relatively fresh tissue model that had been drained of blood. Only refrigerated tissue labelled as “fresh / not frozen” was purchased and used immediately. UK food standards require meats to be refrigerated at below 8° C and recommend temperatures between 0-5° C.

Ablation results were graded visually by the author with the following criteria:

“Ablation” was defined as the appearance of a visible crater with or without signs of carbonisation. “Coagulation” was defined as the appearance of whitening of the tissue, but without the formation of a visible crater. “No effect” was defined as no visible changes on the tissue.

The first dye to be used was ICG.

Two concentrations of ICG were used — 1 mg/ml and 5 mg/ml (w/v). This was applied topically to the chicken leg muscle and allowed to form into a small pool on the tissue surface.

A Diomed 805 nm laser was used at the maximum 25 W of power to expose the tissue with an approximately 2 mm diameter spot. However, only 16.5 W of power was measured exiting the fibre tip using a thermopile power meter, which corresponded to an irradiance of 530 W/cm².

Unstained tissue also was exposed to laser light under the same conditions.

Methylene blue then was used to sensitize tissue for ablation.

Two concentrated solutions of MB – 1 mg/ml and 11 mg/ml (w/v) – were applied topically to chicken muscle tissue and allowed to form into a small pool on the tissue surface.

A Diomed 652 nm PDT laser, which has a calibrated laser output of 2 W, was used at maximum power to illuminate the MB stained tissue with a laser spot size of about 1 mm diameter. This corresponded to an irradiance of 250 W/cm².

Unstained tissue also was exposed to laser light under the same conditions.

The Diomed 805 nm laser also was used with MB dye using the previous experimental setup for ICG ablation, substituting MB for the ICG.

Finally, the chicken muscle was ablated using the CO₂ laser as a control. Since 10.6 μm light is highly absorbed by water, which is the largest component of tissue, the addition of dyes was not necessary. The 30 W self-calibrated laser output illuminated the tissue with a ~3 mm diameter spot. This corresponded to an irradiance of 420 W/cm².

Results

The overall results of the experiments are summarized in Table 3-2:

Table 3-2. Results of dye-mediated laser ablation.

Dye	Laser	Result (dye concentration, runs)
-	Carbon dioxide 10.6 μm laser (30 W maximum)	Ablation (n=5)
-	Diomed 805 nm laser (25 W maximum)	No effect (n=5)
Indocyanine green	Diomed 805 nm laser (25 W maximum)	Ablation (n=10)
Methylene blue	Diomed 805nm laser (25 W maximum)	Ablation* (5 mg/ml, n=5)
-	Diomed 652 nm PDT laser (2 W maximum)	No effect (n=3)
Methylene blue	Diomed 652 nm PDT laser (2 W maximum)	Coagulation (1mg/ml , n=5) Ablation (11mg/ml , n=3, t >> 9.9 s)

* No effect, then the appearance of carbonisation and then sustained ablation.

See the results below and the discussion in Section 3.4.6.

For tissue stained with ICG, in all cases (n=10) at 25 W set power with 1 mg/ml or 5 mg/ml concentration ICG, ablation was observed with a margin of coagulation around the edges of the crater. A copious amount of char formation within the crater was observed, manifesting as islands of carbonisation surrounded by regions of desiccated tissue (see Figure 3-3). The white

desiccated region appeared dried and shrunken with a broken, irregular surface reminiscent of cauliflower.



Figure 3-3. A linear incision made an 805 nm Diomed laser in chicken tissue stained with ICG. Features of the ablation crater are typical of ICG-mediated ablation.

All cases of unstained tissue ($n=5$) exposed to 9.9 s of 805 nm laser light at 25 W set power showed no signs of any visible changes.

For tissue stained with MB, ablation was observed ($n=3$) at 2 W of power using the higher concentration of MB (11 mg/ml) to stain the tissue (see Figure 3-4). A dark, charred crater could be observed surrounded by a faint whitening of tissue around the periphery of the crater. However, this was hard to distinguish from natural variations in shade of the very dark colour of the higher concentration MB solution.

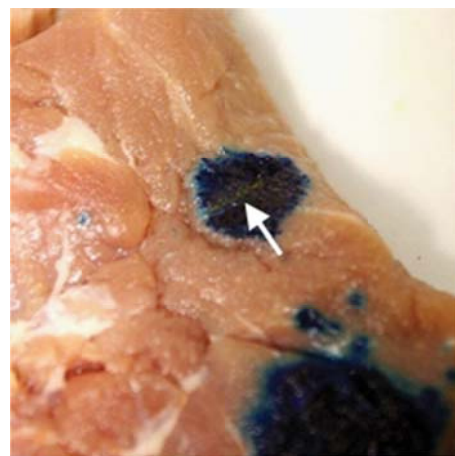


Figure 3-4. Tissue stained with the higher concentration (11 mg/ml) MB was ablated when exposed to the laser.

Tissue stained with the lower concentration of MB (1 mg/ml) was coagulated (n=5) when exposed to the 652 nm PDT laser with a maximum exposure of 9.9 s (see Figure 3-5). This was clearly visible as a whitening of the tissue, which was easy to see through the less intense and more transparent blue of the lower concentration MB solution.

When the 9.9 s experimental time limit was lifted, occasionally the tissue could be ablated. When ablation was observed, this process took on the order of tens of seconds to occur.

Initial vaporization of the dye pool on the surface of the tissue was followed by a period of relative calm. After tens of seconds, carbonization would be observed along with a smoke plume and an enlarging ablation crater.

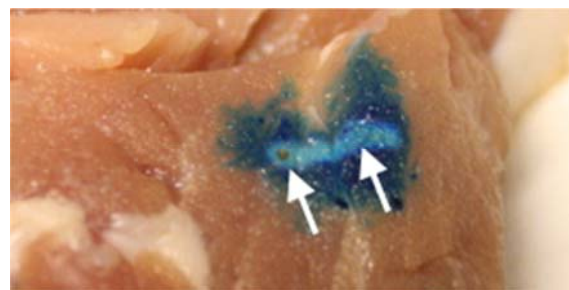


Figure 3-5. Tissue stained with the lower concentration (1 mg/ml) MB typically was coagulated when exposed to the laser (right arrow), although occasionally ablation was observed (left arrow). However, when ablation was observed, the process took tens of seconds to occur, which is above the 9.9 s exposure time limit set in these experiments.

All cases of unstained tissue (n=3) exposed to 9.9 s of 652 nm laser light at 2 W power exhibited no visible changes.

MB stained tissue exposed to the Diomed 805 nm laser displayed signs of ablation (n=5) in a process that appeared similar to MB-mediated ablation using the lower concentration MB solution (see Figure 3-6).

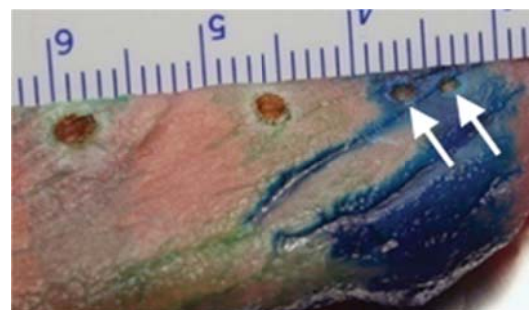


Figure 3-6. MB-stained tissue ablated by an 805 nm Diomed laser.

Initial vaporisation of the pool of dye was followed by a period of relative calm (a few seconds) followed by carbonisation and the formation of an ablation crater with a corresponding smoke plume. Islands of carbonisation could be found within the ablation crater surrounded by small regions of desiccated tissue. A thin annulus of coagulated tissue could be found beyond the ablation crater.

Finally, all unstained tissue ($n=5$) exposed to $10.6 \mu\text{m}$ carbon dioxide laser showed clear signs of ablation (see Figure 3-7). Islands of carbonisation surrounded by desiccated tissue could be found inside the crater, which itself was surrounded by a region of coagulated tissue.

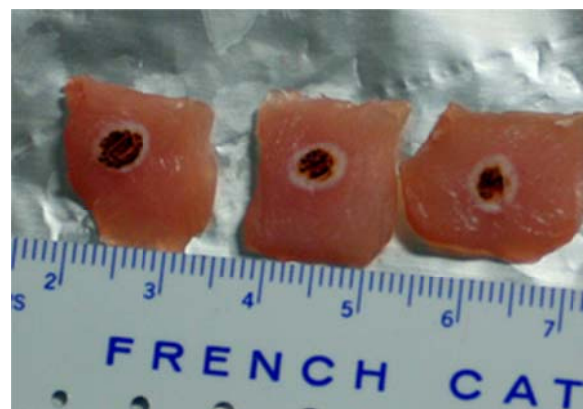


Figure 3-7. Ablation with the carbon dioxide laser.

Discussion

From these exploratory experiments, it can be concluded that ICG and MB have the capability to mediate laser ablation of tissue when paired with low-powered lasers with output wavelengths near the peak absorption wavelengths of the dyes. In these experiments, such pairings resulted in clear tissue ablation and removal of tissue.

The craters from ICG- and MB-mediated ablation qualitatively were similar in appearance to craters created by the gold standard carbon dioxide laser. The same lasers that ablated tissue when used with the dyes did not ablate tissue in the absence of the dyes, meaning that the ablation action potentially can be gated effectively by the presence or absence of dye.

A suboptimal pairing between laser and dye, or the use of a low concentration dye also can result in ablation. In both cases, ablation was observed to occur, but only after a delay and after tissue had been carbonised.

In the experiments with the lower concentration MB solution paired with the 2 W PDT laser, ablation occurred only sporadically and only after tens of seconds. This probably was due to the low maximum irradiance from the PDT laser.

Original experiments with the PDT laser exposing a 2 mm spot similar to the ICG setup (instead of 1 mm diameter used in these experiments) did not result in any ablation at all, even coupled with higher concentration MB solutions or pure MB powder applied directly to the tissue.

Even with the smaller 1 mm spot used in these experiments, the irradiance on the tissue from the PDT laser was still only about half that from the 25 W Diomed laser.

Still, with long enough exposure of tissue stained with the lower concentration MB solution, the PDT laser could heat, desiccate and carbonise tissue. This carbon then acted to absorb light, heat up and ablate tissue through direct thermal conduction. This idea will be explored later in this chapter and in depth in subsequent chapters.

The irradiance from the Diomed laser was slightly greater even than from the 30 W carbon dioxide laser. This was because the collimated beam from the carbon dioxide laser was used instead of a focused beam (at this point in the research, we could find neither the hand piece nor any IR-compatible focusing optics), which resulted in using a 3 mm spot that was larger than the 2 mm spot of the Diomed.

Because irradiance is defined as power per unit area, and area increases with the square of the radius, irradiance is more sensitive to an increase in spot diameter than it is to an increase in overall laser power delivered.

Irradiance is not the only important factor involved with laser ablation. How this light is absorbed and transformed into heat is also vital. This also is important for thinking about ablation with the mismatched MB dye and the Diomed laser.

At around the laser wavelength of 805 nm, the molar extinction coefficients of ICG, MB and HbO₂ are 1.89e5 cm⁻¹/M (@ 806 nm), 121 cm⁻¹/M (@ 800 nm) and 844 cm⁻¹/M (@ 806 nm) respectively.

The molar extinction coefficient is the extinction coefficient of the chromophore divided by its concentration. It comes from Beer's 1852 law stating that the optical density of a substance is

directly proportional to its concentration, assuming that the chromophore is dissolved in a non-absorbing medium.

Deoxyhemoglobin is not considered as any blood exposed to the oxygen-rich atmosphere rapidly would be converted to oxyhemoglobin.

Clearly, ICG is the winner by many orders of magnitude in terms of absorption at this wavelength. But haemoglobin actually absorbs 805 nm light better than methylene blue.

However, haemoglobin usually is confined physically within the vascular system in the capillaries and blood vessels and the tissue used was observed to be pretty well drained of blood. (This probably would not be the case in a clinical setting in which there is blood perfusion and usually a lot of blood in the surgical field. But with the market-bought chicken legs used in this experiment, there was almost no blood to be found.)

So taking the relative concentrations of MB and Hb chromophores in these experiments into account, the effect of MB as an absorber probably dominated haemoglobin.

This is supported by the control experiments in which the laser is used to illuminate unstained tissue. If intrinsic haemoglobin was the dominant chromophore responsible for ablation, then the unstained tissue also should ablate in the same manner as the MB stained tissue, which it did not.

Due to the relative low power of the PDT laser and to the practical consideration that it was hardly ever available for research use, it was decided to focus on the pairing of ICG with the 805 nm Diomed laser for dye-mediated laser ablation.

3.4.3. Selectivity of tissue ablation due to the presence of dye

The next sets of experiments were designed to demonstrate proof-of-concept that the ICG could be used for selective tissue ablation.

Previously, the dye was applied to a bulk area of tissue and the ablation was performed in a small sector of this marked area.

However, in these experiments, dye is applied only to where ablation is desired, and the laser exposure path is started from a non-stained spot, moved through the marked area and then terminated at another non-stained spot.

Methods

A 5 mg/ml mixture of ICG in de-ionized water was prepared and used as the sensitizing dye. Fresh British chicken legs was obtained from the local supermarket and used as the tissue model. The Diomed 805 nm laser was used as the laser source.

In the first set of experiments, a 1 ml bolus of ICG solution was injected just under the surface of the chicken muscle tissue. The activated laser which was set to 25 W set power was slowly scanned from a non-stained spot through the marked area to another non-stained spot with the fibre tip hovering about 1.5 mm above the tissue surface. The laser was swept back and forth along this path multiple times with each sweep taking approximately 3 s for a total time of approximately 30 s.

This corresponded to an average speed of about 10 mm/s for an average exposure of 1.3 J/mm², assuming constant sweep speed.

In the second set of experiments, a needleless syringe filled with ICG was used as a fountain pen to paint the word "HI" onto the tissue surface.

With the laser set to 25 W, the beam was activated and the optical fibre slowly scanned by hand back and forth across the painted letters, the fibre tip hovering approximately 1.5 mm above the tissue surface. Each pass of the fibre across the letters took about 3 s for a total time of approximately 30 s.

Results

For the experiments with sub-surface ICG injection, ablation was very well confined to the area above where the dye was injected (see Figure 3-8). The area of ablation manifested as a char-filled crater located immediately superficial to the ICG injection extending some depth into it. Two small ablation craters also were seen at the two ends of the path. Everywhere else along the scan path, coagulation was observed manifesting as a white swatch of muscle tissue. The results of all runs were similar (n=3).



Figure 3-8. Ablation is confined laterally above sub-surface injection of ICG.

In the second set of experiments with the word "HI" painted on the surface of the tissue, patchy areas of carbonisation and coagulation and small ablation craters could be found within the painted areas (see Figure 3-9). No visible ablation or coagulation was seen outside of the painted areas. The results of all runs were similar ($n=3$).

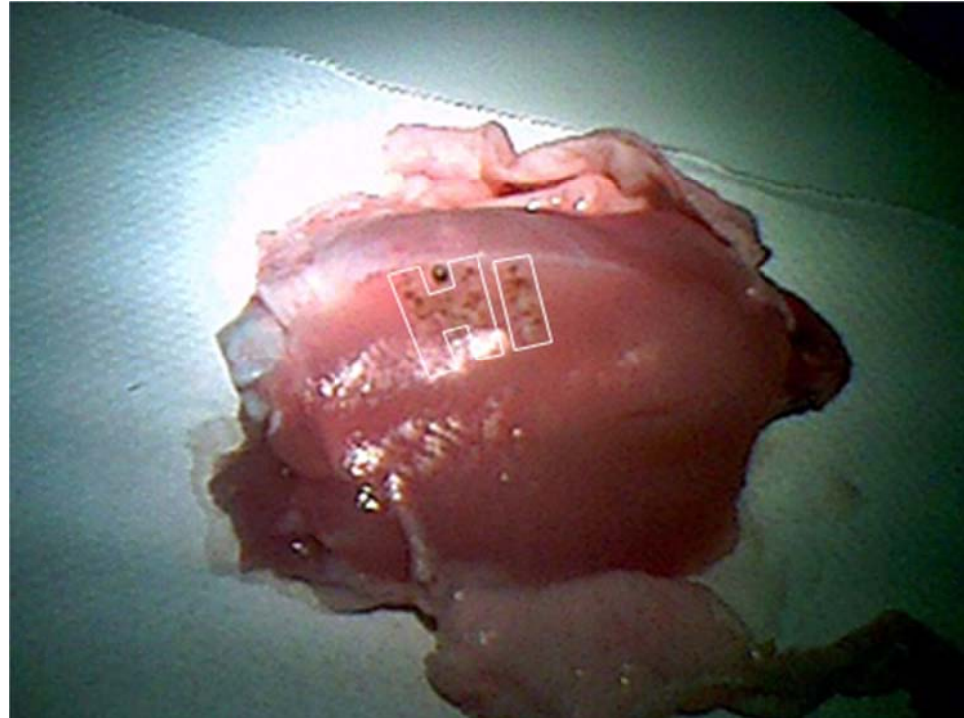


Figure 3-9. Islands of ablation are confined to where "HI" (outlined in white) was painted in ICG on the tissue surface.

Discussion

As these experiments were designed purely for proof-of-concept, the results obtained were very qualitative in nature. However, these results lend support to the idea that careful placement of dye onto or within tissue can be used to control where ablation occurs.

In the experiments with injected ICG, ablation is confined very clearly above areas of green-stained tissue. However, it is slightly concerning that slow, repeated passes over unstained tissue resulted in coagulated tissue as evidenced by the white line of coagulation along the path. Also, at the endpoints of the path that received a higher total fluence because of higher dwell time from changing direction in the back and forth sweep, carbonisation and small craters were seen.

This might mean that careful monitoring of laser irradiance and how much overall fluence is delivered to the tissue might be necessary. However, in the presence of blood profusion shuttling away heat faster than simple thermal diffusion, this problem potentially could be less important.

Because the laser fibre was handheld, the distance between the fibre tip and the tissue probably varied by a reasonable amount. As a result, the spot size, and correspondingly, the irradiance also varied. But the most important outcome — the gating effect by the presence of the dye — still was expressed, perhaps suggesting a degree of robustness to the effect for a wide range of irradiances.

The mechanism for how laser ablation occurs with sub-surface injection or tattooing also is interesting. If unstained tissue only has a low (but not zero) potential for being ablated and the laser absorbing dye is located under the surface of the tissue, then how does ablation of the thin superficial layer of unstained tissue occur?

Could ablation function primarily through decrepitation — subsurface explosions of water vapour at the dyed tissue disrupting and ejecting tissue as it makes its way to the surface? Logically this would make sense, although these experiments provide no evidence to confirm or refute this.

In the experiments with the painted letters “HI” on the surface of the tissue, the results support the idea that controlled ablation is feasible with ICG demarcation of ablation zones. However, the quality of the ablation was not great, i.e. the ablation was not very pronounced

and manifested as multiple small craters interspaced in the painted area rather than one, sharply defined “H” shaped crater.

One explanation for why the ablation was not so “clean” could be that the sloppy hand-held scanning of the laser over the painted areas resulted in lower dwell time over dyed areas and lower overall fluence of laser energy. Scanning back and forth over a relatively large area could mean that local areas of tissue were allowed to cool too much before the laser could scan back to them.

These experiments do raise some interesting questions. Still, the results overall do provide anecdotal evidence to support the conclusion that ICG control of laser ablation is possible and feasible.

3.4.4. Dependence of ablation on tissue type

The next set of experiments was designed to provide some qualitative feedback that dye-mediated laser ablation can work in a variety of tissue types. It was not intended to be a comprehensive survey of all tissue types to provide conclusive evidence that ablation will work, but rather to gain confidence that it can work in different post mortem tissues.

Methods

ICG-mediated laser ablation was attempted on a variety of tissue types from three animal species — chicken skin, chicken thigh muscle, lamb kidney, beef muscle, beef liver, beef kidney. These tissues varied in the amount of water and fat content.

5 mg/ml ICG dye solution was used as per previous experiments.

The Diomed 805 nm laser was used with a hand-held 600 μm fibre to target tissues. The power used was varied between 5 and 25 W. The fibre was held in place over the ablation target for single spot ablation as well as swept over a linear path to simulate dissection.

Results

All tissue types — chicken skin, chicken muscle, lamb kidney, beef muscle, beef liver and beef kidney — were able to be ablated with the ICG and the Diomed laser (see Figure 3-10).



Figure 3-10. ICG-mediated laser ablation of liver, kidney, muscle.

As little as 5 W set power could be used to ablate tissue. However the tip of the fibre used needed to be nearly touching the tissue for this to occur. This introduced the problem where debris ejected from the tissue surface during ablation would soil the fibre tip, burn and then damage the fibre.

The fibre could be used at a farther distance from the tissue surface, however higher laser power was required for ablation. A microlens fibre potentially could be used to enable the required laser irradiances with the fibre positioned farther away from the tissue surface.

The different tissue types qualitatively were not dissimilar in their ability to be ablated. There were differences in time to ablation, but they could not conclusively be attributed to tissue type or variations from run to run.

Discussion

Although overall the human body is composed approximately of 60 percent water, different tissues have different compositions. Percentagewise, the water content in gastrointestinal tissues is in the mid- to high-seventies, while skin on average is about 65% water. Fat, or adipose tissue, on average is only about 21% water. Selected percentage constituents of adult human tissues are given in Table 3-3.

Tissue composition can also very slightly between animals of different species. And for *ex vivo* tissue, the harvesting and storage conditions can affect water content as well. Factors such as the dryness of the air, osmosis and freezing can change the amount of water in tissues, which may bias benchtop results when compared with results from tissue *in vivo*.

Table 3-3. Percentage constituents of adult human tissues. (Selected data compiled from Duck [279].) Overall ranges given except when in square brackets, which represent ± 1 SD.

Tissue	Water, %	Ash, %	Lipid, %	Protein, %
Whole body	60	4.8-5.8	19 (5.3)	15-30
Blood	79.0-80.8	1.0	0.65	18-19
Fatty, adipose	[11.4-30.5] (21.2)	0.3	[61.4-87.3] (71.4)	[1.0-7.9] (4.4)
Intestine	77.4-82.2 (79)	0.4-1.3 (0.8)	1.3-9.2 (6.2)	10.9-14.9 (13)
Kidney	[72.3-80.5]	0.9	[2.8-6.9] (4.8)	[15.8-19.9] (17.7)
Liver	[72.8-75.6] (74.5)	1.2	[1.5-7.8] (4.6)	[16.1-19.6] (17.6)
Muscle (skeletal)	[70.0-78.6] (74.1)	1.0	[1.6-6.8] (4.2)	[17.9-21.3] (19.8)
Oesophagus	76	0.5-1.1 (0.9)
Skin	[58.6-72.1] (65.3)	0.7	[5.2-13.5] (9.4)	[22.0-27.2] (24.6)
Stomach	60-78 (75)	0.8	6.2	17.0

Still, for typical visceral tissues other than fat, these variations are not huge, especially when considering water content.

If one considers the widely accepted idea that ablation results from explosive vaporization of intracellular water, then this is consistent with the experimental results in which all the tissues were qualitatively similar in succumbing to ablation.

Adipose tissue with its low water (21.2%) and high lipid content (71.4%) poses unique issues that are consistent with previous experiences experienced by the author with ICG mediated laser ablation as well as conventional electrosurgical diathermy.

The high electrical impedance of lipids makes for a difficult environment in which to use monopolar electrosurgery.

Even with bipolar electrofulguration (see Section 3.8) and dye-mediated laser ablation both of which are not dependent of the tissue electrical impedance, the low water content made for difficult dissection as the tissue appeared to liquefy rather than explosively vaporize.

Perhaps a brute force approach increasing the power density by using short pulses of energy could vaporize the lipids in adipose tissue, assuming the heat energy does not diffuse away too much between pulses. But existing mechanical methods for cutting fatty tissues with scalpels and scissors work well enough, and stretching, compressing and ripping tissue while applying energy means also works.

For many other tissue types, dye-mediated laser ablation can be used for tissue dissection, as was demonstrated in these proof-of-concept experiments.

3.4.5. The potential for dye-erasure

The separation of the marking and dissection tasks provides the opportunity to invent techniques to undo or erase wrong markings.

One idea to erase marked tissue — using hydrogen peroxide to bleach ICG stained tissue — was explored to investigate whether the overall possibility of dye erasure or interference was plausible.

Although this particular technique ultimately was rejected because successful dye erasure always was accompanied by unacceptable, collateral tissue damage, these experiments do suggest that the general concept of dye erasure may be feasible.

The concept explored in these experiments was based on the ability of hydrogen peroxide to bleach biological materials such as human hair and teeth. In particular, hydrogen peroxide has been used to bleach hair so safely and frequently that the colloquial term “peroxide blonde” has made its way into our culture.

Hydrogen peroxide, H_2O_2 , is a slightly viscous, pale blue liquid that has a very high oxidizing capacity. It removes colours by oxidation of chromophores, either by breaking chemical bonds or by converting double bonds into single bonds in the chromophore, either way destroying the chromophore’s light absorbing capability.

It naturally decomposes exothermically into liquid water and oxygen gas:



That the hydrogen peroxide disproportionates exothermically and that oxygen is produced in the process makes the use of catalysts like manganese dioxide and silver slightly dangerous.

However, this ability to decompose explosively in the presence of a catalyst has been harnessed in the past, and high concentration peroxide solutions above 70%, called high test peroxide (HTP), have been used with catalytic screens to generate thrust for rocketry.

Methods

These proof-of-concept experiments were designed to demonstrate that the addition of hydrogen peroxide solution to ICG stained tissue could disrupt dye-mediated ablation.

Although the bleaching effect might be predicted by measuring the absorption spectrum at 805 nm of ICG and hydrogen peroxide mixtures, performing *ex vivo* experiments was desirable to account for any unanticipated interactions between the chemicals and the tissue.

The first set of experiments involved mixing 5 mg/ml (m/v) ICG solution with a 6% (wt%) hydrogen peroxide solution to see the effects of peroxide on ICG in solution. A commercial hair bleaching product that contained 6% hydrogen peroxide — Sun-In Super (Chattem Ltd; Hampshire, UK) —was used.

Approximately 5 ml of ICG solution and 5 ml of peroxide solution were mixed together and allowed to sit for 10 minutes. Any changes visible to the naked eye were noted.

The second set of experiments involved injections of either ICG or ICG followed by hydrogen peroxide into chicken thigh muscle. These blebs of subsurface liquid were exposed to 805 nm laser light from the Diomed laser and the results were observed.

For the test runs, 0.1 ml of ICG solution was injected into tissue followed by 0.1 ml of the hydrogen peroxide solution into the same spot. Control runs consisted of two sequential 0.1 mg injections of ICG solutions to create control blebs with volumes similar to the test blebs.

The Diomed laser, set to 10 W indicated power, was scanned across test and control blebs, taking between 2 to 3 s to scan across each bleb. A scalpel was used to slice along the centre of the laser burn lines to reveal the laser damage to the tissue in cross-section.

0.2 ml of hydrogen peroxide also was injected into tissue to observe the effect of peroxide alone in tissue.

Results

In the first set of experiments in which liquid solutions of ICG and hydrogen peroxide were mixed ($n=2$), there was an immediate and noticeable decrease in the green colour of the both mixtures. After approximately ten minutes, one mixture appeared to be completely clear to the naked eye, while the second mixture was almost but not completely clear, still maintaining a slight green tint.

In the second set of experiments that involved injected solutions into tissue ($n=3$ pairs, control/test), the peroxide injection into ICG-filled blebs resulted in the immediate appearance of bubbles that leaked out of the injection injury. Visible whitening of the tissue above the bleb was observed.

The control blebs had a similar appearance to ICG injections observed in previous experiments — a slight bulge in the tissue from the injected tissue with the green colour of the dye visible through the tissue above it.

In the blebs in which only hydrogen peroxide was injected, the visible whitening of the tissue above the bleb was observed.

When the laser was scanned across the blebs, ablation craters were formed in tissue in locations where the dye was located (see Figure 3-13).

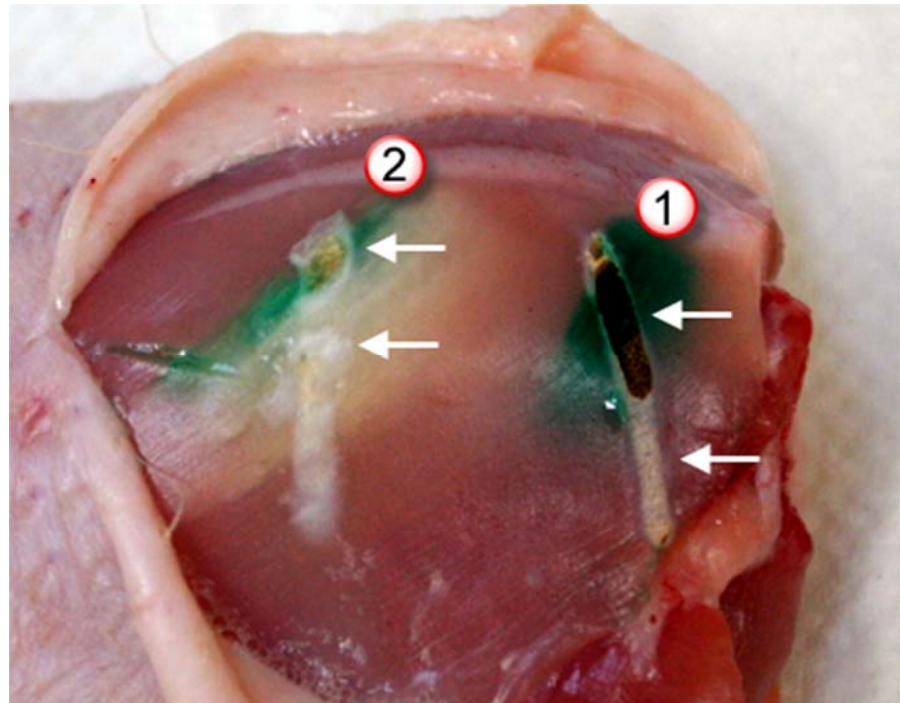


Figure 3-11. (1) Subsurface injection of ICG into chicken muscle could mediate laser ablation. Ablation occurred where the tissue was stained green by the ICG (top arrow), while ICG-free regions were not ablated (bottom arrow).

(2) Subsurface injection of ICG followed by injection of hydrogen peroxide resulted in a whitening of tissue. Whitened areas of tissue were not ablated by the laser (bottom arrow), while areas that remained green were able to be ablated (top arrow).

For the control blebs, the results were similar to previous experiments with ICG-mediated ablation. In the test cases, the presence of the white bleaching effect from the hydrogen peroxide was correlated with the lack of ablation, while areas of ICG-treated tissue that were not whitened and still retained the green hue of ICG could be ablated.

The cross-section views of the control and test blebs cut with a scalpel along the laser path can be seen in Figure 3-12 and Figure 3-13, respectively.

Tissue that had been marked with the ICG dye and then whitened by the peroxide did not ablate when exposed to the laser light. Tissue that was not whitened was able to be ablated.

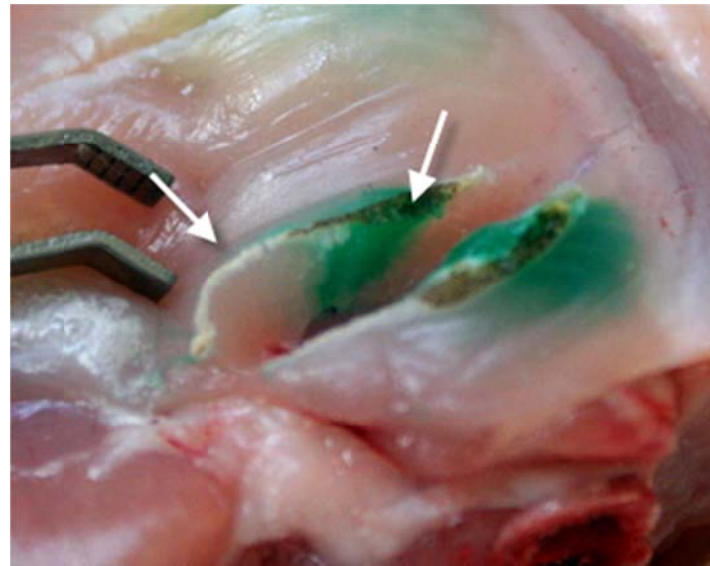


Figure 3-12. Cross-sectional view of the control bleb cut through the laser path. Tissue with green ICG beneath could be ablated by the laser (right arrow). Tissue without ICG could not be ablated (left arrow).

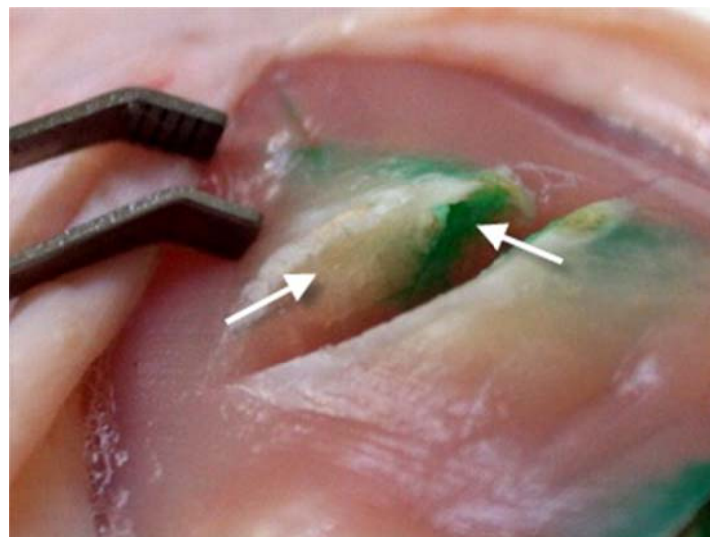


Figure 3-13. Cross-sectional view of the test bleb cut through the laser path. Tissue with green ICG that had been whitened with the hydrogen peroxide injection did not ablate (left arrow). ICG marked tissue that had not been whitened could be ablated (right arrow).

For the set of experiments in which ICG and hydrogen peroxide were applied topically to the surface of the tissue, the qualitative results were similar to the injected ICG and peroxide.

Discussion

From these qualitative, proof-of-concept experiments, there is evidence to support the idea that tissue marked for ablation by ICG injection can be un-marked with a subsequent injection of hydrogen peroxide.

However, it was troubling that tissue injected only with peroxide was turning white. And this begged the question of what exactly was happening in the un-marking process with the peroxide injection to gate the laser's ability to ablate tissue?

To start, from the simple experiments mixing ICG and hydrogen peroxide solutions, one could surmise that the peroxide was bleaching the ICG as evidenced by the mixed solution losing its colour and becoming clear.

It was possible that the initial decrease in colour might be attributed simply to dilution when the two solutions were mixed, and this could be verified by diluting the ICG solution with water instead of peroxide and comparing the colours of the solutions.

However, this would not explain the continued loss of colour over time. A process by which the ICG concentration was continuously decreasing, such as the oxidation of ICG, could much better account for continued fading of colour over time.

So then, the bleaching effect of peroxide on ICG would result in lower concentrations of ICG molecules in the tissue, decreasing the ability of marked tissues to absorb and convert to heat the laser energy, thus resulting in a lower capacity of the tissue to be ablated.

In other words, marking the tissue with ICG added molecules of ICG to the tissue to increase susceptibility to ablation. Hydrogen peroxide took away molecules of ICG by oxidizing it, reducing the ability of the tissue to be ablated.

But what about the whitening of tissue by the peroxide injection?

Well, there is no reason to expect the oxidative effects of hydrogen peroxide to be restricted only to ICG. The peroxide injection probably was chemically coagulating the tissue, breaking and rearranging bonds in biological molecules, resulting in higher optical scatter and an overall whitening of the tissue.

The increased scatter could reduce the amount of laser light able to reach molecules of ICG for it to convert the energy to heat, thus reducing the capability of the tissue to be ablated.

Probably a combination of both the ICG-oxidation effect and the increased tissue scatter effect are responsible for the ability of hydrogen peroxide to block dye-mediated laser ablation.

However, as damage to tissue is an unacceptable side-effect of the erasure of ICG, this particular embodiment of dye erasure was abandoned.

Still, these experiments do demonstrate that effective dye erasure is feasible, although biocompatibility is of key importance if a concept is to be developed for clinical practice.

3.4.6. Carbonisation to sustain laser ablation

In the course of experimenting with ICG-mediated laser ablation, two observations were made:

First, it was observed that all the ablation craters were covered in a layer of carbonisation. This usually took the form of many black islands of charred tissue surrounded by lighter margins of desiccated tissue.

Second, although the presence or absence of the dye could be used to gate initial laser ablation, it was observed that ablation craters could be made that were much deeper than the depth to which the dye was placed.

It then was theorized that ICG could mediate initial laser ablation in tissue, but carbonisation formed in the process allowed laser ablation to be sustained beyond the lifetime of the dye.

The experiments in this section were designed to confirm that this phenomenon did indeed exist, and much of the rest of the thesis was designed to investigate how this process functioned and to explore how it could be controlled.

Methods

In these experiments, laser ablation of pork muscle tissue was attempted without the use of a sensitizing dye. The pork was obtained from a local supermarket.

The 805 nm Diomed laser was used with focusing optics on an optical bench to focus the laser beam to a 1 mm diameter spot at the tissue surface. This corresponded to an irradiance of 2100 W/cm², which was about four times greater than was used in the experiments in Section 3.4.2.

The lens set consisted of two identical planoconvex lenses ($f=63$ mm) used to collimate and then focus the divergent beam emanating from a 600 micron optic fibre (see Figure 3-14).

This setup, in addition to increasing the irradiance, also allowed fragile components like the optic fibre to be located at some distance away from the ablation zone in the tissue. The

horizontal setup with the beam path parallel to the floor allowed the plume ejected from the ablation site to rise up and out of the beam path away from equipment instead of directly towards it as would be with the equipment in a vertical configuration.

This allowed the fibre to withstand almost unlimited laser exposures without the fibre cracking or the cladding being set on fire.

Both sets of experiments in this section utilized the laser setup described below.

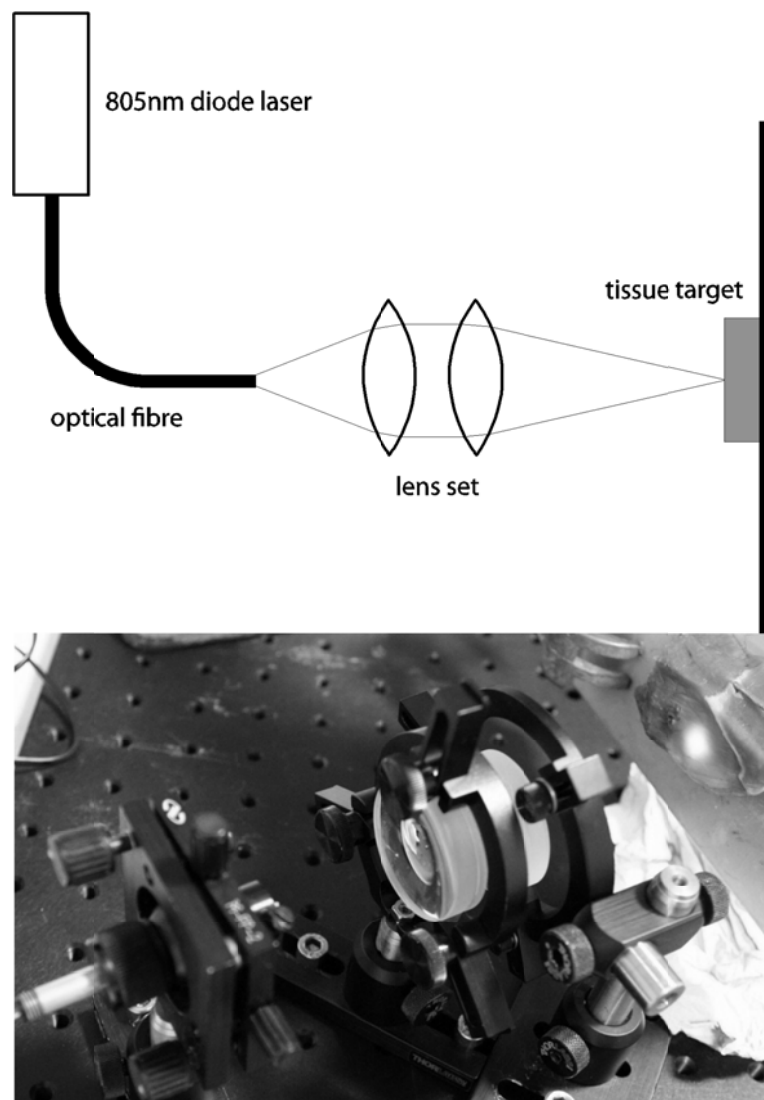


Figure 3-14. Schematic of the experimental laser setup (top). Photograph of the setup (bottom).

The objective of the first set of experiments was to consistently reproduce laser ablation of tissue without the use of a dye.

First, as a reference, ICG was applied to the tissue surface and ablated with the laser setup as described previously. The laser was set to 25 W set power for a 2 s pulse. The laser was deactivated for 10 s and then reactivated for another 2 s pulse.

The laser then was trained onto a location where there was no ICG and laser exposure was set for 9.9 s. The laser was turned off for 10 s before being activated again for another 9.9 s pulse.

Finally, the laser was set to the 2 s exposure used with the ICG ablation, followed by a 10 s delay and then another 2 s pulse.

The second set of experiments was designed to determine how long tissue had to be exposed to laser light before carbonisation and ablation could occur. These are similar to the experiments by Bown et al. in 1979-80 exploring damage to tissue during laser photocoagulation by Argon ion and Nd:YAG laser in canine and human stomach. [280][281][282][283]

The laser was used to illuminate the pork muscle tissue at 25 W set power with pulse durations varying from 2 s to 25 s.

Results

For the first set of experiments, typical results are shown in Figure 3-15 and Figure 3-16.

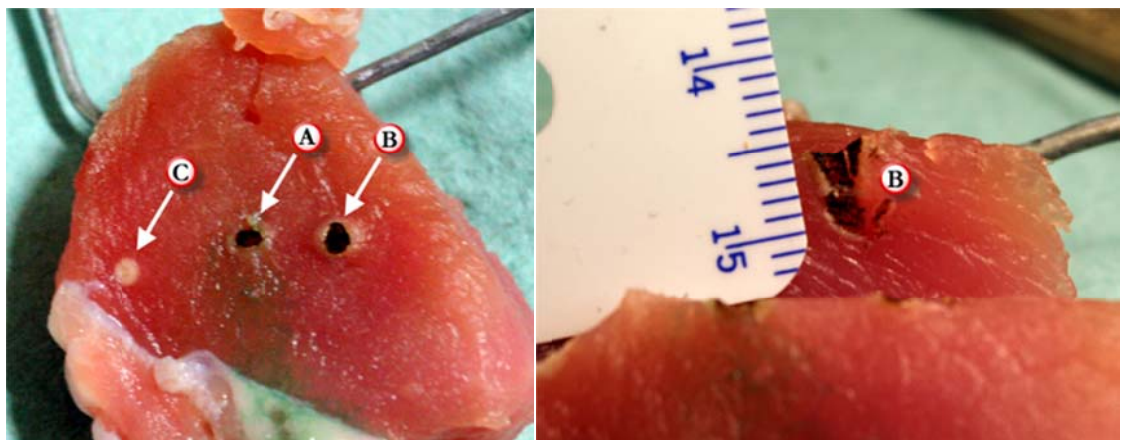


Figure 3-15. (Left image) (A) ICG-mediated laser ablation resulted in ablation.
(B) Two 9.9 s prolonged exposures in tissue with no dye both resulted in ablation.
(C) Two 2 s exposures in tissue with no dye did not result in ablation.
(Right image) Cross-section through the tissue at (B).

ICG-mediated ablation with the new laser setup was similar to results previously observed. Ablation occurred immediately and a well-defined ablation crater could be seen after a 2 s exposure ($n=1$). Ablation reoccurred immediately with the second 2 s pulse ($n=1$).

The same 2 s exposure at a spot on the tissue surface not marked with ICG did not result in ablation ($n=2$). Signs of coagulation manifesting as a white spot on the tissue surface were observed.

After a 10 s delay with the laser turned off, the same spot was exposed to another 2 s pulse of laser light, which also did not result in ablation ($n=2$).

A 9.9 s exposure at another spot on the tissue surface that was free from ICG did result in ablation after a few seconds dwell time ($n=2$).

After a 10 s delay with the laser turned off, a second 9.9 s laser pulse resulted in immediate continuation of laser ablation ($n=2$).

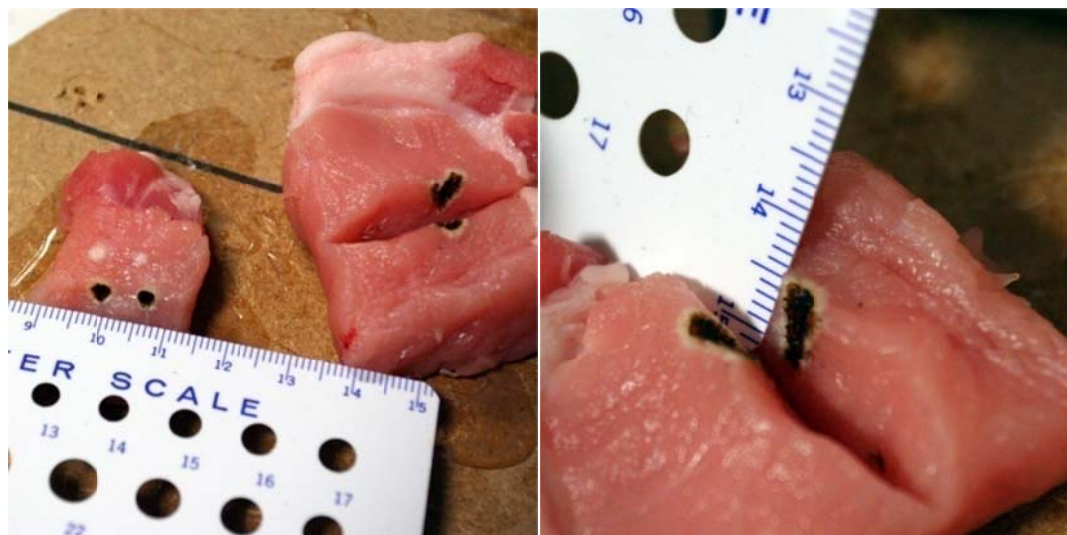
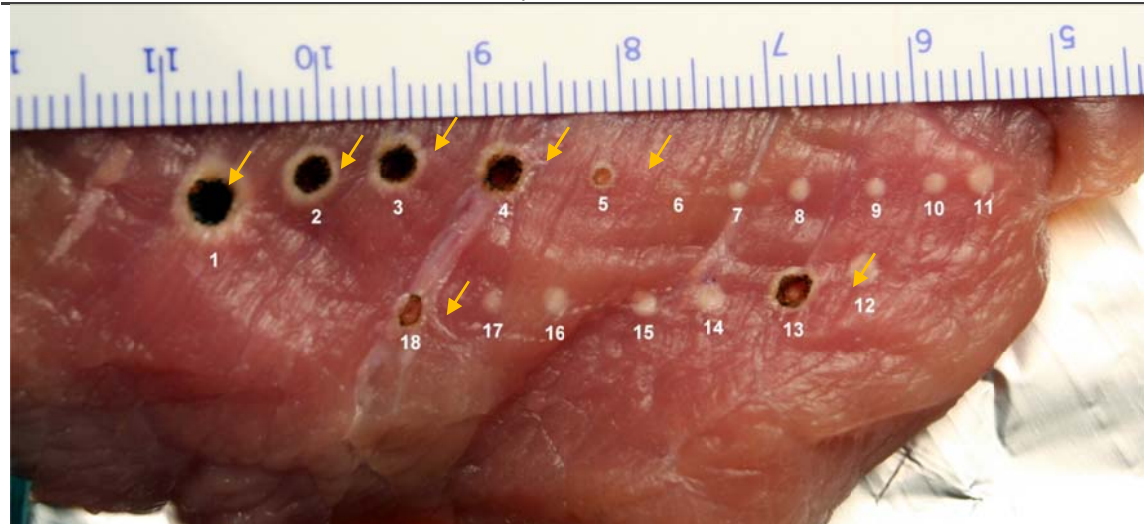


Figure 3-16. Ablation of unstained tissue by a 9.9s pulse of 805nm laser light at 25W. Subsequent pulses result immediately in the generation of smoke and continued ablation. Typical ablation craters are shown (left) and in cross-section (right).

For the second set of experiments with varying laser exposure durations, the results are summarized in Table 3-4 and the ablation craters can be seen in Figure 3-17.

Table 3-4. Exposure times and outcomes for 805nm laser ablation of unstained pork tissue.

Run	Exposure duration (s)	Ablation	Observations / Notes
1	~25	X	Laser timer maximum duration is 9.9s. 25s exposure was timed using a stopwatch. Smoke was observed to come from a blackened crater.
2	9.9	X	Smoke was observed to come from a blackened crater.
3	8.0	X	Smoke was observed to come from a blackened crater.
4	6.0	X	Smoke was observed to come from a blackened crater.
16	4.5		Spot of whitened tissue observed, at the centre of which was a small brown dot.
17	4.5		Spot of whitened tissue observed, at the centre of which was a small brown dot.
18	4.5	X	Smoke was observed to come from a blackened crater.
5	4.0	X	Smoke was observed to come from a blackened crater.
15	4.0		Spot of whitened tissue observed, at the centre of which was a small brown dot.
13	3.9	X	Smoke was observed to come from a crater.
14	3.9		Spot of whitened tissue observed, at the centre of which was a small brown dot.
11	3.8		Spot of whitened tissue observed, at the centre of which was a small brown dot.
12	3.8		Spot of whitened tissue observed, at the centre of which was a small brown dot.
10	3.5		Spot of whitened tissue observed.
9	3.0		Spot of whitened tissue observed.
8	2.8		Spot of whitened tissue observed.
7	2.5		Small spot of whitened tissue observed.
6	2.0		Small spot of whitened tissue observed.

**Figure 3-17.** Laser ablation of unstained tissue by an 805nm diode laser. Each test location with the run number. Arrows denote crater formation and carbonisation indicative of tissue ablation.

The experimental results indicated that with exposure duration of around 4 s or longer, laser ablation of pork muscle tissue is possible without the use of a sensitizing stain like ICG.

Discussion

- (1) Tissue can be ablated without the use of a sensitizing dye if the laser irradiance is high enough.

The irradiance used in experiments in previous sections was not high enough to ablate tissue without the addition of a sensitizer. The focusing optics in the experiments in this section afforded a level of irradiance that was four times higher than the maximum irradiance previously used. This allowed ablation to occur in unstained tissue after about four seconds of continuous laser irradiation.

However, four seconds of irradiation interrupted halfway through by a ten second cool down, i.e., two seconds of irradiation followed by ten seconds of cool down and then another two seconds of irradiation, did not result in ablation. This fact implied that the onset of ablation did not depend simply on the total fluence delivered.

A model of ablation that involves a balance of energy flows — inwards from the laser heating source to a control volume and outwards by means of thermal diffusion with energy imbalances contributing towards raising the tissue temperature — and threshold temperatures at which other physical processes occur might better explain what has been seen experimentally. This will be discussed in more detail in the theoretical modelling chapter.

- (2) The use of a sensitizing dye greatly the time to onset of tissue ablation.

It is worth repeating that the presence of the light-absorbing dye does mediate tissue ablation by, for example, low-power diode lasers.

This has been demonstrated experimentally in previous sections and again in this section, in which ICG-stained tissue was ablated every time by the laser without a delay.

Although the higher irradiance used did allow un-stained tissue to be ablated, the ablation process occurred only after a not insignificant time delay of about 4 s.

- (3) ICG-mediated ablation is accompanied by carbonisation, which self-renews and allows sustained ablation even after the ICG has been consumed.

This, perhaps, is one of the more interesting findings from these experiments.

As described earlier, stained and unstained tissue behaved differently upon initial exposure to laser light — ICG-stained tissue ablated immediately while unstained tissue only started ablating after about 4 s, given the experimental setup and laser settings described previously.

However, once an ablation crater with char had been formed, second attempts at laser ablation resulted in immediate continuation of ablation regardless of whether the initial crater had been formed with or without ICG.

For unstained tissue if carbonisation is not present, second attempts do not result in immediate tissue ablation.

These observations suggest that although initial laser ablation is mediated by the presence of ICG or some other light-absorbing dye, carbonisation formed during this process can mediate laser ablation to sustain it beyond the lifetime of the dye.

This is fascinating because carbonisation traditionally has been considered clinically to be bad — an unwanted by-product of laser ablation. Charred or blackened tissue has been thought to hinder laser ablation because its high absorption as a gray body absorber blocks laser light from penetrating it to reach underlying tissue.

It would be very interesting if this could be turned around so that ablation is enhanced through carbonisation instead of being hindered by it.

3.4.7. Overall conclusions for dye-mediated laser ablation

ICG clearly has the capability to enhance greatly the tissue ablation power of the low power Diomed laser. Tissue can be ablated with the dye/laser combination. The ability to ablate tissue can be demonstrated repeatedly.

Under some conditions, the presence or absence of a dye like ICG can determine whether or not the tissue is ablated. Ablation can thereby be restricted to areas demarcated by ICG.

However, carbonisation formed by the dye-mediated ablation might act as a second wave of sensitizer, mediating continued laser ablation after all the dye has been displaced or consumed. As more char is formed during the ablation process, this sensitizer is self-renewing potentially

allowing ablation depths far beyond the initial depth of the dye. This has been witnessed in some experiments.

Dye-mediated ablation by a low power, normally non-ablative laser shows good promise both as a method to control tissue dissection and as an interesting topic for research. The whole phenomenon of carbonisation mediating a second wave of tissue ablation is scientifically fascinating.

These reasons coupled with the author's childhood fascination with lasers influenced this concept's selection as the topic for further research.

While the ablation-gating promise of dye-mediated ablation is very exciting, a number of key practical areas would need to be resolved before the technique could merit use in a clinical setting.

The specifics of how the gating phenomenon is exploited for spatial control would need to be worked out. What sensitising compound should be used and what is its biocompatibility upon exposure or implantation?

How is the compound applied to the tissue and what engineering challenges need to be resolved to achieve this? Are there methods to erase or remove misapplied compound?

What are potential risk factors and side-effects associated with the dye-mediated ablation technique? Does this technique improve overall safety and control when compared with existing cutting methods?

While many, if not most of these questions will not be answered in this work, they may provide interesting topics for continued research in order to develop this concept into a clinically viable technique.

3.5. Selective tissue stiffening prior to mechanical shearing with scissors

3.5.1. The problem with endoscopic scissors

It is well known in the community of flexible endoscopists that endoscopic scissors are poor performers when it comes to cutting tissue.

Yet, we all use normal scissors in our everyday lives quite effectively to cut everything from paper in the office place to yarn in the sewing room and meats in the kitchen. They are effective, precise and intuitive, and we don't give much thought to their use.

Using laparoscopic scissors requires a bit more skill, as the long instrument length and indirect viewing through a video camera require some specialized hand-eye coordination skills.

Still, the author, who has had no formal training in clinical medicine, has used laparoscopic scissors successfully to perform cholecystectomy in an animal model, and the scissors performed quite well at cutting tissue.

(Although the author had to admit that the ultrasonic dissectors he also tried cut the tissue more easily and provided convenient, instant access to coagulation capability, which probably was the point — the surgery was part of a program provided by the manufacturer of the ultrasonic dissectors to train surgeons in the best use of their products.)

So why do endoscopic scissors work so poorly?

From observations of open and laparoscopic surgery made by the author viewing many dozens of live and recorded surgical procedures, the key technique utilized in open and laparoscopic surgery but missing from endoscopic surgery is the application of counter-traction to lift and stretch tissue before cutting with scissors.

This hardly ever is done at flexible endoscopy because of the limitations of the current endoscopic technology. There simply aren't enough "hands" in the surgical field to apply traction and cut at the same time.

To prove the point with qualitative, anecdotal evidence, the author attempted to cut tissue with endoscopic scissors on the benchtop. Without counter-traction, the tissue to be cut would slip out of the jaws or wedge in between the blades upon closure — all the same problems that doctors who have used them before had described. However, when counter-traction forces were applied to *ex vivo* porcine stomach, the author was able to cut the tissue with relative ease.

One might also consider using scissors with sharper, tighter blades to cut tissue better. This is another potential cutting solution and was explored by the author in previous work.

However, force transmission problems and miniaturisation issues unique to devices designed for use at flexible endoscopy quickly were encountered. These engineering roadblocks probably can be overcome, but it was decided to look for simpler, alternative solutions.

3.5.2. Deployable polymer stiffeners (glue) to mediate cutting with scissors

In a world without countertraction, does a method exist to improve tissue cutting with scissors? In some ways, this is a perfect situation for applying the concepts of deconstructing dissection because the existing technique already is so poor. A method to selectively improve the scissors' cutting ability potentially could allow for a new scheme for controlled cutting.

The concept proposed in this section is to apply a liquid adhesive to the surface of the target tissue to form essentially a rigid polymer-tissue composite. This, in theory, might make it easier to cut the targeted tissue because of the following:

First, the bonding of the tissue to the polymer would allow strains induced by cracks in the polymer to be mirrored locally in the tissue. Because of the high bonding strength and the higher stiffness of the composite, strains induced by the scissoring action would stress tissue more, locally near the crack, rather than being distributed over a larger volume of tissue.

A way to visualize this might be to consider stretching a 10 cm long rubber band by 1 cm. Stretching the entire band by 1 cm would be different from stretching a 1cm portion of the band by 1 cm. The glue would effectively clamp the tissue to itself and reduce the portion of stretchable tissue to an area nearby to the common crack.

Second, the rigidity of the composite might better resist being stretched, and thus getting stuck in between the jaws of the scissors. One common cause of failed cuts with endoscopic scissors is exactly this stretching and jamming of tissue in between scissor blades. A more rigid composite might better resist this failure mode.

Selective cutting would come from unbonded tissue still being difficult to cut. The presence or absence of the polymer glue potentially could act as an effective gating function to control cutting.

What follows are experiments to demonstrate simple proof-of-concept. Of course, to develop the concept into a design that might be clinically relevant, further work would be necessary to investigate the biocompatibility of any adhesives used, characterise the degree of cutting

enhancement that the stiffening provided and explore what additional countertraction or tissue fixation was necessary.

3.5.3. Proof-of-concept in *ex vivo* tissue

These experiments were designed to demonstrate proof-of-concept that tissue stiffening by the addition of glue could make cutting tissue easier and more reliable.

Methods

The tissue used in these experiments was skin resected from fresh chicken drumsticks obtained from the local supermarket.

The adhesive used was Loctite SuperGlue brand cyanoacrylate (CA) (Henkel AG; Düsseldorf, Germany). The main component, ethyl-2-cyanoacrylate ($C_6H_7NO_2$) is an acrylic resin that rapidly polymerises in the presence of water. CA was chosen because it is readily available and relatively cheap.

Medical grade CA is available commercially and provided a direct path to clinical use. However, because it is much more expensive despite being similar in physical properties to commercial-grade CA , store-bought CA was used instead.

Normal metal office scissors were used in these experiments.

The CA glue was painted onto skin tissue and allowed to dry in order to verify that CA could be bonded to tissue.

Next, rectangular swatches of tissue approximately 3 cm wide by 1.5 cm tall were cut out of the chicken skin with a scalpel. Half the surface of each swatch was coated in CA and allowed to dry. The uncoated half served as a control.

The swatches were placed within the open blades of the scissors on a flat table so that the weight of the tissue swatches was supported only by the scissors and the table top. Handling of the tissue was done only to reposition tissue after a failed cut or for a subsequent cut.

Triangular wedges with bases and heights of about 0.5 cm were attempted to be cut from the treated and untreated halves of each swatch and the results recorded.

Finally, to characterize qualitatively how well the selective-stiffening technique could work, another rectangular swatch of tissue was completely covered in glue on one surface. Multiple,

small rectangular pieces with progressively smaller widths were cut from this swatch and observations were made about the quality and ease of the cuts.

Results

CA glue was bonded rapidly and successfully to the moist skin tissue (see Figure 3-18). Bonded tissue was noticeably stiffer to the touch and could maintain its shape when held by one edge with forceps.

Unbonded tissue remained flaccid and soft to the touch. Unbonded tissue also wrinkled and shrivelled immediately upon resection from the source chicken drumstick, whereas tissue bonded before resection retained its shape.

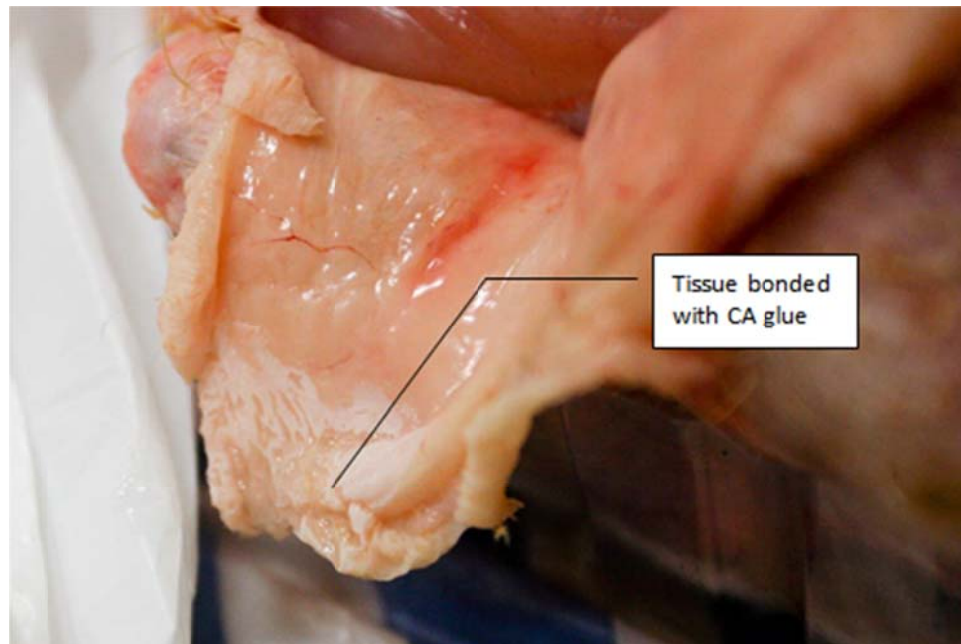


Figure 3-18. Cyanoacrylate adhesive (Loctite SuperGlue brand) applied to chicken skin in order to increase mechanical stiffness.

For the experiments in which triangular wedges were attempted to be cut from half-treated and half-untreated rectangular swatches of skin, all attempts at dissection on the glue-treated halves were successful ($n=3$). The resection defects remaining in the rectangular swatches were sharp and well defined. The actual cutting process felt to the author similar to cutting a piece of cardstock.

In contrast, dissecting the triangular wedges from the untreated halves of the tissue swatches was only marginally successful ($n=3$). Although eventually triangular wedges could be cut, this

was a painstaking process in which repeated nibbles and bites of the scissors were required. The remaining defects were jagged, shrunken and ill-defined (see Figure 3-19).

In the final experiment, multiple small cuts were made in the completely glue-bonded swatch. Qualitatively, each cut was very easy to make with the office scissors, and the definition of the cuts were good (see Figure 3-20). The smallest piece cut from the glue-bonded tissue was about 0.5 mm wide.

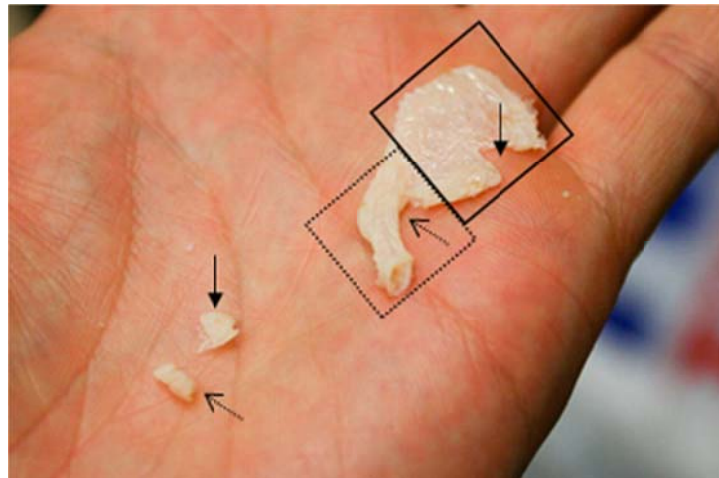


Figure 3-19. Chicken skin tissue stiffened with cyanoacrylate adhesive (solid rectangle), and untreated tissue (dotted rectangle). Scissor cuts in the glue-stiffened region were sharp and easy to make (solid arrows), while the cuts in the control region were jagged and hard to make in the soft, floppy and shrivelled tissue (dotted arrows).



Figure 3-20. The CA glue-tissue composite could be cut with great precision.
A ~0.5 mm wide piece cut from the sample is shown at the arrow.

Discussion

From the results of these qualitative experiments, the application of glue bonded to chicken skin appeared to improve the ability, speed and ease tissue could be cut by standard office shears.

Small, triangular wedges could be cut easily from the glue-bonded swatch and the thinnest rectangular piece cut by the author was about 0.5 mm wide.

Unglued tissue, by contrast, was difficult to cut. Repeated gnawing at the same spot in the tissue was necessary to initiate the cut, and most times the scissors appeared to deform and stretch the tissue rather than cut it. However, ultimately, unbonded tissue could be cut, although it was quite a frustrating exercise to do so.

An unanticipated benefit of the glue was its ability to permit treated tissue to retain its shape, allowing for easier manipulation of tissue that behaved more like a rigid-body than a floppy, deformable mass.

These results suggest that selective stiffening of tissue with an adhesive is feasible to mediate cutting with scissors, although the gating functioning of the technique could be bypassed by a motivated scissor operator. However, as a guard against accidental cutting, the level of gating could be good enough.

Qualitatively, much sharper cuts could be made much more easily with the bonded tissue compared with the unbonded tissue. Amazingly thin pieces could be cut from bonded tissues.

Also, since tissue *in vivo* being cut always will be fixed to something, this might be exploited to provide countertraction and fixation to further enhance control of cuts using this technique.

3.5.4. A physical basis for enhanced cutting

What would the addition of CA glue to form a tissue-glue composite do to the forces required to cut tissue? How can physics contribute to our understanding of how tissue stiffening functions to enhance cutting by scissors?

A relevant model for how cutting with scissors occurs is described by Mahvash et al. [284] They modelled scissors cutting as the result of two main physical phenomena — local deformation and fracture. Local deformation was modelled analytically by making a few assumptions on the

geometry and assuming linear elasticity of the material based on Hooke's Law, and fracture was modelled using an energy based approach with fracture mechanics.

The model geometry of cutting a material with scissors is shown in Figure 3-21.

From their combined model, the torque felt at the scissor handle during the various stages of cutting was predicted (see Figure 3-22). From 0 to 1, the torque is zero as the scissors close to engage the material. From 1 to 2, the torque increases as the material is compressed and loaded up with stress until a fracture occurs at 2. From 2 to 3 represents cutting by means of crack propagation by the scissors. From 3 to 4, the tissue relaxes as the scissors are opened and reset to the beginning of the cutting cycle. Their results were validated by experimental data, but it is not reproduced here.

Copyrighted material

Figure 3-21. Geometry of scissors cutting a swatch of material of thickness h .
(Reproduced from Mahvash et al. [284])

Copyrighted material

Figure 3-22. Stages of cutting by scissors. θ is the angle between the centreline of the scissors blades, and τ is the torque required at the scissors handle. From 0 to 1, the closing scissors blades have not yet engaged the material. From 1 to 2, the material is being deformed until a fracture occurs at 2. From 2 to 3, the material is being cut. From 3 to 4, the material is relaxing as the scissors are opened. (Reproduced from Mahvash et al. [284])

The increasing torque during the cutting could be attributed to the changing scissor geometry and mechanical advantage during the cutting stroke as the crack propagates away from the scissor pivot.

So how does creating the glue/tissue composite affect these two stages of cutting? And how can this enhance cutting?

During the local deformation phase of cutting, the tissue can react by bending like a beam (see Figure 3-23). Beam theory can be applied to model how the beam reacts to the applied forces.

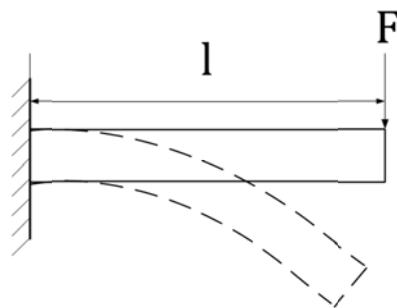


Figure 3-23. The bending of a cantilever beam.

Although the cantilever beam geometry does not exactly describe the scissors cutting geometry, all the common approximate solutions to the beam displacement and end slope for a variety of beam geometries are similar and given by Equations (3.2) and (3.3), respectively:

$$\delta = \frac{Fl^3}{C_1 EI} \quad (3.2)$$

$$\theta = \frac{Fl^2}{C_2 EI} \quad (3.3)$$

Where l is the distance from the fulcrum to the location of the force, E is the Young's modulus, I is the second moment of the beam section, and C₁, C₂ are constants corresponding to various beam-grounding geometries (for a cantilever beam, C₁=3 and C₂=2). More complicated geometries are simple linear superpositions of these solutions.

What is important from these equations is that the deflection and end slope depend inversely on the material stiffness. An increase in the Young's modulus decreases the beam deflection, which makes sense intuitively.

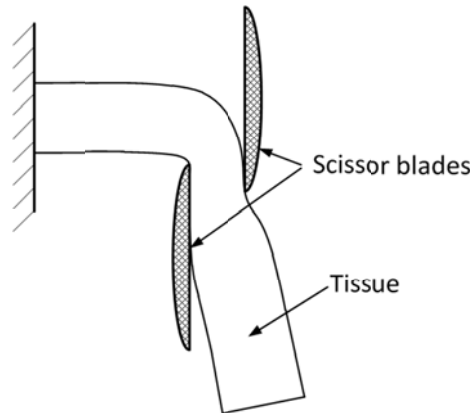


Figure 3-24. A common failure mode when cutting with scissors – the material bends, stretches and gets stuck between the scissor blades instead of being cut.

Tissue, in general, is not a very stiff material when compared with engineering plastics. If during the cutting process, the tissue bends too much before stresses reach a fracture-inducing level, it can become wedged in between the blades of the scissors (see Figure 3-24).

Longer scissors that are made with larger tolerances or more flexible materials are more susceptible to this failure mode than scissors that are tighter and stiffer. However, tighter scissors require higher activation forces because of the higher intrinsic friction with opening and closing tight scissors. This could make actuation at a distance, such as in flexible endoscopy, much harder to do.

The author had spent several months before starting the PhD research trying to solve the tissue wedging problem by balancing tighter tolerances with higher actuation forces in the engineering of new flexible, endoscopic scissors. Getting this design balance correct can be quite a challenging problem indeed!

However, by increasing the material stiffness through the application of the glue to form a laminated composite, one neatly bypasses scissors engineering compromises for a tissue / material engineering solution to solve the tissue wedging problem.

Once the tissue has been loaded with stresses to a critical level, fracture mechanics take over. This theory of material failure takes an energy approach to determine how resistant, or tough, a material is against the growth of cracks.

Fracture mechanics considers the lowest free energy state in a material with cracks, taking into account elastic energy stored in stressed areas near a crack versus the increase in surface

energy in order to propagate the crack. This approach bypasses stress and strain singularities at the crack when using standard linear elasticity theory.

The principal equation in fracture mechanics for the stress condition at the onset of fast fracture is given by Equation (3.4):

$$\sigma\sqrt{\pi a} = \sqrt{EG_c} \quad (3.4)$$

Where σ is the stress, a is the crack length, E is the Young's modulus and G_c is the toughness, or critical strain energy release rate. J_c , as used by Mavash et al., is equivalent to G_c when considering linear elastic fracture mechanics, as opposed to nonlinear, ductile material behaviour.

The left side of (3.4) is defined as the stress intensity factor, K . When K is equal to the right side of (3.4), the threshold for fast fracture, which depends only on material properties, K becomes K_c and is known as the critical stress intensity factor or fracture toughness.

What is important is that K_c depends on (the square root of) the product of the Young's modulus and the toughness of the material.

From Table 3-5, selected material properties for chicken skin and cyanoacrylate can be found.

Although chicken skin is about twice as tough as polymerized CA, its stiffness is lower by almost five orders of magnitude! This is reflected in the fracture toughness of CA being much higher (107x-215x) than chicken skin.

Table 3-5. Selected material properties for chicken skin and cyanoacrylate.

Material	Young's modulus, E	Toughness, G _c	Fracture toughness, K _c
Chicken skin	15-60 kPa [285]	2.8 kJ/m ² [284]	6.5-13.0 kN m ^{-3/2}
Cyanoacrylate	1.17 GPa [286]	1.6 kJ/m ² [287]	1.4 MN m ^{-3/2}

These material properties help explain why chicken skin is hard to cut. The stress necessary to induce fracture can be calculated from (3.4). The corresponding strain can be found from linear elastic theory and Equation (3.5):

$$\sigma = E\varepsilon \quad (3.5)$$

Assuming identical cracks, it can be shown from (3.4) and (3.5) that the strain required to reach the critical fracture criterion is proportional to $1/\sqrt{E}$. In other words, the chicken skin

needs to be stretched much more than the cyanoacrylate for both to reach critical fracture-inducing stresses.

By bonding the two materials together, the laminate can have a higher overall stiffness that requires less strain to reach the critical stresses for fracture. However, this does come at the price of higher overall fracture toughness, which means that higher scissoring forces are necessary.

When cutting with scissors, applying higher stress might be possible by squeezing harder on the handles, but strain is limited by the geometric design of the scissors.

3.5.5. Overall conclusions for selective tissue stiffening

The improvement in the cutting ability of normal office shears to cut glue-bonded tissue compared with untreated tissue was quite remarkable. The differences in the speed, ease of dissection and the cut definition were qualitatively significant, as demonstrated by proof-of-concept experimentation.

These differences might be pushed further with the development of bespoke adhesives and endoscopic scissors to the point at which only tissue that has been pre-treated with glue can be cut by the scissors. This selectivity could be the basis of a controlled dissection scheme in which tissue is “sensitized” to cutting by scissors through the selective application of glue.

An analysis of the mechanics of scissors cutting helped to explain how the “sensitization” physically works. It applied well-known mechanical engineering principles to modelling material deformation and crack propagation.

However, one limitation of this technique was the necessity of the target tissue to be fit within the jaws of the scissors. Incisions perpendicular to large flat surfaces probably would be difficult compared with “plunge-cut” incisions made by scalpel or electrosurgery.

Also, further research into the technique probably would involve optimizing the adhesive, requiring a substantial amount of materials science and chemical engineering work, and optimizing the scissors, which would require design and mechanical engineering expertise. Given the areas of expertise available within the department, to the author this concept did not seem to be ideal for a medical physics research topic.

As a technique, the concept is appealing. However, despite potential engineering contributions and clinical applications, the overall value of the scientific contribution the concept could lead to was questionable in the author's mind.

For researchers interested in developing this idea further to a state useful for clinical work, a number of areas need to be addressed.

What is the appropriate adhesive that should be used to stiffen tissue? What is the biological impact of short and long-term contact with the chemical adhesive?

How is this adhesive applied to the tissue? Can application device be made to be compatible with existing or future endoscopes? Can the endoscopic scissors be improved to function more synergistically with the adhesive? For example, could the scissors be combined physically with the glue application tool?

Can something other than an adhesive that is not left behind in the surgical field be used to perform the same selective stiffening function? These are all exciting questions waiting to be resolved by researchers looking to continue this research.

3.6. Blunt dissection by gas-evolving chemical reaction

3.6.1. A “volcanic” reaction

Chemistry always had been an interesting subject for the author, ever since winning a prize in a primary school science fair for building an erupting papier-mâché model of a volcano.

The required eruption was simulated by mixing two household chemical reagents — baking soda (sodium bicarbonate) and vinegar (acetic acid) — releasing carbon dioxide gas in a frothy, foamy mess. Throw in some red food colouring and the illusion was complete.

When Sumiyama et al. reported in 2007 [237] successful gas dissection of submucosa in *ex vivo* porcine stomach by direct injection of high pressure CO₂ gas (700 kPa), images of that first model volcano resurfaced in the author's mind.

Could the baking soda / vinegar chemical reaction be employed to bluntly dissect and de-laminate layered gastrointestinal tissue by gas emphysema? Could careful placement of one reagent in the tissue control the location of tissue dissection by the second?

3.6.2. Proof-of-concept in post-mortem tissue

These proof-of-concept experiments were designed to explore the effects of injecting baking soda and vinegar into layered tissues. They were meant to study whether the concept was even remotely feasible, and thus the methods used and the results obtained were anecdotal in nature.

Methods

Freshly harvested *ex vivo* porcine stomach and oesophagus were used for the experiments.

Food-grade baking soda and the vinegar purchased from the local supermarket were used as the chemical reagents. Syringes were loaded with the two reagents – one with a solution of baking soda and tap water, and the second with the vinegar (5% acidity).

5 ml of the baking soda solution first was injected into the submucosal layer of stomach tissue to form a bleb. This was followed by an injection of 5 ml of vinegar into the same location.

A control bleb formed from the injection of 10 ml of tap water at an adjacent site served as a control. Both blebs were observed for 20 minutes.

The same procedure was repeated in *ex vivo* porcine oesophagus.

All blebs were sliced across their major diameter to reveal the bleb cross-section.

Results

None of the test cases in either stomach ($n=2$) nor oesophagus ($n=2$) resulted in any visible delaminating or dissection of tissue layers.

None of the control cases ($n=4$) resulted in any visible dissection either.

For the test blebs, a rapid reaction was observed upon injection of the vinegar into the baking soda filled blebs as the volume doubled or tripled in size, reaching a maximum volume over the course of a few seconds. A bubbly whitish liquid could be seen oozing out of the injection wound.

All blebs were hemi-ellipsoid in shape. The blebs were firm, but soft to the touch, and persisted for the duration of the 20 minute observation period at which point the experiment was stopped.

The hemi-ellipsoid control blebs formed by the water injection initially were firm, but soft to the touch. However, they immediately started to decrease in volume upon withdrawal of the injection needle and almost completely disappeared within a few minutes. Liquid could be seen slowly seeping out of the injection wound as well as from the sides of the tissue samples at the excision margins.

Slicing through the experimental and control blebs with a scalpel revealed the bleb cross-sections.

Slicing through the control blebs resulted in the release of most of the remaining water out of the incision. Some areas of submucosa with trapped liquid that had a spongy, clear, pillow-like appearance could be found in the control bleb.

In contrast, cutting through the experimental blebs revealed something very different. The two halves of the sliced tissue were almost completely intact, and much less liquid was observed leaking out than in the control bleb. The submucosa in the cross-sections of the experimental blebs appeared to be almost a gel-like in appearance.

In both the experimental and control blebs, all three layers of the oesophagus and gastric tissues – mucosa, submucosa and *muscularis propria* – visually appeared to be intact and firmly attached to each other. The volume increase from trapped reagents or water appeared to be localised in the submucosa as a stretching or inflation of tissue in that region. No visible delamination or dissection between layers could be seen.

Discussion

These experiments attempted to adapt existing techniques for creating a submucosal fluid cushion to delaminate tissue layers by the injection of gas-producing chemical reagents.

Although the volume increases with the gas-producing reagents were quite dramatic — injections of similar volumes of water resulted in blebs that were two to three times smaller — the technique did not appear to generate the necessary forces needed to delaminate the tissue layers.

Also, because of the difficulty in creating submucosal blebs in geometries other than an ellipsoid shape, it probably would be difficult to define more elaborate regions for dissection even if an appropriate chemical reaction could be found.

However, this technique might be applicable for creating long-lasting blebs for EMR or ESD.

Current techniques for increasing bleb longevity involve the injection of more viscous mixtures such as sodium hyaluronate, hydroxypropyl methylcellulose or chitosan to retard fluid leakage and water dissipation by osmosis. But these viscous fluids are expensive and harder to inject because of their viscosity.

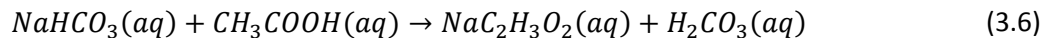
Injection of vinegar and baking soda solution could be useful for surgeons requiring long-lasting blebs, but biocompatibility and adverse reactions need to be investigated.

However, carbon dioxide is readily absorbed by the body and is used for peritoneal cavity insufflation at laparoscopy, and low concentration solutions of both vinegar and baking soda are safely used topically for personal hygiene purposes and have been used over the millennia as part of folk remedies. We also regularly ingest vinegar and baking soda as part of our food without incident.

High concentrations of acetic acid are corrosive and harmful to living tissue, and 50% solutions of acetic acid in saline have been used clinically for sclerotherapy of renal cysts. [288] Still, low concentration 5% solutions of acetic acid have been used safely in humans as a low cost technique to diagnose cervical cancer in developing nations. [289] Are chemical improvements possible?

The vinegar and baking soda reaction appeared to be quite poor in its capability to tear and delaminate layered tissue, at least with the experimental parameters used. Could the reaction be improved to create the higher forces necessary to delaminate tissue layers?

The baking soda and vinegar mixture evolves gas according to the following two reactions:



Equation (3.6) describes the oxidation-reduction reaction of sodium bicarbonate (NaHCO_3) and vinegar (CH_3COOH) to form sodium acetate salt ($\text{NaC}_2\text{H}_3\text{O}_2$) and carbonic acid (H_2CO_3). The carbonic acid produced by (3.6) is unstable at room and body temperatures, and it immediately breaks down into water (H_2O) and carbon dioxide gas (CO_2) as per Equation (3.7).

From the stoichiometry of the two chemical equations, one part of carbon dioxide gas is produced from one part each of baking soda and vinegar.

Given the concentrations and volumes of the reagents used, one could calculate the amount of carbon dioxide gas produced. The pressure to separate the tissue would come from both the pressure of the incompressible, injected liquid and the evolved gas.

One could calculate the pressure exerted by the gas on the tissue using the Ideal Gas Law (3.8),

$$PV = nRT \quad (3.8)$$

Where P is the absolute pressure, V is the volume, n is the amount of gas in moles, R is the universal gas constant (8.314 J/mol-K) and T is the absolute temperature.

This could be solved alongside equations for calculating stresses in the tissue. However, this could get quite complicated due to the complexity of the layered tissue geometry, and the anisotropic, viscoelastic material properties of the tissue.

Also, the fibrous nature of the submucosa and the puncture wound of the injection needle would add leaks to the system that would have to be accounted for.

And this solution models only static loading. Dynamic loading with high pressure impulses and fracture mechanics would require different modelling strategies.

Suffice it to conclude at this stage that the forces produced were not high enough.

What modifications, then, could be used to increase the pressures and the forces generated?

An increase in the amount of gas produced could help.

This could be achieved by increasing the amount of both reagents by increasing the concentrations of the solutions or increasing the volume of solutions used. Increased chemical concentrations, however, could make the reagents more harmful to tissue.

Also, using different chemicals with a better gas yield could help, for example, a reaction in which two parts of gas is produced for each part of reagents used.

Increasing the production rate of the gas could improve the forces exerted on the tissue by loading it dynamically with a fast, short impulse rather than a slow build-up. Chemical kinetics can give some insight into how to achieve this.

The chemistry of the reaction (3.9) can be modelled as a pseudo-first-order reaction if the concentration of B is much greater than A (and thus essentially doesn't change during the reaction). The differential equation for the simplified reaction is (3.10):



$$r = -\frac{d[A]}{dt} = k[A], ([B] \gg [A]) \quad (3.10)$$

Where A and B are the reagents, C is the product, r is the rate of reaction, k is the rate constant and [A], [B] are the concentrations of the reagents.

The integrated rate equation is

$$A = A_0 e^{-kt} \quad (3.11)$$

The concentration of A over time is an exponential decay from the initial concentration A_0 . The half life $t_{1/2}$ for this reaction is $\ln(2)/k$.

The rate constant k is inherent to the specific chemical reaction involved and can be modelled by the Arrhenius equation,

$$k = A e^{-E_a/RT} \quad (3.12)$$

Where A is the pre-exponential factor, E_a is the activation energy required for the reaction to occur, R is the universal gas constant and T is the absolute temperature.

The Arrhenius equation can make sense intuitively if one interprets it as follows:

The rate of the chemical reaction k , is the product of the total frequency of molecular interactions, represented by the pre-exponential or frequency factor A, multiplied by the fraction of the interactions that have energy greater than the activation energy E_a , as given by the Maxwell-Boltzmann distribution, represented by the exponential term $e^{-E_a/RT}$.

From (3.11) and (3.12), it can be seen that the only two ways to increase the rate of reaction is either to increase the temperature to shift the distribution so that more molecular interactions are higher in energy, or to decrease the activation energy, for example, by using a catalyst.

However, increasing temperature to increase the reaction rate could work, although any rate gains would need to be weighed against causing thermal damage to the tissue.

The use of a catalyst could work. But because the vinegar / baking soda reaction is a combination of two sequential reactions – the redox reaction (3.6) and then the chemical decomposition (3.7) — both reactions must be increased else a rate-limiting bottleneck might appear.

3.6.3. Overall conclusions for dissection by gas-evolving chemistry

Separating tissue layers in the oesophagus and stomach by gas evolved from mixing baking soda and vinegar does not seem very promising, based on proof-of-concept experimentation on the benchtop. However, this particular mixture possibly could be useful for creating long-lasting submucosal fluid cushions for ESD or EMR if safety and biocompatibility could be proven.

Potential strategies for improvement exist that could allow the concept to work, including the use of catalysts or different gas-evolving chemical reactions. However, this area of research is very firmly entrenched in chemistry, which is not an area of expertise of either the author or the research supervisors.

Also, the potential for applying the deconstructing dissection strategy is uncertain.

One might question, in the first place, why gas emphysema for tissue separation is being approached by mixing chemicals *in situ* when Sumiyama was able to achieve a better result using a canister of compressed gas?

The answer has to do with control in the context of the deconstructing dissection strategy. Sumiyama was able to separate tissue layers with injections of high pressure gas into the submucosal layer of gastrointestinal tissue. However, there was no real control over where the pressure front from the injection went. Presumably, it followed areas of mechanical weakness or pre-existing channels.

The hope was that by using a gas-evolving chemical reaction involving multiple reagents, one could essentially “plant” demolition charges in desired locations and set them off with the addition of the second reagent.

Although with perseverance this concept might be made to work as originally envisioned, it was deemed not to be a promising avenue of research, and too much unavailable chemistry expertise probably would be needed to make any further progress with this concept.

As with previous concepts proposed in this chapter, the question of which chemical reagents and their biocompatibility are key issues that need to be resolved.

In the specific context of using gas-chemicals for creating long-lasting submucosal cushions, the safety of evolving gas within tissue planes also should be investigated.

Also, deployment mechanisms for the chemical reagents need to be designed, although injection through large-diameter endoscopic injection needles seems to be a likely method.

3.7. Non-Newtonian fluid barrier

3.7.1. Protection from liquid “force fields”

Liquids have been used in the past to protect underlying tissue from procedures being performed on tissue above. Submucosal injection of liquids, in particular, to elevate resectable lesions and protect the underlying muscle layer is a well established technique in EMR and ESD. [122]

In order to create the submucosal fluid cushion, a saline-based injection typically is used, although more viscous substances such as 50% dextrose (D50), glycerol, sodium hyaluronate, hydroxypropyl methylcellulose (HPMC) and fibrinogen also have been used. These more viscous mixtures take a longer time to dissipate, which is advantageous when performing complicated EMR and ESD with long procedure times. [290][291][292][293][294]

It was wondered whether, taken to the logical extreme, an extremely viscous fluid could provide physical protection against mechanical penetration by a sharp object. Also, would it be possible for the fluid to transition reversibly between two states — a less viscous form for easy implantation into tissue and a hardened form to protect underlying tissue?

It is known that non-Newtonian fluids, or liquids that change viscosity with shear rate, have been used experimentally by military research to reinforce Kevlar body armour for protecting soldiers against knives and firearms.

They differ from Newtonian fluids because the viscosity, or the constant of proportionality between stress and strain in the fluid, is not constant and can depend on the shear rate. Non-Newtonian fluids that have lower viscosities at higher shear rates are called shear thinning fluids, and fluids that have higher viscosity at higher shear rates are called shear thickening fluids.

Wetzel et al. [295] used a shear thickening fluid (STF) composed of silica particles suspended in ethylene glycol to reinforce Kevlar fabric against penetration by a sharp object. STF infused into four layers of kevlar was able to withstand firearm penetration comparable to ten layers of Kevlar, while retaining the thinness and flexibility of the uninfused four layer material.

Although glass particles suspended in automotive antifreeze probably is not a very safe substance to inject into tissue, a commonly available shear thickening fluid composed of corn flour and water might be.

The concept proposed was to use this corn flour and water mixture as a submucosal injection to help protect against accidental mechanical perforations by needles and knives at flexible endoscopy.

Injection of the STF might be possible if the shear rate in the substance during injection is kept below the transition point at which shear thickening is induced. This behaviour is similar to the STF impregnated Kevlar armour described above that allows soldiers to move freely and bend the fabric under normal conditions, yet stiffen sufficiently to withstand firearms penetration.

However, this would require the shear rates induced at fluid injection to be distinctively lower than the shear rates induced by accidental needle or knife puncture. This may or may not be possible depending on the physical characteristics of the liquid suspensions used.

Alternatively, the STF suspension might be mixed in the tissue *in situ* by implantation of a core of corn flour or other substance with a large gauge needle followed by injection with water or some other liquid.

To develop this concept into a clinically viable technique, the biocompatibility of these substances would need to be investigated. Also, another important issue is what happens in the aftermath of the procedure — whether these injected substances are bioabsorbable, left as an implant or are physically removed.

3.7.2. Evaluating corn flour and water to protect against needle penetration

How well can the corn flour and water mixture protect against penetration by a sharp object? An experiment was designed to determine the effectiveness of the corn flour mixture in reducing the penetration depth of a sharp needle.

Methods

In the experimental setup (see Figure 3-25), a 19 gauge hypodermic needle attached to a trolley fixture and was dropped from various heights into a container of the shear-thickening corn starch mixture. The penetration capability at the end of the trajectory was measured by penetration into a layered foil target at the bottom of the container under the fluid.

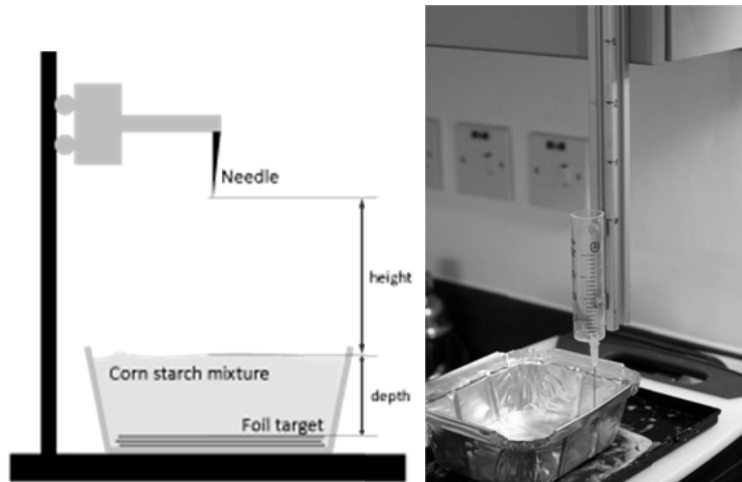


Figure 3-25. Schematic (left) and photograph (right) of the experimental setup.

The combined mass of the trolley and the needle measured on a Sartorius BP211D analytic scale was 21.977 g.

The aluminium foil target consisted of 101 individual layers of foil plus one outside binder layer. The thickness of individual layers of aluminium foil measured by Mitutoyo digital callipers was 0.01 mm thick.

Two corn flour mixtures were used. Mixture "2" consisted of two parts of corn flour to one part water (v/v) and had a cake-mix-like consistency. Mixture "4" consisted of four parts of corn flour to one part water and had a clay-like consistency. Mixture "0" was the baseline mixture and consisted of only pure water with no added corn flour.

Three depths of the each fluid mixture (10 mm, 20 mm, 30 mm) and five starting heights (38.1 mm, 76.2 mm, 114.3 mm, 152.4 mm, 190.5 mm) for the needle / trolley were used. The needle was dropped into the fluid to come to a complete stop after penetrating some distance into the foil target. The target was removed and the number of layers penetrated by the needle was counted.

The experimental design used was a full factorial design of experiment (DOE) type study with needle height, fluid depth and fluid composition as the inputs factors and the penetration depth as the output response. The statistical package Minitab (Minitab, Inc; State College, PA, USA) was used to generate the factorial design and statistically analyze the data.

Overall, the experiment consisted of forty-five runs with composition, depth and height set at different levels according to the factorial design.

Results

In general, the shear-thickening behaviour of corn flour and water manifested as a very discernable increase in the firmness of the material when strained with quick, forceful motions.

Qualitatively, it was very difficult to stir the mixture with a spoon, and striking the material on edge felt like hitting a solid object. Slow, languid motions were met with much less resistance, and slowly stirring the mixtures felt akin to stirring cake batter.

The results of the experiments are displayed in scatterplots in Figure 3-26 and Figure 3-27.

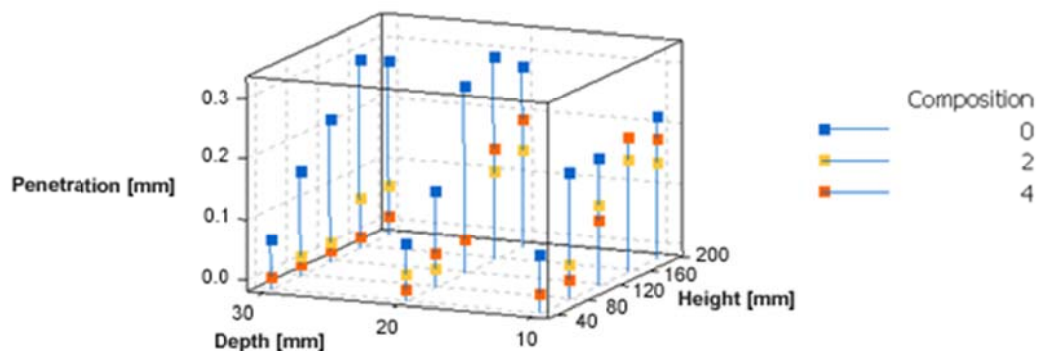


Figure 3-26. 3D scatterplot of layers of foil penetration versus initial needle height versus depth of liquid barrier. Composition "0" is water, "2" is the corn flour/water liquid and "4" is the corn flour/water "mud".

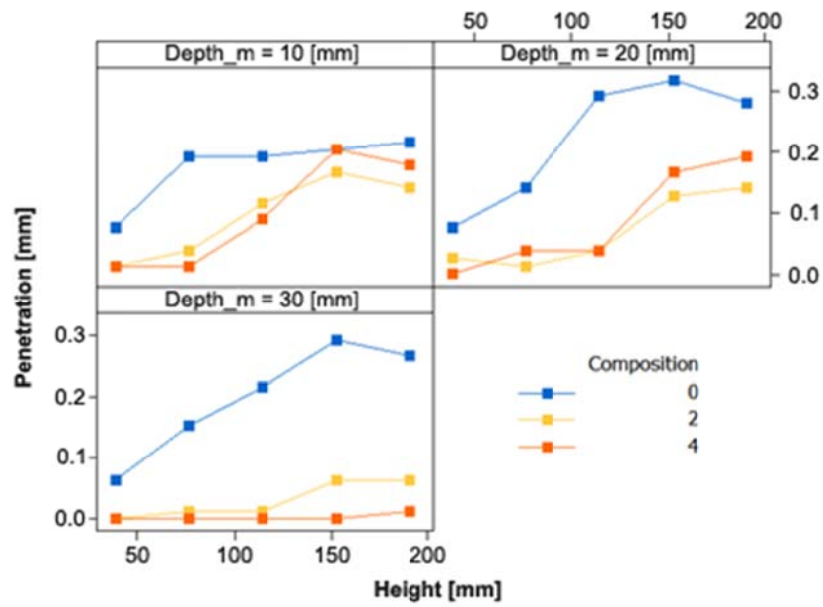


Figure 3-27. 2D scatterplot of foil penetration versus initial needle height for each liquid barrier composition. Composition “0” is water, “2” is the corn flour/water fluid and “4” is the corn flour/water “mud”.

Analysis of variance (ANOVA) of the data suggested that the correlation between the penetration and the fluid composition ($p=0.000$), depth of fluid ($p=0.004$), initial needle height ($p=0.000$) and the interaction between composition and height ($p=0.028$) were larger than could be explained statistically by random variability.

Therefore, composition, depth, height and composition*height were chosen as factors in the DOE. Higher order interactions, with p-values larger than 0.05, were used to estimate the error.

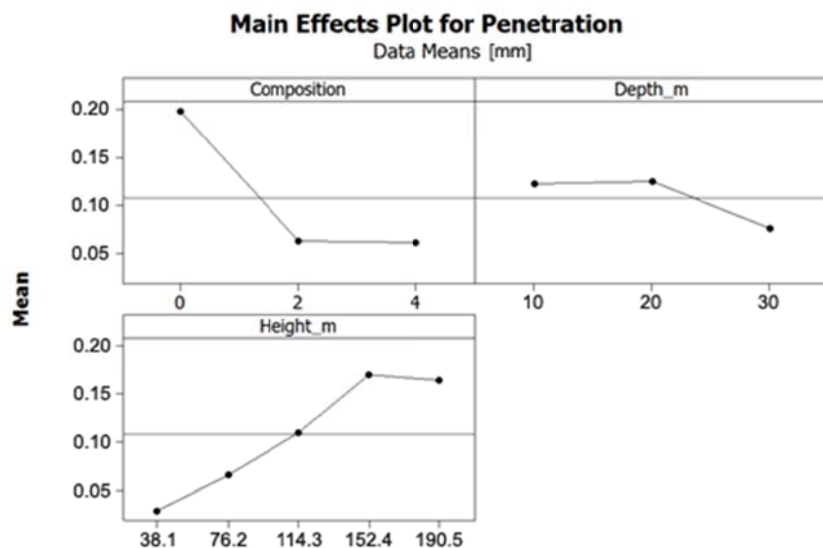


Figure 3-28. The main effects plot for penetration based on data means.

From the DOE model, the main effects can be seen in Figure 3-28. The model coefficients for the piecewise linear DOE model can be found in Table 3-6.

Table 3-6. DOE model coefficients.

Term		Coef	SE Coef	T	P
Constant		0.000108	0.000006	17.83	0.000
Composition					
0		0.000090	0.000009	10.44	0.000
2		-0.000044	0.000009	-5.12	0.000
Depth_m					
0.01		0.000014	0.000009	1.67	0.104
0.02		0.000017	0.000009	1.97	0.058
Height_m					
0.0381		-0.000079	0.000012	-6.48	0.000
0.0762		-0.000042	0.000012	-3.46	0.002
0.1143		0.000002	0.000012	0.14	0.890
0.1524		0.000062	0.000012	5.13	0.000
Composition*Depth_m					
0	0.01	-0.000037	0.000012	-3.06	0.004
0	0.02	0.000006	0.000012	0.49	0.629
2	0.01	0.000015	0.000012	1.25	0.219
2	0.02	-0.000013	0.000012	-1.04	0.304

It can be seen that the change in composition of the fluid from water to the liquid corn flour mixture had a significant correlation with a reduction in penetration, but this reduction, although still significant, was much smaller changing from the liquid corn flour mixture to the clay-like corn flour mixture.

The increase in the depth of the liquid barrier used from 2 cm to 3 cm also had a significant correlation with the penetration reduction. However, the slight increase in mean depth from 1 cm to 2 cm correlating with the increased penetration was not significant.

For starting height versus penetration, there was a positive correlation followed by a slightly negative correlation. However, the p-value of the coefficient from the third to fourth height coupled with a statistically unusual observation at the fourth height (an observation a large standardized residual compared to the model) may account for this unusual model behaviour.

The composition*depth interaction was only significant at the lowest settings of both factors. All other factorial combinations had p-values greater than 0.05. This possibly could indicate the

presence of a real interaction at the low settings of composition and depth, but it is also likely the interaction was a statistical anomaly.

Discussion

In general, the corn flour and water mixture in either liquid or the clay form provided more protection against needle penetration than water, reducing the amount of penetration the needle made into the foil target. However, the protection gained from changing from the liquid to the clay-like corn flour mixture was much smaller. Both these correlations were statistically significant and could not be accounted for to a 95% confidence level by random variation.

These results are consistent with our understanding of how shear thickening in colloidal suspensions can occur (see Figure 3-29).

The liquid phase (water) of the corn flour mixture is highly filled with rigid, colloidal particles (corn flour) in suspension. When the liquid experiences high shear rates, the forces that keep particles separated are overcome by hydrodynamic forces causing formation of hydroclusters, or clumps. These clumps “jam up” the particles as they collide and result in the mixture exhibiting macroscopic rigidity.

Copyrighted material

Figure 3-29. A model for the mechanism for shear thinning and shear thickening in non-Newtonian fluids.
(Reproduced from Wetzel et al. [296])

In other words, the STF behaves like a liquid until a shear thickening transition point after which microscopic clumping leads to jamming and macroscopic behaviour like a solid.

This might explain why there was a large difference in the protection offered by both the liquid and the mud-like mixtures of corn flour when compared with pure water, but why there was no significant difference between the liquid and the mud-like mixtures.

Thicker layers of barrier fluid were more effective at reducing penetration than thinner layers when going from 2 cm of liquid to 3 cm. This made sense as having a deeper layer of the protective fluid would allow for a longer interaction for the liquid to slow down and dissipate the kinetic energy in the falling needle as it made its way through the liquid.

The very slight increase in the data means of penetration correlating to the increase in depth from 1 cm to 2 cm was not significant.

Increasing the initial height of the needle in general corresponded to a deeper penetration into the foil target.

This makes sense because the higher starting distances of the needle/trolley assembly corresponded to higher initial potential energy and higher final kinetic energy at the end of freefall before contacting the protective liquid.

The assumption made is that the shear rate always was high enough to induce the transition of the corn flour mixture to the rigid state, thus providing far more protection than the liquid state and allowing for lower penetration into the foil witness.

This, in general, is supported by the data as the mean penetration of the corn flour mixtures was much lower than the water.

However, it also is possible that the shear thickening transition threshold was not reached until the needle was placed at an initial starting height of about 15 cm, explaining the discontinuity between increasing penetration up to about 15 cm starting height and the slightly decreasing penetration after 15 cm.

But the DOE model for the region between 11 cm and 15 cm height was not associated with a p-value below 0.05, and one could imagine a slightly different coefficient for the model in that region to make the overall model look much more linear.

One method to settle this question would be to use a rheometer to explicitly measure the viscosity of the corn flour mixture at different shear rates to determine the shear-thickening transition point, and then compare the shear rates induced by the needle falling from the various starting heights to this threshold.

However, this measuring equipment was not readily available and the experiment was not performed for this exploratory phase of the PhD.

Overall, the corn flour mixtures appeared to provide some protection against needle penetration. However, even with up to 3 cm of corn flour mixture to serve as a protective barrier, the needle still was able to penetrate some depth of aluminium foil. This raised the question of whether an injection resulting in a thin layer of the substance could provide adequate protection.

Injection of the corn flour into the “spongy” submucosal layer probably would perform better than the layer of only corn flour mixture in the experiment, as the interconnected layers of tissue might disperse the impact energy of the needle to a larger volume of liquid and induce shear thickening in more of the liquid. Wetzel et al. demonstrated better penetration resistance of their STF when impregnated into Kevlar compared with STF in a layer above or below the Kevlar.

Using a larger needle with a larger frontal surface area also might produce a similar effect by inducing shear thickening in more of the liquid. However, this also would impede its penetration capability for cutting the tissue above the protective layer.

It also was wondered what effect sending vibrations through the mixture would have? Could it induce sustained stiffening? What would happen with standing waves and rarefaction waves? Was it possible to use this effect to selectively control where tissue was protected, vis-à-vis the deconstructing dissection strategy?

3.7.3. Overall conclusions for protective shear-thickening liquid barriers

Playing with non-Newtonian fluids proved to be fascinating and provided many avenues for potential research. There was plenty of science to explore and the potential to bring novel mechanical engineering concepts into the realm of medical physics.

However, although the corn flour mixtures did seem to provide some protection against needle puncture, improving the protective performance would involve synthesizing non-Newtonian fluid mixtures with better performance and/or exploring further the speculative interaction between vibrations and shear-thickening.

Also, much of the equipment and expertise necessary was not available in the medical physics department where this research was being conducted, although help might be available from the mechanical engineering department.

Given these uncertainties, it was decided not to pursue this concept further.

If an appropriate, biocompatible shear-thickening fluid could be engineered, the next research steps could involve developing a suitable deployment and cutting method. Also, methods to make the solid fraction of the liquid suspension to be bio-absorbable would be quite desirable.

3.8. Monopolar and bipolar electrofulguration

3.8.1. Improvements to electrosurgical diathermy

Electrosurgical diathermy is one of the most common methods for cutting tissue at flexible endoscopy. Hot biopsy forceps, hot snares, sphincterotomes and needle knives all use electricity to dissect tissue.

However, certain tissues such as skin, adipose and mesentery can be difficult to cut with monopolar electrosurgery. It is thought that the relatively high impedance and relatively low water content of these tissues make them challenging to cut.

One possible solution is the use of electrofulguration to cut tissue.

Electrofulguration is the use of electrical sparks or controlled streams of plasma (ionised gas) to cut and coagulate tissue. Like with electrosurgery, this can be achieved in a monopolar configuration in which an active electrode and a grounding plate are physically separated by a large distance, or in a bipolar configuration in which the two electrodes are in close physical proximity.

Monopolar electrofulguration used for coagulation is employed in argon plasma coagulation. Bipolar electrofulguration might be considered conceptually by imagining tissue placed into the spark gap of an automotive spark plug.

The existing spray coagulation modes of some electrosurgical generators can produce voltages in the range of thousands of volts. The high voltage can cause electrical breakdown in air and form electrical arcs to coagulate (but not cut) tissue in a non-contact manner.

Used off-label (in a manner not officially recommended by the manufacturer), fulguration can be used to cut tissue when used with sharp or pointed electrodes like the tip of a bare wire or the edge of scissor blades.

Private conversations with two colorectal surgeons who also perform flexible endoscopy revealed that they have used fulguration to dissect tissue successfully clinically for laparoscopic cholecystectomy and experimentally in pre-clinical NOTES procedures.

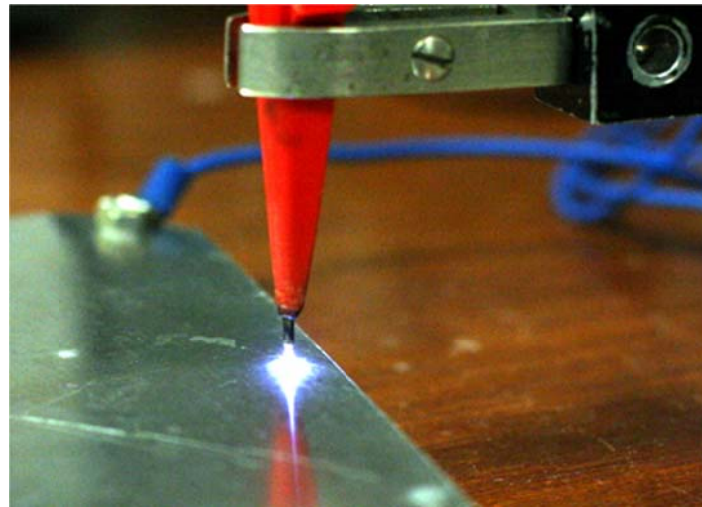


Figure 3-30. A spark can be made to jump a small air gap by using the high voltage spray coagulation mode to induce electrical breakdown.

What was started to be investigated was whether an existing ERBE ICC 200 electrosurgical generator could be used with a custom electrode geometry to reliably dissect tissue by both monopolar and bipolar electrofulguration (see Figure 3-30).

Unfortunately, while this experimental research was being conducted, two commercial products that employed fulguration to cut tissue were introduced and discovered as part of the ongoing literature review.

Further research on electrofulguration was discontinued; however highlights of the experiences are presented here.

3.8.2. Proof-of-concept experiments with electrofulguration

The purpose of these proof-of-concept experiments was to verify the feasibility of cutting tissue using electrofulguration.

A variety of *ex vivo* tissue types from a number of animal species were used to test a prototype electrofulguration setup using an existing, commercially available electrosurgical generator.

Both monopolar and bipolar electrical configurations were tested.

Methods

An ERBE ICC 200 electrosurgical generator (ERBE Elektromedizin GmbH; Tübingen, Germany) was used in spray coagulation mode, which is rated to generate 4000 V at a maximum power of 120 W at 500 ohms load.

Because of the low electrical load impedance in the benchtop experiments with the grounding pad positioned on the tissue in very close proximity of the cutting electrode, the electrical arcing generated during fulguration often would trigger the safety mechanism and shut down the system.

To prevent unwanted triggering of the safety mechanism, a 100 ohm thick-film resistor designed for high power dissipation was placed in series with the cutting electrode to ensure that the electrical load would not fall to a level that would cause the generator to switch off.

For the experiments using the monopolar electrode configuration, the standard flat-paddle shaped electrosurgical knife for open surgery was used as the cutting electrode and a larger metal grounding plate was used as the return electrode. The generator was set to spray coagulation mode and the active electrode was used to cut in a non-contact mode.

For the experiments using the bipolar electrode configuration, the metal grounding pad was replaced with a segment of exposed wire held by alligator clips. The generator again was set to spray coagulation mode and the two electrodes were held about 2 mm apart to cut in a non-contact mode.

The grounding pad safety mechanism in the generator that ensured, in normal operation, the proper attachment of the pad to the tissue needed to be bypassed by short circuiting the safety pins in the grounding pad port.

Desiccated and salted porcine small intestinal serosa, mesentery connected to freshly harvested porcine small and large intestine, chicken muscle, fat and skin were cut by electro-fulguration in both monopolar and bipolar electrode configurations and experiences noted.

In the final set of experiments, monopolar and bipolar electrofulguration was attempted *in vivo* in one live porcine model on mesenteric tissue. These experiments were performed at the end of the surgery after the unrelated, primary study had been completed. All relevant animal regulations and protocols were followed and the procedure was performed by a licensed practitioner.

Results

In all the experiments, the ERBE generator could be made to cut tissue using fulguration by bypassing some safety mechanisms and employing the spray coagulation mode of the generator.

Incisions made into chicken skin and muscle from tissue bought from the local supermarket can be seen in Figure 3-31.

The wounds produced by electrofulguration in general tended to be larger and resulted in more desiccation and charring during the dissection process. Also, the electrical arc tended to "wander" as it would spark to different tissue locations near the hovering active electrode.

However, with fulguration, one could reliably make incisions into the skin and underlying muscle tissue. Both skin and muscle were easily cut by fulguration.

Electrosurgical diathermy was much less reliable for making the initial incision into the skin. However, once an incision was able to be started, both the skin and the muscle could be cut. Unlike the skin, muscle was cut easily with diathermy.

Much less tissue desiccation and charring was seen with diathermy. Some coagulation was observed, although the amount was much less than with fulguration.

For comparison, cutting with a scalpel was relatively easy when the skin was pretensioned with the other hand between two fingers. As the knife was at room temperature and no additional energy means for coagulation was used, there was no coagulation, desiccation or charring observed with the scalpel-made incision.

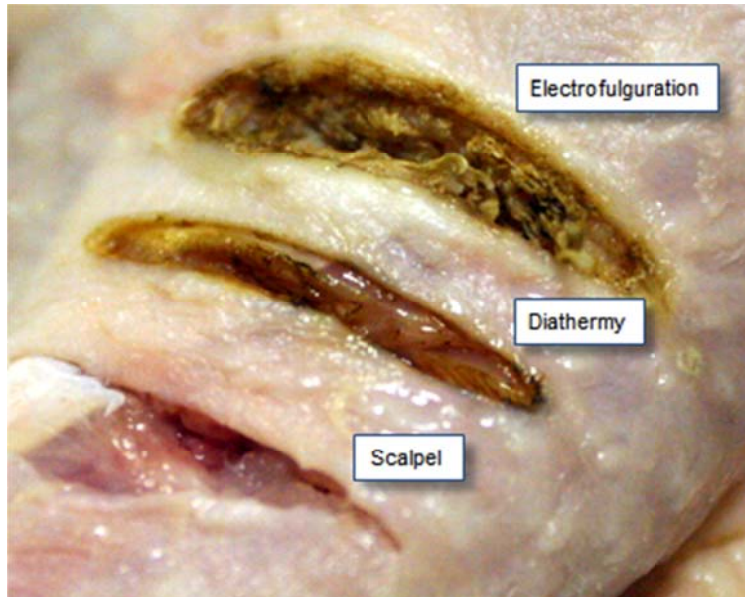


Figure 3-31. Comparison of incisions in chicken thigh made by electrofulguration, electrosurgical diathermy and scalpel.

The results of bipolar fulguration in chicken thigh can be seen in Figure 3-32.

The bipolar electrodes were used in two configurations. For tissue with an edge protruding from the surface, the tips of the two electrodes were placed in close proximity to each other on opposite sides of the exposed edge with the electrical arc penetrating the tissue.

For flat surfaces, one electrode was used to pierce the tissue like a needle, and the second then was brought into close proximity to the first. The electrical arc would form between the embedded and the exposed electrodes and vaporize the tissue in between.

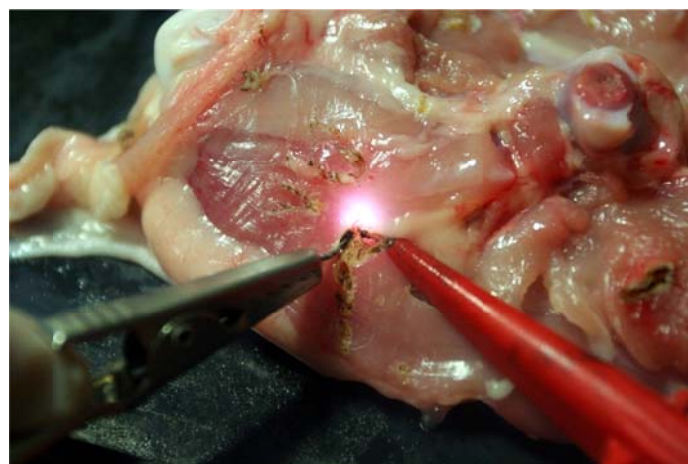


Figure 3-32. Tissue dissection by bipolar electrofulguration.

Overall, bipolar fulguration to cut tissue was possible and in these experiments appeared to be more controllable than monopolar fulguration. The electrical arc always was contained between the two electrodes. Damage to tissue appeared similar to monopolar fulguration with more tissue desiccation and charring than was found with diathermy.

Cutting salted sausage casings with electrofulguration is shown in Figure 3-33. The electrodes were used in a monopolar configuration.

The sausage casings (intestinal serosa) were able to be dissected using monopolar electrofulguration. However, a lot of tissue shrinkage was observed in the tissue in between the cut location and the area where the tissue was placed atop the grounding plate.

During fulguration, a plume of black smoke could be seen, and after fulguration, a visible area of charring could be found around the dissection margins.

Dissection through the sausage casings with normal electrosurgical diathermy was difficult. Very often the attempt would result in a large amount of tissue shrinkage without an actual incision being made.



Figure 3-33. Electrosurgical dissection through the serosa of the small intestine.

The results of monopolar fulguration of freshly harvested mesentery attached to small intestine can be seen in Figure 3-34.

As with the previous experiments, fulguration resulted in larger, more heavily charred incision wounds than with diathermy.

However, unlike previously, dissection with diathermy was relatively reliable and was performed more easily. Observed differences between these experiments and previous ones

include the tissue type used, the condition of the tissue and the location of the grounding electrode.

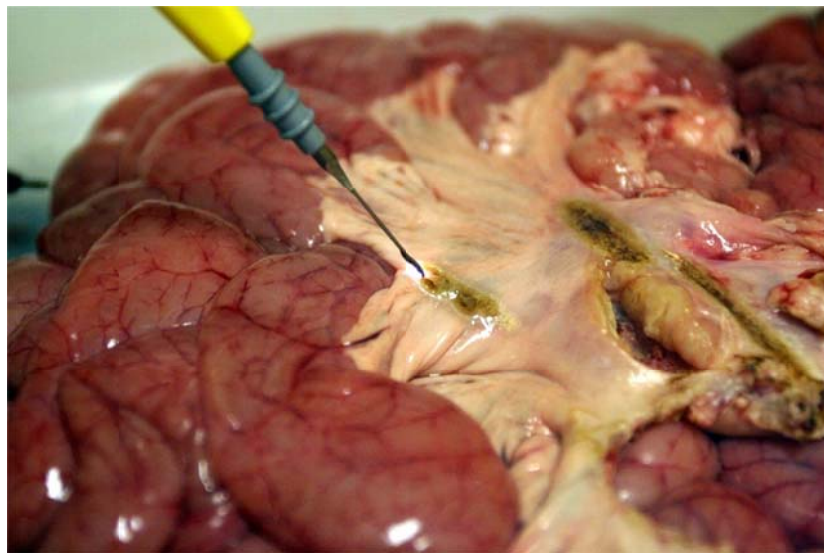


Figure 3-34. Tissue dissection by monopolar electrofulguration.

In the *in vivo* experiments in a live porcine model, both monopolar and bipolar electro-fulguration were used successfully to cut mesentery in open surgery. Bipolar fulguration, in particular, allowed for easy and rapid dissection of mesentery by moving the two electrodes in tandem on opposite sides of the tissue with the electrical arc serving as the “blade”.

In general, using monopolar electro-fulguration for tissue dissection was feasible with commercially available generators designed for electrosurgical diathermy.

Although incisions made by fulguration were associated with more charring and desiccation than with diathermy, in general, tissues like fat and skin that are considered to be difficult to cut by diathermy could be cut more easily with fulguration.

However, fulguration performed in this experimental setup resulted in less precise and predictable cuts, as the spark would jump around wildly from spot to spot on the tissue. Bipolar electro-fulguration was more predictable when the two electrodes could be maintained at a fixed separation.

Discussion

From the experiments conducted, fulguration appeared to be a viable method for cutting many types of tissue, including skin and mesentery which traditionally have been more difficult to cut with electrosurgical diathermy. However, a number of issues were observed.

In the monopolar electrode configuration, the location where the plasma arc would contact tissue was hard to predict, as the arc would skip around on the tissue. As the electrical impedance changed when tissue became coagulated, desiccated and charred, the path of least resistance also changed and the electrical arc jumped back and forth to different spots on the tissue to reflect this. This behaviour actually is exploited in spray coagulation and argon plasma coagulation to prevent localised heating and perforation of tissue, promoting more widespread but superficial coagulation instead.

The bipolar electrode configuration appeared to better control the location of the arc. Cutting performance was best when the two electrodes could be held in close proximity on opposite sides of thin tissue. Incisions into flat surfaces were more difficult, but a technique in which one electrode was used to impale the tissue functioned as a reasonable workaround.

Bipolar fulguration also avoided the dangers from accidental coagulation of tissue in a pedicle or connecting structure by geometric focusing of electrical energy. This was seen as the tissue shrinkage induced in the sausage casings when cut with monopolar fulguration. It also is a common problem with monopolar diathermy.

More smoke and charring was observed with fulguration than with standard cut diathermy. This probably is due to vaporization and combustion of tissue from the high temperature plasma arc. The high temperatures that allow for disruption of high impedance tissues like skin and mesentery also cause more desiccation, charring and smoke production.

A careful balance might be achieved by actively monitoring and limiting the power delivered to the electrodes. Design and construction of custom equipment tailored to fulguration might yield more desirable dissection results with less collateral damage to surrounding tissue.

In terms of selective control vis-à-vis deconstructing dissection, a number of control schemes were identified including injection of conductive or insulating masks described in the next section, feedback control, implantable grounding electrodes and mechanical schemes that limited cutting by fulguration to inside repositionable grasping jaws. However, none of these control concepts were taken beyond the ideation phase.

3.8.3. Overall conclusions for electrofulguration

Electro-fulguration in both monopolar and bipolar electrode configurations appeared to be a promising method for dissection of tissue.

Initial experimentation in feasibility using an electrosurgical generator yielded positive results. The promise of optimized fulguration using a custom electrical signal generator was good, and the prospects of modelling the physics seemed scientifically interesting.

Control schemes involving electrical insulating masks and grounding plates employing the deconstructing dissection strategy could be imagined.

However, in light of the commercial introduction of two devices that function by electro-fulguration, it was decided not to take this concept further.

The lack of publications on scientific research conducted by corporations in secret for strategic marketing and patent law reasons is an ongoing problem for academic researchers. Perhaps only by better engagement and cooperation between academic and commercial researchers can we mitigate these problems in the future.

3.9. Conductive or insulating masks for directing RF energy

3.9.1. Rubber tires and lightning rods

In a previous section, fluid injections of viscous fluids for protecting underlying tissue were described. Submucosa engorged with a shear-thickening fluid was shown to provide some degree of protection to underlying tissue from mechanical damage from a needle puncture.

What was wondered was whether fluid injections could afford electrical protection to underlying tissue from assault by electrosurgical diathermy or fulguration. Specifically, could insulating and conducting fluids be used like rubber tires and lightning rods to insulate against or divert electric currents around crucial anatomy?

For example, could electrical insulation or diversion be set up around the bile duct and the sensitive pancreas before sphincterotomy for ERCP or NOTES cholecystectomy?

3.9.2. Computer modelling of conductive and insulating masks

It was desirable to quickly explore the potential effects the presence of conductive and insulating materials would have on the electrical environment of tissue. A simplified finite element model was created in COMSOL Multiphysics (COMSOL AB; Stockholm, Sweden) to explore this problem.

Methods

A number of assumptions were made to simplify the model. Diathermy was modelled as a direct current problem instead of alternating current. The electrical properties of saline were used to model tissue, and the electrical properties of glass and copper were used to model the implantation of a good electrical insulator and a good electrical conductor, respectively.

A simplified 3D axis-symmetric geometry was used and consisted of a homogenous cylindrical slab of tissue with a smaller disc-shaped volume inside, hovering 1 mm under the top surface of the tissue and representing the implanted material. A 1 mm diameter area centred on the top surface of the volume represented the point of contact of the tissue with the ablation electrode. Taking advantage of the axis-symmetry, this 3D geometry could be simplified to the more simulation-friendly 2D geometry shown in Figure 3-36.

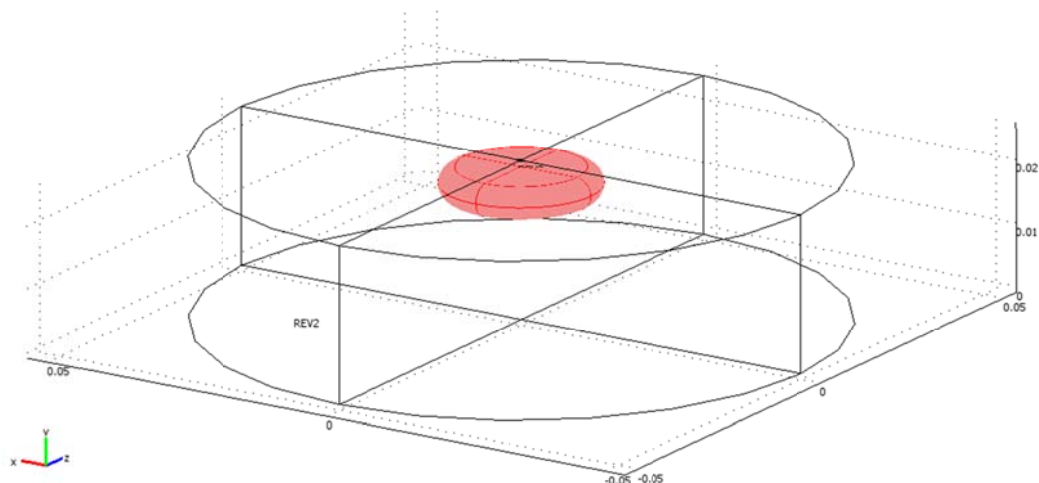


Figure 3-35. Axis-symmetric geometry of the model.

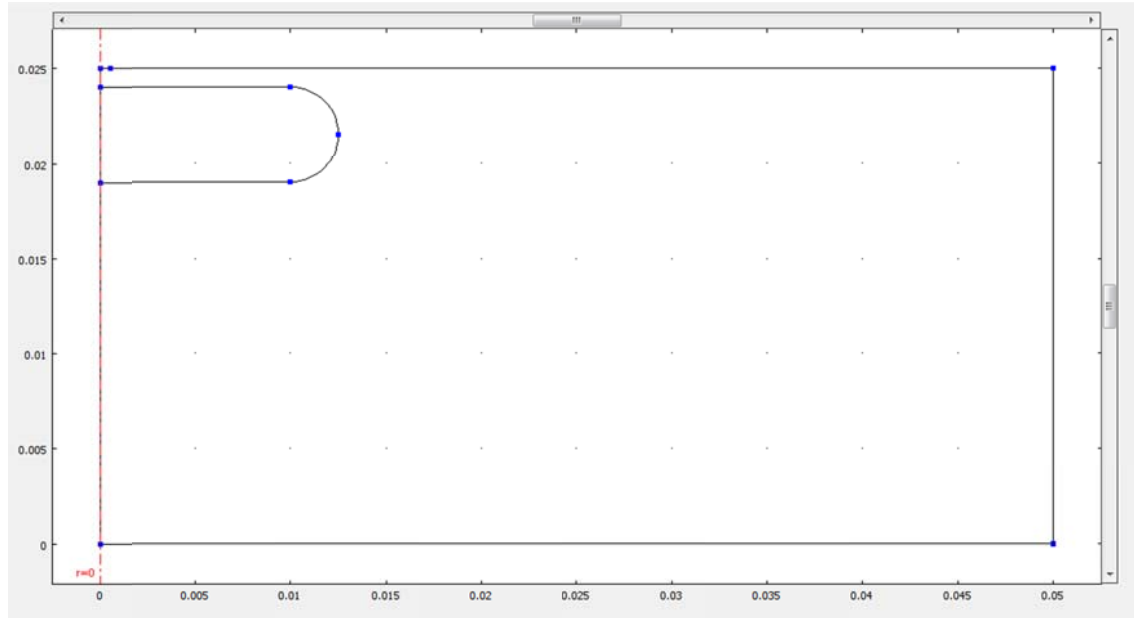


Figure 3-36. 2D cross-section of the 3D axis-symmetric model geometry.

The material properties of the implant region were set to the electrical properties of saline for the control case (no implant), to glass for the case with the implanted insulator and to copper for the case with the implanted conductor.

In the 2D model, the line segment representing the active electrode was set to a DC voltage potential of 400 V. The bottom and right-side edges of the slab were set to electrical ground. The left-side edge was set as the axis of symmetry.

A fine triangular mesh was created for the 2D geometry (see Figure 3-37).

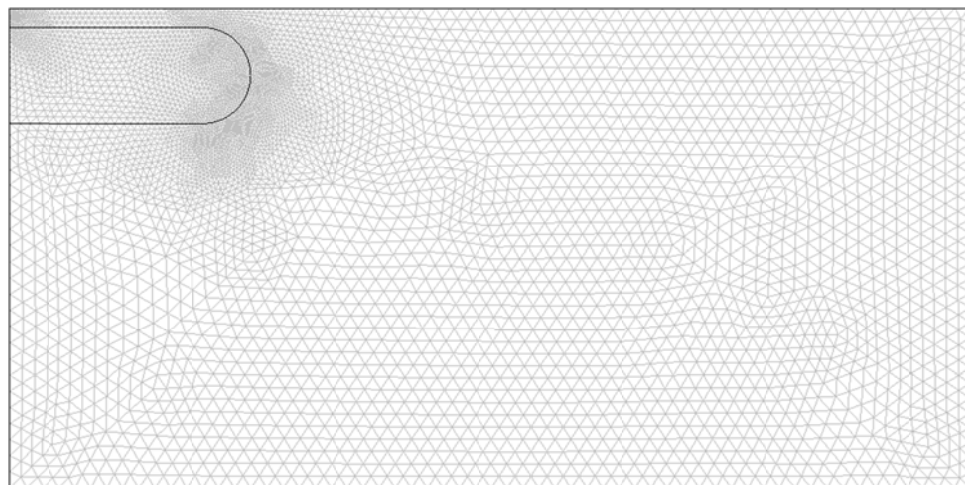


Figure 3-37. The meshed 2D geometry.

The conductive media DC mode in Comsol that was used to model the system employed the finite element method to solve the following governing equation:

$$\nabla \cdot (-c\nabla V - aV + \gamma) + aV + \beta \cdot \nabla V = f \quad (3.13)$$

Where c is the diffusion coefficient, a is the absorption coefficient, f is the source term, a is the conservative flux convection coefficient, beta is the convection coefficient and gamma is the conservative flux source term.

The model was run with the appropriate electrical properties to simulate the control, insulator and conductor cases. Stationary solutions were found using the built-in direct linear solver.

Results

The results from the model for the control, insulator, and conductor cases are shown in Figure 3-38. The graphs depict the magnitude of total current density in pseudo-colour and total current density streamlines as a red overlay.

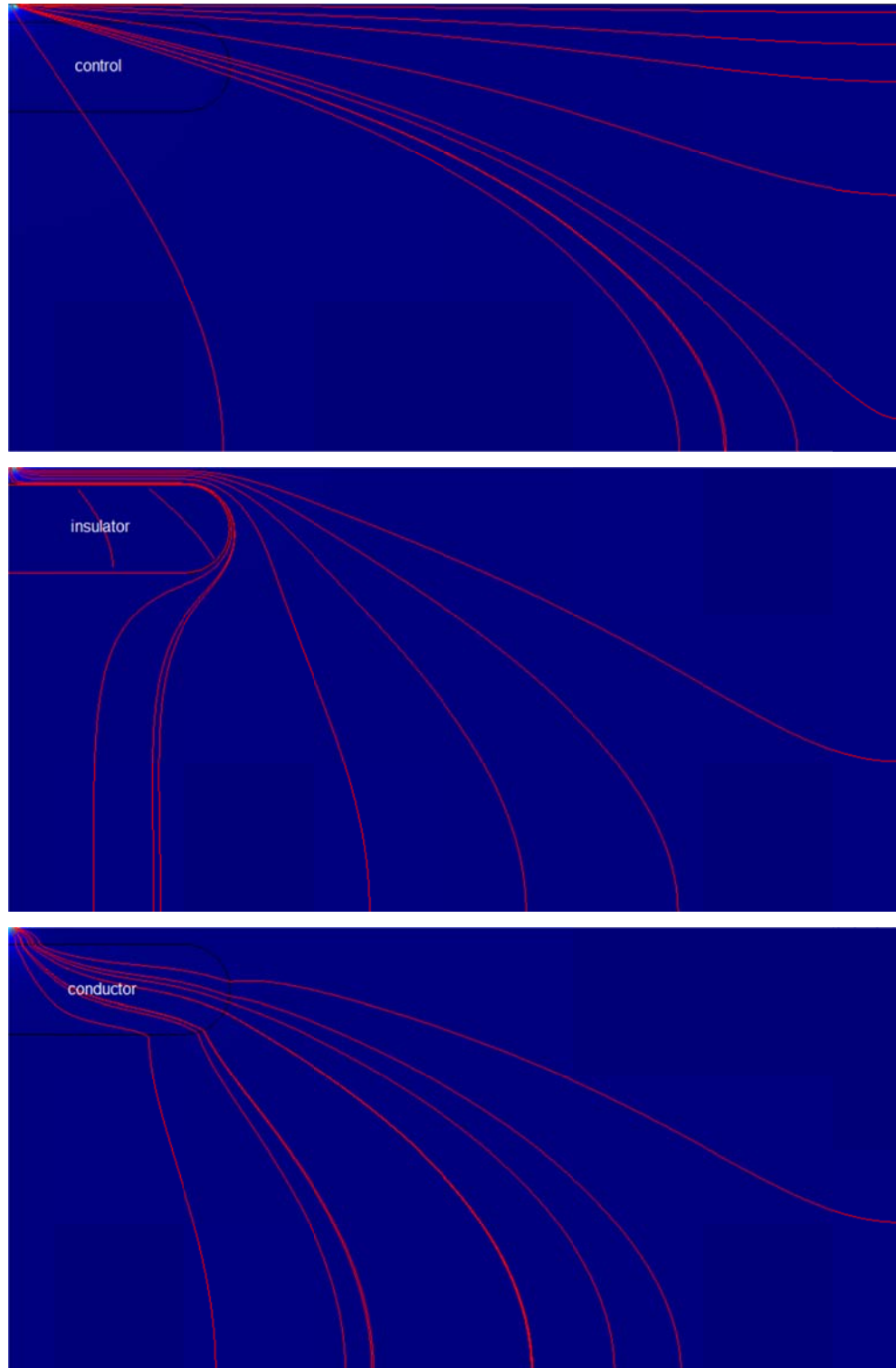


Figure 3-38. Results FEM simulation of monopolar electrosurgical diathermy with no implant (top), an implanted insulator (middle) and an implanted conductor (bottom). Surface colours represent the magnitude of total current density and the red lines are streamlines for total current density.

Discussion

It is interesting to compare the results from the control, insulator and conductor cases. In general, the highest magnitude of total current density appears in a small area around the active electrode in the upper left corner of the model in all three scenarios. However, it is interesting to observe the effects of the implants on the current density streamlines.

In the scenario with the embedded insulator, the high number of streamlines in the area between the top model edge and the top edge of the insulator indicate higher currents in this area compared with the control.

Because the presence of the insulator has “blocked off” direct paths to ground, much of the current is routed around the insulator. These higher currents in this area might result in thermal damage from Joule heating if the increase were high enough.

In the scenario with the embedded conductor, the streamlines are drawn towards the conductor and then exit from the conductor surface towards electrical ground.

The conductor appears to act as conduit, drawing current towards it and spreading it out in the tissue. Although more current may pass through the conductor than if the volume were made of tissue, much higher current would be necessary for the low resistance in the conductor to result in significant Joule heating.

Based on these simulations, it was concluded that, at least in theory, the use of implanted materials to alter current flows and current densities in tissue was possible. However, much work would be required to formulate and produce suitable biocompatible materials that would have the desired electrical and material properties.

One speculative concept that was of particular interest to the author was the potential formulation of a magnetorheological (MR) fluid that could change electrical resistance and fluid viscosity upon the application of a magnetic field.

Personal correspondence with Prof. Quentin Pankhurst, an expert in bio- and nano-magnetism at UCL, suggested that this might be possible with a suspension of magnetic nanoparticles in an electrically insulating liquid.

The application of a magnetic field theoretically could both increase viscosity and provide mechanical protection similar to the non-Newtonian fluid barrier concept, and increase

electrically conductivity as the nanoparticles clump together and provide a continuous electrical path for current.

Theoretically, an MR fluid with the potential to act as either conductor or insulator might be used *in vivo* by injecting it into an area under the target tissue. Multiple magnets can be used to create local regions of electrical conductivity and insulation in the fluid to “guide” the current from the electrosurgical generator. The spatial geometry of where regions of conductivity and insulation are located might be modified by manipulating the magnetic field.

However, there probably are severe limitations to the geometry and spatial resolution of these areas of local conductivity and insulation, and much research would be necessary to understand and characterise the behaviour of the fluid and its limitations.

3.9.3. Overall conclusions on conductive or insulating masks

Although the theoretical simulations were interesting and suggested that embedding insulators or conductors into tissue could produce scientifically interesting results, the overall research topic was considered to be too uncertain given the limited time and resources available for PhD research.

Primarily for this reason, no further work on this topic was pursued.

As before, further development of this concept would have to include study of the biocompatibility and safety of new materials and methods.

The complete lifecycle of these materials in relationship to the body would have to be explored as these materials essentially would be implanted into tissue. Whether the materials remain in place encapsulated in scar tissue or are absorbed and cleared out from the body would be a key issue defining the regulatory pathway the materials would need to follow for government approval.

Also, the safety and practicality of any electromagnetic systems and associated with activating MR fluids would have to be evaluated.

Still, these aspirational, blue-skies concepts could inspire others to look at old problems in new ways.

3.10. Miscellaneous Ideas

These concepts did not fit into the overall “deconstructing dissection” framework but were interesting, nevertheless, to the author. The majority of these were not taken beyond the brainstorming / ideation phase, and the feasibility of implementing them was not proven.

However, in the spirit of academic openness and cooperation, they are shared here with the hopes that they might inspire new research by other investigators working to improve technology for minimally invasive surgery.

3.10.1. Endoscopic scissors with local-tensioning

This concept builds on the observation that cutting tissue with scissors required countertraction to stretch tissue before the scissor blades could efficiently shear it. The idea was to build scissors with a built-in mechanism to locally tension tissue before shearing it. This perhaps could be accomplished mechanically by a tissue spreader mechanism, through suction, by electro-stimulation of muscular tissue or by some other means (see Figure 3-39).

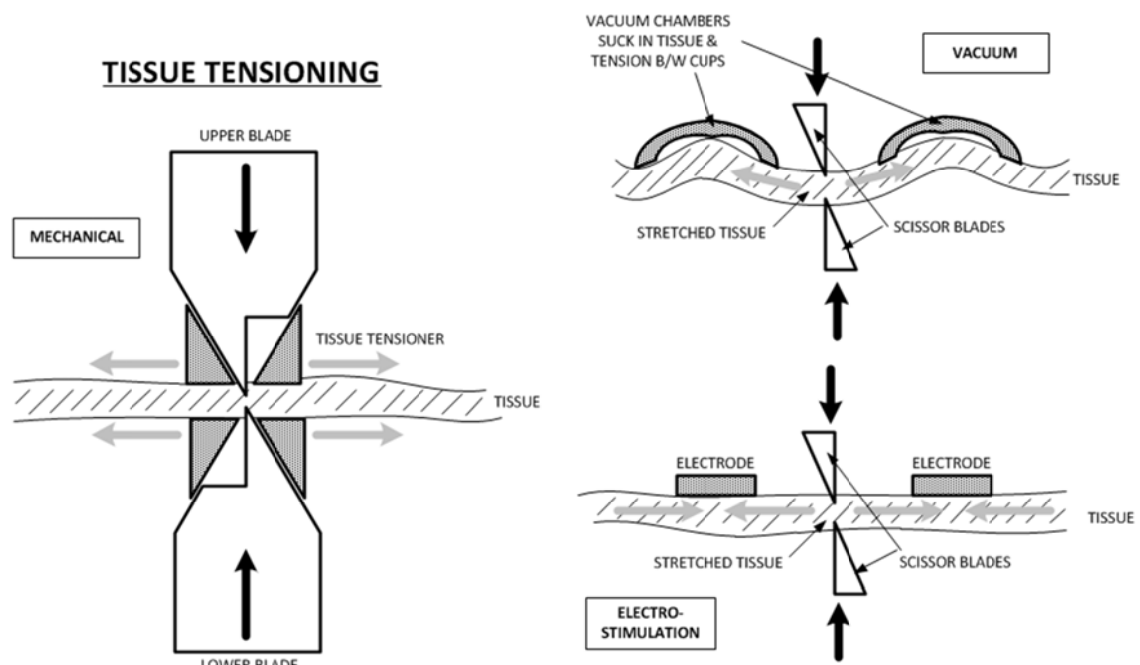


Figure 3-39. Mechanical, vacuum-based and electro-stimulation concepts for tissue stiffening.

3.10.2. Cheesewire cutter with tissue-depth stop

This concept aspired to use the cheesewire or bandsaw effect to cut tissue (see Figure 3-40). First, a curved needle would be used to place a metal wire at the maximum depth of tissue to be cut. The needle and wire would be recaptured by the cutting device. The cheesewiring

effect then is created by simultaneously drawing the wire and cinching it against the captured tissue. When the tissue has been cut and the wire has been fully retracted into the device, it can be reset in order to make another incision into the tissue.

The cheesewire cutter might be of value clinically when controlled endoscopic cutting of tissue to a specified depth is necessary. A depth guide mechanism could be implemented to adjust the depth of each incision.

Incisions made with this device might be safer to perform than with an endoscopic needle-knife because the cutting motion is made away from the tissue rather than towards it.

The cheesewire cutter might also be useful for difficult polypectomy because the stalk can be approached directly and the wire looped around it (before cinching down and transsecting the stalk) instead of having to maneuver a loop of wire over the top of the polyp or pseudo-polyp.

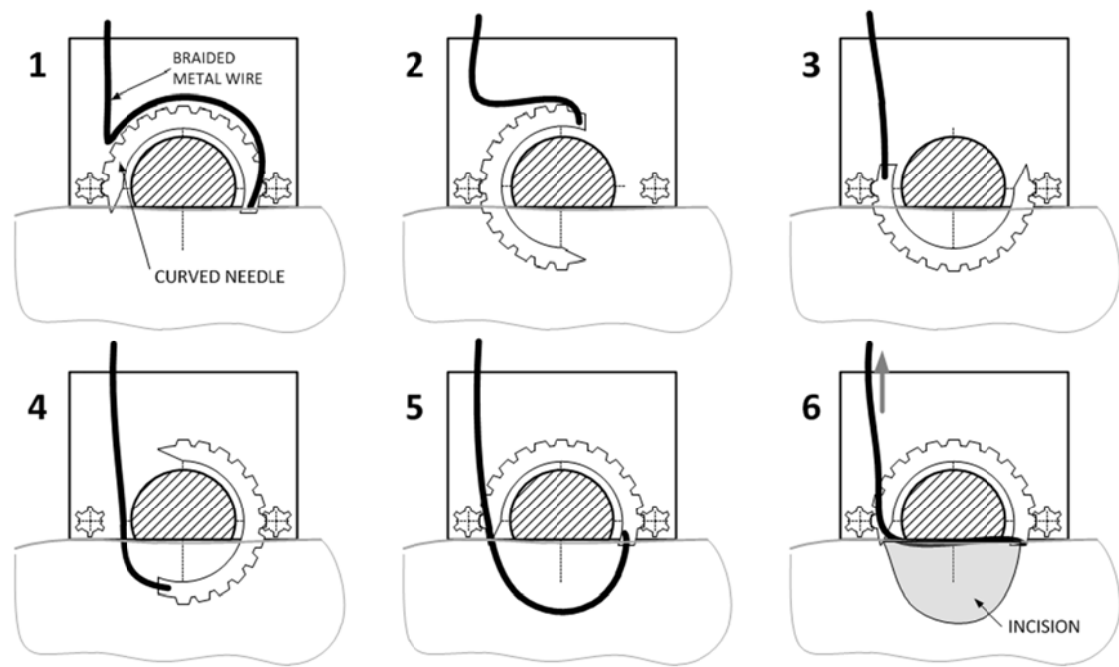


Figure 3-40. The Cheesewire cutting concept. (1) The metal wire is placed at depth into tissue with a curved needle and regrasped with the device. (2) Cheesewiring effect used to cut tissue by sliding the wire and cinching it against the captured tissue at the same time. (3) When the wire is fully retracted back into the device, it can be reset to make another incision.

3.10.3. Tissue differentiation by acoustic fingerprinting

This was a concept to identify the tissue type based on what was hoped to be distinctive acoustic emissions from tissue undergoing laser ablation with a carbon dioxide laser. This

information then could be used in as a feedback mechanism to control the laser to ablate only desired tissue types.

The idea was that because the carbon dioxide laser is very good at explosively vaporising intracellular water and different tissues have different microscopic structures, the “explosions” from the water would “ring” the tissue with an acoustic signature specific to the tissue type.

An initial exploratory experimental setup is shown in Figure 3-41, however no useful data suggesting these signatures might exist was collected from this kit. If a unique acoustic signature did exist, the signal-to-noise ratio simply was too low for this specific setup to detect the signal.

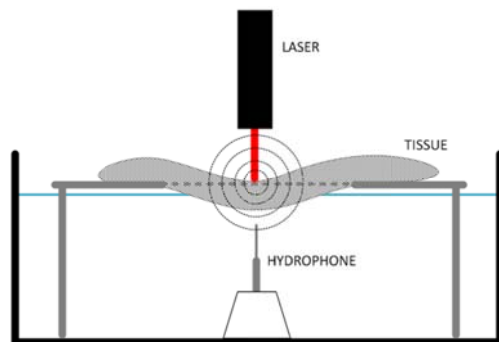


Figure 3-41. Acoustic “fingerprinting” experimental setup with CO₂ laser, tissue, and needle hydrophone submersed in a water bath.

3.10.4. Circular and rotary saw cutter

The original concept was to investigate whether high speed rotational cutting tools such as circular saws and drills could be used to cut soft tissues. Initial experimentation with a high

speed Dremel tool (maximum rotational speed of 35,000 RPM) using standard cutting bits to cut freshly harvested porcine gastric tissue occasionally were successful (see Figure 3-42 and Figure 3-43).

The cut-off disk was approximately 25 mm in diameter and 1 mm thick. The other drill and grinding bits were approximately 3 mm in diameter.

However, often the tissue was dangerously entangled around the spinning cutting tool, randomly and forcefully catapulting it into the air. Perhaps more suitable cutting blades for soft tissues and cutting guards to protect against collateral damage could be designed. Sharp circular blades such as in the delicatessen meat/cheese slicing machines might yield better results than Dremel tool bits and blades used.

However, even if cutting could be optimised, control of bleeding would still be a problem. This potentially could be addressed by incorporating electrosurgical coagulation capabilities into the device as the metal cutting blades would be electrically conductive.

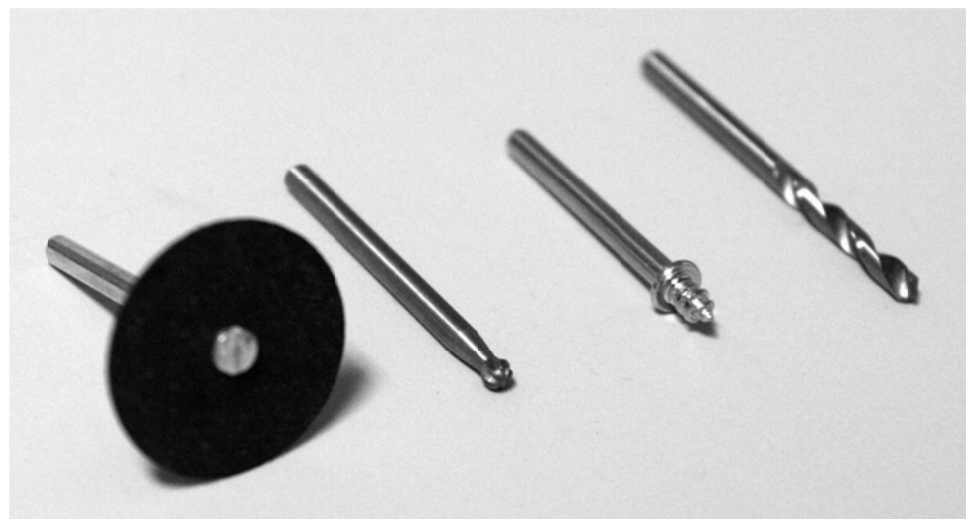


Figure 3-42. Rotary grinding and drilling tools used with a high speed rotary instrument.



Figure 3-43. Of the cutting tools in the Dremel kit, the circular cut-off disk was the most effective at cutting the slippery, mucus coated porcine gastric tissue.

3.10.5. RF-vaporisation or hydrogen peroxide decomposition for waterjet cutting and rotary steam engine

The concept involved harnessing the enormous volume change generated by either saline vaporised by passing a high voltage current through it, or hydrogen peroxide catalytically decomposed by passing it through a silver screen to create a forceful jet of water.

This jet potentially could be used to cut soft tissues directly or to drive a rotary steam engine to create high torque rotary motion *in situ* inside the body at the distal end of the endoscope.

The ability to generate high speed or high torque rotational motion at flexible endoscopy could be important as currently there are no reliable methods to do so.

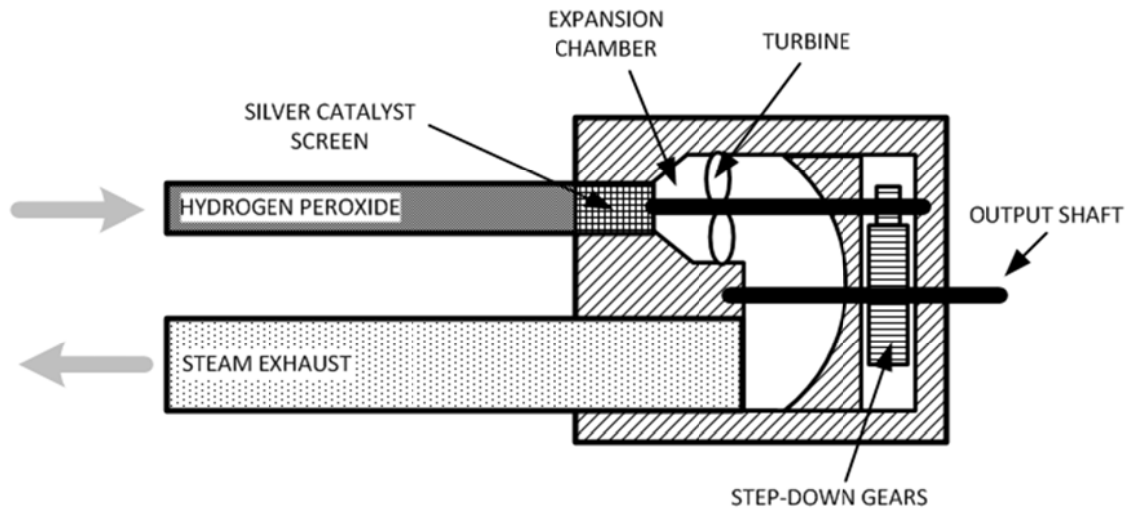


Figure 3-44. One embodiment of a miniature hydrogen peroxide steam engine to generate rotary motion *in situ*.
(Reproduced from author's personal design notebook.)

3.10.6. Vibrating blade

This concept involved using the small pager motor inside a Gillette M3 Power razor blade to vibrate a cutting blade. Two patents found during the literature search [297][298] describe the use of vibrations to augment the cutting power of razor blades for men's' shaving and it was wondered whether this effect could improve cutting with a razor blade (see Figure 3-45).

Although cutting forces were not rigorously measured, no difference could be discerned qualitatively between the vibration assisted blade and a standard scalpel.



Figure 3-45. A crude attempt at a vibrating blade using a commercial vibrating shaving razor handle.

3.10.7. Shear-thickening fluids for transmitting ultrasonic vibrations

Ultrasonic dissectors that are compatible with flexible endoscopy often have been requested by physicians and surgeons. However, these devices currently do not exist at flexible endoscopy probably because of difficulties with miniaturizing piezoelectric actuators and designing flexible acoustic waveguides.

Could shear thickening fluids be used in the design of a flexible acoustic waveguide?

Although this idea was never taken beyond fanciful speculation, the shear-rate-dependent viscosity of shear-thickening fluids might be a beneficial property. Instrument and scope manipulations probably would induce low shear-rates in the material while ultrasound vibrations might cause high-shear rates.

Of course, questions of whether shear thickening fluids could be used as part of a waveguide design and the efficiencies of such a system would need to be answered to evaluate whether this concept would be feasible in practice.

3.11. Summary of concepts, selection criteria and selection results

Except for the concepts in the miscellaneous ideas section, all the deconstructing dissection concepts presented along with evaluation criteria are listed a concept selection Pugh chart in Table 3-7.

Seven subjective selection criteria were used to compare the concepts against each other. These criteria were:

1. Feasibility or likelihood of success.
2. Availability of equipment and materials, given budget constraints.
3. Likelihood of biocompatibility and/or complications.
4. The anticipated safety both to patients and operators.
5. Available expertise and guidance.
6. Physics and science content enough to make a reasonable contribution to the field?
7. Author's personal bias.

The electro-fulguration concept was chosen to be the baseline because of its similarities to existing dissection technology at flexible endoscopy. Each concept was compared to this baseline concept and evaluated for each selection criterion to be better, similar or worse than the baseline.

The results are tabulated in Table 3-7.

Based on attributes such as feasibility / likelihood of success, availability of equipment and materials, biocompatibility and likelihood of complications, safety to patients and operators, available technical expertise, perceived scientific content and author's personal bias, the concept with the highest overall score was dye-mediated laser ablation.

Table 3-7. Concept selection Pugh chart.

Concepts	Each concept is compared against the baseline and evaluated for each attribute. '+' indicates better, easier, more positive than the baseline, '0' represents similar to baseline, and '-' denotes worse, harder, more negative than the baseline. Scoring is subjective, based on impressions from proof-of-concept experimentation, theoretical models, and resource and expertise considerations.	Attributes							TOTAL SCORE
		Feasibility / likelihood of success.	Availability of equipment, materials.	Biocompatibility, complications.	Safety to patient & operator.	Available expertise.	Physics / science content.	Author's bias.	
Dye-mediated laser ablation.	+	+	0	0	+	+	+	-	5
Selective tissue stiffening prior to mechanical shearing with scissors.	0	+	0	0	-	-	-	-	2
Blunt dissection by gas-evolving chemical reaction.	-	+	-	-	-	-	-	-	5
Non-Newtonian fluid barrier.	-	0	-	0	0	0	0	-	2
Hyper-conductive or insulating masks for directing RF energy.	-	0	-	-	-	+	0	-	3
Monopolar and bipolar electro-fulguration.*	BASELINE							*	

*The monopolar and bipolar electro-fulguration concept was chosen as the baseline because it is most similar to existing cutting technology at flexible endoscopy.

3.12. Chapter Conclusions

The strategic concept of deconstructing dissection was presented along with arguments for potential benefits offered by the idea.

With the restrictions of feasibility, practicality and historical precedence removed to allow for unlimited blue skies brainstorming, many new and hopefully creative concepts were generated.

These were evaluated using the scientific method, and data from the initial investigations into a number of these concepts were presented, along with discussions and evaluations of the suitability of the concepts for continued research.

Using the Pugh chart method for concept selection, one concept was chosen for further research. The dye-mediated laser ablation concept showed the most promise in terms of likelihood of success, scientific content and author bias and was chosen to be the conceptual focus for the rest of the PhD research.

Chapter 4:

Dye-mediated laser ablation

When you want something, all the universe conspires to help you achieve it.

Paulo Coelho
The Alchemist

4.1. Chapter Overview

This chapter explores dye-mediated laser ablation in detail, reviews experiments conducted to understand the ablation process and statistically models the dye-mediated ablation process in response to laser irradiance, exposure time and applied dye volumes.

A theoretical framework is offered to explain the mechanism of ablation. First, the McKenzie theoretical model for laser ablation of tissue is modified for dye-mediated ablation. Then a numerical computer model is presented.

4.2. The concept

In order to cut tissue, bonds holding the solid mass of tissue together need to be broken. Energy needs to be deposited in tissue to cause a thermal, mechanical or chemical stresses large enough to break bonds and relocate mass. If this process is used to reshape the topography or physical configuration of tissue, we typically can call this tissue dissection or cutting.

Different lasers can be used to provide this energy to the tissue in a variety of different ways.

Excimer lasers, for example, affect tissues in a photochemical manner by breaking molecular bonds directly without causing excessive tissue heating. Excimer lasers are used for corrective eye surgery because they can cut corneal tissue without thermally changing its optical properties.

Nanosecond or picosecond pulsed lasers can affect tissues in a photomechanical manner by forming plasmas that cause high-pressure acoustic waves to travel through the tissue and break it apart mechanically. These photomechanical effects have been used clinically, for example, to disrupt opaque membranes in the eye or fragment kidney stones impacted in the ureter.

For lasers that affect tissue primarily in a photothermal manner, laser energy is absorbed by chromophores within the tissue and is converted into heat.

10.6 μm carbon dioxide laser light, for example, is absorbed very strongly by water. The energy deposited in tissue by the carbon dioxide laser goes into rapidly heating the intracellular water and causes a phase change from liquid to gas that is accompanied by a large change in volume. If this process happens rapidly, this explosive vaporisation of water rips cells apart and results in displacement of tissue mass and cutting of tissue.

How well the light is absorbed by the tissue is quantified by its wavelength-specific absorption coefficient, μ_a , which, for a non-turbid medium where the scattering coefficient $\mu_s=0$, relates incident and transmitted light by the Lambert-Bouguer Law:

$$I = I_0 e^{-\mu_a d} \quad (4.1)$$

Where I_0 is the irradiance of the incident light, I is the irradiance of the transmitted light and d is depth.

This equation describes an exponential decay of light intensity within non-turbid tissue where at a characteristic distance of $1/\mu_a$ the light has fallen to an intensity of $1/e$ of the initial intensity.

It must be emphasised that (4.1) holds true only when $\mu_a > \mu_s$. Nevertheless, we can see from (4.1) a number of strategies to increase laser heating of tissue.

One strategy is to increase I_0 . We can increase the irradiance by using a more powerful laser with a higher power output or by decreasing the spot size by focusing the laser light to a smaller spot.

Another strategy is to increase μ_a . This can be achieved by selecting lasers with output wavelengths that are highly absorbed by existing chromophores found in the tissue. For example, 2.94 μm light from an Er:YAG laser and 10.6 μm light from a carbon dioxide laser both are strongly absorbed by water, which is a major component of most tissues. As a result, these two lasers can ablate tissue very effectively and are used clinically for cutting and resurfacing tissue.

The final strategy for boosting laser heating is to increase μ_a by adding an extrinsic chromophore that is highly absorbent at the light wavelength of whatever laser one would like to use.

This is the strategy that we employ by matching a low power, 805 nm semiconductor diode laser such as the Diomed 25 (Angiodynamics Co; Queensbury, NY, USA) with indocyanine green dye.

4.3. Lasers

4.3.1. Light amplification by stimulated emission of radiation

A laser, which stands for light amplification by stimulated emission of radiation, is an optical device that emits intense beams of light by the process of stimulated emission.

Unlike light generated by other processes such as incandescence or fluorescence, the laser light usually is coherent, meaning that the emitted light waves have identical frequency, phase and polarisation. The emitted beam of light also usually exhibits low-divergence and can travel long distances while maintaining high beam intensity.

Stimulated emission is a process by which an atom or molecule in an excited energy state is struck by a photon of the correct energy to produce a second photon of identical frequency, phase, polarisation and direction to the original photon. A laser takes advantage of this phenomenon by bouncing these photons back and forth through the gain medium of excited atoms or molecules to cause a cascade amplification of light.

Energy is required to raise the atoms or molecules in the gain medium to the excited state, and they may decay back to the ground state by spontaneous emission. However, if the rate of excitation can be made greater than the rates of spontaneous emission so that there are more atoms in the excited state than in the ground state, a population inversion can be achieved and the laser can work as an optical amplifier.

4.3.2. The Diomed 805 nm semiconductor laser

The Diomed 25 laser (Angiodynamics Co; Queensbury, NY, USA) that was used for all the ICG-mediated laser experiments is a medical semiconductor diode laser that can emit up to 25 W of 805 nm near-infrared laser light.

It often is used clinically in interstitial laser photocoagulation (ILP), for example, for coagulating spinal osteoid osteomas, [299] prostate cancers, [300] and liver metastases. [301]

It also has been used in research for ablating tissue by using a 300 µm fibre in contact mode. [302]

Because technical documentation could not be found for this relatively old and discontinued laser model, measurements were made to characterize the laser output.

4.3.3. Laser output power measurements

A power calibration between laser set power and power measured at the tip of the optic fibre was performed because transmission losses were expected due to the mode scrambling fixture used with the 600 micron optic fibre to smooth out the beam profile.

The fixture consisted of a small wooden plank with seven nails protruding from it around which the optic fibre was looped slalom style and in small circles. Light leakage from the cladding of the fibre in the region of the mode scrambler would lead to less power being emitted from the fibre tip.

Methods

Power calibration was performed using a Coherent 210 thermopile laser power meter (Coherent, Inc; Santa Clara, CA, USA).

A thermopile is an optically absorbing ceramic disc to which is bonded an array of thermocouples. The array senses the temperature gradient produced by optical radiation incident on the disc. The temperature gradient, and hence, the voltage produced by the array, is proportional to the power of the incident radiation.

The laser power was set to 5W, 15W and 25W and the laser output measured with the power meter. The run order was randomized to minimize any systemic effects on the data.

Transmission efficiencies at individual power settings were calculated by dividing measured power by set power.

A statistical analysis was run and a linear regression was fit to the data.

Results

From linear regression of the calibration data ($n=28$), the output power from the fibre tip was measured to be about 66% of the set power (see Figure 4-1). The regression model had an R-squared value of 0.9996.

Discussion

Much of the lost laser power probably was due to losses in the mode scrambler, imperfect coupling at the laser-fibre interface due to the numeric aperture of the fibre and some degree of absorption by the optic fibre.

Transmission efficiency stayed essentially constant over the measured power range as the linear regression model was a very good fit for the experimental data.

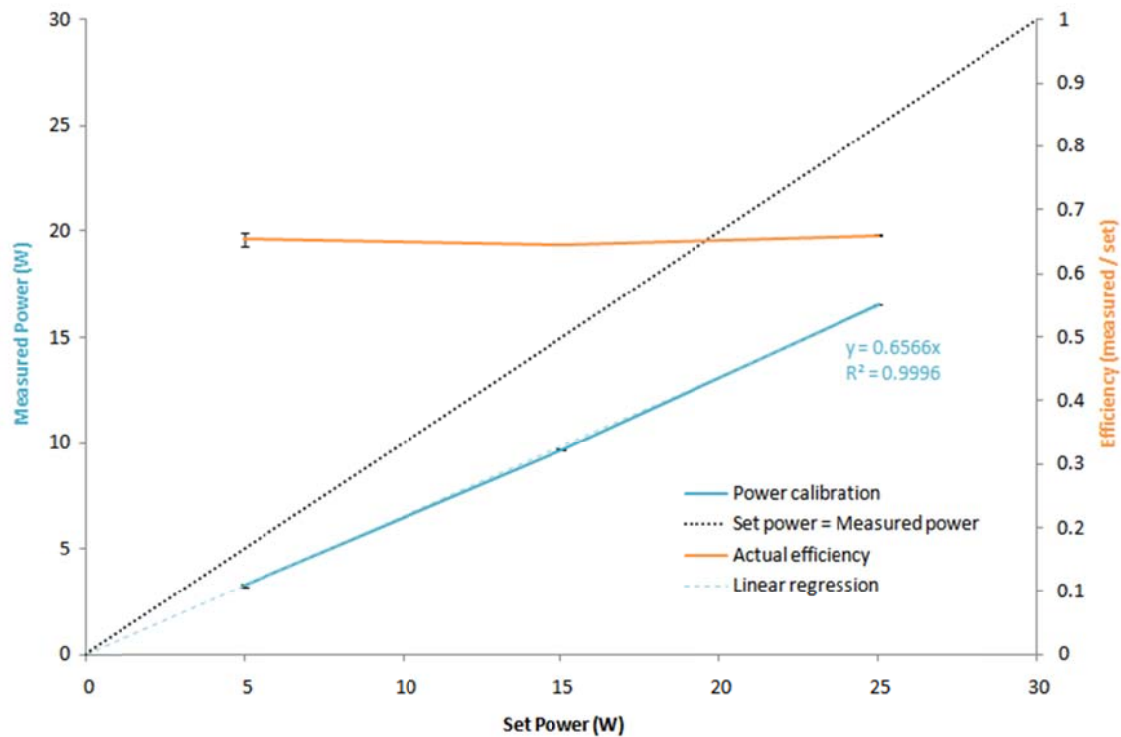


Figure 4-1 - Calibration of the set power vs. measured output power for the Diomed 25 laser ($n=28$). Error bars are standard errors. The overall laser system with the fibre and mode scrambler has an output efficiency of ~66%.

4.3.4. Beam profile and divergence

The laser beam emitted from the Diomed 25 laser consists of an invisible, circular NIR beam for treatment and a red annular aiming beam that circumscribes the therapeutic beam (see Figure 4-2). This red aiming beam optionally can be disabled.

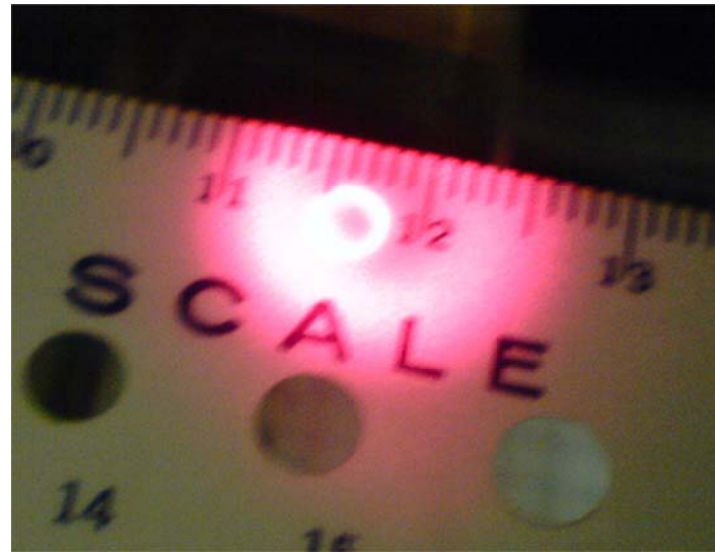


Figure 4-2. The visible red aiming annulus circumscribes the targeting area of the invisible NIR treatment beam.

The Diomed laser itself is composed of a linear array of semiconductor laser diodes that can be powered in different firing configurations depending on how much output power is required. At high power settings, all the diodes are activated. For low power settings, alternating diodes can be activated on successive laser firings to even out wear and extend the overall life of the instrument.

Axis-symmetric smoothing of the output beam is imparted by transmission of the laser light through the optic fibre, and some degree of radial smoothing is gained by mode scrambling from winding the fibre through a fixture with a tortuous path.

However, when viewing the beam enlarged and projected onto the wall through an Electrophysics Model 7215 electroviewer (Electrophysics Corp; Fairfield, NJ, USA) (see Figure 4-4), irregularities in the beam profile were revealed.

Specifically, at lower power settings, the various laser diode firing configurations could be observed in successive firings at a constant laser power setting (Figure 4-4). The beam profile at high power settings appeared qualitatively not to change visibly.

It was unknown what the magnitude of these variations were and if they were exaggerated by non-linear signal amplification in the electroviewer.

Therefore, it was desirable to explicitly measure the profile of the beam emitted from the Diomed 25 laser.



Figure 4-3. An electroviewer is used to visualize the near-infrared radiation from the Diomed laser.

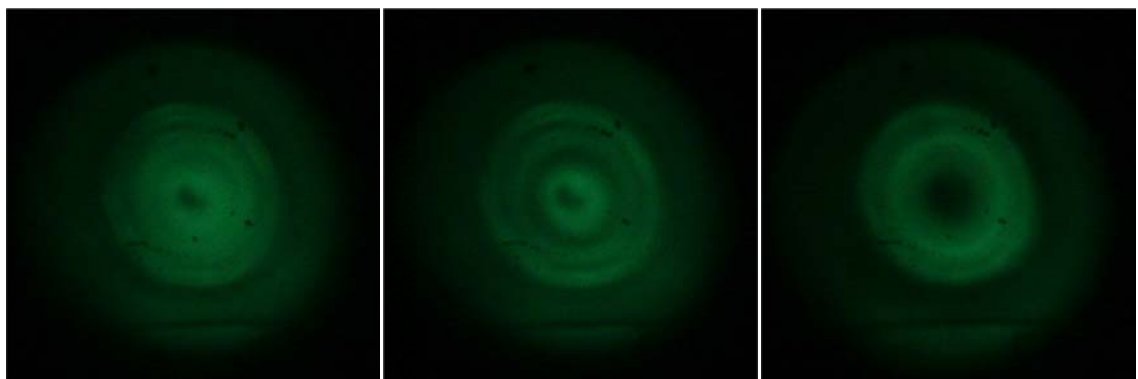


Figure 4-4 – At low power settings, the beam profile from the Diomed 25 laser set to a constant power, projected onto a white screen and viewed through an electroviewer varied from one activation to the next.
At high power settings, the profile was relatively consistent between activations.

Methods

A 600 µm clinical optic fibre with a coaxial blower sleeve was connected to the Diomed laser and an Olympus air blower unit (Olympus Medical Corp; Tokyo, Japan).

The fibre was passed through a mode scrambling fixture and the divergent laser beam output was projected onto graph paper 28 cm away measured from the fibre tip to the projection surface (see Figure 4-6). Normality between the fibre and the projection plane was obtained by adjusting the fibre holder position until the projected aiming beam annulus was circular.

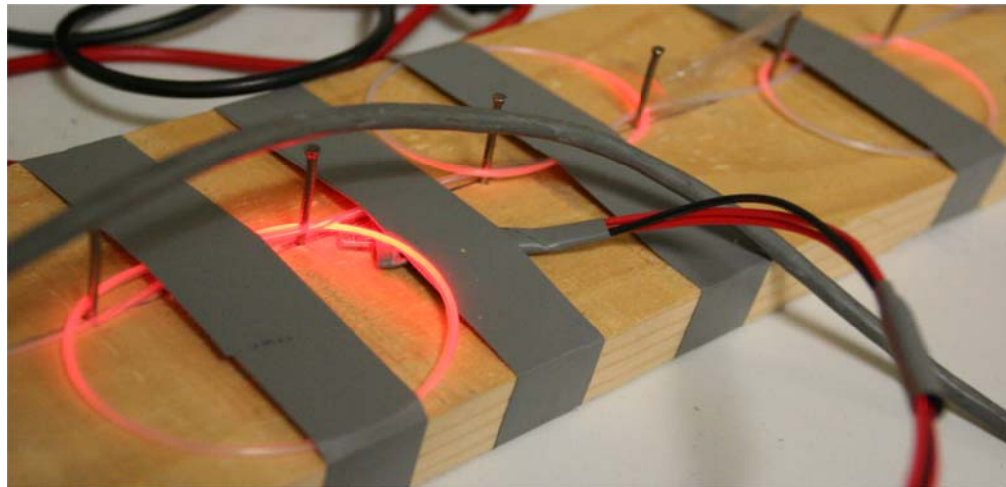


Figure 4-5. Mode scrambling fixture.

The beam was centred on guide marks made on the graph paper. Once all positioning adjustments had been made, the red aiming beam was switched off.

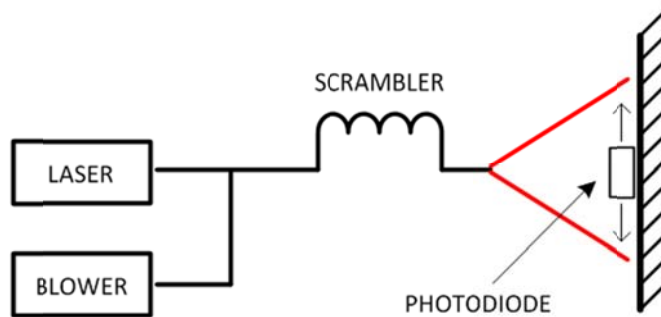


Figure 4-6. Experimental setup for the beam profile measurement experiments.

A Centronic OSD5-5T photodiode (Centronic Ltd; Croydon, UK) with a 5 mm^2 sensor that had a maximum sensitivity between 820-850 nm was used as a light sensor in photovoltaic mode to measure light intensity (see Figure 4-7).

Operating in this mode, there is zero bias and generated current is linearly proportional to the illuminance. Current flow was measured by a Fluke FL112 digital multimeter (Fluke Corp; Everett, WA, USA) connected in series to the photodiode.

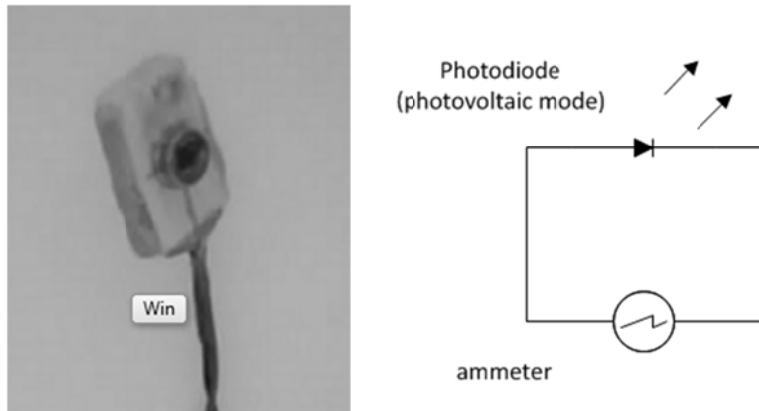


Figure 4-7. The photodiode fixtured into a block of wood (left). It was used in photovoltaic mode and the generated current was measured with a digital multimeter (right).

The photodiode was embedded into a wooden fixture for stability and was scanned across the diameter of the projected beam in a randomized order that covered diameter positions from -12 cm to 12 cm on the graph paper. This procedure was repeated for all three laser power settings (25 W, 20 W, 15 W) used.

The beam profile was measured for three successive laser firings at 15 W to determine whether the profile differences seen through the electroviewer were numerically significant.

Approximate beam divergence was calculated by measuring the diameter of the aiming beam with the projection surface at three distances away from the fibre tip.

Results

The beam profile data at the three laser power settings ($n=75$ for each power setting) are summarized in Figure 4-8. Before the aiming laser was switched off, it was observed that it projected a red annulus with inner and outer radii of 8 and 10 cm respectively.

At 25 W and 20 W power settings, the beam profiles were relatively flat with small “humps” at the two extremes of the flat region before the rapid decline in intensity. However, these “humps” were at a maximum were about 5% of the average intensity of the flat region.

The beam profile data for three successive firings of the laser at 15 W are summarized in Figure 4-9.

Although there were slight variations in the measured light intensities at 15 W power setting, they were within 7% of the average of the “flat” region. This variation was slightly higher than

at 20 W and 25 W, but this might be explained by a statistically unusual observation during the first firing at 15 W.

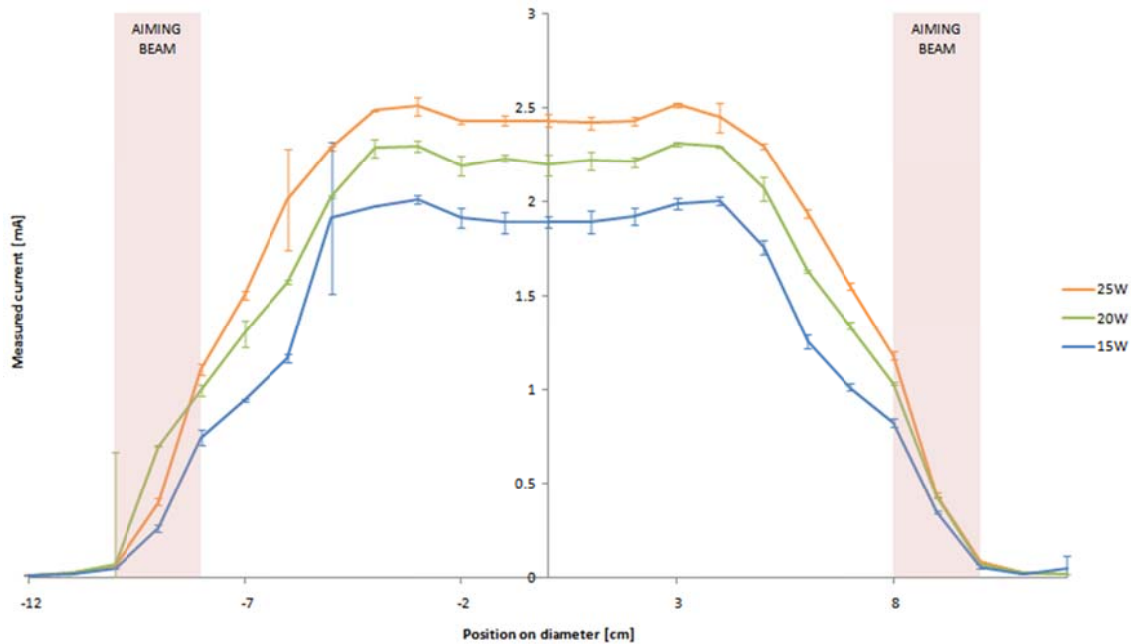


Figure 4-8. Beam profile of the Diomed 25 laser at 25 W, 20 W and 15 W set power. Error bars represent 95% CI. Red areas represent where the aiming annulus would be located. The aiming beam was disabled for the experiments.

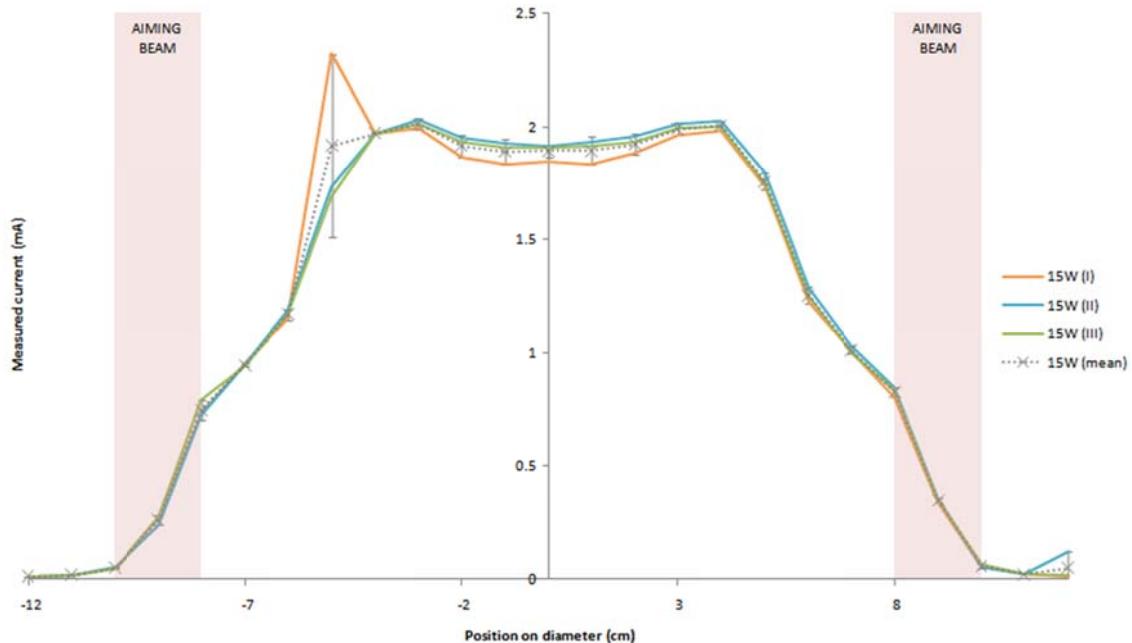


Figure 4-9. Variation in the beam profile in three sequential firings of the Diomed 25 laser at 15 W set power. The data in the dotted profile are data means at each radial position, and error bars represent 95% CI. Red areas represent where the aiming annulus would be located. The aiming beam was disabled for these experiments.

Measurements of the radius of the annular aiming beam were plotted against the separation between the tip of the optic fibre and the projection surface, and a linear regression was fitted to the data (see Figure 4-10). The regression model fit the data with an R-squared value of 0.9999.

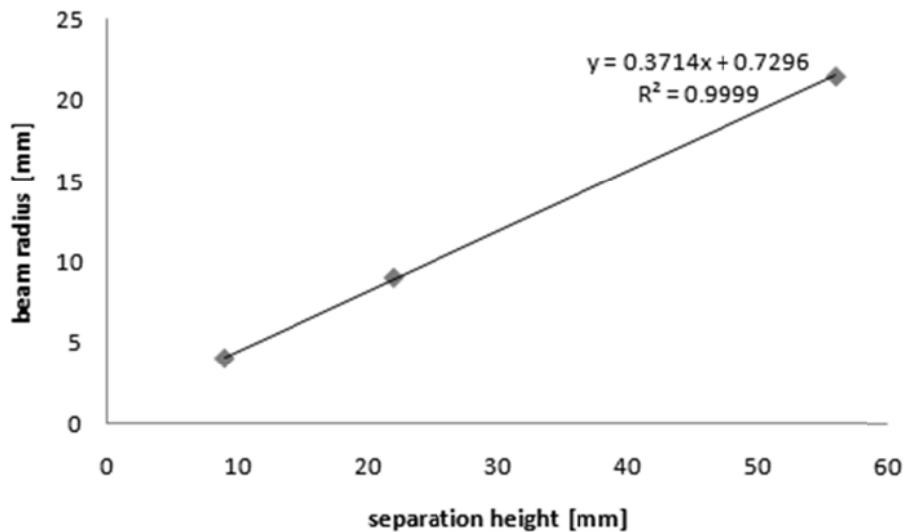


Figure 4-10. Measurements and linear regression of beam radius v the separation height between the tip of the optic fibre and the projection surface.

The slope of the model, 0.3714, gives the ratio between the beam radius and the separation height. The beam divergence was found by taking the inverse tangent of the slope, giving a beam divergence of 20.4 degrees.

Discussion

Although there was some concern from the beam profile visualization with the electoviewer revealing visible profile differences at lower power settings, these differences were not significant upon measurement of the light intensity along the beam diameter.

The overall beam profile appears to be relatively flat with a rapid drop-off in intensity at the edges of the beam.

Variations in relative intensity in the flat region were around 5% at 25 W and 20 W set power, and less than 7% at 15 W. The slightly higher variations could be due to the configuration of activated diodes at lower power, but possibly could be due to some unexplained events that led to statistically unusual measurements in the data for this power setting.

4.3.5. Wavelength

The wavelength of light emitted by semiconductor lasers is dependent on junction temperature and hence, output power. Therefore, it was necessary to quantify the magnitude of this dependence.

Methods

An Ocean Optics spectrometer USB4000-FL (Ocean Optics, Inc; Dunedin, Florida, USA) was used to analyze the spectral characteristics of the Diomed laser output.

This spectrometer contains a high-performance 3648-element linear CCD-array detector that is optimized for fluorescence measurements of light wavelengths from 360-1000 nm. It has a spectral resolution of \sim 10 nm FWHM.

Using the spectrometer to analyze the spectrum of a known laser source — a 1 mW Melles Griot HeNe laser with a wavelength of 632.8 nm — the limitations of the spectrometer could be seen. What with a higher resolution spectrometer would have appeared to be a single spike at 632.8 nm appeared as a broader spread at least 10 nm wide (see Figure 4-11).

But this resolution was adequate to verify if drift of laser wavelengths at power was something about which to be concerned.

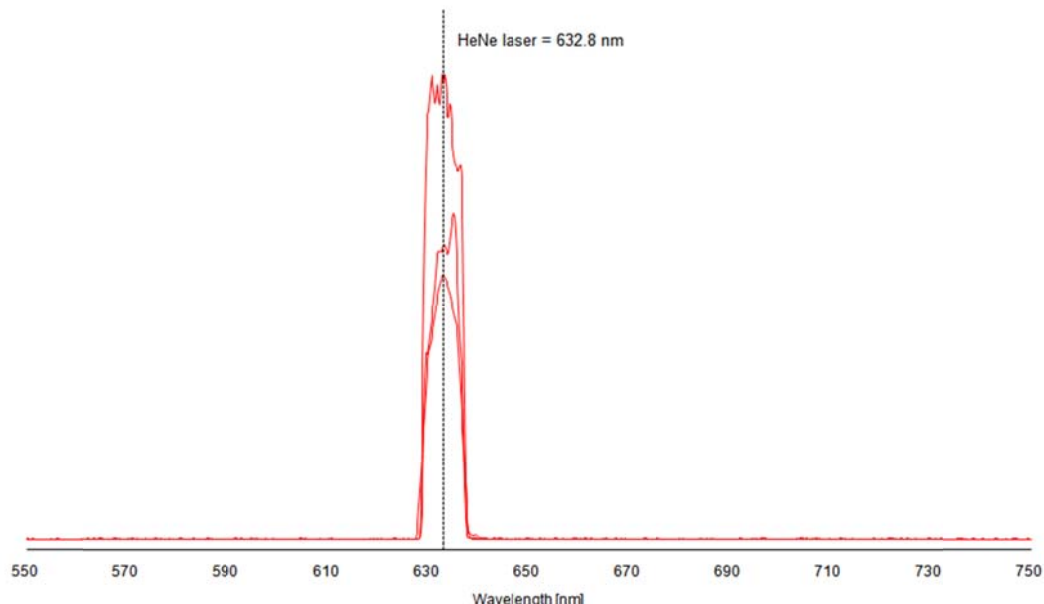


Figure 4-11. Spectral measurements of a HeNe laser with wavelength of 632.8 nm confirmed the spectrometer's poor spectral resolution.

The spectrometer was used to measure the spectrum of the laser output at various power settings from 1 W to 25 W.

The laser was aimed towards a diffusely reflecting surface. The reflected light was sampled by the spectrometer and spectral data was collected. The spectra were averaged temporally through time integration by the spectrometer software.

Results

The collected spectra for the range of the Diomed power settings used can be seen in Figure 4-12.

The wavelength corresponding to the peak intensity for each spectrum was extracted and plotted versus the set power in Figure 4-13. The spread of wavelengths at half maximum is shown by the dotted lines.

Overall, the wavelength at maximum intensity increased about 5 nm when set power was increased from 1 to 25 W. The average wavelength at maximum intensity was 797 nm. Average spread at FWHM was 8.5 nm.

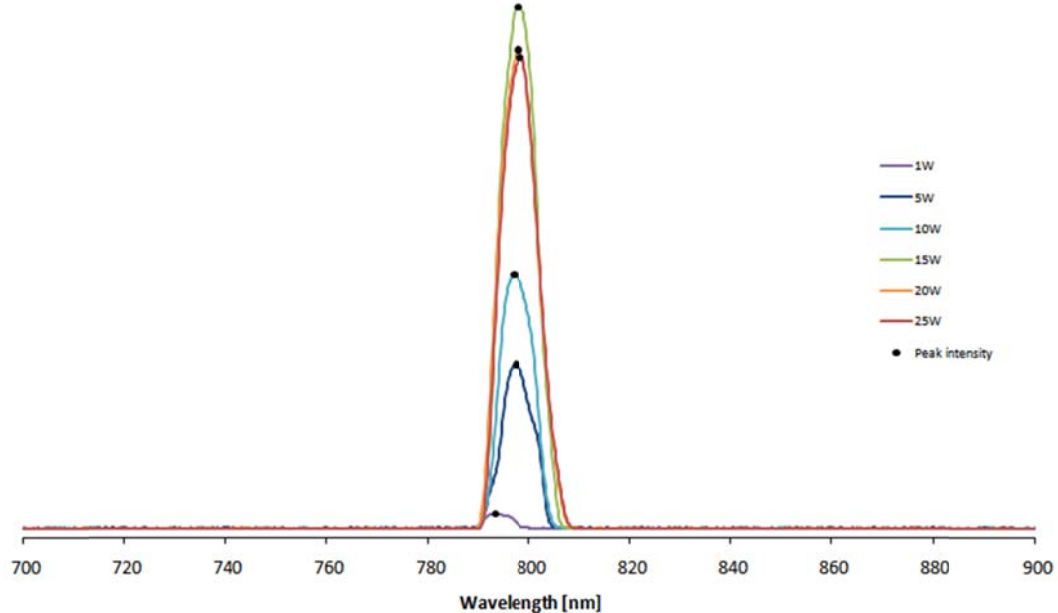


Figure 4-12. Wavelength spectra of Diomed laser at power settings from 1 W to 25 W.

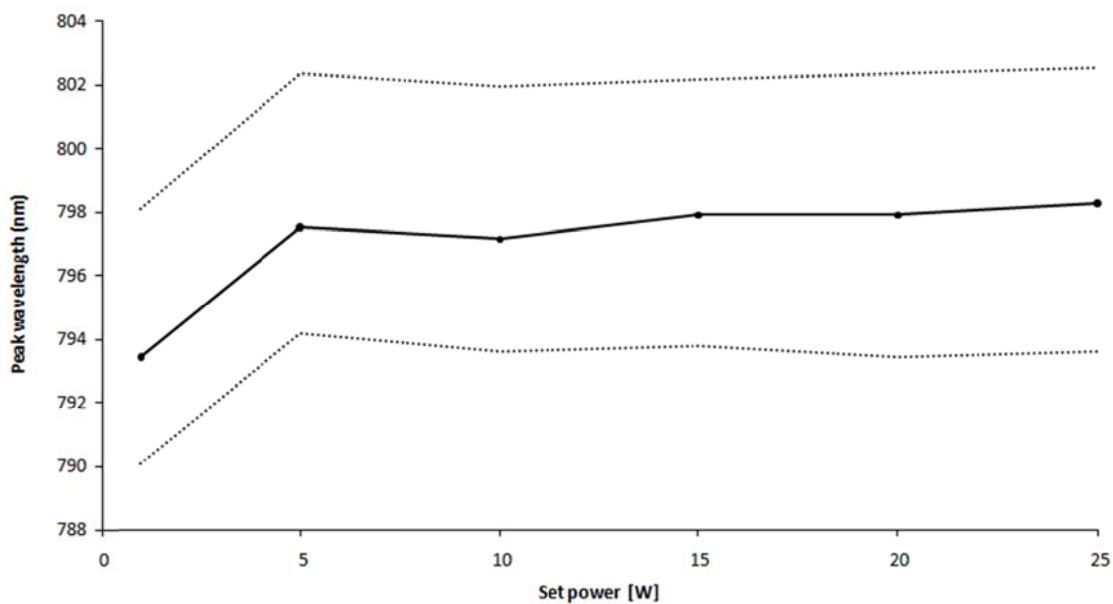


Figure 4-13. The wavelength corresponding to peak intensity for each power Diomed power setting. Dotted lines correspond to the wavelength spread at half maximum intensity.

Discussion

Although there was a slight increase in the peak intensity wavelength with increasing laser set power, the increase was smaller than the ability of the spectrometer to resolve wavelength. The dependence of wavelength on power output probably is insignificant for the purpose of the experiments described in this thesis.

4.4. Absorbers

4.4.1. Indocyanine green dye

Indocyanine green, $C_{43}H_{47}N_2O_6S_2Na$, which we use to improve absorption of 805 nm laser energy in dye-mediated ablation, is a tricarbocyanine dye with molecular weight of 775. It is a large molecule with complex chemical structure that allows it to be both hydrophilic and lipophilic (see Figure 4-14). [303]

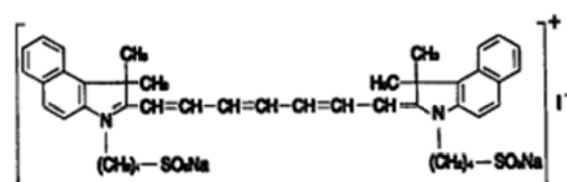


Figure 4-14. The molecular structure of indocyanine green sodium iodide.

This substance, first written about by Fox and Wood in 1960, [304] is safe and approved for clinical use in humans. It has a long history of clinical use and is administered routinely as a contrast agent for measuring perfusion in ocular vasculature, blood volume, cardiac output and hepatic function.

The principal advantages of the ICG for medical use according to Landsman are (1) an absorption maximum near the isobestic point of oxy- and deoxyhemoglobin, (2) confinement to blood due to binding to blood plasma proteins, (3) very low toxicity and (4) rapid clearance by the liver out of the body as bile, with a plasmatic half-life of 3-4 minutes. [305]

4.4.2. Absorption spectrum of ICG solutions

ICG is a good absorber of near infrared light. It strongly absorbs light between 600 and 900 nm, and when dissolved in blood plasma, has an absorption peak at around 805 nm.

The wavelength corresponding to the peak absorption is different depending on the solvent used and the ICG concentration. [305][306] For high concentration solutions in water, ICG tends to polymerize to form oligomers. In physiological saline solutions of ICG, the molecules tend to clump through molecular aggregation.

The oligomers formed at high concentrations can shift the wavelength of peak absorption (see Figure 4-15). According to Desmettre, Devoisselle and Morden, this is why ICG need to be dissolved in water before injection. [303]

Upon mixing with blood, the lipophilic nature of ICG results in binding to major plasma proteins and, to a lesser extent, to human serum albumin. This results in spectral stabilization and a 25 nm spectral shift towards higher wavelengths so that the absorption peak is at around 805 nm.

Landsman's spectra for ICG/water and ICG/plasma are shown in Figure 4-15. The dependence of the optical density at 805 nm ($\lambda = 0.5 \text{ cm}$) on the concentration of ICG in human plasma is shown in Figure 4-16.

Copyrighted material

Figure 4-15. Absorption spectra of ICG in water and plasma for different concentration solutions.
(Reproduced from Landsman. [305])

Copyrighted material

Figure 4-16. The dependence of optical density at $\lambda=805$ nm on concentration of ICG in human plasma.
Concentrations for data points denoted by triangles should be multiplied by 0.1 as this data represents
concentrations
of 0-20 mg/l. (Reproduced from Landsman. [305])

Unfortunately, these concentrations are much too low, and no absorption spectra of ICG at high concentrations could be found in the literature. Therefore, experiments were conducted to measure high concentration solutions of ICG.

Methods

Absorbance spectra of ICG solutions dissolved in water and in bovine serum albumin (BSA) solution were measured with a Shimadzu UV-2401PC spectrometer (Shimadzu Corporation; Kyoto, Japan) using a glass cuvette with 1 mm path length (Starna Scientific Ltd; Essex, UK).

Measurement data was normalised and combined with literature data from Landsman and Barofsky.

Results

The absorption spectra data for ICG/plasma and ICG/water can be found in Figure 4-17 and Figure 4-18, respectively. The spectra are given in terms of absorption coefficient, μ_a [cm^{-1}] versus wavelength [nm].

Since we are interested specifically in the coefficients at $\lambda=805$ nm, these data have been extracted and can be found for ICG/plasma and ICG/water in Figure 4-19 and Figure 4-20, respectively.

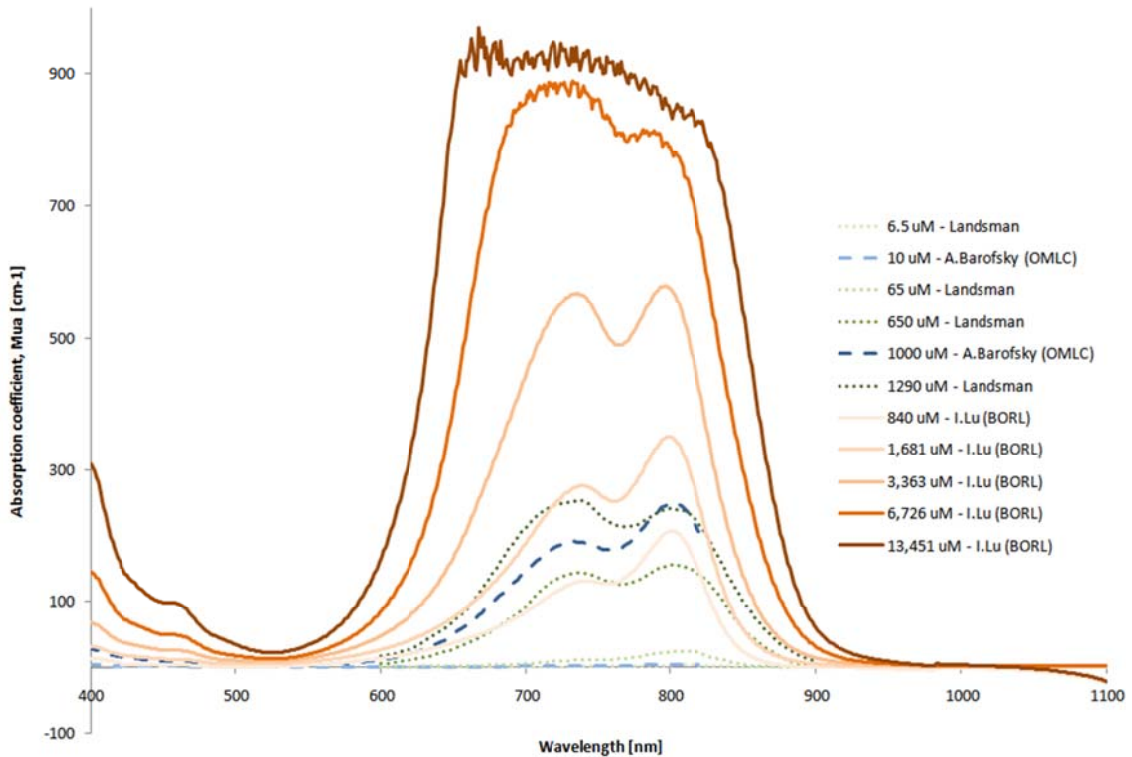


Figure 4-17. Absorption spectra of ICG in plasma at various high concentrations. Experimental data (solid) were combined with literature data (dashed, dotted).

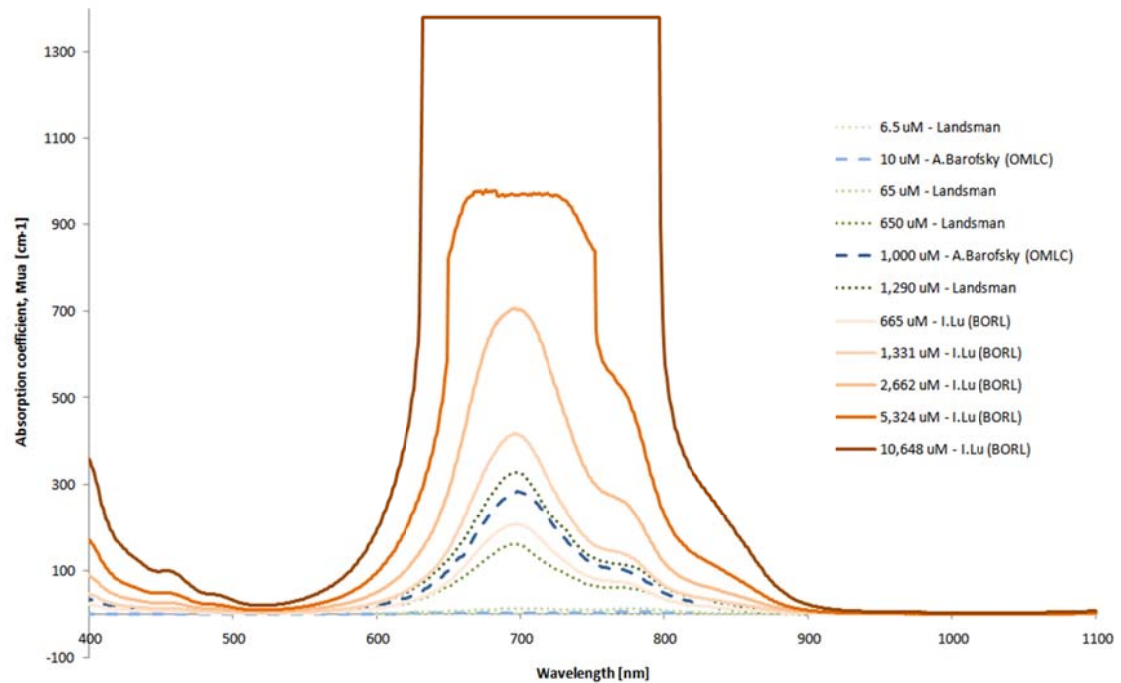


Figure 4-18. Absorption spectra of ICG in water at various high concentrations. Experimental data (solid) were combined with literature data (dashed, dotted).

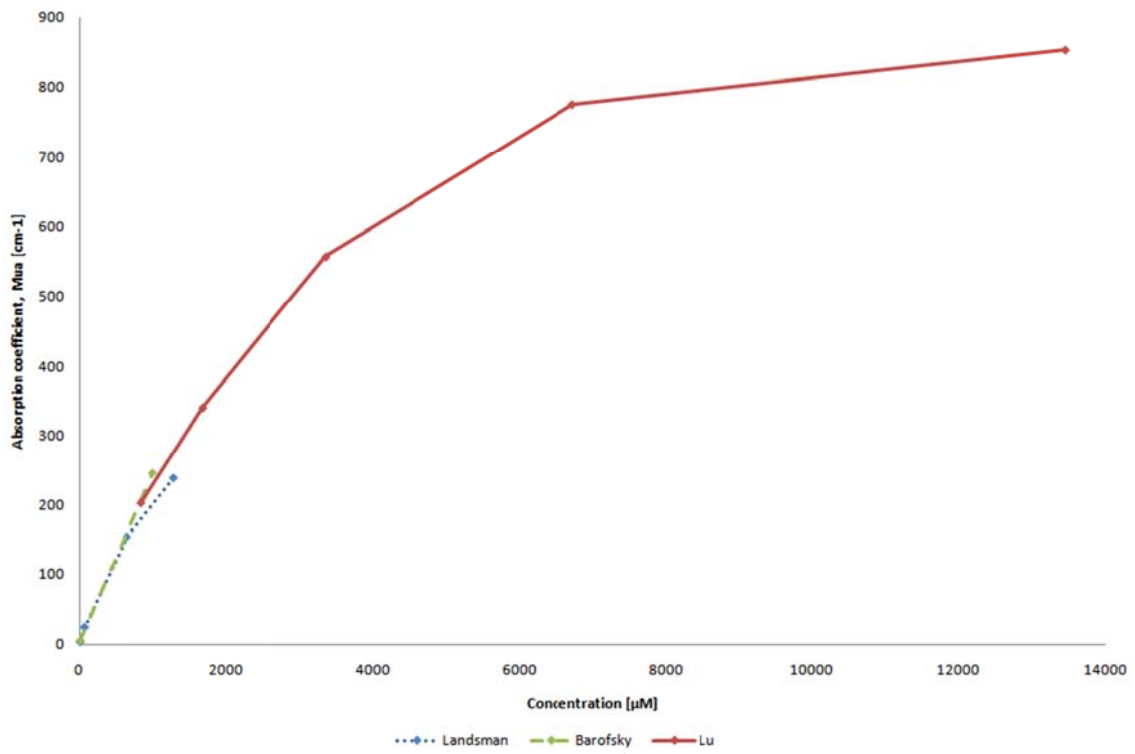


Figure 4-19. The dependence of the absorption coefficient at 805 nm on the concentration of ICG in plasma. Experimental data (solid) and literature data (dashed, dotted) have been combined.

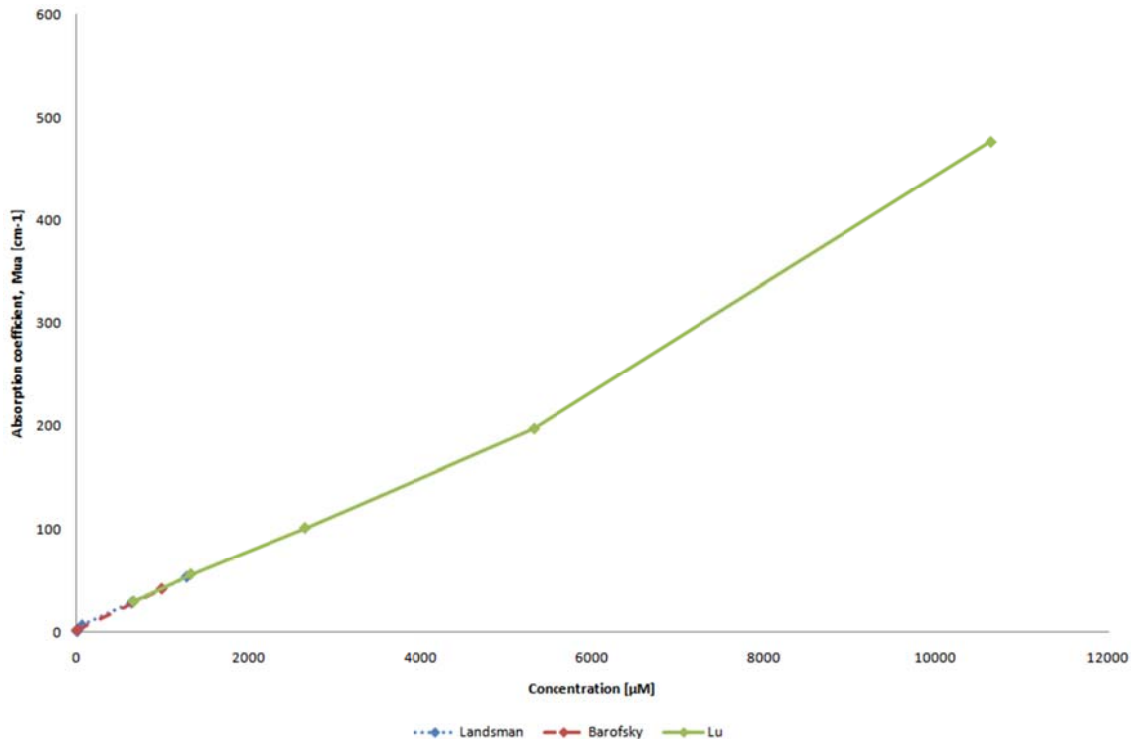


Figure 4-20. The dependence of the absorption coefficient at 805 nm on the concentration of ICG in water. Experimental data (solid) and literature data (dashed, dotted) have been combined.

Discussion

Clinical use of ICG usually involves injections of ICG solutions in water and not mixtures in plasma or albumin. This likely is done to avoid introduction of foreign lipoproteins and plasma proteins that might provoke an adverse reaction.

For the dye-mediated ablation experiments, ICG solutions in water also were used to follow clinical practice. For ICG/water mixed with blood, it is rapidly bound to lipoproteins and plasma proteins and its absorption characteristics quickly become those of ICG/plasma.

However, since we are applying the dye to tissue and not blood, the exact absorption coefficient is not known. Most likely some blood plasma would be present as surgery does create bleeding in the surgical field. Also, ICG is lipophilic and other lipoproteins probably are available in the tissue to which the ICG can bind.

It probably is safe to estimate the absorption coefficient of ICG when applied to tissue as somewhere in between the coefficients at ICG/water and ICG/plasma. With opportunity for it to bind to lipoproteins, the actual coefficient probably is on the higher end of the range.

4.4.3. Diffusion into tissue

The initial concept with ICG-mediated ablation assumed that the dye would diffuse readily into tissue. If the chromophore could penetrate into intracellular water in cells up to a predictable depth from the application point, this would assist explosive vaporisation for ablation and could provide a degree of control over where it occurred.

Diffusion rates through tissue depend on both properties of the molecule and properties of the tissue. Transport can occur passively through diffusion down a concentration gradient, or actively by molecular carrier mechanisms that require energy.

Of course, the majority of the experimentation in this thesis was performed in post-mortem *ex vivo* tissue in which active transport mechanisms for ICG probably were not functioning, if these active transport mechanisms existed at all.

Study of ICG active transport in the literature seemed to focus on the removal of intravenous ICG by the liver in the form of biliary excretions, and generally agreed that the ICG did not escape the cardiovascular system except by this route.

Devoisselle, Mordon and Desmettre, however, did report in 2000 that slow leakage by diffusion through the fenestrated chorio-capillaris allowed staining of choroidal stroma within 12 minutes after injection. [303]

In general, research on active transport mechanisms for ICG in other parts of the anatomy could not be found in the literature.

While searching for a potential carrier transport pathway for ICG is beyond the scope of this thesis, a study of passive diffusion would be beneficial. Therefore, it was desirable to quantify the diffusion rate into tissue through experimentation.

Methods

Fresh porcine muscle tissue obtained from the local supermarket was cut into 1 cm cubes and submersed for 24 hours in 5 mg/ml solutions of either ICG in water or ICG in dimethyl sulfoxide, (CH₃)₂SO.

Dimethyl sulfoxide (DMSO) is a polar solvent that can penetrate skin readily. It has been used, both purposefully and accidentally, to help carry chemicals across skin and was used to attempt to increase diffusion depths into tissue.

The mechanism of action is thought to be by expansion or swelling of proteins to allow passage through these barriers rather than by an active transfer process or by a direct carrier effect. [307][308]

Tissue specimens were recovered from solution and cut in half to reveal the cross-section. Images of the tissue after submersion for 24 hours in ICG/water and ICG/DMSO can be seen in Figure 4-21.

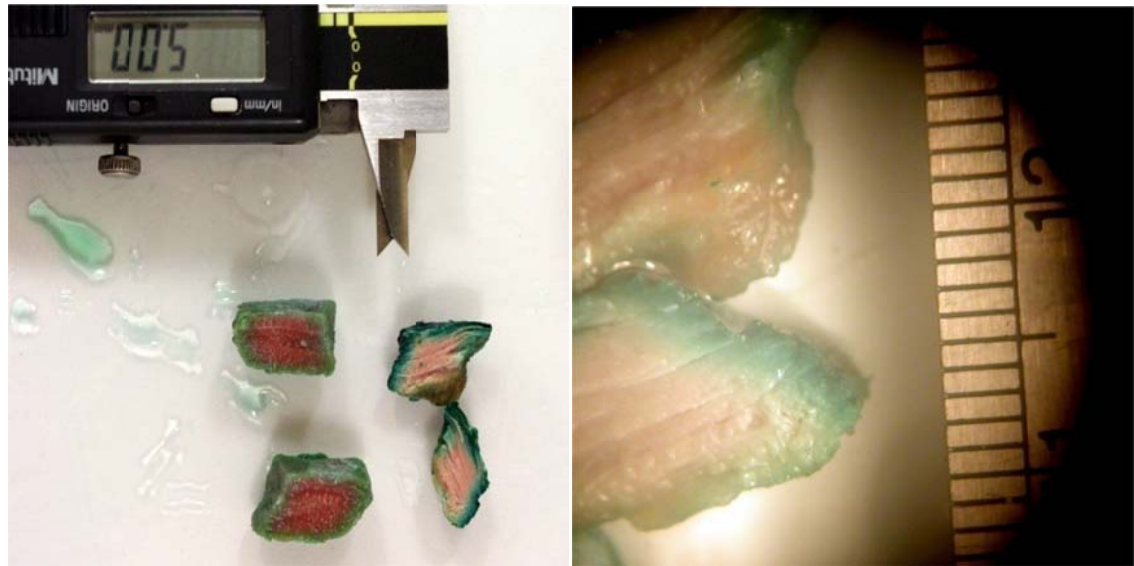


Figure 4-21. Cross section through tissue samples after immersion in ICG/water and ICG/DMSO for 24 hours.

Images of the cross-sections were split digitally in the hue-saturation-brightness colourspace, and diffusion depths were extracted from the hue images after thresholding with the open-source ImageJ program. [309] The results of digital separation into the hue-saturation-brightness colourspace can be seen in Figure 4-22 and depth annotation of the thresholded images can be seen in Figure 4-23.

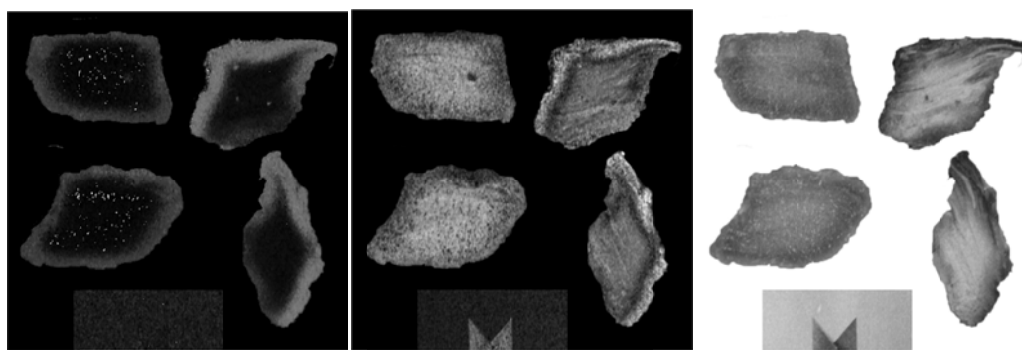


Figure 4-22. Image of the tissue digitally split into hue (left), saturation (middle) and brightness (right) channels. The hue channel provided the best visual contrast for detecting the green colour of ICG.

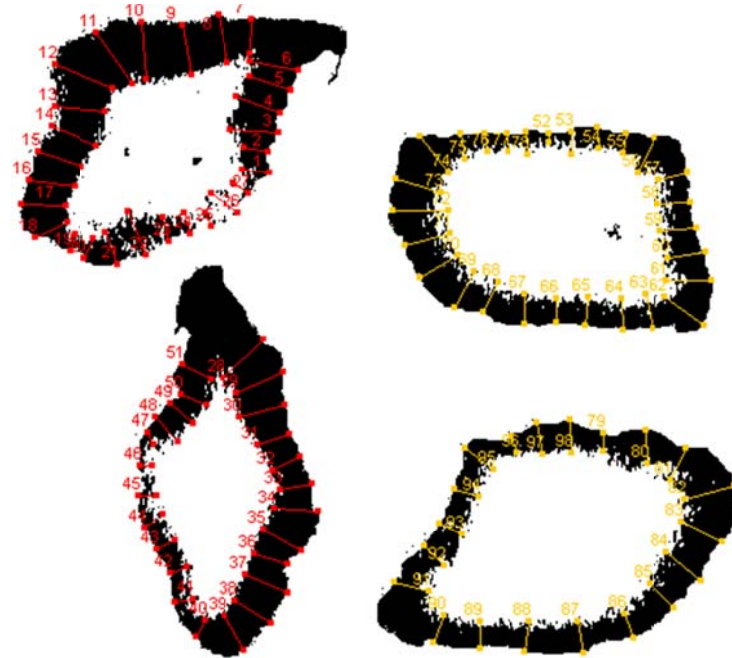


Figure 4-23. The thickness of the thresholded regions are measured in ImageJ. ICG/water (left) and ICG/DMSO (right).

Statistical analysis was performed in SigmaPlot (Systat Software, Inc; San Jose, CA, USA). Algebraic calculations to determine diffusion depth were performed in Mathematica (Wolfram Research, Inc; Champaign, IL, USA).

Results

A box-and-whisker plot of the distribution of measured diffusion depths is in Figure 4-24.

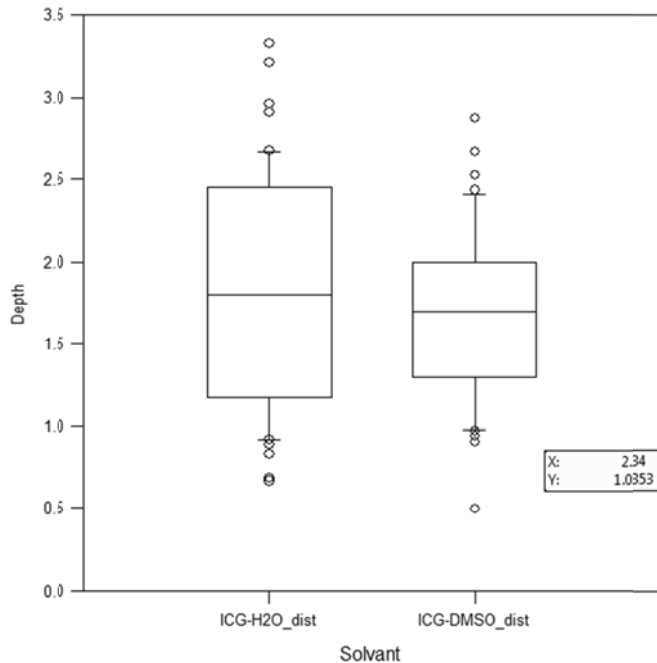


Figure 4-24. Box-and-whisker plot of the data.

To compare the two data sets to see if there was a significant difference, typically a T-test would be used. However, not all assumptions for the T-test were met — although the data passed the normality test, it failed the equal variance test.

Therefore a Mann-Whitney rank sum test was performed instead of a T-test to compare the data medians of ICG diffusion depth dissolved in water and DMSO for a significant difference.

The statistical results are summarized in Table 4-1. After 24 hours, the median diffusion depth was 1.8 mm for ICG/water and 1.7 for ICG/DMSO. However, the difference between the two test groups was not significant ($p=0.291$). Therefore, the difference in population medians due to randomness could not be ruled out at the 95% confidence level.

Table 4-1. Summary of Mann-Whitney rank sum test.

Group	N	Missing	Median	25%	75%
ICGH2O_dist	51	0	1.803	1.199	2.439
ICG-DMSO_dist	47	0	1.697	1.299	1.982
Mann-Whitney U Statistic= 1049.500 T = 2177.500 n(small)= 47 n(big)= 51 (P = 0.291)					

Assuming that diffusion into tissue occurred only by passive diffusion, it can be modelled by Fick's second law of diffusion (4.2):

$$\frac{\partial \varphi}{\partial t} = D \frac{\partial^2 \varphi}{\partial x^2} \quad (4.2)$$

Where φ is the concentration, D is the diffusion coefficient, t is time and x is position.

The 1D diffusion problem can be solved analytically:

$$\frac{n(x, t)}{n(0)} = erfc\left(\frac{x}{2\sqrt{Dt}}\right) \quad (4.3)$$

Where $erfc$ is the complementary error function.

If we define the depth of diffusion as corresponding to an arbitrary threshold concentration the boundary of which moves into tissue over time, then we can solve for this distance as a function of time without having to know the actual diffusion coefficient.

Five minutes probably is the longest amount of time a physician could be asked to wait between application of the dye to tissue and activating the laser for ablation. The diffusion depth from (4.3) corresponding to 5 mins diffusion time is 0.11 mm.

Discussion

This model of diffusion seems to confirm our experiences with ICG-mediated ablation. ICG appears to diffuse into post mortem tissue very slowly, diffusing a depth of 1.8 mm in *ex vivo* porcine muscle after immersion in 5 mg/ml solution for 24 hours.

Assuming that dye transport was due only to passive diffusion, ICG would penetrate into tissue only about 0.1 mm from the surface 5 minutes after application.

Diffusion rates might be different in other tissue types. Muscle tissue is very anisotropic and possibly gaps and tears along the muscle fibres might provide a path for dye transport by capillary action.

Diffusion of ICG into living tissue might be different due to active transport by a carrier mechanism. Whether the rate would be higher or lower is unknown as it would depend on whether the cell pumped ICG in or out of the cell membrane.

Active transport might be identified by observation of a plateau in transport rate due to saturation of the carrier mechanism. However, this was beyond the scope of the thesis and was not studied.

It might be concluded that aside from a small diffusion depth, the majority of the applied ICG sits on the tissue surface, adhered perhaps by surface tension forces in rough topology of tissue.

4.4.4. Lateral spread on the surface of porcine muscle

If most of the ICG applied to the tissue remained on the surface, then how much area would a volume of dye cover on tissue? And how deep would this dye layer be?

Of course, this is a complicated problem depending on many factors including the surface tension of the dye solution, the type, geometry and texture of the tissue. Because of the complexity, it was decided to quantify this by experimentation rather than by theory.

Because pork muscle tissue is used for the majority of the laser experiments, it is used here as the test substrate to quantify lateral spread of dye as well.

Methods

Three volumes of dye — 1 μ l, 3 μ l, 5 μ l — were applied to the surface of pork muscle tissue with an Eppendorf Reference 10 pipette (Eppendorf AG; Hamburg, Germany) in a randomized order.

The pipette could dispense volumes between 0.5 and 10 μ l and has an inaccuracy of $\pm 2.5\%$ and imprecision of $\leq 1.8\%$ at 1 μ l, and $\pm 1.5\%$ and $\leq 0.8\%$ respectively at 5 μ l.

Photographs of the dyed areas were taken at 5 minutes and 15 minutes after dye application and analyzed in ImageJ. From hand drawn outlines, coverage areas were calculated and the data was analysed. A typical photograph if the outlined dye areas can be seen in Figure 4-25.

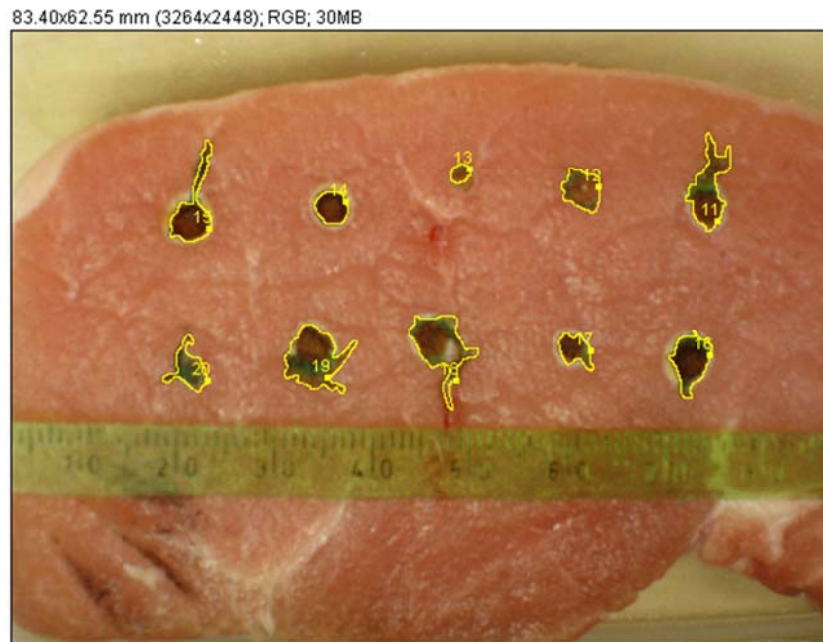


Figure 4-25. Outlines traced around dyed muscle in ImageJ.

Statistical analysis was performed in SigmaPlot.

Assuming that the dye layer was a constant height throughout the coverage area, the average depth of the dye layer was calculated.

Results

From these images, surface coverage area data were extracted and summarized in Figure 4-26 and Table 4-2. Volumes of ICG dispensed to the tissue surface appeared to cover roughly round areas, but also tended to follow the path of surface creases and valleys to form “fingers” extending from the main areas.

Table 4-2. Mean dye coverage areas vs. volume and time.

Dye volume	After 5 s, mean area (std. error)	After 15 s, mean area (std. error)
1 μ l	10.9 mm ² (1.2) (n=10)	11.7 mm ² (1.4) (n=10)
3 μ l	21.1 mm ² (0.8) (n=10)	22.3 mm ² (0.8) (n=10)
5 μ l	29.0 mm ² (1.7) (n=10)	30.2 mm ² (2.3) (n=10)

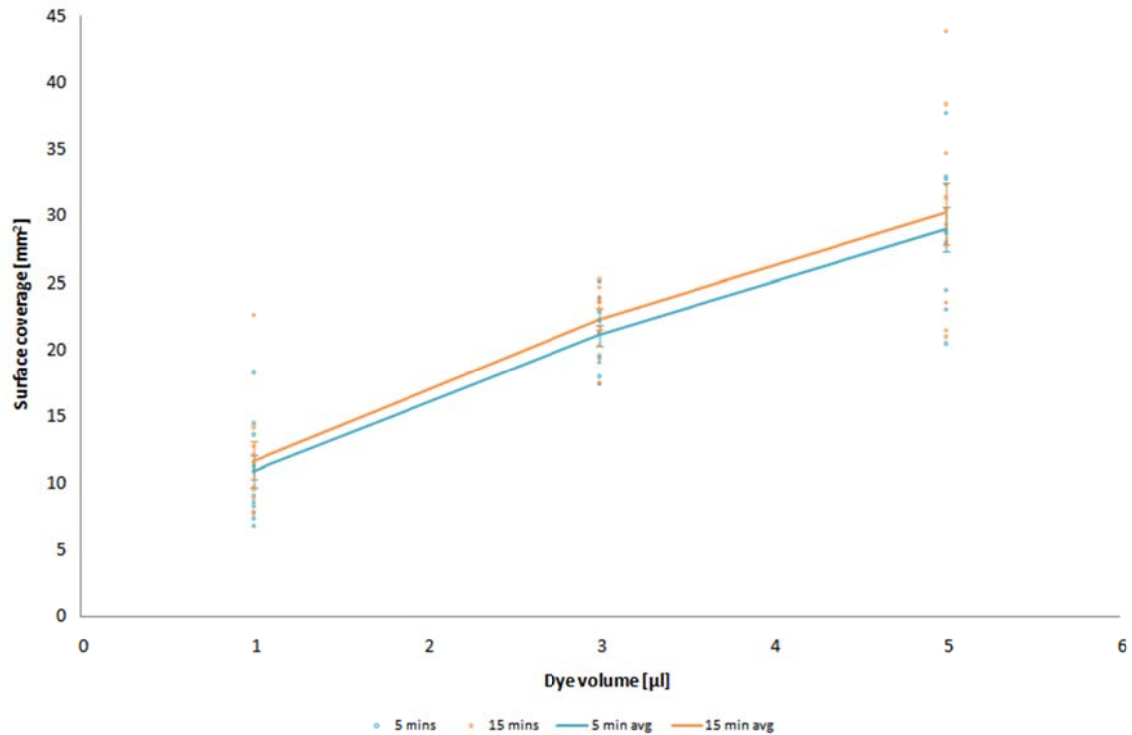


Figure 4-26. Dotplot and data means for surface coverage data vs. dye volume. Error bars represent standard error.

Two-way ANOVA was performed to examine the effects of volume and time on the coverage. The results are summarized in Table 4-3:

Table 4-3. Summary of ANOVA analysis.

Normality Test:	Passed	(P = 0.262)			
Equal Variance Test:	Passed	(P = 0.063)			
Source of Variation	DF	SS	MS	F	P
Volume	2	3370.456	1685.228	79.448	<0.001
Time	1	17.971	17.971	0.847	0.361
Volume x Time	2	0.600	0.300	0.0141	0.986
Residual	54	1145.438	21.212		
Total	59	4534.465	76.855		

From ANOVA, the change in area coverage due to volume after allowing for the effects of time were greater than would be expected by chance ($p<0.001$). The effects of time and the volume-time interaction were found to be not significant.

Assuming the thickness of the dye layer was constant throughout the area, the average thickness can be calculated by dividing the total volume of dye used by the average surface

area. The average thickness of the dye for each volume of applied dye can be found in Table 4-4:

Table 4-4. Thickness of the dye layer.

Dye Volume	1 μ l	3 μ l	5 μ l
Thickness	85.5 μ m	134.5 μ m	165.6 μ m

Discussion

ICG was observed to spread when known volumes of the solution was dispensed onto the surface or porcine muscle tissue.

It tended to cover areas that were roughly round, although the dye had the tendency to follow creases and valleys in the surface to form “fingers” extending from the main area.

The volume of dye dispensed correlated with the area of tissue covered. This was to be expected, barring any changes in density, as tendency for the volume to “flatten” was balanced by the surface tension holding the drop together.

Although a slight increase in the mean area covered by dye was observed at 5 minutes vs. 15 minutes, this change was not significant. This might indicate that the changes were occurring at a slow pace undetectable by these experiments, or that force equilibrium in the volume of dye already had been achieved.

4.5. Feasibility of dye-mediated ablation *in vivo*

The opportunity to perform a “piggyback” experiment at the end of an unrelated *in vivo* study arose and was used to evaluate the feasibility of dye-mediated ablation *in vivo* in a live porcine model. These experiments helped to provide confidence that the ICG-mediated laser ablation method could be made feasible in a pre-clinical setting with a live animal.

All experimental procedures were carried out with ethics approval from the Royal Veterinary Collage by doctors and veterinarians licensed to work with live animals. Verbal instructions were provided by the author to the physicians to facilitate adherence to the experimental protocol.

However, because the experiments were performed under time pressure at the tail end of the primary study when the animal was about to expire, experimental protocols set by the author were not always followed and were not completed.

Methods

The goal of these experiments was to demonstrate feasibility of ICG-mediated laser ablation in a live animal model.

An Olympus dual-channel therapeutic gastroscope (GIF-2T100; Olympus; Tokyo, Japan) was used for the procedure. Transgastric access to the peritoneal cavity was gained via gastrotomy and the endoscope was manoeuvred to the lower abdominal wall on the right side.

The two working channels of the scope were loaded with an endoscopic injection needle in the first channel and a 300 µm fibre optic connected to the Diomed 805 nm laser in the second channel.

The injection needle was used to create small, submucosal blebs in the abdominal wall by injection of approximately 3 ml of ICG solution (1 mg/ml concentration ICG in water).

The laser fibre optic was used to expose the tissue to 10 W (set power) of laser radiation for 2 s. This was repeated for each submucosal bleb (n=3).

Nearby locations without any ICG injections were exposed to 10 W (set power) for 2 s as a control (n=2).

After the animal was euthanized, sections of the abdominal wall ablated by the laser were excised and examined visually.

Results

ICG injection presented as a greenish tinting of the abdominal wall tissue. There was slight leakage out of the injection wound. However, the bleb did not immediately dissipate.

All areas of the abdominal wall without ICG injection (n=2) showed no visible signs of coagulation or ablation after exposure to laser light.

When areas with ICG injection (n=3) were exposed to laser light, smoke was seen emanating from the laser spot. On the video monitor, an area surrounding the laser site saturated white during exposure, obscuring the view. After exposure, vision was restored and ablation craters with charring were found.

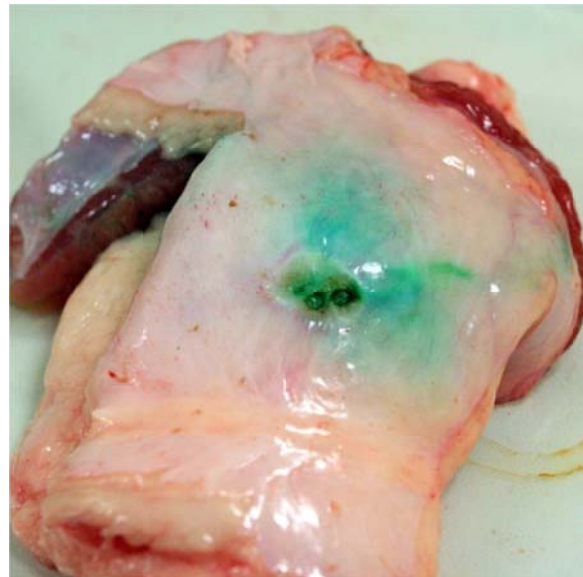


Figure 4-27. Craters, charring and tissue whitening on the surface of an ICG/H₂O filled sub-surface bleb.

One excised specimen from the abdominal wall can be seen in Figure 4-27. Ablation craters can be seen with visible charring in and around the crater. An area of whitened, coagulated tissue can be found surrounding the crater. These results were typical for all the specimens resected.

Discussion

The positive ablation results with ICG/water helped to support the idea that ICG-mediated laser ablation is feasible *in vivo* at flexible endoscopy.

In benchtop experimental work, there always is the concern that it is not representative of the surgical environment *in vivo*. From this experiment, ICG-mediated ablation *in vivo* in a porcine model did not reveal any large, unexpected problems that impeded successful tissue ablation.

However, two issues were noticed during the procedure. The first was the smoke generation from laser ablation that somewhat obscured vision. This also occurs with electrosurgical diathermy, but not with ultrasonic dissection or cutting with scissors.

The second issue was the saturation of video brightness in the immediate vicinity of the laser ablation. This could be remedied with the use of an infrared filter on the endoscope camera.

Spatial specificity depending on the presence or absence of ICG dye was demonstrated in this experiment. Tissue over an injected volume of ICG could be ablated, while tissue without injection was not, given the laser power and duration used.

Spatial control over the dye application would be desirable for useful application of the deconstructing dissection strategy.

4.6. Theoretical model of laser ablation

Theories of the physics describing laser ablation of tissue can be found in the literature, although the papers on ablation are dwarfed in numbers by the reports on laser coagulation. Below, the literature on theoretical modelling of laser ablation is reviewed and is followed by a detailed discussion of the important three damage zone model by Alan McKenzie.

4.6.1. Modelling laser ablation in tissue

Since Schawlow and Townes published the first paper on lasers in 1958 and the first working laser was constructed by Maiman in 1960, applications for lasers in medicine also have been explored and grew rapidly in subsequent years as new technologies for generating and transmitting laser light became available.

McKenzie analyzed in 1983 the extent of thermal damage beneath the surface of CO₂ laser ablation craters by considering the ablation process to be boiling water in a state of dynamic equilibrium. In a dynamic steady-state, the damage wave from heat diffusion moves at the same speed as the ablation front. [310]

By simplifying the laser heat source as a single planar source at the surface and modelling the heat diffusion into the tissue as an exponential decay, McKenzie calculated the maximum distance the 60° C temperature wave could reach into the tissue.

He considered that tissue proteins raised to 60° C even for a short time period would be irreparably and permanently damaged. Ablation occurred at the ablation front at the surface when water was vaporised at a temperature of 100° C.

Welch reviewed in 1984 various methods to model light and heat distribution in laser irradiated tissue for predicting its thermal response. [311]

He included in his comprehensive review a section on Henriques' tissue damage model based on the Arrhenius equation for first order chemical kinetics, which took into account both temperature and time for calculating the probability of cell death.

However, Welch also lamented that no perfect model existed that accounted for all the changes that occur in tissue during ablation, including the fact that “charring creates a highly absorbing layer.”

Welsch et al. also published in 1985 a model for laser angioplasty. [312] Their model tried to incorporate a number of different factors including:

- (1) accounting for light lost through scatter by a modified Beer’s law,
- (2) incorporating Henrique’s damage integral to represent irreversible heat damage to tissue,
- (3) modelling water losses by assuming a linear relationship between water content and thermal conductivity and specific heat.

One of their key conclusions based on their models and video scanning thermography was that tissue ablation occurred at temperatures significantly higher than 100° C — for plaque ablation, temperatures were measured to be 160-310° C.

Van Gemert et al. also described in 1985 a model for coronary laser angioplasty. [313] Although they acknowledged the findings of Welch et al. of ablation temperatures higher than 100° C, their work nevertheless used the 100° C threshold for the “evaporation” of tissue volume from the onset of laser ablation.

Despite the self-described “crude nature” of their model assumptions, including constant optical and thermal properties in tissue despite clear changes due to coagulation and ablation, the model was able to achieve reasonable agreement with data.

They described the general behaviour of ablation to include a “relatively fast initial ablation followed by a much slower almost linear rate of ablation,” which led them to predict that faster ablation velocities could be achieved by intermittent pulses preferably much shorter than the thermal relaxation time rather than one long, continuous pulse.

Jacques and Prahl in 1987 described a one-dimensional model that incorporated solutions for optical transport by the diffusion approximation, thermal diffusion by a Green’s function and tissue coagulation by an Arrhenius equation. [314] They were able to predict optical and thermal distributions inside tissue, and experimentally determined the threshold temperature for coagulation to be 60-70° C.

Probably one of the most complete models of tissue damage caused by laser ablation was proposed by McKenzie in 1986. [315] This model of CO₂ laser ablation, like the one in 1983, used a moving coordinate system at the ablation front and assumed a state of dynamic equilibrium.

McKenzie modelled the region of laser damaged tissue as three distinct zones — a carbonised zone, a vacuolated zone, and a sub-boiling coagulated zone. This model will be discussed in detail in the next section.

McKenzie followed up his research in 1989 with an extension of the three-zone model for pulsed mid-infrared lasers like the Er:YAG and Ho:YAG lasers, [316] and in 1990 with a review of the physics of thermal processes in laser-tissue interaction. [317]

Subsequently, researchers have attempted to expand the model, for example, by extending the model to four damage zones and accounting for the movement of heat through convection of liquid water and vapour as Zhang, Shen and Zhang did in 2009. [318]

4.6.2. The McKenzie model

The simple and three-layer McKenzie models essentially are 1D energy balance models that relate input energy (from absorbed laser energy and, in the three-layer model, tissue combustion) with the energy required to cause physical changes in the tissue (like temperature rise and phase change) and energy diffused away by thermal conduction.

When soft tissue is exposed to laser energy, absorbed energy heats up intracellular water. Temperatures that reach a threshold 60-70° C cause protein denaturisation leading to cell death, and temperatures that reach 100° C cause water to boil. The phase change associated with boiling water corresponds to a one-thousand-fold expansion in volume that physically and explosively disrupts cells.

McKenzie in 1983 modelled CO₂ laser ablation speed by assuming that all the laser energy were used to raise the temperature of water from 37 to 100° C and then to vaporise the tissue by overcoming the latent heat:

$$u = \frac{I}{\rho(c\Delta T + L)} \quad (4.4)$$

Where u is the velocity of the vaporisation front, I is the beam irradiance, ρ is the density of water, c is the specific heat of water, ΔT is 63° C (to raise water from body temperature = 37° C

to 100° C), and L is the molar heat of vaporisation of water. A top-hat, or flat beam profile is assumed in which the irradiance is constant throughout the beam profile.

For a Gaussian profile, the irradiance as a function of radius, r , from the centre of the beam is given by the equation:

$$I = I_0 e^{-\frac{2r^2}{w_0^2}} \quad (4.5)$$

Where w_0 is the beam waist, or the radius at which the intensity drops to $1/e^2$ or about 0.135 of the axial value.

Integrating (4.5), the total power of the beam is:

$$P = \frac{1}{2}\pi w_0^2 I_0 \quad (4.6)$$

This reveals that the peak irradiance at the centre of the Gaussian beam is twice the average irradiance found by dividing the total power by the beam area (with radius = w_0). This results in twice the ablation speed in the centre of the crater based on (4.4) and twice the maximum ablation depth by multiplying (4.4) by the exposure duration.

McKenzie subsequently proposed in 1986 a more realistic model of laser ablation to explain the formation of three distinct zones of tissue damage as a result of CO₂ laser ablation. These three damage zones are the carbonised zone, the vacuolated zone and the sub-boiling coagulation zone. Beyond the coagulation zone lies undamaged tissue (see Figure 4-28).

This new model was required to explain the presence of the vacuolated zone, which could not exist in the 1983 model which assumed an infinite absorption coefficient for CO₂ laser radiation in soft tissue and heat transfer by conduction only. In the older model, only an infinitely thin volume of tissue at the surface would be at 100° C with temperatures decreasing monotonically the deeper one moves into the tissue.

Figure 4-28. McKenzie's three zone model of laser ablation.
(Reproduced from McKenzie. [317])

The carbonised zone

The most superficial layer in McKenzie's three zone model is the carbonised zone. The most noticeable feature of tissue in this region is the blackening or charring of tissue from carbonisation.

At the very surface of this damage zone at the ablation front, the tissue mass is completely vaporised by combustion at temperatures around 500° C. Underneath the ablation front, the remains of a tissue network can be found that is marred by fissures and vacuoles created from explosive vaporisation of water underneath in the vacuolated zone.

Free from the thermal clamp of liquid water, the temperature in this desiccated region is free to rise above the 100° C phase transition temperature of water, hot enough for the carbonisation processes of pyrolysis and combustion to occur.

For CO₂ laser ablation, McKenzie considered two extreme cases for power delivery to the tissue in this region to estimate the layer thickness. Although it was unknown how much of the power came from laser light absorbed by the carbonised tissue and how much came from the heat of combustion, two extreme cases provided an estimated range that the layer thickness should fall within.

For the first case, it was considered that none of the heat of combustion heated the tissue in the carbonised zone and that all the heating power came from light absorption. This lead to a predicted depth, z of

$$z = \left(\frac{\beta_{carb} \Delta T_{carb}}{P k_{carb}} \right)^{\frac{1}{2}} \quad (4.7)$$

Where β_{carb} is the thermal conductivity of charcoal, ΔT_{carb} is 400° C, P is the laser power absorbed per unit area and k_{carb} is the absorption coefficient of charcoal modified to account for the low density in tissue.

For the second case, all the heating power from combustion was used to heat the carbonised region and the power from light absorption was small in comparison (only 9%, calculated retrospectively by McKenzie). In this case, the predicted depth z is

$$z = \frac{\beta_{carb} \Delta T_{carb}}{\sigma \rho_{carb} v P} \quad (4.8)$$

Where σ is the heat of combustion of charcoal, ρ_{carb} is the density and v is the ablation speed. McKenzie used 3.4e4 J/g as the exothermic heat of combustion for charcoal.

According to McKenzie, whichever extreme case is used, the calculated carbonised depth for CO₂ ablation is in the range of tens of microns, decreasing with increasing absorbed power.

The vacuolated zone

Beneath the carbonised zone in McKenzie's model lies the vacuolated zone in which a region of coagulated tissue has been raised to the 100° C boiling point of water. This region exists because of the non-zero penetration depth of laser light resulting in direct volumetric heating from absorbed laser power in addition to heat conduction from adjacent regions.

Power from laser absorption in this region is used to boil water, creating bubbles of steam that create vacuoles in the tissue. Nearer to the surface, these bubbles grow and coalesce resulting in larger vacuoles and the emergence of fissures and gaps.

The vacuoles and gaps created in this sponge-like region allow more light penetration than would occur in a solid region due to decreasing water content and thus the local absorption coefficient, as water is the main light absorber at 10.6 μm.

However, to simplify, McKenzie defined an effective thickness $\xi(x)$, which can physically be thought of as the “condensed” thickness of vacuolated tissue between the surface and a depth x .

Using (4.4) and the effective thickness transformation, the maximum effective thickness ξ_{max} can be determined.

$$\xi_{max} = k^{-1} \ln \left(\frac{c\Delta T + L}{C\Delta T} \right) \quad (4.9)$$

McKenzie pointed out that ξ_{max} is independent of the details of the density distribution in the zone as well as the irradiance of the beam. Also, ξ_{max} depends inversely on the absorption coefficient.

One weakness of this approach is that predictions are not for the actual “expanded” thickness of the region but rather for a theoretical “condensed” effective thickness, which by McKenzie’s account “may only be half that of the physical extent of the zone.”

The sub-boiling coagulated zone

The sub-boiling coagulated zone is a region of coagulated tissue below the vacuolated zone with temperatures under the 100° C boiling point but higher than the threshold temperature for tissue coagulation. Physical characteristics of tissue in this region include whitening in colour due to increased light scatter from protein denaturisation and some degree of geometrical shrinkage.

Although, technically speaking, the probability of cell death is most accurately modelled as a time integral of local temperature according to the Arrhenius damage integral, it can, as a practical approximation, be defined as a threshold temperature in the range of 60-70° C. McKenzie used a threshold temperature of 60° C for his model.

By considering light absorption with intensity reduced by absorption in more superficial layers and heat diffusion from 100° C at the boundary between the vacuolated and the sub-boiling coagulated zones, a relationship of energy balance can be derived:

$$\frac{23}{\Delta T} \left(\frac{\alpha k}{v} - P \right) = \frac{\alpha k}{v} \exp \left(\frac{-Pvx_{eq}}{\alpha} \right) - \exp(-kx_{eq}) \quad (4.10)$$

x_{eq} is the distance from the boundary between the vacuolated and the sub-boiling coagulated zones (at a temperature of 100° C) to the 60° C isotherm below, i.e. the thickness of the

coagulated zone. It can be solved for by numeric methods and was found by McKenzie to be larger, but of the same order of magnitude as depths of damage calculated by the simple McKenzie model of 1983.

4.6.3. The importance of carbonisation

McKenzie in his three-zone model hinted at the importance of carbonisation by explicitly modelling this region containing the ablation front and used the high absorption coefficient of charcoal to model carbonised tissue as the main light absorber in this region.

However, he also argued that because this region is thin for CO₂ laser ablation (at most, a few tens of microns), most of the absorption of laser energy occurred in the vacuolated zone where essentially water is being boiled. In fact, McKenzie ignored the heat contribution from the carbonised zone completely when considering the energy balance in the vacuolated zone, although he did say that the model could be adjusted to include this term if it were necessary.

For CO₂ laser ablation, these simplifications are reasonable and make the problem more tractable. However, for other lasers in other situations, carbonisation may play a larger role than generally is considered.

Verdaasdonk, Borst and van Gemert in 1990 described their experiences with Nd:YAG (10-60 W) and argon (3.5 W) laser ablation of bovine aortic and myocardial tissue. [319] They were able to observe three distinct phases at the onset and during laser tissue ablation – tissue denaturation (coagulation), explosive vaporisation and cyclic carbonisation.

While McKenzie provided a good theoretical model for laser ablation once it had reached a dynamic steady state, Verdaasdonk et al. helped to paint a more complete picture by providing experimental insights into the processes leading up to the onset of ablation, and revealed the fascinating cyclical waves of carbonisation and vaporisation during steady-state laser ablation by a laser with a Gaussian profile (see Figure 4-29).

Figure 4-29. Cyclical waves of carbonisation and ablation as revealed by videography.
(Reproduced from Verdaasdonk, Borst and van Gemert. [319])

They theorised that these cyclic waves of “expanding, ring-shaped, carbonised tissue layers” were formed from temperatures high enough to cause carbonisation of tissue which immediately was vaporised from enhanced absorption, consistent with McKenzie’s model.

This would expose and also cool the underlying uncarbonised tissue below the carbonisation temperature, assuming that the final evaporation process was endothermic. This process would repeat in a cyclical pattern of expanding rings of carbonisation and vaporisation due to the higher relative irradiance at the centre of a Gaussian beam.

Overall, Verdaasdonk et al. concluded that the experimental observations best fit with McKenzie’s description of ablation, despite the use of lasers different from the CO₂ laser assumed for McKenzie’s model.

They did discuss, though, that it is not well known whether carbon formed by tissue decomposition is vaporised (phase transition at 3550° C). If it is, they speculated that

exothermic chemical combustion “may contribute substantially” to the final endothermic carbon evaporation.

However, as alternatives to evaporation, this carbon might also be removed intact, physically ejected as part of the smoke plume, or chemically bonded to other atoms as part of hydrocarbon gases released from oxidative combustion.

In the lead up to exothermic combustion, mass may also be removed by endothermic pyrolytic reactions releasing hydrocarbon gasses and leaving behind a blackened char.

Jacques argued for the importance of carbonisation in high irradiance tissue ablation in 1993. [320] He described a process by which elevated temperatures in tissue from laser heating lead to browning of muscle by chemical reactions such as the Maillard reaction, which increased absorption and thusly accelerated carbonisation of the tissue.

Although the browning of meats often has been referred to as a Maillard reaction, lean meats like muscle tissue contain very little, if any, reducing sugars to react with amino acids in proper Maillard browning reactions.

More likely, the initial browning at temperatures under 100° C comes from the denaturisation of myoglobin, the protein which gives meat its red colour. The red heme group containing iron (II) when bound to oxygen becomes yellow/brown iron (III) after denaturisation.

Unfortunately, at wavelengths above 650 nm, denatured myoglobin is a poor absorber, and absorption decreased further with increased temperature. [321] Although the measured absorption spectra by Trout covered only 450-700 nm, it is likely that absorption remained low at the 805 nm Diomed laser wavelength used for our application (see Figure 4-30).

Figure 4-30. Absorbance spectra of denatured myoglobin from 450-700 nm.
(Reproduced from Trout. [321])

Regardless, Jacques probably is correct that browning of tissue does occur (although it is unknown at what temperature), and perhaps the formation of intermediary absorbers might improve the local absorption and increase the tendency of tissue to be carbonised. However, these browning processes are a complicated family of numerous chemical reactions requiring different reagents and occurring at different temperatures. [322]

Without a clear understanding of the specific chemistry involved, probably it is sufficient to focus on carbonisation rather than low temperature browning. Char is known to be an excellent gray-body light absorber, and once it has formed, absorption of 805 nm laser light is greatly increased.

Returning to the main point made by Jacques, carbonisation was required for successful laser ablation of chicken breast muscle by Nd:YAG laser (1064 nm, 90 W, 7mm spot, $\sim 230 \text{ W/cm}^2$).

He described an experiment in which tissue exposed to Nd:YAG laser light sequentially was coagulated and desiccated in the first 30 s of irradiance. At around 30 s, carbonisation occurred followed by rapid tissue ablation over the next 20 s.

Jacques explained this process as “a cycle of removing char and renewing char, which allowed the efficient ablation to proceed at a steady rate,” and cited Verdaasdonk et al. for their observations of the cyclical removal and renewal of carbonisation.

Jacques also made the interesting point that “although char absorption depends on wavelength, the fraction of total laser energy absorbed by the char is always quite high, and all lasers tend to operate similarly once char formation has been initiated.”

The absorbance spectrum of char was measured by Jacques by referencing reflectance from charred tissue with uncharred tissue and can be found in Figure 4-31.

These findings by Verdaasdonk et al. and Jacques suggest that carbonisation may play an important role in dye-mediated laser ablation, and that the standard McKenzie model of laser ablation may have to be modified to account for the importance of carbonisation.

This will be revisited later when considering numeric modelling of dye- and carbonised tissue-mediated laser ablation.

Copyrighted material

Figure 4-31. Measurement of the absorbance spectrum of char. (Reproduced from Jacques. [320])

4.7. Ablation tissue effects revealed by histology

Returning to the dye-mediated laser ablation experiments, the examination of the aftermath of ablation thus far had been on only a macroscopic level. Histological techniques were used to examine ablation craters in cross-section under high magnification. This was done to examine tissue for the morphology of carbonisation, explosive vaporisation and coagulation.

Methods

In the first set of experiments, we wanted to visualise the effects of dye-mediated laser ablation on tissue on a microscopic scale.

Laser-ablated porcine muscle tissue was prepared using 1 mg/ml solution of ICG/water and the 805 nm laser at 25 W set power.

Histological slides with frozen sections were cut according to the protocols detailed in “Appendix A: Histology slide preparation techniques.” These procedures included flash freezing in liquid nitrogen, slicing cross-sections on a microtome within a chilled cryostat and tissue staining with hematoxylin and eosin (H&E). Cross-sections were made as close to the centres of the ablation craters as possible.

Images were captured using a high-magnification laboratory microscope with an attached camera device and stitched together algorithmically using Adobe Photoshop (Adobe Systems Inc; San Jose, CA, USA).

Frozen sections were used because the superficial carbonised regions did not survive the formalin fixation and wax embedding processes.

In the second set of experiments, workarounds for difficulties differentiating between coagulated and uncoagulated tissues at histology in the first experiments were sought by experimenting with alternative histological staining techniques. Dr. Thomas Jacques, clinical scientist and honorary consultant of histopathology at the UCL Institute of Child Health, was consulted in this effort.

Gömöri trichrome and NADH reductase histology protocols were used to stain frozen sections prepared by the author. Stained slides were reviewed by Dr. Jacques.

Results

Three frozen section specimens of ICG-mediated laser ablated porcine muscle taken in cross-section at the middle of the ablation crater can be seen in Figure 4-32. The location of the ablation laser coming from the top surface of the tissue is indicated by the red arrow. Lower areas in the image represent deeper depths within tissue.

In general, the ablated tissue viewed by frozen section histology can be sub-divided into three regions of interest.

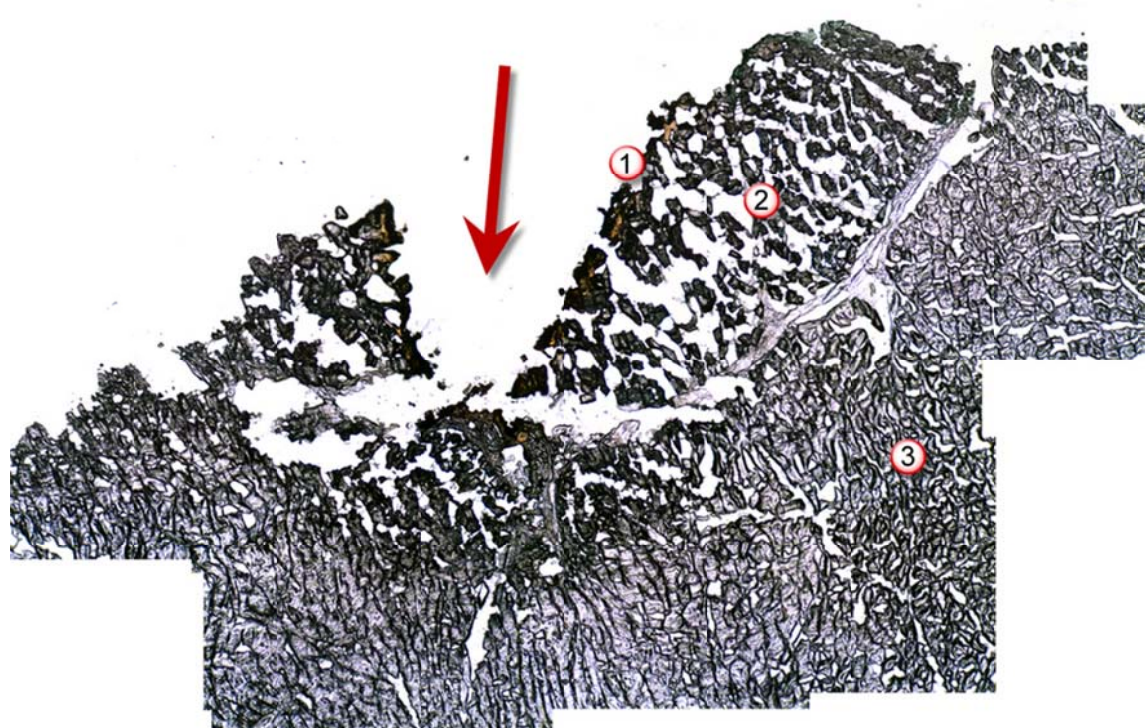
The first region, denoted by the number one in the histology images, is the ablation crater which is defined primarily by the absence of visible cells. At the edge of the crater at the tissue boundary, a band of dark brownish-black can be found.

The most prominent feature in the second region, denoted by the number two in the histology images, is the sponge-like gaps found in and between cells. At higher magnifications, the highly distorted remains of fragmented cells can be seen. This region also appears darker than deeper tissues.

The third region, denoted by the number three in the histology images, comprises the bulk of the remaining tissue. In this region, cells appear whole and cell nuclei do not appear to have been disrupted.

It must be noted that before sectioning by the microtome in the cryostat, two regions could be differentiated within this third region. In the immediate vicinity of the crater, whitened tissue could be seen. Further away, the tissue retained the reddish hue typical of muscular tissue. However, after sectioning, this colour distinction could not be seen.

The result of the frozen slides after undergoing the protocol for H&E staining are shown in Figure 4-33. Although the staining process increased the contrast of intracellular structures, it also debonded parts of the specimen, especially in regions 1 & 2, as loosely adhered cells in these regions did not survive repeated submersion and washing in various chemicals as part of the staining protocol.



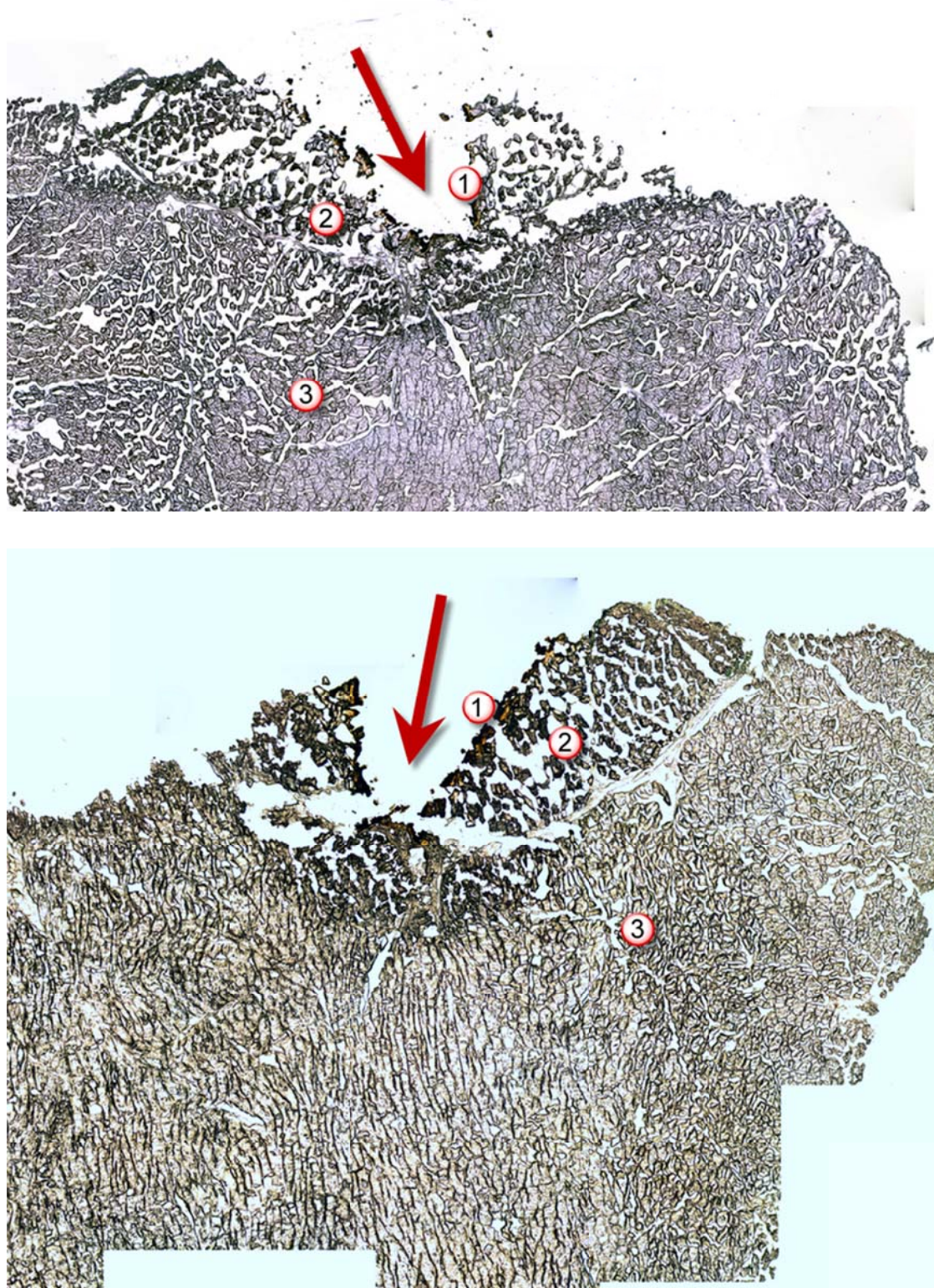


Figure 4-32. Three frozen histology section of ICG-mediated laser ablation in pork muscle tissue.
The red arrows indicate the location of the laser beam. In region (1),

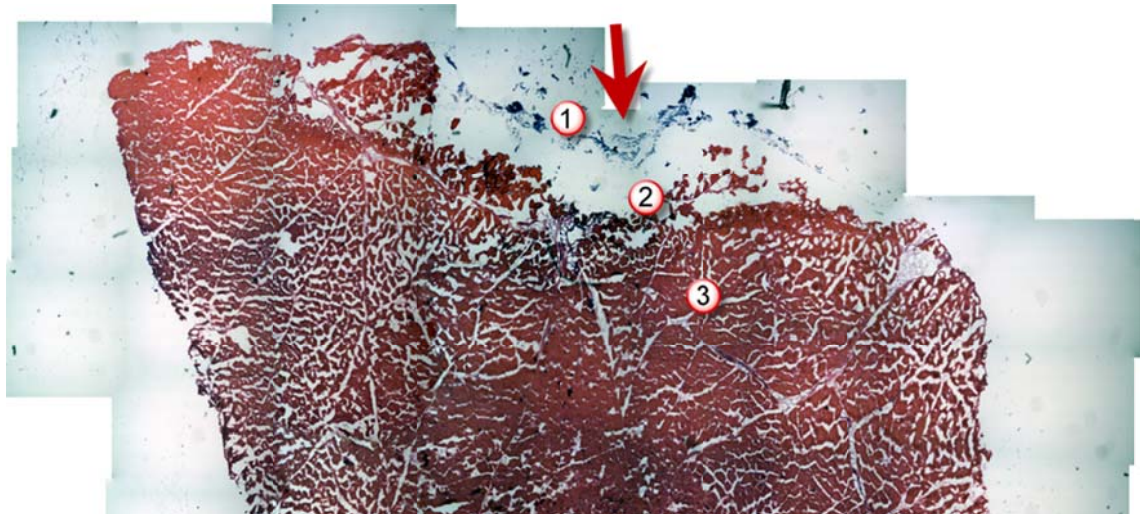


Figure 4-33. A frozen section that subsequently has undergone H&E staining.
As can be seen when compared with slides not stained with H&E, much of the tissue at (1) and (2) has been lost.

The results of Gömöri trichrome staining and NADH reductase can be found in Figure 4-34 and Figure 4-35, respectively.



Figure 4-34. Gömöri trichrome staining of ICG-mediated laser ablation of tissue — control (left) and test (right).

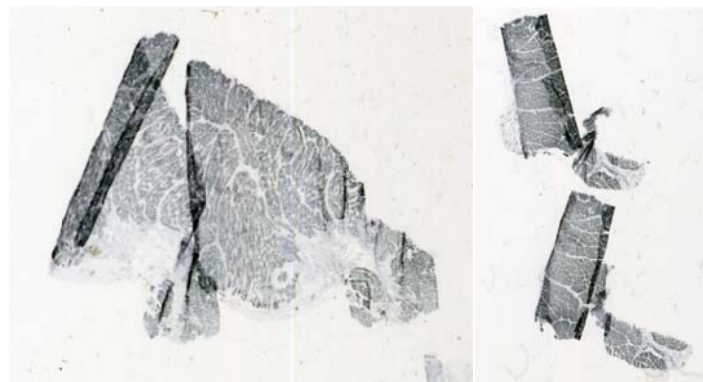


Figure 4-35. Staining for NADH reductase in ICG-mediated laser ablation of tissue — control (left) and test (right).

After review of all the histology slides, Dr. Jacques concluded in his expert opinion that a definitive differentiation between coagulated and uncoagulated tissue could not be made based on the slides he had viewed.

Discussion

Histology performed on dye-mediated, laser-ablated tissue revealed structural changes roughly in accordance with the McKenzie three-zone model.

A visible ablation crater and carbonised zone could be seen, however no vacuolated zone was found. The coagulated zone could be visualised in the bulk tissue before histological sectioning, but could not be differentiated from undamaged tissue afterward.

Looking at the histology results in Figure 4-32, the ablation crater left behind by vaporised tissue can be seen, with the number (1) placed in each image near the ablation front.

The carbonised zone can be seen at (2) where the tissue is vacuolated and darker than tissue at the deeper location (3). Temperatures in this region probably were between 100-500° C, hot enough for carbonisation to occur by a combination of pyrolysis and combustion and for vaporisation at the ablation front.

One might believe that the region at (2) is the vacuolated zone rather than an expanded carbonised zone due to the extensive vacuolisation seen here. However, in McKenzie's model, vacuoles and fissures also can be found in the carbonised region.

Furthermore, in McKenzie's model, the temperature of the vacuolated zone is held constant at 100° C by the thermal clamp of vaporising water, which makes it difficult to explain the dark colour of the region as seen in the histology images. The carbonisation processes all take place at temperatures above 100° C.

In the region at (3), presumably a coagulation zone can be found directly where temperatures have reached the notional coagulation temperature of 60° C, high enough to denature proteins and destroy cell viability, but not to the boiling point of water at 100° C.

However, this cannot be seen directly at histology, as definitive visual cues cannot be found to differentiate it from undamaged tissue. Perhaps the area immediately below the dark carbonised region is subtly lighter than deeper tissues in some of the histology images, but this was not conclusively supported by image analysis using level thresholding.

In the lasered tissue before sectioning with the microtome for histology, the coagulation zone can be identified by the white colour in the tissue due to increased optical scatter largely from proteins being denatured. However, in the 10 µm thick histology sections, one could not visually differentiate between coagulated tissue and undamaged tissue.

In clinical practice, necrosis is tracked by animal survival studies — allowing the animal to heal for a period of time after the test procedure and then sacrificing the animal for histopathological study. For scientific studies, the coagulation area might be calculated immediately after the procedure by visually segmenting the area turned white by thermal damage.

However, the relationship between necrosis, or cell death, and coagulation is slightly tricky. Although cells that have been coagulated as indicated by a colour change almost certainly have died, cells that have been exposed to lower temperatures for long periods of time also may die. Therefore, regions of necrosis potentially can be bigger than visible regions of coagulation depending on how the thermal damage was administered to the tissue.

It was conjectured that although the tissue whitening effect was too subtle to be detected in a 10 µm slice, perhaps the coagulative damage would be expressed in other, more discernable changes, perhaps, in the cellular microstructure or metabolic enzyme concentrations. Dr. Jacques recommended using the Gömöri trichrome and NADH reductase staining to visualise these changes.

However, these efforts did not bear fruit as these alternative histological test results were inconclusive. Therefore, in later experiments, coagulation was evaluated by measuring tissue areas that had turned white in bulk sectioned tissues and not at histology.

4.8. Ablation sequence of events revealed by high speed videography

Two high-speed video cameras, a Phantom MIRO4 monochrome camera (Vision Research; Wayne, NJ, USA) and a Fastcam SA1 colour camera (Photron, Ltd; San Diego, CA, USA), were borrowed from the EPSRC equipment loan scheme to film in slow-motion the tissue effects of ICG-mediated laser ablation in the first few seconds of laser irradiation.

An overview timeline of events during ablation is presented in this section, while details of ablation filmed *en face* and in cross-section are presented in the next two sections.

Methods

The Vision Research Phantom MIRO4 camera is a compact, high-speed, 8-bit monochrome, CMOS-based video camera that can capture video at up to 1,200 fps at the maximum sensor resolution of 800x600 pixels (see Figure 4-36). The camera has the capability to trade image resolution for framerate — at the 256x256 pixel resolution used in the experiments, the camera had a maximum frame rate of over 11,000 fps.

The Photron Fastcam SA1 high-performance, high-speed, 12-bit colour (Bayer GRGB filter array), CMOS-based video camera that can capture video at up to 5,400 fps at the maximum sensor resolution of 1,024x1,024 pixels (see Figure 4-36). Like the MIRO4, it has the ability to trade image resolution for framerate. At the 256x256 pixel resolution used in the experiments, the camera had a maximum frame rate of 67,500 fps.



Figure 4-36. The Vision Research Phantom MIRO4 (left) and the Photron Fastcam SA1 (right) shown to approximate scale.

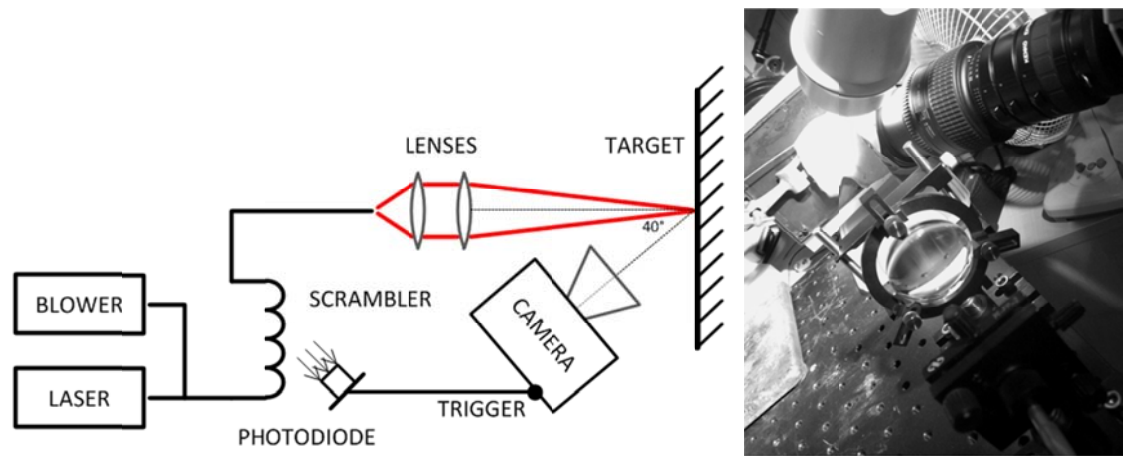


Figure 4-37. Experimental setup for producing the *en face* ablation videos.

The experimental setup on the optical bench is shown in Figure 4-37.

A 600 µm clinical optic fibre with a concentric blower sheath was attached to the Diomed 25 laser and the Olympus blower. The fibre was fixtured into a tortuous path in the mode scrambling fixture as done previously. The fibre tip was held in a fibre holder, and beam was focused using two lenses ($f = 50.8\text{mm}$, 200 mm) (Comar Optics Inc; Regina, SK, Canada) to collimate and focus the beam.

A Photologic Plastic Sensors Type OPL550 (Optek Inc; Carrollton, TX, USA) which incorporated into a single package a photodiode with maximum sensitivity at 800 nm, a linear amplifier and a Schmitt trigger, was used to trigger video recording in the camera upon firing of the laser. Powered by a 5 V DC supply, it detected the laser light leaking out from the fibre in the mode scrambling fixture and sent a TTL signal to the camera to initiate recording.

Two halogen lamps (one in the nearfield and one in the farfield) provided illumination and a small fan produced a small amount of air flow to blow the generated smoke plume away from the camera.

A Nikon macro lens provided by the EPSRC was used with both cameras. Macro extension tubes were used with the MIRO4 to magnify further the image on the sensor. However, due to constraints imposed by the large physical size of the SA1 camera, the extension tubes were not used with this camera.

The MIRO4 and SA1 cameras were placed 40 degrees off-axis to the right of the laser beam. The laser spot on target was positioned in the centre of the camera field of view. Although off-axis visualisation was not optimal, this was required due to the macro-lens focal length and the physical size of the camera body.

The Diomed laser was set to 25 W in a 3 mm diameter spot, which corresponded to an irradiance of 230 W/cm^2 after transmission losses. The target consisted of pork muscle tissue purchased from the local supermarket. 5 mg/ml ICG in water was used. The MIRO4 camera captured the laser ablation at 4000 fps for almost 8 seconds. The SA1 filmed at a frame rate of 20,000 fps for just over 4 seconds.

Recorded pixels through the centre of the ablation crater were plotted against time in ImageJ.

Results

Selected frames from the SA1 video can be seen in Figure 4-38, and from the MIRO4 in Figure 4-39. The SA1 images are in colour, and the monochrome images from the MIRO4 have a higher magnification because of the use of macro extension tubes.

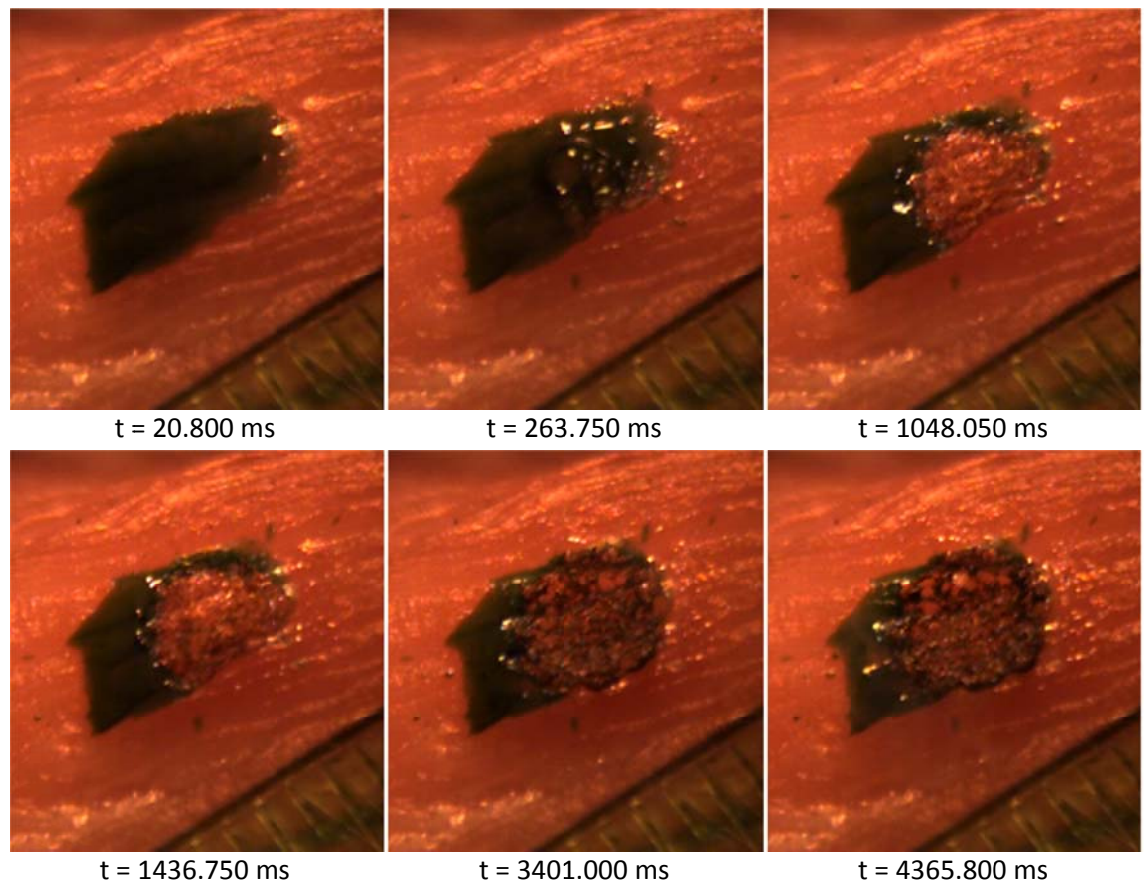


Figure 4-38. Dye-mediated laser ablation of pork muscle captured with the Phantom SA1.

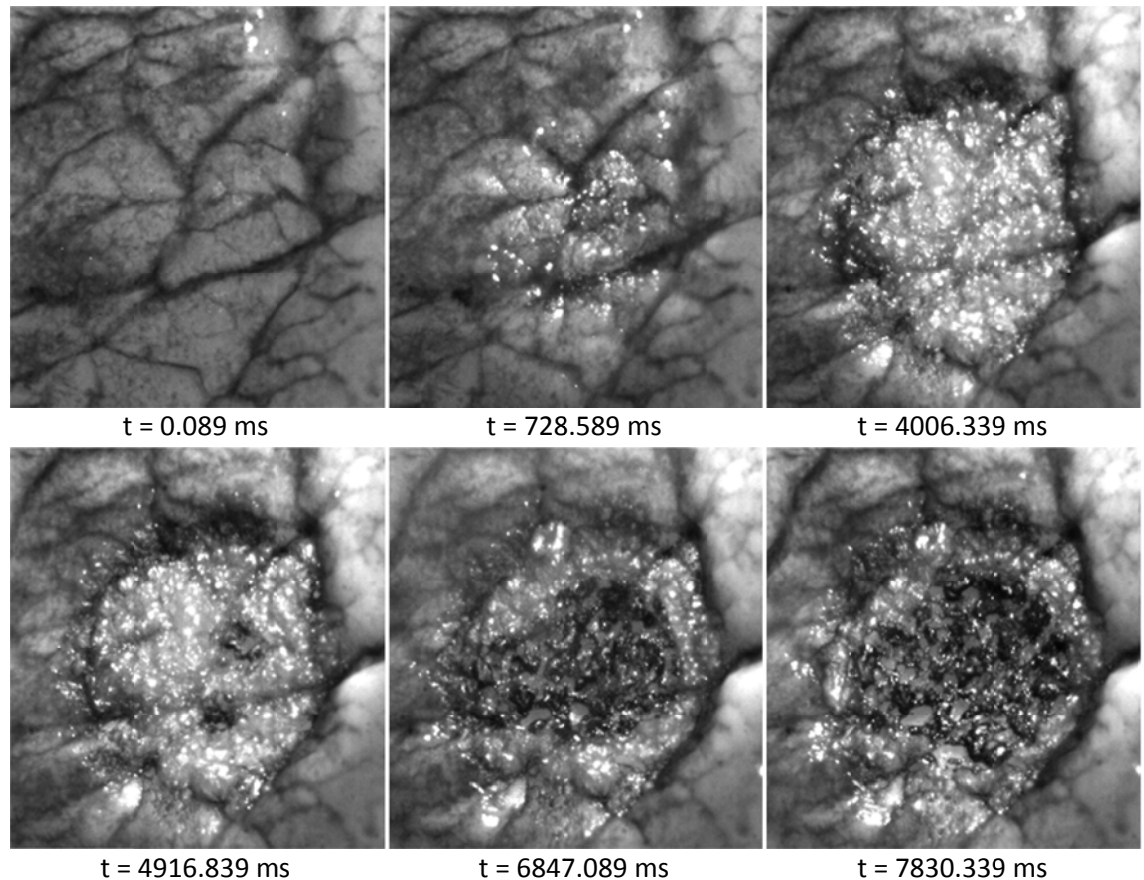


Figure 4-39. Dye-mediated laser ablation of pork muscle captured with the Phantom MIRO4.

In general, both series reveal a similar sequence of events:

1. Boiling of the pool of dye upon activation of the laser. The boiling was observed to be quite violent, occasionally erupting and sending small droplets of the liquid away from the main pool. During this phase, a whitening of the image can be seen starting from near the centre of the image growing outwards.
2. Disappearance of the dye layer from the centre of the pool outwards to reveal light-coloured, pock-marked tissue underneath.
3. Appearance of small regions of blackened tissue that grow and converge into a single, large blackened area. A large amount of black smoke is generated during this phase of the ablation.

The results of extracting a vertical line of pixels through the centre of the ablation crater plotted against time can be seen in Figure 4-40. Regions in time corresponding to the above sequence of events have been tagged with the numbers (1), (2) and (3) in the plots.

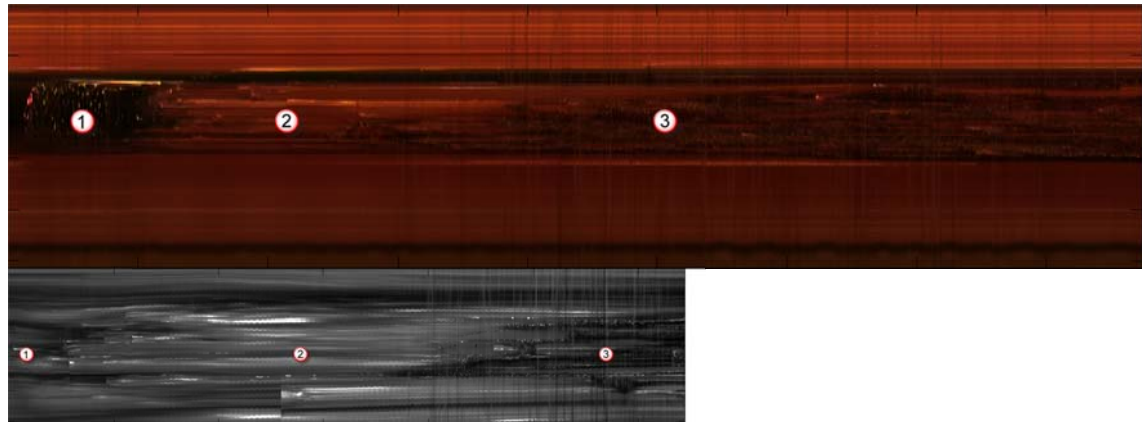


Figure 4-40. Plot of the pixels in a vertical line through the centre of the ablation crater (y-axis) versus time (x-axis). (Top) Photron SA1 filmed at 20,000 fps for 4.3658 s; (Bottom) Phantom MIRO4 filmed at 4000 fps for 7.8303 s. Time axes (horizontal) were scaled and aligned. The space axes (vertical) were scaled to maintain the aspect ratio.

Discussion

In general, the events revealed by high speed videography of the onset and continuation of laser ablation in porcine muscle tissue roughly corresponded with observations made by Verdaasdonk et al. of laser ablation in three phases — coagulation, ablation and carbonisation.

Upon activation of the laser, the pool of dye on the tissue surface started to boil vigorously, occasionally ejecting droplets of dye away from the pool. The initial coagulation of tissue could be seen as a whitening of the laser-exposed region, although this was partially obscured by the dark pool of dye.

Once a circular area of the dye pool, approximately the same size as the beam diameter, had been vaporised, the coagulated tissue underneath was revealed. Dark specks assumed to be dye remained on the tissue surface, and bubbles from boiling appeared to be centred on these areas.

This continued for a short time until blistering and popping of the tissue surface started to occur. This probably corresponded to the “popcorn” ablation phenomenon observed by Verdaasdonk et al.

Finally dark areas of char appeared accompanied by smoke plumes that grew and then coalesced into one large dark spot. Deepening of the crater appeared to accelerate during this phase, which corresponded to Verdaasdonk’s cyclical carbonisation phase.

The cyclical renewal of carbonisation did not appear as expanding rings of char, probably because a top-hat profile beam was used instead of a Gaussian profile beam. However, char

renewal process could be seen in the videos — uncarbonised tissue revealed after chunks had been blown off the surface was seen to be carbonised.

By McKenzie's model, increased absorbed power would be necessary to decrease the thickness of the char to the point where uncharred tissue underneath would be revealed. (The thickness of the carbonised layer is inversely proportional to the absorbed power.) This newly exposed tissue then would be carbonised and the cyclic process continued.

This might suggest a method, at least theoretically, for permanent termination of dye-mediated ablation, at least until dye is re-applied. If a short, high-irradiance pulse can vaporise the carbonised layer, then further exposure to the lower irradiance beam would not result in any more tissue ablation due to the elimination of good absorbers on the tissue.

However, actually engineering a method for doing this cleanly could be very challenging indeed.

4.9. Growth of the ablation crater assessed by *en face* videography

To understand the ablation process better, further experimentation was conducted with the high speed cameras to capture the dye-mediated ablation process under a number of different conditions. This section deals with visualisation of laser ablation *en face*. The next section will present data viewed through cross-section.

Methods

The experimental setup on the optical bench from the previous section was used for the experiments in this section as well.

Three power settings on the Diomed laser — 15 W, 20 W, 25 W — were used and the laser beam was focused onto a 3 mm spot, corresponding to laser irradiances of 140 W/cm^2 , 190 W/cm^2 , 230 W/cm^2 .

The ablation run order was randomised and the MIRO4 camera used to document the ablation events for each experimental run. Video capture was set to 256x256 pixel resolution at 4000 fps for about 8 seconds of capture time.

Pork muscle tissue from the supermarket was used as the laser target. 5 mg/ml ICG in water was used as the sensitising dye.

Captured videos were reviewed for qualitative generalisations about dye-mediated laser ablation.

Quantitative measurements were made by extracting individual video frames at 500 ms increments in time and annotating regions of interest (ROI) with fitted ellipses designated “black” for blackened, “white” for desiccated and “coag” for coagulated. Frame extraction and ROI annotation was performed in ImageJ.

Criteria for marking the ROIs were as follows:

Regions marked as “coag” displayed some degree of whitening as seen in the video over time.

Regions marked as “white” exhibited surface blistering and roughening in addition to a whitening of colour. The blistered and roughened surface often appeared similar in texture to cauliflower. Tissue in this region may be seen to shrivel and shrink, leading to more blistered and roughened surface.

Regions marked as “black” appeared initially with similar texture characteristics as regions marked as “white” but quickly darken in colour to a black or brown hue. Bits of material may be seen ejected and black smoke may be seen to be emitted from these areas. Tissue in this region may be seen to recede and vaporise.

A typical ablation crater and regions of interest marked in Image J can be seen in Figure 4-41.

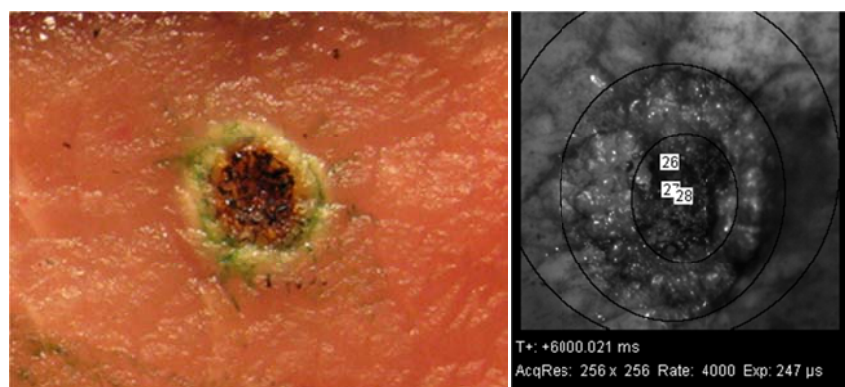


Figure 4-41. A typical ablation crater and regions of interest are marked in ImageJ.

Results

A summary of the growth of average diameters of the “black”, “white” and “coag” ROIs over time can be seen in Figure 4-42. The different colours in the graph represent the three laser irradiances used. Error bars represent 95% confidence intervals.

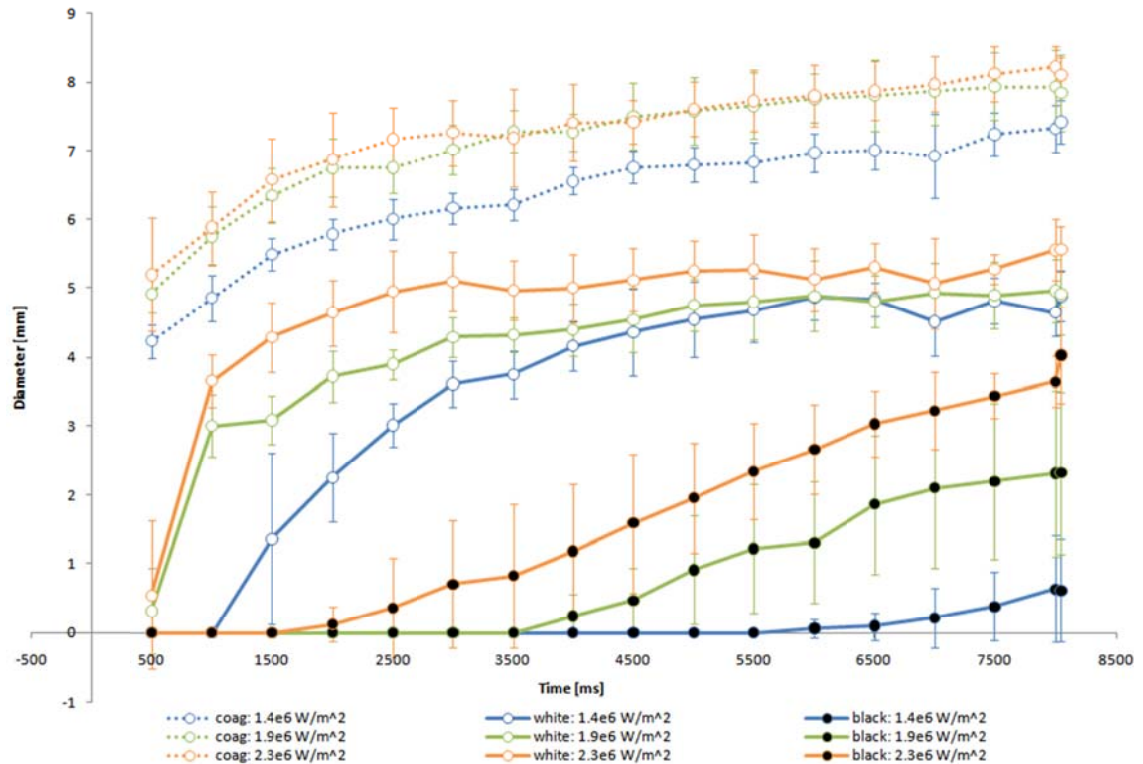


Figure 4-42. The diameter growth of regions denoted as black, white and coag at three laser irradiances. ($n=255$, x- and y- error bars represent 95% CI)

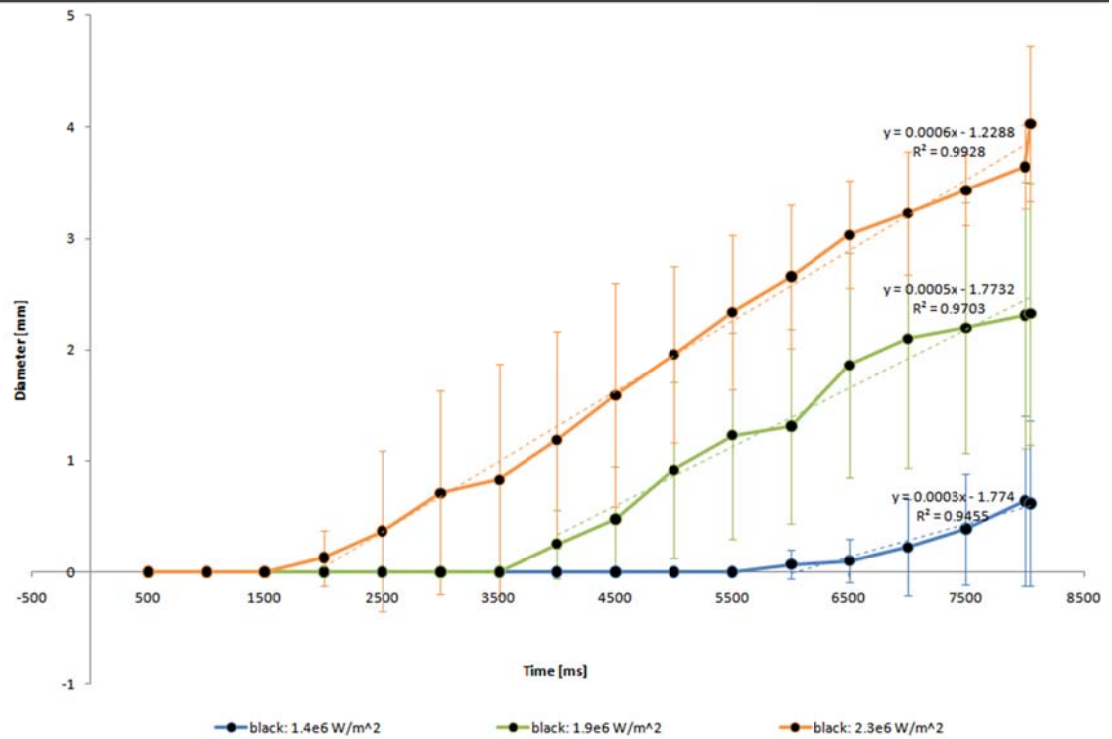
Upon activation of the laser, there was an immediate growth in size of the “coag” region, followed by growth of the “white” region after a delay, and finally growth of the “black” region. The ablation events as viewed in the videos always occurred in this order without exception ($n=101$ videos). However, depending on the laser irradiance and the particular experimental run, appearance of “white” and “black” ROI did not always occur.

Focusing on the appearance and growth of the “black” region, linear regression seemed to fit the non-zero data well with R-squared values of 0.95, 0.97 and 0.99 for the three irradiances (see Figure 4-43).

Continuing the assumption of linear growth of the “black” region diameter, then the onset could be found by determining the x-intercept. The rate of diameter growth is given by the slope of the regression. These results are summarised in Table 4-5.

Table 4-5. Summary of “black” region growth assuming a linear model.

Irradiance	140 W/cm ²	190 W/cm ²	230 W/cm ²
Start time after trigger	6 s	3.5 s	2.0 s
Diameter growth rate	0.3 mm/s	0.5 mm/s	0.6 mm/s

**Figure 4-43.** Linear regression of the “black” region growth over time at three irradiances.
Error bars represent 95% CI.

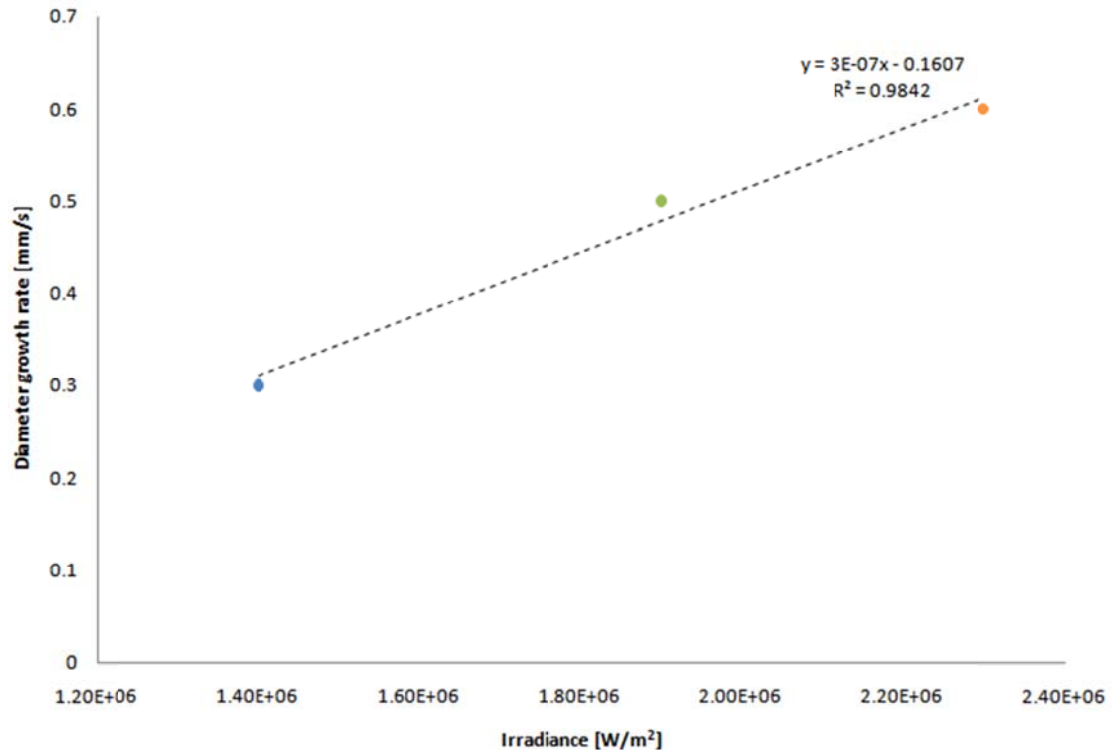


Figure 4-44. Diameter growth of the “black” region increased with larger laser irradiances.

The diameter growth rate of the “black” region increased with increased laser irradiance, and within the range of irradiance used, could be modelled well by linear regression with an R-squared value of 0.98 (see Figure 4-44).

The “white” regions in general appeared initially to grow rapidly before appearing to level off after a few seconds (see Figure 4-45).

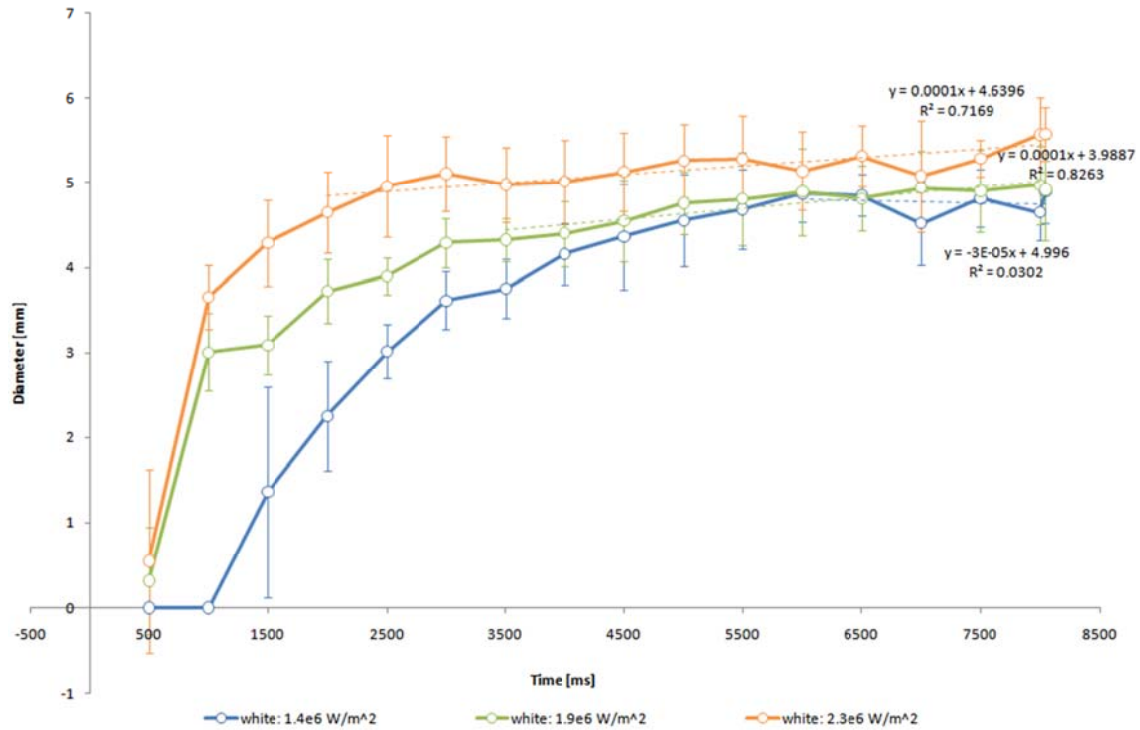


Figure 4-45. The growth of the “white” region over time at three irradiances. Error bars represent 95% CI.

For each irradiance level, a linear regression was fitted to data corresponding to times after the first appearance of a “black” region. These regressions fit the data moderately well at the high and middle irradiance levels with R-squared values of 0.72 and 0.82 respectively. However, the regression at the low irradiance level was poor, with an R-squared value of 0.03.

Finally, the thickness of the “coag” region was determined by subtracting the “white” diameter from the “coag” diameter and dividing by two to reveal the results found in Figure 4-46.

The general trends seen for the “coag” ROI were that there appeared to be an initial increase in the thickness of the “coag” region followed by a decrease that appeared to level off. Average “coag” thicknesses were lower at the highest irradiance compared with thicknesses at the middle irradiance level. However, at the lowest irradiance level, the thicknesses started out higher and then became lower than at either the middle or high irradiance cases.

There was a lot of overlap in the 95% CI for the results at all three irradiances.

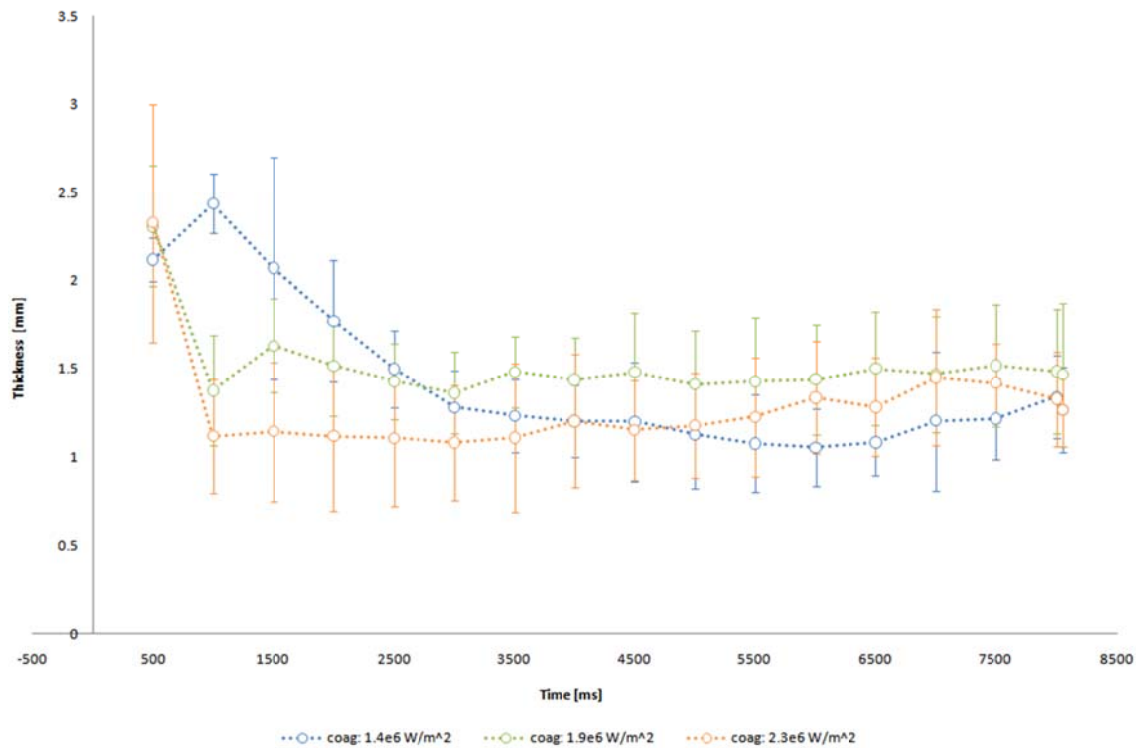


Figure 4-46. Average thickness of the coagulated region at three irradiances over time.. Error bars represent 95% CI.

Discussion

We can explain the observed experimental behaviour of the *en face* aspect of the ablation crater by first examining ablation by CO₂ laser, and then considering the similarities and differences with dye-mediated laser ablation.

The water in tissue is a good absorber of 10.6 μm light from the CO₂ laser.

Upon activation of the laser, the temperature of the tissue within the diameter of the laser beam on the surface (and a small depth underneath) increases rapidly, first high enough to coagulate the tissue and then hot enough to vaporise explosively the water within cells.

Vaporised water mass and probably some amount of non-water tissue mass are removed by the violent migration of steam to the atmosphere.

Free from the thermal clamp of liquid water, the pock-marked and vacuolated remains of desiccated tissue then are free to increase further in temperature beyond 100° C until it becomes carbonised by pyrolytic and combustion processes and the remaining mass is removed.

This is the general description of the axial ablation process in the direction parallel to the laser beam — what happens to tissue from the surface at the ablation front to some depth beneath — as proposed by McKenzie.

Unfortunately, the model offers no predictions for what might happen for a finite beam in the radial direction because the model is a theoretical framework in one dimension (McKenzie assumes an infinitely wide beam of laser light falling upon a semi-infinite slab of tissue).

However, we can expect that, for a circular beam with top hat beam profile and sufficient irradiance, ablation should occur everywhere within the full diameter of the laser beam.

At the centre of the beam, because of the radial symmetry and because the penetration depth is small compared with the beam diameter, the conditions essentially are equivalent to those in McKenzie's 1D model and the damage to tissue in the direction parallel to the beam are well described by the model.

However, at the edges of the laser beam, the conditions are very different. In the case of a finite beam with a flat beam profile and assuming no scattering, differential heating on the two sides of the beam boundary (heating inside the boundary and no heating outside) result in a thermal gradient and heat loss from conduction radially away from the irradiated tissue (in addition to axial conduction). Because of this, one would expect the laser heating from absorbed light to decrease from a maximum at the centre to the boundary of the beam.

Being the hottest in the centre, one would expect coagulation, water vaporisation and carbonisation to occur first in the centre and then to spread out towards the edges.

We would expect the "black" area of carbonisation to grow and then stabilise at about the diameter of the laser beam. Because, at this point, the walls of the ablation crater are essentially tangential to the beam, the laser irradiance of the laser light incident on the walls is much smaller than at the bottom of the crater.

However, the side walls probably remain at an elevated temperature, due to heating from some incident and some reflected laser light, but also from contact with hot gasses, hot particulates and water vapour released from inside the crater, and by thermal conduction from tissue inside the crater.

The area of desiccation corresponding to the “white” area would grow to and stabilise at a larger diameter than the black region. The boundary of the white area would correspond to the 100°C isotherm.

The thickness of coagulation corresponding to the “coag” area initially would grow until tissue started to be vaporised. It would settle to a steady state thickness.

These effects were confirmed in separate experiments using a CO₂ laser to replace the Diomed 805 nm laser in the above setup.

Dye-mediated laser ablation with the 805 nm laser is decidedly more complicated, but overall, we would expect similar behaviour because of the high absorption from both ICG and carbonised tissue.

The overall behaviour of the “black”, “white”, and “coag” regions in these experiments were in agreement with expectations.

For each irradiance level, the thickness of the “coag” region initially grew from zero but then approached an almost constant thickness as measured from the boundary of the “white” region.

The diameter of the “white” region grew initially but then approached a maximum diameter for each of irradiance level. Linear regression of data points corresponding to times after the “black” region had appeared fit the data well. The slope of the regressions at each irradiance level all were close to zero.

The diameter of the “black” region appeared to grow linearly — the data for each irradiance level were fit well by linear regression with high R-squared values. Although the diameter of the “black” region did not appear to level off, given more time than the maximum 9.9 s exposure used, it is expected that they would have.

The correlation between the diameter growth rate of the “black” region and the irradiance was fit well by linear regression with a high R-squared value of 0.98.

The time sequence of the “black” region growth in ICG-mediated laser ablation in actuality was more complicated than an expanding black circular region. Multiple small black regions would appear and grow, eventually combining into a single large black region.

An explanation for this might come from the locations of where carbonisation had been seeded, which appeared to be random. But the carbonised regions always converged into one large circular black region over time.

4.10. Growth of the ablation crater from cross-section photography

While visualising the growth of the ablation crater and tissue damage zones with a video camera from an *en face* perspective was relatively straightforward, it was much more difficult to track the growth of the damage zones in cross section in real time.

McKenzie and Byrne in 1987 used the method of plane photography to visualise isodose pattern of HeNe laser in tissue, delivered by an optic fibre with a diffusing bulb tip embedded within the tissue volume. [323]

They split the slab of tissue in half to visualise the isodose pattern at the cross-section corresponding to a plane of symmetry. A mirror, placed in contact with the tissue at the symmetry plane, restored the space irradiance back to the distribution before splitting the tissue in half.

By using a partially silvered mirror, photons passing through the mirror could be recorded by a camera, revealing the cross-sectional isodose pattern within the tissue without changing it significantly from that with a fully reflecting mirror.

An approach inspired by this was taken here to visualise the evolution of tissue damage in a planar cross-section through the centre of the beam / crater, with the understanding that the conditions for ablating a half-slab of tissue was not equivalent to ablating a full-slab.

In the ideal case, a material would be found for use at the boundary which would function as both an optical and thermal mirror, as laser tissue ablation operated in both the light transport and thermal diffusion domains. The material ideally would be reflective at 805 nm and be thermally insulating. It also needed to allow transmission of visible wavelengths for capture by video equipment.

Unfortunately, an appropriate material that also was cost effective could not be found. Dielectric mirrors that reflect at 805 nm were expensive, and probably would not survive the localised thermal expansion stresses induced during laser ablation. They also would not have been particularly good thermal insulators.

Soda-lime glass was used instead. As this material is the most common form of glass, it was cheap and easy to obtain. Also retrospectively, using soda-lime glass was good because it needed to be replaced after each experimental run. Build-up of carbonisation on the glass surface in all cases was very difficult to remove.

Also, in some cases after some runs, cracks could be found in the glass, probably due to mechanical stresses from localised thermal expansion due to heating of the carbonised residue adhered to the glass.

Unfortunately, soda-lime glass is neither a good thermal insulator — the thermal conductivity of soda-lime glass is 0.9-1.3 W/(m K) — nor is it a good reflector at 805 nm.

The latter factor, however, is mitigated by the laser beam being aimed parallel to the glass and by dye-mediated laser ablation being an absorption dominated process.

Still, it is acknowledged that videography of a half-slab of tissue with glass at the symmetry plane is not equivalent to that of a full-slab.

However, it was thought that high speed videography could reveal insights into the time evolution of dye-mediated laser ablation from direct visualisation, even if conditions are not exactly equivalent. The black pixels of the carbonised tissue and the white ones of the coagulated tissue were tracked.

Ablation of tissue in the full-slab configuration followed by physical sectioning with a scalpel to reveal the cross-section also was conducted and will be discussed in the next section.

Methods

Laser damage to tissue was visualised directly by ablating a half-slab of porcine muscle tissue fixtured in a glass box with a replaceable front glass plate. The overall experimental setup was essentially identical to the previous *en face* experiments with the laser and lenses positioned on an optical bench, with the exception that the camera was positioned 90 degrees to the laser target (see Figure 4-47).

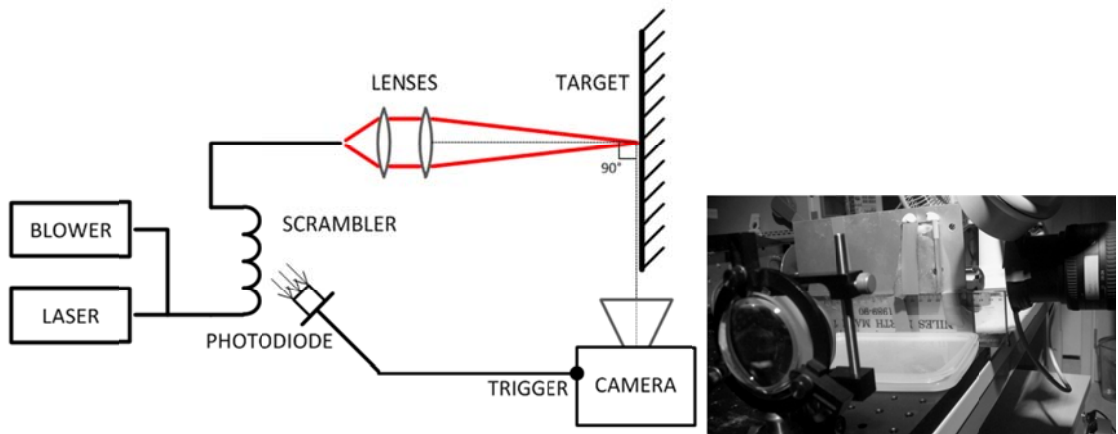


Figure 4-47. Experimental setup for cross-section laser ablation videography.

A glass fixture with a replaceable front glass plate was used to position the porcine muscle tissue. The tissue was positioned so that the tissue-glass interface was located on the diameter of the laser beam.

Three power settings on the Diomed laser — 15 W, 20 W, 25 W — were used and the laser beam was focused onto a 3 mm spot, corresponding to laser irradiances of 140 W/cm^2 , 190 W/cm^2 , 230 W/cm^2 . The ablation run order was randomised.

$5 \mu\text{m}$ of 5 mg/ml ICG in water was used for each run and applied with an Eppendorf pipette. The ablation crater resulting from a typical experimental run can be seen in Figure 4-48.



Figure 4-48. Porcine muscle tissue target after laser ablation run.

The same photo-diode with TTL output as previous was used to trigger the Phantom SA-1 high speed camera, which recorded video at 512x256 pixel resolution at 500 fps for about 11 s of recording time. The laser was activated for 9.9 s in each run and deactivated for about 1 s of each video (see Figure 4-49).

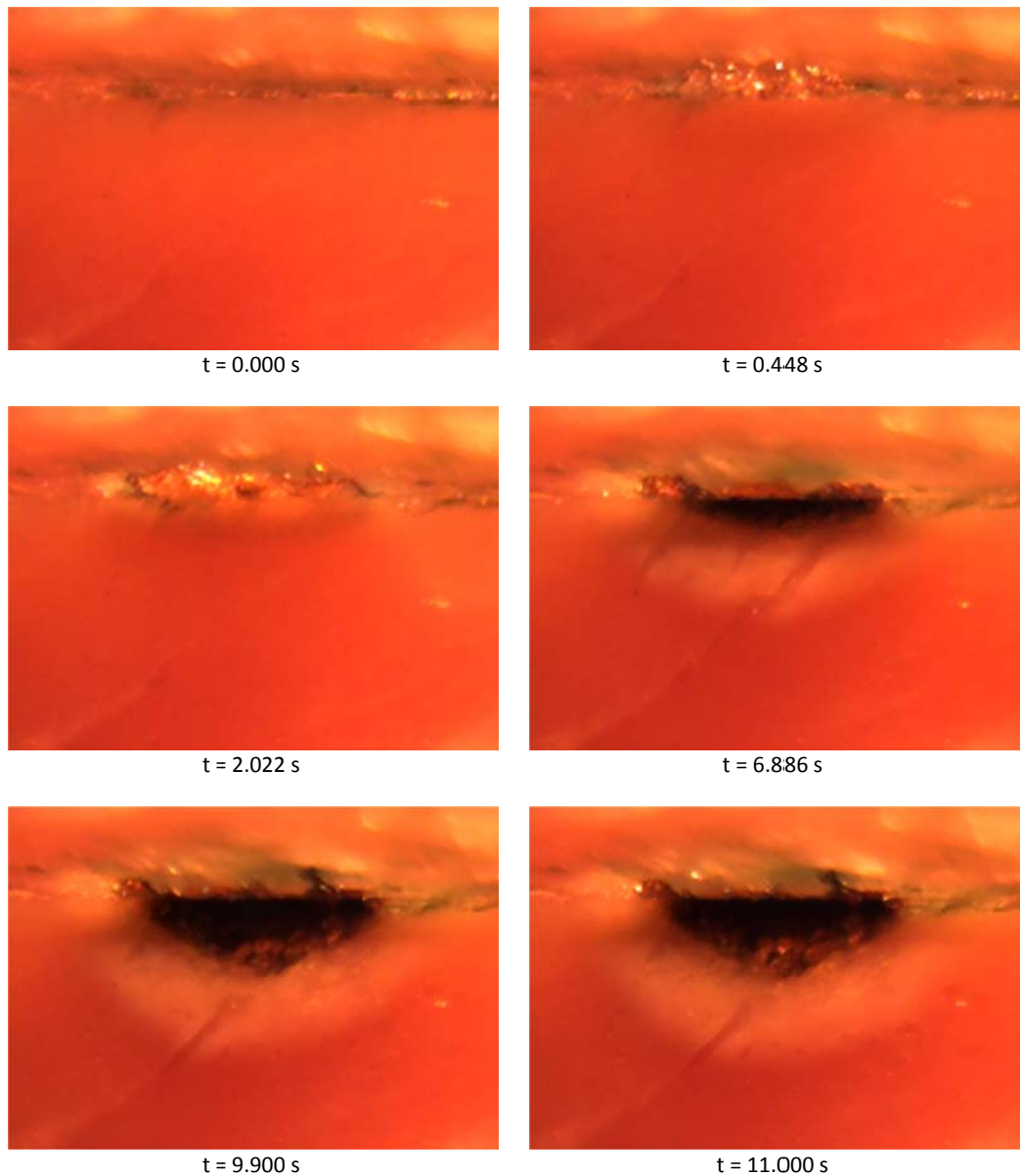


Figure 4-49. Cross-section view of laser ablation. The laser is active from $t=0$ to 9.9 s.

128 pixels along the vertical axis of symmetry of the ablation crater were extracted for each frame and plotted in sequence to show the time evolution of tissue ablation (see Figure 4-50).

These pixel vs. frame plots were analysed in ImageJ to segment out regions of interest by thresholding the images for regions of black (top) and regions of white (bottom), and typical segmentation results can be seen in Figure 4-51.

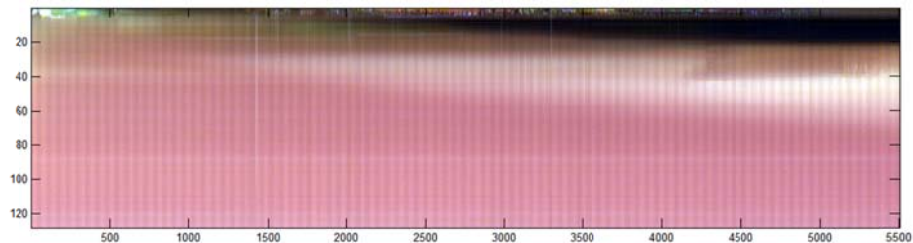


Figure 4-50. The vertical pixels through the centre of the crater section in each frame (y-axis) are plotted against frame / time (x-axis).

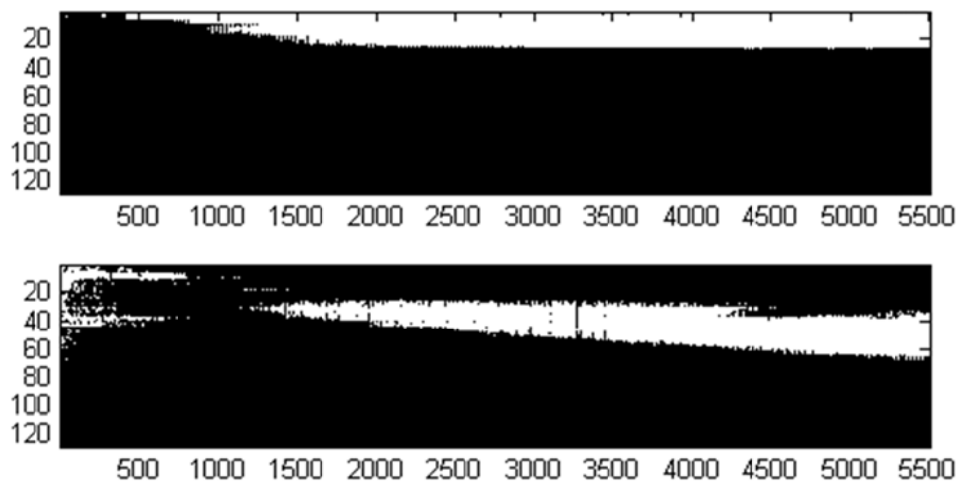


Figure 4-51. Computer segmentation of regions of black corresponding to the ablation crater and carbonisation (top) and regions of white corresponding to coagulation (bottom).

These black and white segmented images then were processed in Matlab to extract for each frame the top and bottom pixels for each region of interest.

From these data, the depth of the black region and the thickness of the white region could be extracted, smoothed by a moving average filter and averaged across experimental runs for each of the three power settings.

The depth of the black region was determined by locating the bottom-most pixel in the thresholded image for pixels with low luminance. This region corresponded to the sum of the areas corresponding to the ablation crater and the carbonised layer.

The confounding of these two regions was due, in part, to the residue left on the glass from areas where tissue had been carbonised and ablated. Also, because we viewed 3D crater geometry in 2D in the videos, the carbonised tissue on the far side of the crater was visible through the glass in the void where the ablation crater should be.

Because of these two factors, the ablation crater void appeared black in the videos and could not be differentiated from the carbonised layer.

The thickness of the white region was calculated by subtracting the top-most pixel from the bottom-most pixel in the thresholded image for pixels with both high saturation and high brightness. This region corresponded to the layer of coagulated tissue.

Results

The average behaviour over time for the black and white ROIs can be found in Figure 4-52. The three colours correspond to low ($n=5$), mid ($n=6$) and high ($n=6$) laser irradiances.

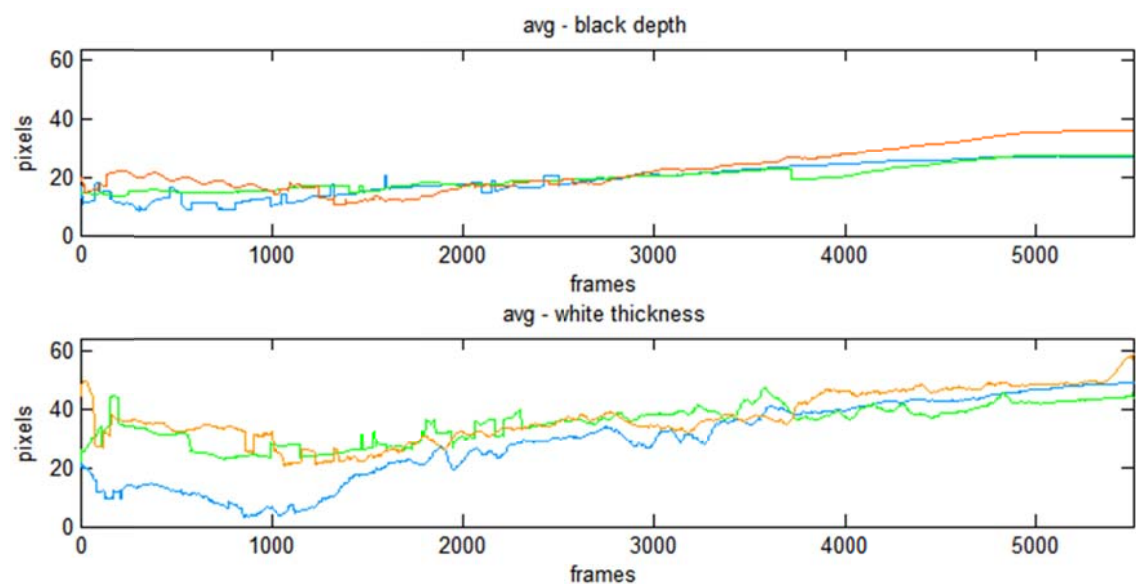


Figure 4-52. Average boundary location at three laser irradiances (orange = high, green = mid, blue = low) for the maximum depth in pixels of the black region (top) and the thickness of the white region (bottom).

The time plots of the bottom boundary of the black region of interest at the three irradiance levels can be seen in Figure 4-53.

The behaviour of the black ROI bottom boundary varied quite a bit for about the first 1000-1500 frames (2-3 s). However, after this initial variability, the data appeared to be described well by linear regression.

At around frame 4950 (9.9 s), the depth of bottom boundary of the black region at all three irradiances appeared to level off. This corresponded to the time when the laser was deactivated.

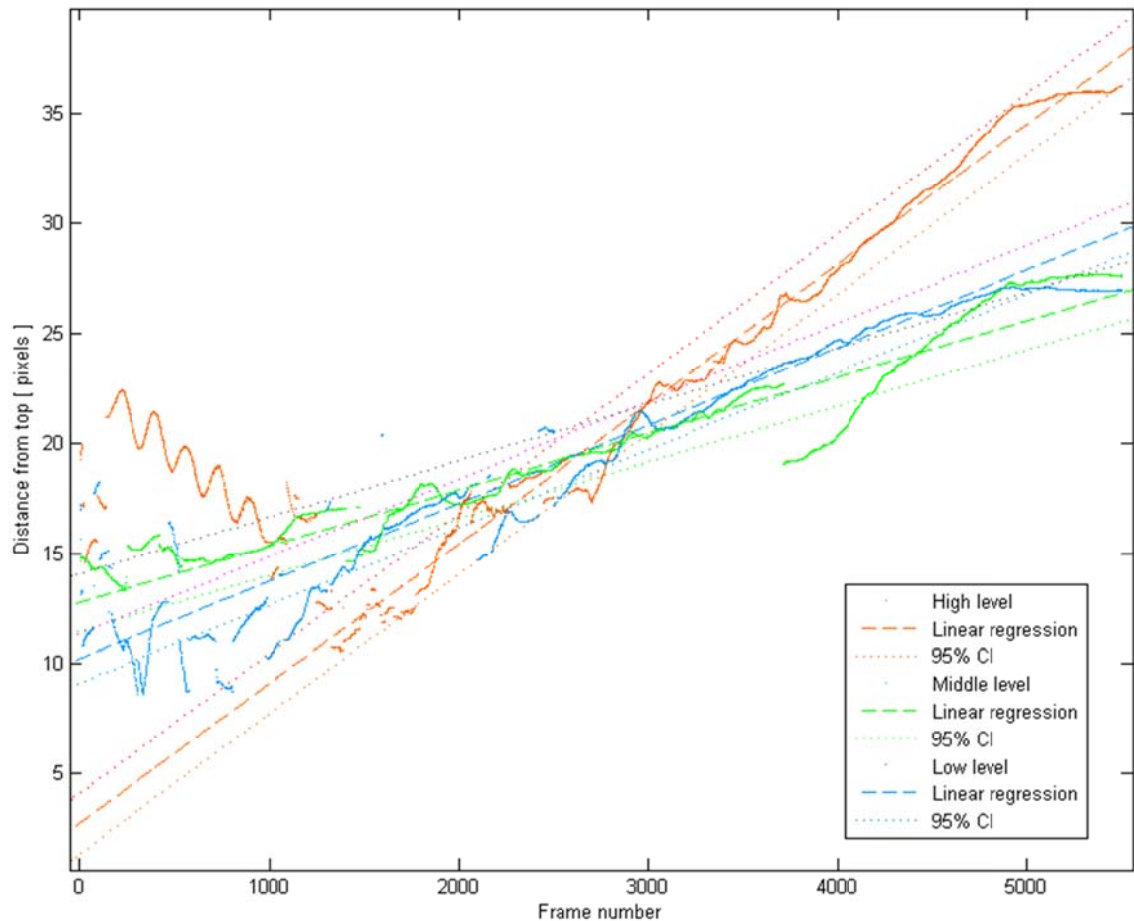


Figure 4-53. Linear regression of average distance from top of image to the bottom of black region.

A summary of the rate of growth of the black region as determined from the slope of the linear regression equations can be seen in Table 4-6 and in Figure 4-54.

Table 4-6. Summary of the black region growth rate, assuming a linear model.

Irradiance	140 W/cm ²	190 W/cm ²	230 W/cm ²
Black region growth rate	0.003524 px/frame (95% CI: ± 0.000020)	0.002554 px/frame (95% CI: ± 0.000020)	0.006342 px/frame (95% CI: ± 0.000030)
y-axis: 29.1 px/mm x-axis: 500 frames/s	0.06 mm/s	0.04 mm/s	0.11 mm/s

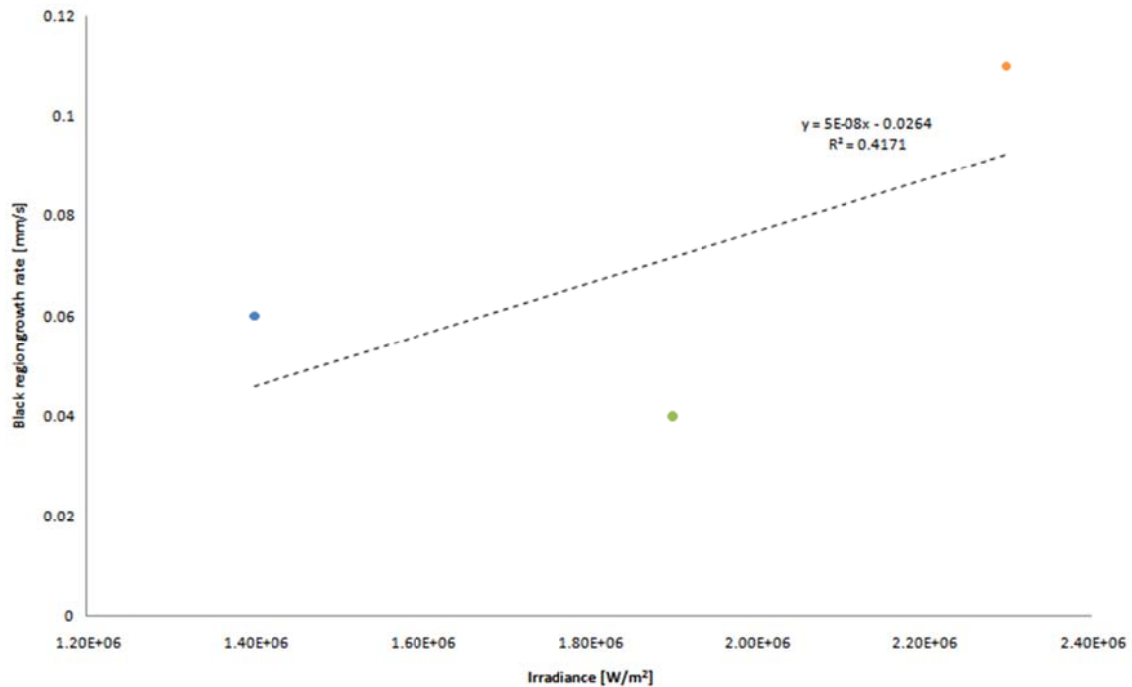


Figure 4-54. Positive correlation between the growth rate of the black region and the irradiance.

Irradiance and the growth rate of the black region were generally positively correlated and were fit by a linear regression model with an R^2 value of 0.4171.

The behaviour of the thickness of the white region can be seen in the time plots at the three irradiance levels in Figure 4-55.

Similar to the black ROI, the data traces at all three irradiance levels exhibited large variability until after around 1000-1500 frames (2-3 s). After this, the thickness of the white region appeared to increase with time at all three irradiances. However, at the high level of irradiance, the thickness appeared to start levelling off. After frame 4950 (9.9 s) when the laser was shut off, the magnitude of the variability in the data appeared to decrease, although thickness continued to increase with time.

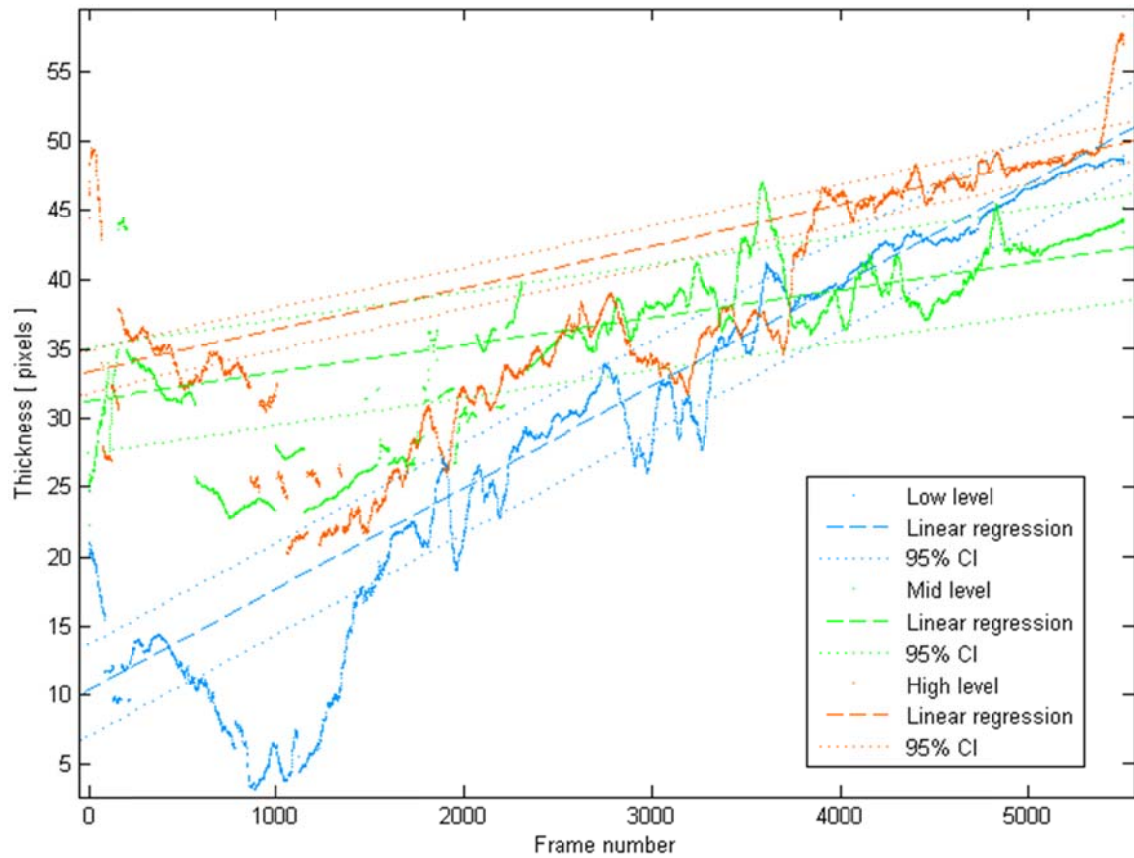


Figure 4-55. Linear regression of the thickness of the white region.

The rate of increase of the thickness of the white region as determined by the slope of the linear regression equations is summarised in Table 4-7 and Figure 4-56.

Table 4-7. Summary of the white region growth rate, assuming a linear model.

Irradiance	140 W/cm ²	190W/cm ²	230 W/cm ²
White thickness growth rate	0.007319 px/frame (95% CI: ±0.000061)	0.001988 px/frame (95% CI: ±0.000100)	0.002997 px/frame (95% CI: ±0.000134)
y-axis: 29.1 px/mm x-axis: 500 frames/s	0.13 mm/s	0.03 mm/s	0.05 mm/s

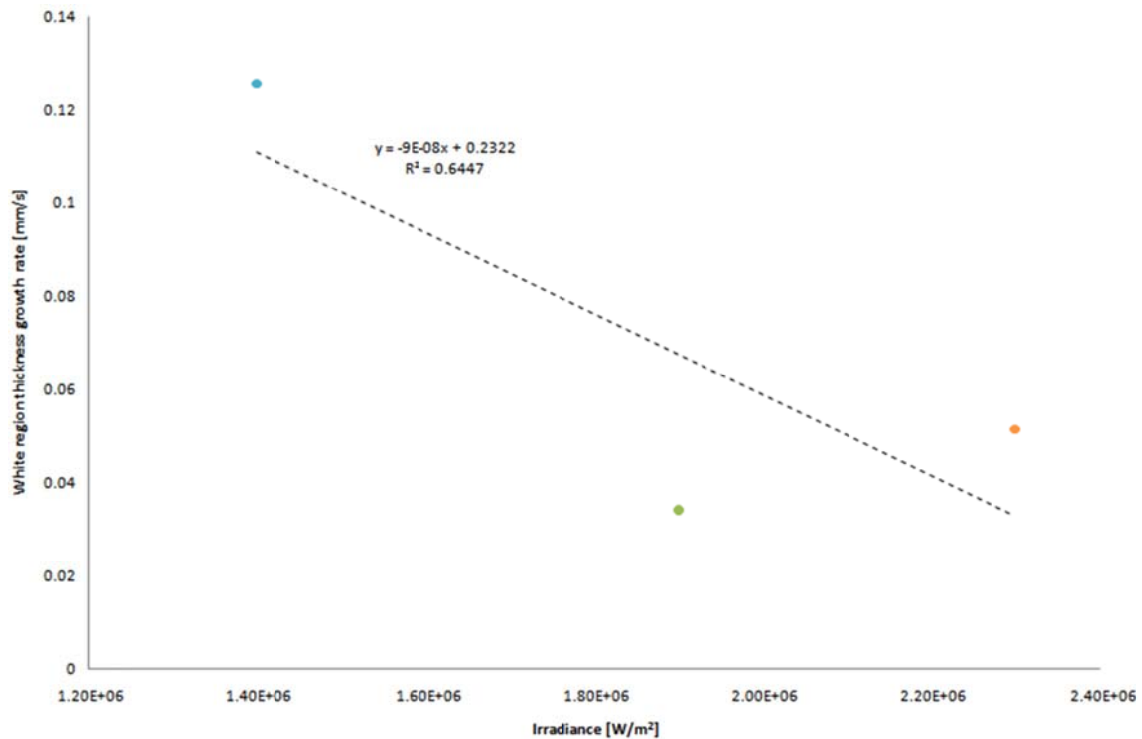


Figure 4-56. Negative correlation between the growth rate of the thickness of the white region and irradiance.

In general, the thickness of the white region was negatively correlated with irradiance and could be fit by a linear regression model with an R^2 value of 0.6447.

Discussion

These experiments provided some insights into ICG mediated laser ablation. The data tended to be very noisy, and averaging between trial runs as well as temporal averaging with a moving window was necessary to smooth the data to tease out trends.

Much of this noise probably can be attributed to the randomness of the ablation process, the sub-optimal lighting setup and the computer segmentation of the ROIs. Still, trends in the data were found that can provide some information about what might be happening during the dye-mediated ablation process.

For the black region, after a few seconds the depth of the bottom boundary appeared to grow fairly linearly. This might suggest that the “ablation” rate as inferred from the growth of the black region was fairly constant at a given irradiance, although this cannot be said definitively because the depth of the ablation crater was confounded with the thickness of the carbonised zone.

If we knew that the thickness of the carbonised zone was relatively constant over time, then we could say with more certainty that the ablation rate was constant.

Overall, the rate of growth of the black region depth and irradiance were positively correlated and was reasonably fit by a linear regression with an R^2 value of 0.42. At the highest irradiance, the growth rate was fairly slow at 0.11 mm/s.

The growth appeared to be very dependent on active irradiation of the tissue by the laser. The deactivation of the laser after 9.9 s corresponded in the data with the cessation or a dramatic decrease in the growth of the black region.

This supports the idea that active laser irradiation of tissue is necessary for ablation, suggesting that any heat contribution from exothermic tissue combustion reactions is not self sustaining. Spontaneous and total tissue combustion probably is unlikely.

The thickness of the white region corresponding to the zone of coagulated tissue increased over time, a trend that appeared after initial variability seen in the first few seconds.

Unlike the predictions of McKenzie, the thickness of the white region did not grow to a steady state thickness, but rather continued to grow within the time frame of filming.

This could suggest that a state of dynamic equilibrium had not yet been achieved. If so, this could be due to the half-slab geometry used.

The plate glass used at the symmetry plane was not a good reflector of 805 nm light, although this probably was mitigated by the very high angle of incidence of the beam to the glass resulting mainly in reflection rather than transmission.

However, the relatively high thermal diffusivity of the glass meant that there was heat loss through the glass that reduced the amount of heat that could be used to raise the tissue temperature at a given laser irradiance when compared with the full slab of tissue.

Also, the assumptions to use the McKenzie model as essentially equivalent to what was happening directly under the centre of the beam may not be true. Although we would expect the penetration depth to be low due to the high absorption coefficient of carbon, in actuality, the depth might be higher due to the carbonised layer being porous rather than a solid layer. Fissures might allow light to penetrate much deeper than might be predicted by $1/\mu_a$.

The penetration depth then might not be significantly smaller than the beam diameter, resulting in curved isotherm surfaces rather than relatively flat ones directly under the centre of the beam. This would make the attainment of a stable dynamic equilibrium less likely in the time observed.

The growth of the thickness of the white region appeared to be negatively correlated with the laser irradiance, and was fit by a linear regression model with an R-squared value of 0.64.

This is in general agreement with McKenzie's inverse relationship between the thickness of the coagulated zone and laser irradiance.

4.11. Statistical analysis of ablation response due to power, time, dye

Statistical modelling of the tissue response to laser ablation can help understanding of physical phenomena by providing interpolating power for factor levels within observation ranges and predictive power for some range of factors outside.

While it provides only statistical correlations between responses and inputs, trends seen can be useful for formulating physical explanations.

The Response Surface Method (RSM) is a well-known experimental design to fit a second-order empirical model to experimental data and was used as the experimental design for this section. RSM uses analysis-of-variance (ANOVA) techniques to determine the effects of factors and interactions in fewer experimental runs than with a one-factor-at-a-time design.

Introduced by Box and Wilson in 1951, the methodology uses a series of designed experiments to obtain data efficiently and approximately model the system response (second order polynomial) without having to know much about the process itself. [324]

With combinatorial design, multiple factors are varied simultaneously in factorial experiments rather than one-factor-at-a-time. Effects and interactions between variables can be partitioned by analysis of variance.

Overall precision is increased because multiple observations are used for estimation. However, estimate errors are all correlated with each other.

Methods

The Diomed laser was used in a similar configuration as previously. 5 mg/ml ICG in water was used as the sensitizing dye. Pork muscle tissue was used as the laser target.

A combinatorial experimental design was used with three input factors — irradiance, exposure time and dye volume used. Each factor was tested at three levels (see Table 4-8) and the entire factorial design was replicated in two blocks. Run order was randomised.

Table 4-8. Low, mid and high levels for irradiance, exposure time and dye volume.

Levels	Irradiance	Exposure time	Dye volume
Low	140 W/cm ²	1 s	1 µl
Mid	190 W/cm ²	5 s	3 µl
High	230 W/cm ²	9 s	5 µl

After laser exposure, photographs were taken of the ablation craters *en face* before the specimens were sectioned through the centre of the crater with a scalpel. Photographs then were taken of the crater cross-sections.

All images were analyzed in ImageJ. Two regions of interest were annotated by hand on each image. The “black” region was marked using the same criteria as used previously. However, regions previously designated as “white” and “coag” previously were combined together and designated “white”.

For the *en face* images, the outline of these regions of interest were traced onto the images, and ellipses were fit onto these outline (see Figure 4-57). For the cross-section images, these two regions also were annotated. Two additional lines — a line aligned with the top of the crater and a bisecting perpendicular line — also were overlaid onto the cross-section images (see Figure 4-58).

Major features representing the tissue response to laser ablation were extracted from the images. For the *en face* data, the areas of the black and white ROIs were assumed to come from circular regions and the “average” radii were calculated. The “average” thickness of the white region was calculated by subtracting the white radius from the black radius.

For the cross-section data, the depth of the black region and the thickness of the white region were measured directly from the images.

The extracted data then was analysed in Minitab.

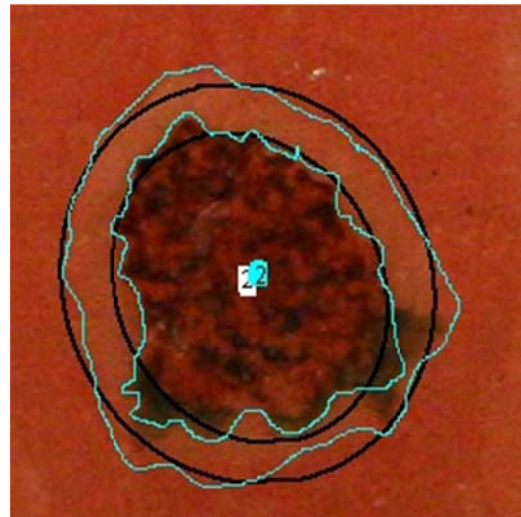


Figure 4-57. An *en face* view of an ablation crater after ROI annotation.

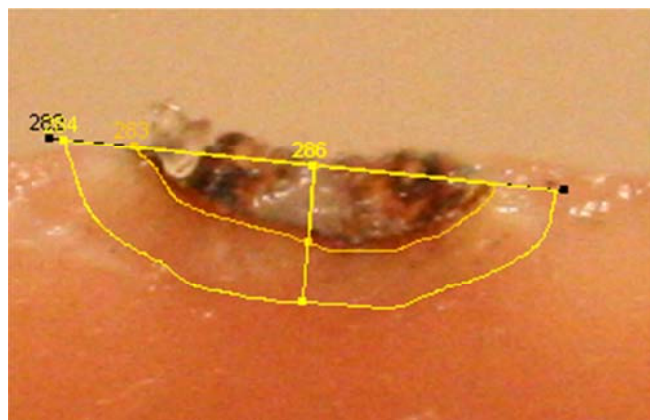


Figure 4-58. A cross-section view of an ablation crater after ROI annotation.

Results

The RSM regression coefficients relating the two measured responses for the *en face* data — (1) the diameter of the black ROI (*en face*) and (2) the thickness of the white ROI (*en face*) — to the three input factors — (1) laser set power, (2) laser exposure time and (3) dye volume — can be found in Table 4-9.

The coefficients for the cross-section data relating the two measured responses — (3) the depth of the black ROI (*x*-section) and (4) the thickness of the white ROI (*x*-section) — to the same three inputs can be found in Table 4-10.

For the thickness of the white ROI for both *en face* and cross-section data, only the linear terms were significant based on ANOVA.

For the black ROI for both *en face* and cross-section data, the linear and square terms were significant, but the interaction terms were not, based on ANOVA.

Table 4-9. RSM regression coefficients for the *en face* data relating the input factors to the output responses.

Thickness of the white ROI (<i>en face</i>)	Diameter of the black ROI (<i>en face</i>)																										
$S = 0.145563$ $\text{PRESS} = 0.617807$ $R-\text{Sq} = 42.40\%$ $R-\text{Sq}(\text{pred}) = 30.03\%$ $R-\text{Sq}(\text{adj}) = 35.21\%$ Estimated Regression Coefficients for EF-W-thick using data in uncoded units <table> <thead> <tr> <th>Term</th> <th>Coef</th> </tr> </thead> <tbody> <tr> <td>Constant</td> <td>0.289256</td> </tr> <tr> <td>Power</td> <td>0.00274219</td> </tr> <tr> <td>Time</td> <td>0.0371504</td> </tr> <tr> <td>Dye</td> <td>0.0292643</td> </tr> </tbody> </table>	Term	Coef	Constant	0.289256	Power	0.00274219	Time	0.0371504	Dye	0.0292643	$S = 0.514188$ $\text{PRESS} = 10.7108$ $R-\text{Sq} = 66.85\%$ $R-\text{Sq}(\text{pred}) = 41.62\%$ $R-\text{Sq}(\text{adj}) = 58.21\%$ Estimated Regression Coefficients for EF-B-dia using data in uncoded units <table> <thead> <tr> <th>Term</th> <th>Coef</th> </tr> </thead> <tbody> <tr> <td>Constant</td> <td>-0.687691</td> </tr> <tr> <td>Power</td> <td>0.208987</td> </tr> <tr> <td>Time</td> <td>0.553146</td> </tr> <tr> <td>Dye</td> <td>0.284268</td> </tr> <tr> <td>Power*Power</td> <td>-0.00504995</td> </tr> <tr> <td>Time*Time</td> <td>-0.0383951</td> </tr> <tr> <td>Dye*Dye</td> <td>-0.0173219</td> </tr> </tbody> </table>	Term	Coef	Constant	-0.687691	Power	0.208987	Time	0.553146	Dye	0.284268	Power*Power	-0.00504995	Time*Time	-0.0383951	Dye*Dye	-0.0173219
Term	Coef																										
Constant	0.289256																										
Power	0.00274219																										
Time	0.0371504																										
Dye	0.0292643																										
Term	Coef																										
Constant	-0.687691																										
Power	0.208987																										
Time	0.553146																										
Dye	0.284268																										
Power*Power	-0.00504995																										
Time*Time	-0.0383951																										
Dye*Dye	-0.0173219																										

Table 4-10. RSM regression coefficients for the cross-section data relating the input factors to the output responses.

Thickness of the white ROI (cross-section)	Depth of the black ROI (cross-section)																										
$S = 0.244147$ $\text{PRESS} = 2.06137$ $R-\text{Sq} = 54.85\%$ $R-\text{Sq}(\text{pred}) = 37.54\%$ $R-\text{Sq}(\text{adj}) = 49.43\%$ Estimated Regression Coefficients for X-W-lg using data in uncoded units <table> <thead> <tr> <th>Term</th> <th>Coef</th> </tr> </thead> <tbody> <tr> <td>Constant</td> <td>0.626722</td> </tr> <tr> <td>Power</td> <td>0.0111633</td> </tr> <tr> <td>Time</td> <td>0.0844521</td> </tr> <tr> <td>Dye</td> <td>0.0161031</td> </tr> </tbody> </table>	Term	Coef	Constant	0.626722	Power	0.0111633	Time	0.0844521	Dye	0.0161031	$S = 0.179180$ $\text{PRESS} = 1.26958$ $R-\text{Sq} = 49.28\%$ $R-\text{Sq}(\text{pred}) = 12.79\%$ $R-\text{Sq}(\text{adj}) = 36.04\%$ Estimated Regression Coefficients for X-B-lg using data in uncoded units <table> <thead> <tr> <th>Term</th> <th>Coef</th> </tr> </thead> <tbody> <tr> <td>Constant</td> <td>0.563564</td> </tr> <tr> <td>Power</td> <td>-0.0223531</td> </tr> <tr> <td>Time</td> <td>-0.0580469</td> </tr> <tr> <td>Dye</td> <td>0.162292</td> </tr> <tr> <td>Power*Power</td> <td>0.000778750</td> </tr> <tr> <td>Time*Time</td> <td>0.00970781</td> </tr> <tr> <td>Dye*Dye</td> <td>-0.0280016</td> </tr> </tbody> </table>	Term	Coef	Constant	0.563564	Power	-0.0223531	Time	-0.0580469	Dye	0.162292	Power*Power	0.000778750	Time*Time	0.00970781	Dye*Dye	-0.0280016
Term	Coef																										
Constant	0.626722																										
Power	0.0111633																										
Time	0.0844521																										
Dye	0.0161031																										
Term	Coef																										
Constant	0.563564																										
Power	-0.0223531																										
Time	-0.0580469																										
Dye	0.162292																										
Power*Power	0.000778750																										
Time*Time	0.00970781																										
Dye*Dye	-0.0280016																										

Plots of the regression models for the *en face* responses can be seen in Figure 4-59, and for the cross-section responses in Figure 4-60.

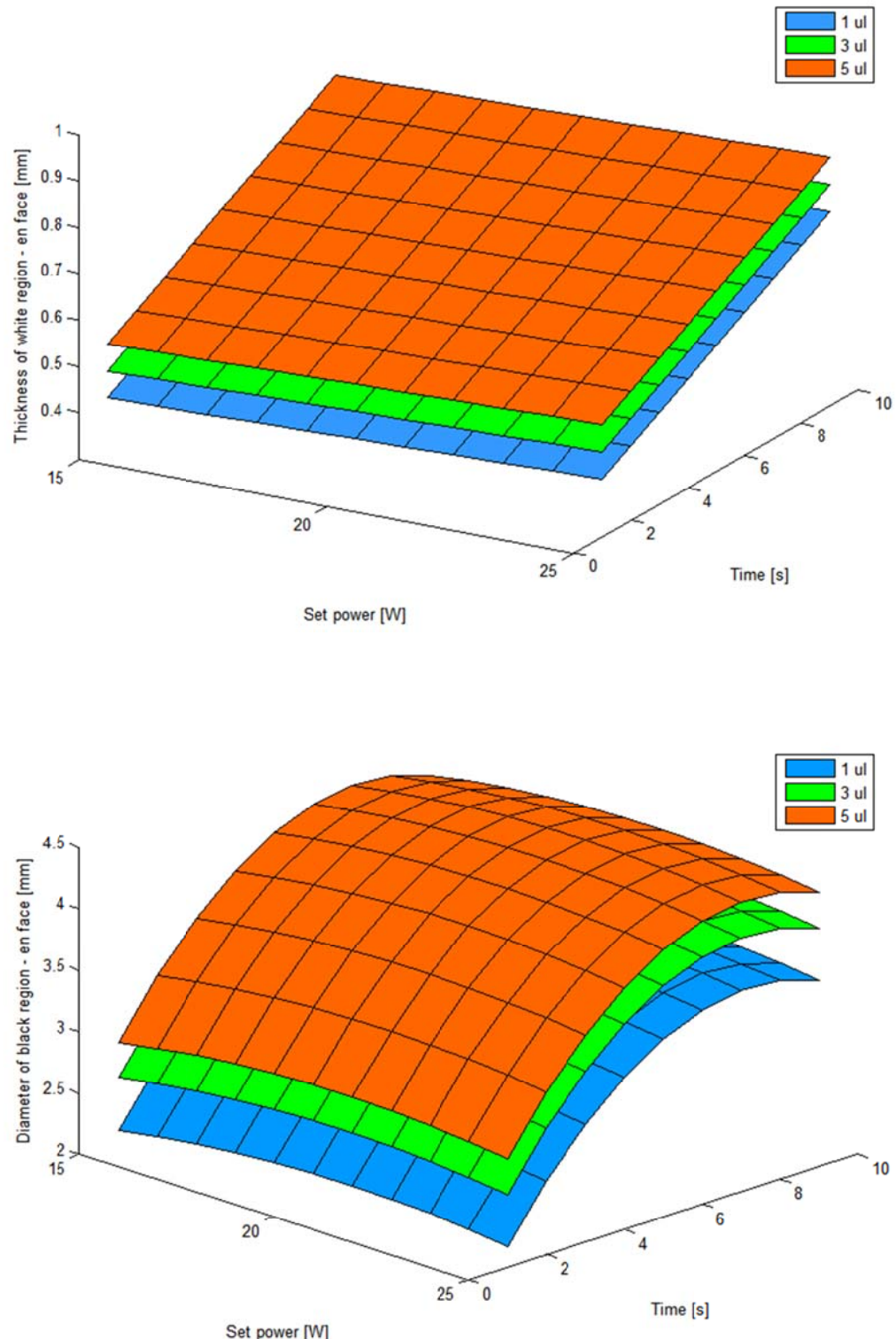


Figure 4-59. RSM regression for the *en face* data. The thickness of the white region (top) and the diameter of the black region (bottom) as reaction to set power, time and dye volume.

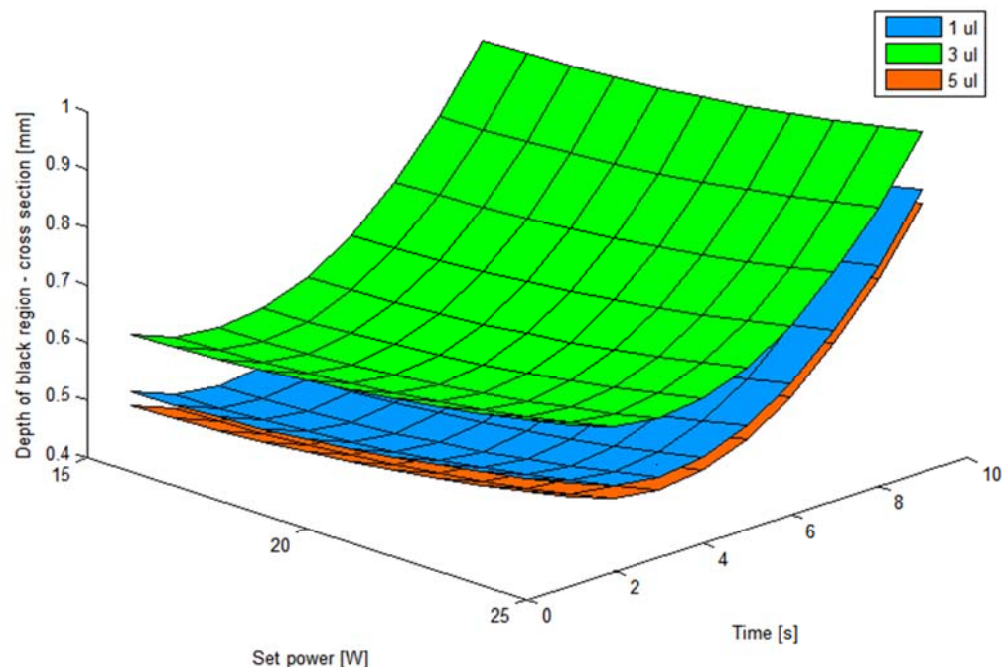
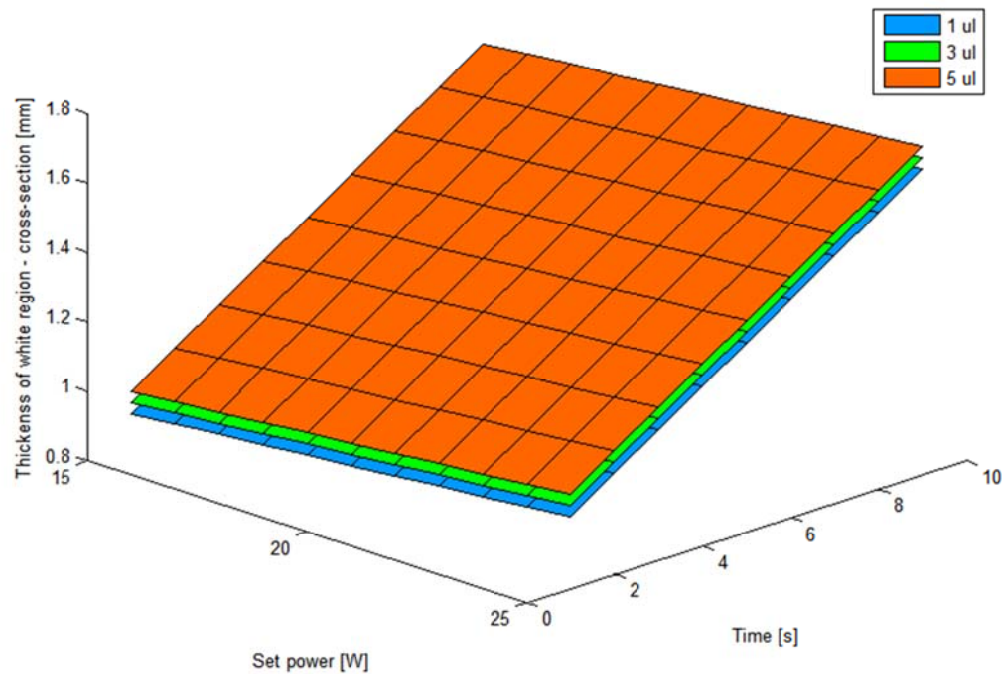


Figure 4-60. RSM regression for the cross-section data. The thickness of the white region (top) and the diameter of the black region (bottom) as reaction to set power, time and dye volume.

Discussion

RSM often is used in industry for modelling manufacturing processes with limited resources when predictive statistical models of systems are required, but an absolute understanding of why inputs cause outputs is not.

The design of the experiments by varying multiple inputs simultaneously in specified combinations allows the use of statistics to de-confound and estimate the contribution of each input factor to each output response. RSM uses higher order interactions between inputs that are insignificant ($p\text{-value} < 0.05$) from analysis of variance to help recover an estimate of error.

The main advantage is that one can get a better estimation of experimental error with fewer runs than one could get in a standard “vary-one-factor-at-a-time” experimental design.

However, experiments on biological materials are notorious for their variability, and this particular set of experiments, which required manual manipulation of tissue after ablation but before photography, may have been more prone to error than previous ones in which photography was concurrent with ablation.

This may explain the relatively poor fit of the statistical models to the noisy data as reflected in the low R-squared values. Still, some insights may be extracted from these data.

For the *en face* experiments, the increase in the diameter of the black region representing the sum of the ablated crater and the carbonised layer increased initially and subsequently levelled off over time, as expected for a beam of finite diameter. This effect was evidenced by the time*time term being the largest of the three squared terms that indicate how much curvature is due to each factor.

The positive correlation between the dye volume used and the diameter of the black region might be due to thicker layers of dye leaving behind larger masses of absorbers on the surface of the tissue once the water of the dye solution has been evaporated.

However, the dye*dye squared term representing curvature in the regression might suggest diminishing returns for additional volumes of dye. This might be due to increased spreading of the dye volume over a larger area resulting in decreasing marginal depth gains.

Power is positively correlated with the diameter of the black region. However, the curvature in the model due to the squared power*power term probably is insignificant as it is numerically small compared with the other coefficients in the model.

The thickness of the coagulation annulus around the black region as indicated by average thickness of the white region appeared to be positively and linearly correlated with exposure time, laser power and dye volume.

Although one would expect the thickness of this region to level off once a steady state had been reached, the overall fit of the model to the data was low, with an adjusted R-squared value of 35%.

For the cross-section experiments, the depth of the black region (ablation crater and carbonisation layer) increased with increased time, as expected. After an initial section with a low growth rate, the ablation rate increased and then stabilised to become almost linear, which fits our understanding of ablation.

In the linear section, the ablation rate was approximately 0.08 mm/s at the high power setting at all three dye volume levels (see Figure 4-61). This is close to the 0.11 mm/s growth rate found from cross-section videography.

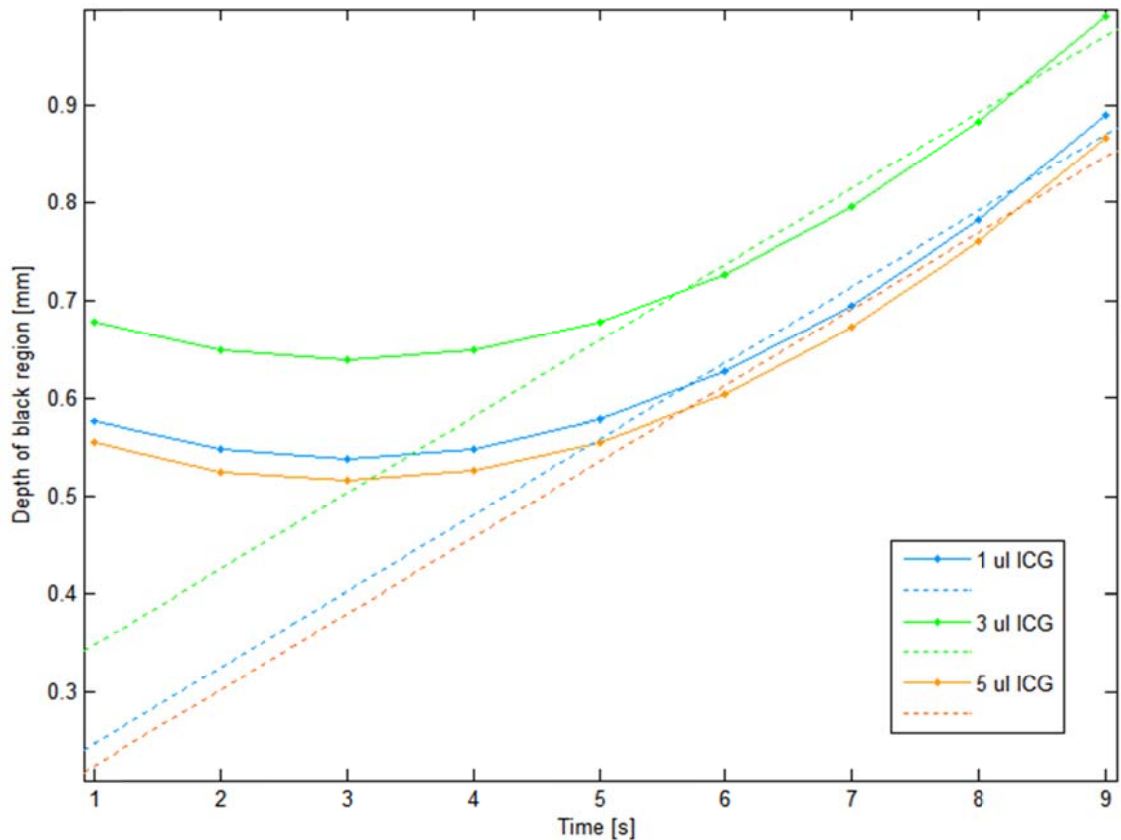


Figure 4-61. Growth of the black region depth at the high power setting.

There was an overall positive correlation between power and the depth of the black region, which also was expected. As previously, the squared power*power term was numerically small compared with the other coefficients and probably is insignificant.

The model for the volume of dye behaved in an unexpected manner. Increase in dye volume from the low to mid level corresponded to increase in the depth of the black region. However, further increase in dye volume from the mid to high levels was correlated to a dramatic decrease in ablation depths to lower than that achieved at the low dye level.

Perhaps with the thickest dye layers, the rapid heating resulted in violent splatter and more displacement of the dye away from the ablation area before much carbonisation of tissue could occur.

However, it also should be considered that the fit between the model and the data for the thickness of the black layer was the second lowest with an adjusted R-squared value of 36%.

The thickness of the white coagulation region in cross section appeared to be positively and linearly correlated with all three factors of exposure time, laser set power and dye volume.

4.12. Modification to the theory for dye-mediated laser ablation

From the various experiments we have conducted, we have seen that dye-mediated laser ablation, in general, appears to be similar to normal laser ablation such as by CO₂ laser, but there appear to be some differences as well. With our experimental observations in mind, we can make modifications to the general theory for laser ablation of tissue to account for the specifics of dye-mediated laser ablation.

The onset and continuation of ICG-mediated laser ablation can be divided into three phases similar to Verdaasdonk et al. These phases are (1) ICG-mediated coagulation, (2) ICG-mediated desiccation and vaporisation, and (3) cyclic carbonisation.

In the first phase, the ICG solution, being a strong absorber at 805 nm, heats up rapidly to 100° C upon irradiation by the laser, and the water starts to boil away. Heat conduction from the boiling dye layer coagulates underlying tissue, resulting in a spreading area of whiteness under the dye layer. Once enough of the liquid dye solution has been boiled away, the underlying coagulated tissue is revealed.

According to Engel et al., molecules of ICG can remain intact at temperatures above the boiling point of water and decompose thermally by two distinct thermally induced processes with threshold temperatures at 180° C and 220° C respectively. [325]

As the water component of the dye solution evaporates, ICG molecules remaining on the coagulated tissue in the second phase of dye-mediated ablation to continue absorbing the laser radiation efficiently, raising the temperature even higher now that the thermal clamp of liquid water has been removed.

The high temperature ICG helps to “seed” areas of carbonisation in the tissue. At some point in the process, the ICG molecules are destroyed or displaced, but its role as light absorber is replaced by the char that is helps to form.

The ablation process then transitions to the third phase in which carbonisation (and its cyclic renewal) acts to mediate laser ablation. The carbonised tissue acts as a good absorber of light,

heats up rapidly and encourages more carbonisation to form until the entire surface of the crater has become carbonised.

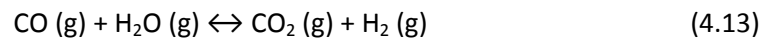
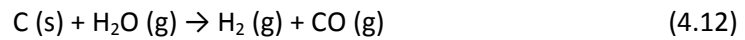
Solid tissue mass is further lost by pyrolysis at temperatures starting above 200° C, releasing volatiles, water vapour and soot particulates and leaving char behind.

Pyrolytic processes can account for up to 70% weight loss for coal, but specifics on the processes for burning tissue are not well known.

The most superficial layers eventually reach temperatures above 500° C at which point the carbon / oxygen combustion process dominates, vaporizing the char into carbon monoxide.



In the presence of water vapour, the gasification of char also can occur, releasing hydrogen gas and carbon monoxide. The carbon monoxide can react further with water vapour to form carbon dioxide and more hydrogen gas.



However, as the gasification processes requires elevated temperatures greater than 700° C (often in excess of 1000° C), it seems more likely that the previously mentioned pyrolytic and combustion processes that occur at lower temperatures can account adequately for complete loss of tissue mass. [326]

Likewise, previously proposed vaporisation of solid carbon at the extremely high 3350° C vaporisation temperature for carbon probably is unnecessary to explain loss of tissue mass. [319]

Because of the high light absorption of char and the correspondingly low penetration depth, the carbonised layer very likely blocks the majority of laser light from penetrating beyond the carbonised region. The fraction of light that does make it past the depth of char does not result in significant heating due to low absorption by uncarbonised or unstained tissue.

Therefore, we assume that light transport is dominated completely by absorption. Although modelling scatter usually is important in tissue optics, we will ignore its effects because the

small amount light that passes through the char or dye will end up in tissue with low absorption that will not result in significant tissue heating in the exposure times used.

Coagulated tissue does result in higher backscatter of light, which would return to the carbonised zone and contribute to heat production. But we argue that this is a small fraction of the heat generated in the carbonised zone which, by neglecting it, would cause a small underestimation of the heat generation and rate of ablation.

Thus we assume that heating below the carbonised layer is due mainly to thermal conduction rather than photothermal heating. Because of this, there is no vacuolated zone of discrete thickness.

The conducted heat from the hot carbonised layer creates zones of desiccated, desiccating and coagulated tissue ahead of the ablation front.

4.13. An Arrhenius-based model for carbonisation

An Arrhenius-based model of molecular kinetics already is used to model coagulation. The damage integral is a standard method for modelling the transition from uncoagulated to coagulated tissue.

But to the author's knowledge, no such model for carbonisation formed during laser ablation has been proposed in the context of tissue ablation in biophotonics.

Therefore, an Arrhenius-based model for carbonisation is proposed in order to adequately model the cyclically renewing carbonisation process that is essential to maintain dye-mediated laser ablation.

4.14. Multiphysics computer model

Comsol Multiphysics (Comsol AB; Stockholm, Sweden) was used to model ICG-mediated laser ablation.

A useful capability of this commercially available finite element program is the ability to model phenomena in multiple physical domains and link them to model interactions between these domains. Simulations can be run and the time evolution of the partial differential equations representing these physics can be solved in a relatively straightforward manner.

An FEM model was created in Comsol to simulate ICG-mediated laser ablation. The model consisted of three sub-models — the light transport model, the heat transfer model and the tissue model (see Figure 4-62).

In overview, the light transport model calculated the light distribution within the tissue after the laser light enters the tissue volume. Absorbed light energy from the light transport model served as the heat source for the heat transfer model, which then calculated how the heat was conducted through the tissue mass. Calculated temperatures and time were used by the tissue model to determine the tissue state, which updated state-dependent optical and thermal coefficients in the model.

This sequence of calculations was run for each time step in the simulation until the modelled time interval was completed.

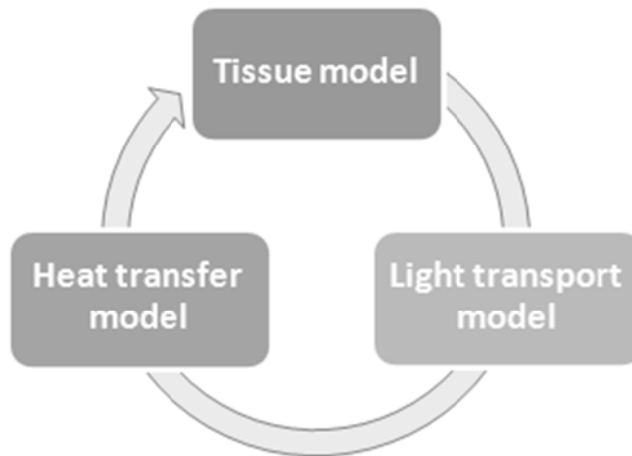


Figure 4-62. The FEM model consists of three sub-models that are linked to each other — the light transport model, the heat transfer model, and the tissue model.

4.14.1. Light transport model

Light transport in tissue was modelled based on the Lambert-Bouguer Law. Using this principle, we model light transport as a simple exponential decay with the rate of decay dependent on only the absorption coefficient.

The spatial heat source from absorbed laser light can be found by multiplying the local irradiance by the local absorption coefficient, assuming all absorbed light energy is converted into heat.

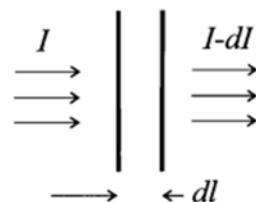
This method to determine the light distribution within tissue was chosen because dye-mediated laser ablation is absorption dominated (absorption is much greater than scatter), and because the simplicity of this model allowed for fast numeric integration of the solution using FEM. Descriptions of other standard methods for modelling light transport are provided in “Appendix B: Alternative light transport models.”

This simplest model of light transport was used because the absorption coefficients are high — the coefficients for 4 mg/ml ICG in water and ICG in albumin are 197 cm^{-1} and 854 cm^{-1} , respectively. This corresponds to penetration depths of $50 \mu\text{m}$ and $12 \mu\text{m}$.

The thickness of the dye layer was estimated to be about $86 \mu\text{m}$ thick when $1 \mu\text{l}$ of ICG was applied to the surface of tissue — this is thicker than the light penetration depth in ICG. In the experiments described in this thesis, typically $5 \mu\text{l}$ volumes of ICG were applied which would correspond to even thicker dye layers.

Light that did penetrate the dye layer would encounter a volume of tissue with relatively very low absorption at 805 nm. This huge difference in absorption between tissue and ICG is the basis for selective ablation in the first place.

The argument therefore is that almost all of the light absorption will occur in the dye and carbon layers, and any light that made it through would not raise the temperature of unstained tissue much (let alone to ablation temperatures) in the few seconds that dye-mediated laser ablation would occur.



The Lambert-Bouguer Law states that light falloff in a purely absorbing substance is defined by the following:

$$-\frac{dI}{I} = \mu_a \delta l \quad (4.14)$$

Where I is the light intensity, μ_a is the absorption coefficient and δl is the layer thickness.

Equation (4.14) essentially states that successive layers of material δl absorb the same fraction of light dI/l dependent on the absorption coefficient μ_a .

Integrating in one dimension in y , the solution to (4.14) with the boundary condition that $I=I_0$ at $y=0$ is a decaying exponential in y :

$$I = I_0 e^{-\mu_a y} \quad (4.15)$$

4.14.2. Heat diffusion model

The standard model for the diffusion of heat in tissue is Penne's bioheat equation [327]:

$$\rho C \frac{\partial T}{\partial t} + \nabla \cdot (-k \nabla T) = \rho_b C_b \omega_b (T_b - T) + Q_{met} + Q_{ext} \quad (4.16)$$

Where ρ is the tissue density, C is the specific heat of tissue, T is temperature of the tissue, k is the tissue thermal conductivity, ρ_b is the density of blood, C_b is the specific heat of blood, ω_b is the blood perfusion rate, T_b is the arterial blood temperature, Q_{met} is the metabolic heat source and Q_{ext} is the spatial heat source.

This equation represents the conservation of energy for each infinitesimal volume of tissue. It states that the sum of the heat energy used to raise its temperature and the energy diffusing out of the volume is balanced by the sum of the energy lost due to cooling by blood perfusion, the heat generated from metabolic processes and extrinsic spatial heat sources such as laser heating.

The spatial heat source Q_{ext} is calculated from the light transport model as a product of the local irradiance and the local absorption coefficient.

Blood perfusion could have an effect on ablation as heat losses to circulating blood would result in a model which did not account for this heat sink to overestimate local temperatures.

However, because *ex vivo* porcine tissue was used in the experimental portion of the thesis, there was no blood perfusion or metabolic heat source, and corresponding terms in the bioheat equation were set to zero for this model.

If necessary, these terms could be reactivated in the bioheat equation.

4.14.3. Tissue model

While the models of light transport and heat diffusion in tissue are fairly standard, the tissue state and temperature dependence of optical and thermal coefficients can make the overall problem highly complicated and extremely non-linear.

The overall purpose of the tissue model is to track the journey as tissue transforms from an undamaged state through coagulated, desiccated, carbonised and finally vaporised states and provide the light transport and heat diffusion portions of the simulation with appropriate optical and thermal coefficients depending on the tissue state and temperature.

While the physics of the simulation are, by definition, relatively straightforward as one tries to describe complicated situations with relatively simple constitutive equations, the proverbial devil is in the details as relevant and accurate physical coefficients are notoriously hard to find.

Coagulation

Tissue coagulation is associated with denaturisation of proteins by exposure to elevated temperatures (and other external stresses) that lead to disruption of cell activity and potentially cell death. It often is characterised by optical whitening of the tissue as the denatured proteins increase in optical scatter when compared with the uncoagulated state.

Henriques in 1948 described a method to predict irreversible tissue injury that took into account temperature and time exposure. [328] Modelling thermal coagulation of tissue as a first-order chemical kinetic process, he proposed the Arrhenius damage integral, Ω , as a measure of the degree of tissue damage caused by elevated temperatures:

$$\Omega = \ln\left(\frac{c_x(0)}{c_x(t)}\right) = \int_0^t Ae^{-\left(\frac{\Delta E}{RT}\right)} dt' \quad (4.17)$$

Where $c_x(0)$ and $c_x(t)$ are concentrations of undamaged molecules initially and at time t , A is the pre-exponential factor, ΔE is the activation energy, R is the universal gas constant and T is the temperature.

In the model, $A = 3.1e98 s^{-1}$ and $\Delta E = 6.3e5 J/mol$ were used as the Arrhenius coefficients. These are the values derived by Henriques for porcine basal epidermis — unfortunately, coefficients for coagulation for porcine skeletal muscle could not be found.

The surviving fraction of undamaged molecules, $F_{uncoagulated}$, is

$$F_{uncoagulated} = \frac{c_x(t)}{c_x(0)} = e^{-\Omega} \quad (4.18)$$

Henriques chose the endpoint for complete tissue necrosis of thermally damaged pig basal epidermis to be $\Omega=1$, which corresponds to $1/e$, or 37% surviving fraction of undenatured molecules.

Coagulation primarily affects optical coefficients, causing changes in the absorption and scattering coefficients and the anisotropy factor. In this model, only the change in the absorption coefficient is considered.

The absorption coefficient is modelled as a linear combination of the uncoagulated and coagulated coefficients multiplied by the corresponding fraction from the damage integral:

$$\mu_a = F_{uncoagulated} \mu_a^{uncoagulated} + F_{coagulated} \mu_a^{coagulated} \quad (4.19)$$

$$F_{uncoagulated} + F_{coagulated} = 1 \quad (4.20)$$

Equation (4.20) reflects the fact that denaturisation of proteins is a binary state. The fractions of uncoagulated and coagulated molecules must sum to 100 percent.

Desiccation

Tissue that has been raised to the 100° C boiling point of water cannot increase in temperature until all the liquid water locally has been evaporated. This thermal clamping effect is quite large because water has a large heat of vaporisation (2257 kJ/kg) due to hydrogen bonding between the polar water molecules.

This latent heat is modelled as a modified heat capacity that incorporates the heat of vaporisation as a Dirac delta pulse that increases the heat capacity at 100° C.

Because numeric models typically do not like discontinuous functions, the actual modified heat capacity is modelled as a Gaussian pulse, D , to approximate the Dirac delta function and the enthalpy change.

$$D = \frac{1}{\sqrt{\pi dT^2}} \exp\left(-\frac{(T - T_{boil})^2}{dT^2}\right) \quad (4.21)$$

$$C_p^{enthalpy} = DL \quad (4.22)$$

T is the temperature, T_{boil} is the boiling point of water, dT is the width of the Gaussian pulse and L is the heat of vaporisation.

The step change in thermal properties before and after the phase change is modelled using the smooth Heaviside step function, $H_{desiccation}$, centred on $T = 100^\circ \text{C}$.

$$C_p^{step} = (1 - H_{desiccation})C_p^{liquid} + H_{desiccation}C_p^{gas} \quad (4.23)$$

The complete modified heat capacity thus is

$$C_p = C_p^{step} + C_p^{enthalpy} \quad (4.24)$$

The phase change of water to steam also is associated with a step change in thermal conductivity, k , and density, ρ , and these are modelled in a similar manner using the smooth Heaviside function.

$$k = (1 - H_{desiccation})k^{liquid} + H_{desiccation}k^{gas} \quad (4.25)$$

$$\rho = (1 - H_{desiccation})\rho^{liquid} + H_{desiccation}\rho^{gas} \quad (4.26)$$

In this model, we do not consider tissue desiccation to affect the optical properties in order to keep the model relatively simple. In reality, optical properties probably do change in reflectance and transmittance due to changes in numeric index.

Carbonisation

Not much could be found in the literature on modelling the chemistry of carbonising animal tissue (although there are many clinical reports on skin burns and studies of the subsequent healing response).

However, there is quite a lot of research on the pyrolysis and combustion of wood and coal materials, probably due to their importance to the industrial chemical and energy realms.

Therefore, tissue carbonisation is modelled as the pyrolysis of wet wood to form char. Thurner and Mann provide the kinetic parameters for the pyrolytic reaction for wood — $A = 2.47\text{e}6 \text{ s}^{-1}$ and $E_a = 106.5 \text{ kJ/mol}$. [329]

According to Shen et al., pyrolysis, or the endothermic breakdown ($\Delta H = 420 \text{ kJ/kg}$) of organic matter into char, volatile gasses and water vapour, can start to occur slowly after the desiccation of the material at 100°C . From $240\text{-}320^\circ \text{C}$, primarily CO_2 and water vapour are

produced. From 320-450° C, the material pyrolyses rapidly and releases increased amounts of flammable volatiles. [330]

Pyrolysis can continue to happen at higher temperatures, but from 500-900° C, the carbon – oxygen combustion reaction dominates. McKenzie chose 500° C as the combustion point, and we do so as well.

Similar to coagulation, the fraction of uncarbonised tissue can be obtained from the Arrhenius equation.

$$F_{uncarbonised} = \frac{c_x(t)}{c_x(0)} = e^{-\Omega} \quad (4.27)$$

As before, the dynamic material properties can be represented as a linear combination of the carbonised and uncarbonised properties.

$$\begin{aligned} coeff_i &= F_{unccarbonised} coeff_i^{uncarbonised} \\ &\quad + F_{carbonised} coeff_i^{carbonised} \end{aligned} \quad (4.28)$$

$$F_{uncarbonised} + F_{carbonised} = 1 \quad (4.29)$$

With an equation in *coeff*, representing the dynamic behaviour of each thermal and optical property.

For the ICG dye layer, the exact reactions and sequence of decomposition are not known, nor are the absorption coefficients of the intermediaries. But because ICG is an organic dye, we assume that it and its decomposition by-products carbonise in the same manner as tissue.

Therefore, $F_{uncarbonised}$ and $F_{carbonised}$ also can be used to model the dynamic absorption coefficient of ICG as a linear combination of the absorption coefficient for ICG and the coefficient for char.

Vaporisation

We model 500° C as an endpoint temperature at which all remaining char is vaporised by combustion. Char reaching this temperature is considered to be irreversibly vaporised, and the tissue model adopts the optical and thermal properties of air saturated with steam at atmospheric pressure. This was chosen because the air in the crater must also serve as the migration path for water vapour from ablating tissue to vent to atmosphere.

The vaporisation of tissue was modelled similar to tissue desiccation using a smooth Heaviside step function centred at a temperature of 500° C.

$$\begin{aligned}coeff_i = & (1 - H_{vapourisation}) coeff_i^{unvapourised} \\& + H_{vapourisation} coeff_i^{vapourised}\end{aligned}\quad (4.30)$$

Where an equation for $coeff_i$ corresponds to each material property.

Summary of changes in coefficients

The thermal and optical coefficients used in the model are tabulated in

Table 4-11 and Table 4-12, respectively. The methods for modelling changes between material states described above are summarised in

Table 4-13.

Table 4-11. Summary of changes in thermal coefficients.

THERMAL	Undamaged (C1)	Desiccated @ 100° C (C2)	Carbonised (C3)	Vaporised @ 500° C
Specific heat, Cp [J/(kg K)]	3448 avg. pig skeletal muscle (Duck [276])	1696 pig skin (Knox et al. [333])	1390 char (Shen et al. [330])	2135 steam (NIST)
Thermal conductivity, k [W/(m K)]	0.49 avg. pig skeletal muscle (Duck [276])	0.084 biological fluids (Spells [335])	0.105 char (Shen et al. [330])	0.07 steam (NIST)
Density, ρ [kg/m ³]	1041 human skeletal muscle (Duck [276])	270 25.9% not water (Duck [276])	25 10% of charcoal (McKenzie [306])	0.3 steam (NIST)

Table 4-12. Summary of changes in optical coefficients.

OPTICAL	Undamaged (C1)	Coagulated (C2)	Carbonised (C3)	Vaporised @ 500° C
Absorption, μ _a [1/cm]	0.30 @ 800 nm pig skeletal muscle (Birth et al. [335])	0.63 (best guess) rat prostate (Skinner et al. [331])	1380 @ 800 nm 10% compact soot (Koylu, Faeth [336])	0.0195 @ 806 nm steam (OMLC)
ICG absorption, μ _a [1/cm]	854 @ 805 nm (measured)	854 @ 805 nm (measured)	1380 @ 800 nm 10% compact soot (Koylu, Faeth [336])	0.0195 @ 806 nm steam (OMLC)

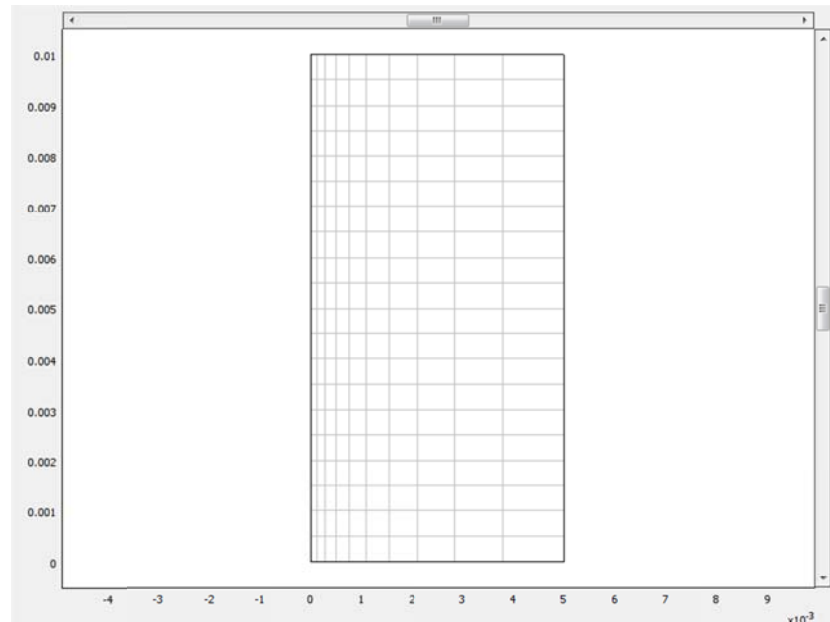
Table 4-13. Summary of how state changes are modelled.

State transition		Model
undamaged	→	coagulated
		Arrhenius damage integral drives property changes.
coagulated	→	desiccated
		Smooth Heaviside function for property changes. Impulse increase in heat capacity at 100° C for vaporisation.
desiccated	→	carbonised
		Arrhenius integral for carbonisation drives property changes.
carbonised	→	vaporised
		Smooth Heaviside function for property changes. Impulse decrease in heat capacity at 500° C from combustion.

4.14.4. Model geometry

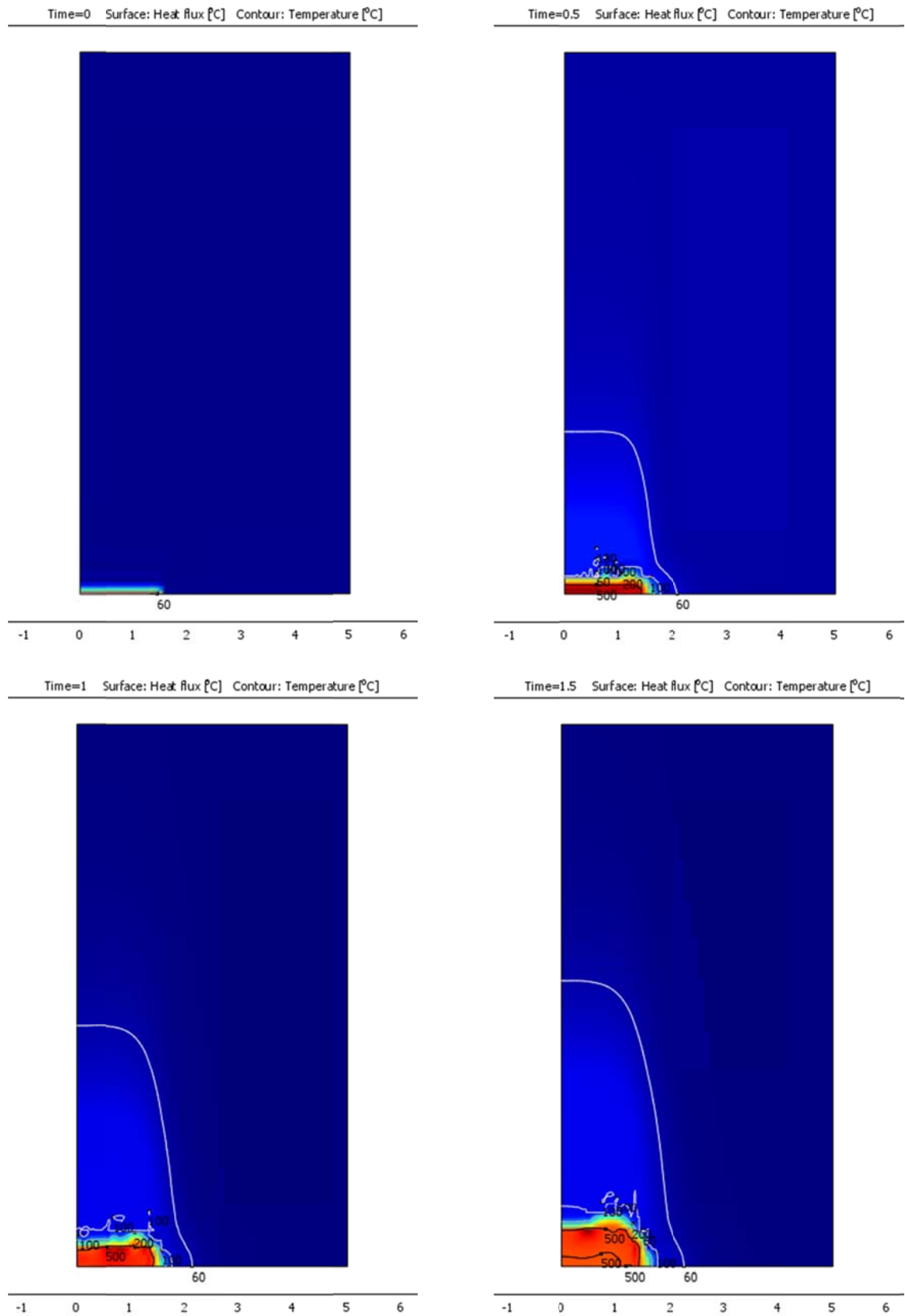
The tissue was modelled as a 2D axis-symmetric geometry with the laser beam centred on the axis of symmetry at $r=0$. The modelled domain was a cylinder of tissue that was irradiated by a laser beam with a finite radius and flat profile (see Figure 4-63).

The 2D model was solved as a transient problem with simulation time from 0 to 3 s.

**Figure 4-63.** Model geometry and mesh.

4.14.5. Results

The results from the FEM model can be seen in Figure 4-64. The growth of the *en face* diameter at $z=0$ is summarised in Figure 4-64.



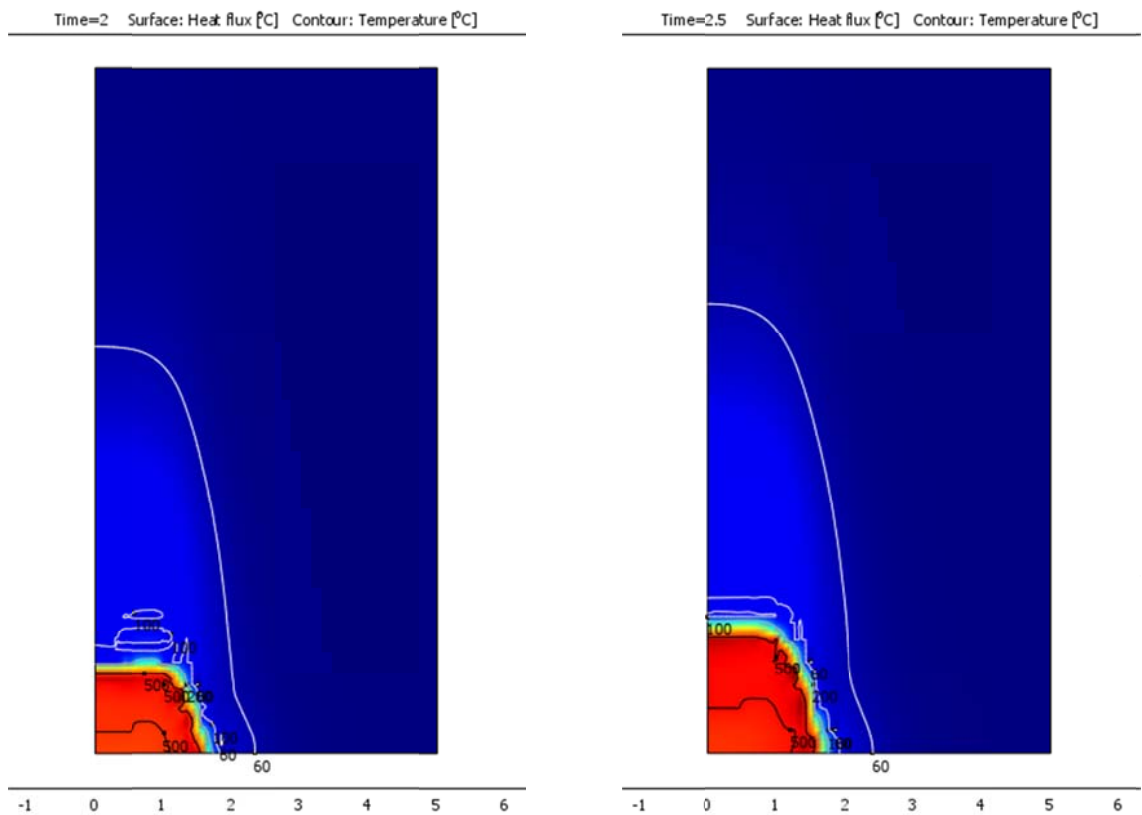


Figure 4-64. Results of FEM model over 2.5 seconds of simulation time.

The growth of the radius of the ablation crater and the thickness of the damage zones in the en-face view at $z=0$ are summarised in Figure 4-65.

The depth of the crater and the thickness of the damage zones in the cross-sectional view at $r=0$ are summarised in Figure 4-66.

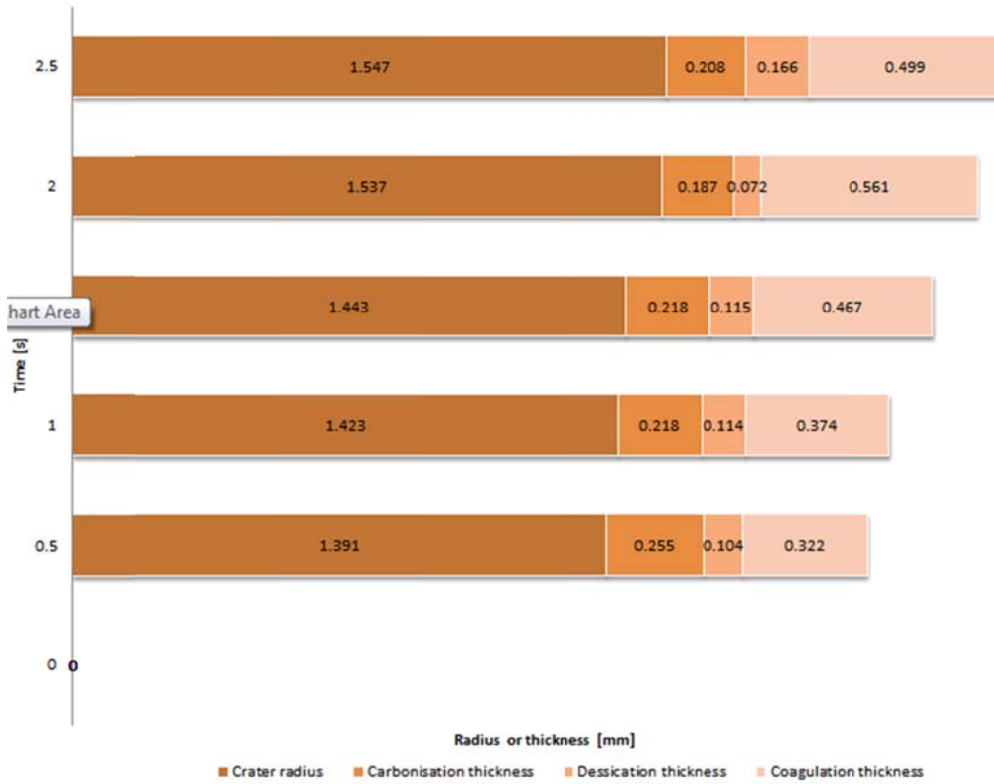


Figure 4-65. En face results. Growth of the crater radius and thicknesses of damage zones at $z=0$.

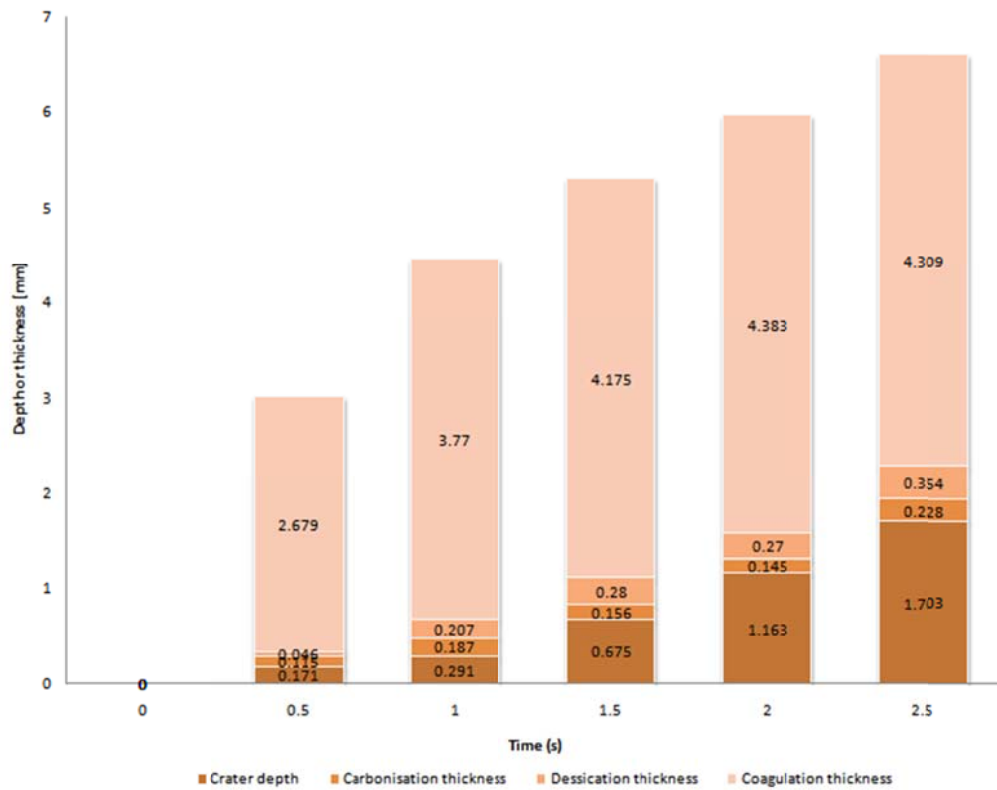


Figure 4-66. Cross-section results. Growth of the crater depth and thicknesses of damage zones at $r=0$.

4.14.6. Discussion

The ablation rate from the computer model is about 0.95 mm/s, which is about twelve times greater than the rate obtained from the RSM model — 0.08 mm/s. This is not a very good match between model and experiment and probably was due to the RSM model being a rather poor fit for the noisy data in the RSM experiments.

However, when one considers the half slab ablation experiments with the high speed camera in which the ablation rate was 0.11 mm/s, the mismatch between model and data is reduced to about 8x. Since probably half of the thermal energy was lost through the glass plate, with the full slab, the ablation rate potentially could have been twice as fast, which would make the overestimation of the ablation speed by the computer model to be only a factor of four.

Also, as with any computational model, the results are only as good as the model coefficients used.

As was stated in the model formulation, the carbonisation of tissue was modelled as the pyrolysis of wood producing char because kinetic models of tissue carbonisation could not be found.

It is entirely possible that wood carbonises slower than animal tissues do, and that the Arrhenius coefficients result in slower carbonisation in the model than in reality.

A subtle hint that this might be the case can be seen in the extended “plume” of coagulated tissue “above” the ablation crater in the model results in Figure 4-46. The depth of coagulation is much larger than was observed in our experimentation.

This might suggest direct heating of this tissue by laser light penetrating the carbonised layer due to a low mass fraction of carbonised tissue versus desiccated tissue. This might be the case if the carbonisation process modelled was slower than the actual reactions in tissue.

Guided by this hypothesis, the rate of the carbonisation reaction in the model was amplified arbitrarily by increasing the frequency factor, A, by 100 fold. The simulation was run for 1 s and the results were plotted in Figure 4-67.

The top image represents the spatial distribution of absorption in the model, the middle image is the light irradiance within the tissue, and the bottom image is the spatial heating generated by multiplying the local irradiance by the local absorption.

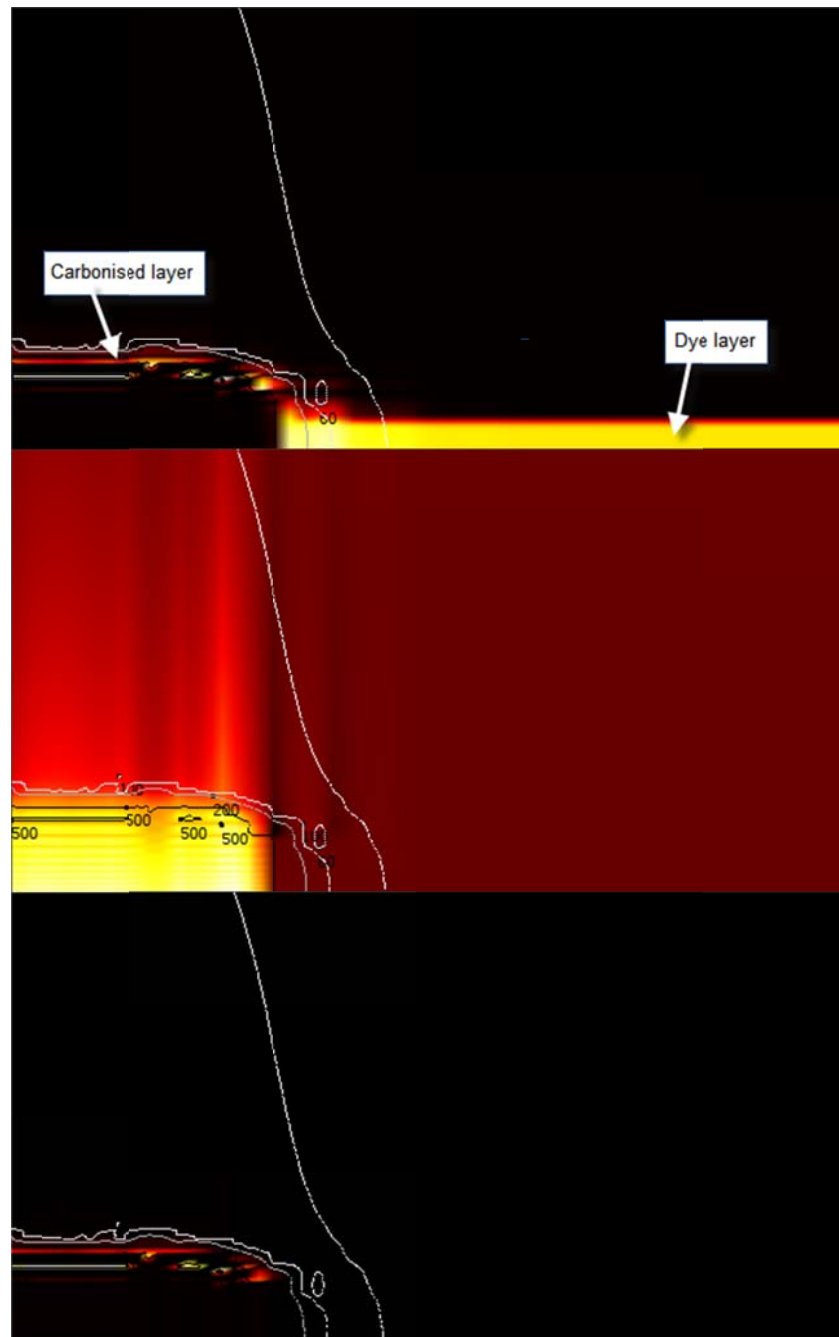


Figure 4-67. Absorption (top), irradiance (middle) and the spatial heat source (bottom) one second into the ablation simulation after replacing the frequency factor in the Arrhenius equation for carbonisation with a higher coefficient.

Indeed, with the increase in the rate of the carbonisation reaction in the model, the light able to penetrate the carbonised layer decreases dramatically and the spatial heating is confined primarily to the carbonised layer.

This type of iterative investigation might be useful for finding appropriate kinetic rate coefficients that improve the accuracy and predictive power of the model.

4.15. Dye-mediated ablation compared with existing techniques

From experimentation and computer model we have estimated the coagulation damage for ICG-mediated laser ablation. How does this compare with existing cutting methods?

Devices for cutting tissue usually trade off between providing acute haemostasis during surgery to control bleeding and longer term healing of the incision wound.

Studies in the literature comparing cutting technologies typically quantify haemostatic capability using a subjective measure, and characterise tissue damage in terms of the margin of coagulative necrosis during the healing response.

However, there does not seem to be standard scientific protocols for producing these comparisons, for example, by taking into account the power being put into the tissue and standardising on a specific tissue type.

Often, the comparisons are made using the “normal operating settings” for each instrument to make incisions on various anatomies. As such, many of these comparisons probably are qualitative and anecdotal, at best.

At one end of the continuum is the standard scalpel blade which provides no haemostatic capability but results in the fastest and most cosmetically appealing healing.

At the other end, it appears that the various laser modalities and electrosurgery compete in providing excellent haemostatic ability but also for causing more coagulation necrosis.

Because of high absorption by tissue, CO₂ laser does not provide much haemostatic capability and in theory should not cause much heating beneath a very thin superficial layer. However, some studies have found CO₂ laser ablation to cause equivalent or more damage than electrosurgery. [332] [333]

Ultrasonic knives have been praised widely by laparoscopic surgeons for their capability to cut and coagulate tissue, in theory, without generating excessive heat. This was supported by von Bloomberg et al. [334] However, Morosolli et al. found it to cause similar levels of tissue damage as electrosurgery and CO₂ laser. [332]

A table of damage caused by various cutting instruments can be found in Table 4-14.

Table 4-14. Depth of coagulation necrosis from various cutting instruments using “normal operating settings” for different surgical procedures. Various power settings used on different tissue types. Data provided for qualitative comparison only.

Modality	Depth of coagulation necrosis	Source
Scalpel	< 0.01 mm	Molgat et al. [333]
Ultrasonic knife	0.05 mm	von Blomberg et al. [334]
CO2 laser (ideal)	0.07 mm	Molgat et al. [333]
Ultrasonic knife	0.30 – 0.38 mm	Morosolli et al. [332]
Monopolar electrosurgery	0.30 – 0.38 mm	Morosolli et al. [332]
CO2 laser	0.30 – 0.38 mm	Morosolli et al. [332]
Monopolar electrosurgery	0.35 mm	von Blomberg et al. [334]
Hot scalpel	0.34 mm	Molgat et al. [333]
Bipolar electrosurgery	1 mm	Botto et al. [243]
Monopolar electrosurgery	1.01 mm	Molgat et al. [333]
ICG-MEDIATED LASER	<u>1.07 – 1.75 mm</u>	From experiments in this thesis
CO2 laser	1.88 mm	Molgat et al. [333]
Ho:YAG laser	3-4 mm	Botto et al. [243]

From the statistical model, at 25 W set power and 5 μ l ICG, dye mediated laser ablation would cause a coagulation depth beneath the ablation crater of 1.07 – 1.75 mm with exposure times of 1 – 9 s.

This is comparable to reported damage caused by electrosurgery and ablation by other types of lasers.

With refinement of the technique from experimentation and further development of the computer model, perhaps the depth of collateral damage can be reduced further.

4.16. Other factors for consideration

Two areas of research for dye-mediated laser ablation that were considered but not explored in detail due to time and resource constraints were (1) methods for dye application and (2) methods for dye removal. Thoughts on both of these topics are presented next.

4.16.1. Methods for dye application

One significant hurdle to overcome in order for dye-mediated laser ablation to be feasible in a clinical setting is engineering a method for fast, effective and reliable application of the dye to

the tissue. A number of concepts for doing so are discussed. A few qualitative experiments were performed to provide anecdotal evidence for discussion purposes.

On droplets and marker pens

For the majority of the experiments in this thesis, the ICG dye was applied topically to the surface of the tissue by depositing droplets using a pipette or a syringe. This worked adequately in the controlled environment of the laboratory benchtop, although overall spatial control left a lot to be desired.

The biggest problem with this dye application method came from depositing the volumes of dye as one large droplet. Although these droplets would stabilize into a thin pool on the surface of the tissue, occasionally the droplet would roll over the tissue surface and settle in unwanted locations.

Also, the fissures and cracks in the tissue surface had the tendency to draw the dye into them, again resulting in poor control over where the dye went (see Figure 4-68).



Figure 4-68. Droplets of ICG applied to the surface of tissue tends to seep into and follow fissures and cracks.

And it is not hard to imagine that in the wet, chaotic environment of the endoscopic surgical field, large dye droplets ejected onto tissue might be hard to control indeed.

As a solution, the application of smaller volumes of liquid might enhance the spatial controllability of marking the tissue.

This might be achieved passively in a manner similar to how a felt-tip marker or a ball-point pen functions to smear small volumes of dye onto the tissue surface.

Alternatively, perhaps the dye could be atomised into a mist and deposited onto the tissue as one would cover a surface with spray paint.

A high technology alternative would involve using piezo-electric or thermal inkjet heads to eject the dye out of miniature nozzles directly onto tissue.

While the sky is the limit when considering complex solutions, simple and cheap usually are good guidelines for schemes to be used clinically, as the domain of medical practice usually is subjected disproportionately to Sod's Law.

Perhaps increasing the viscosity and wettability of the dye could improve placement control when used with an endoscopic syringe. Adhesives might be mixed with the dye, for example, although care would have to be taken to prevent premature curing, and to ensure that the mixture and ablated by-products are biocompatible.

Ad hoc mixtures of ICG powder with cyanoacrylate glue adhered well to tissue and were ablatable by the Diomed laser. However, the fumes released were not pleasant to inhale.

On injections and tattoos

Injection of a relatively large volume of ICG was used in a few experiments in this thesis to good effect for dye-mediated laser ablation. Other research groups also have taken this approach applying ICG as injected dye physically is well contained by surrounding tissues (see Figure 4-69).

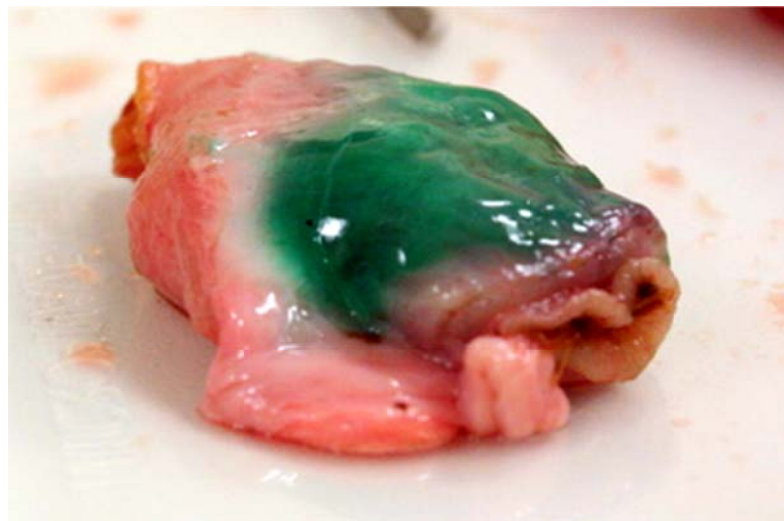


Figure 4-69. ICG injected into tissue is contained within tissue planes.

As with superficial application of ICG, perhaps injection of smaller volumes of dye might improve the spatial controllability of the technique. Vibrating tattoo needles are used by street artists to inject small volumes of tattoo pigments into the skin for decoration.

Perhaps a similar mechanism could be miniaturized for use endoscopically to apply sensitizing dyes to target tissue.

On chalk-lines and stitches

In the world of home improvement and construction, the chalk-line tool often is used to mark long, straight lines quickly and efficiently. The marking device typically consists of a spool of string wholly contained within a box full of powdered chalk.

The string is unwound and stretched over the line to be marked. Then by drawing the middle of the string in a direction normal to the surface and quickly releasing it, the snap of the string deposits a temporary line of chalk mirroring the line of the string.

A similar concept was explored using a cotton sewing thread soaked in ICG solution and dragging it across tissue. This method proved to be rather effective for drawing straight lines on tissue that could be ablated with the Diomed laser (see Figure 4-70).

One possible embodiment of this thread dragging concept which could be made to be compatible with the working channel of an endoscope is shown in Figure 4-71. The conceptual device would resemble large endoscopic forceps with hollow jaws designed not for gripping tissue but to deploy and guide dye-saturated thread. When the thread is fed through the device, a line of dye the length of the open device jaws is deposited on to the tissue surface.

A second concept using a curved needle to implant into tissue the ICG-soaked thread used previously also was attempted. Ablation with the Diomed laser was successful at the edges of implantation where the soaked thread was exposed. Tissue surrounding the implanted thread was coagulated, but no ablation was found after examining the tissue in cross section.

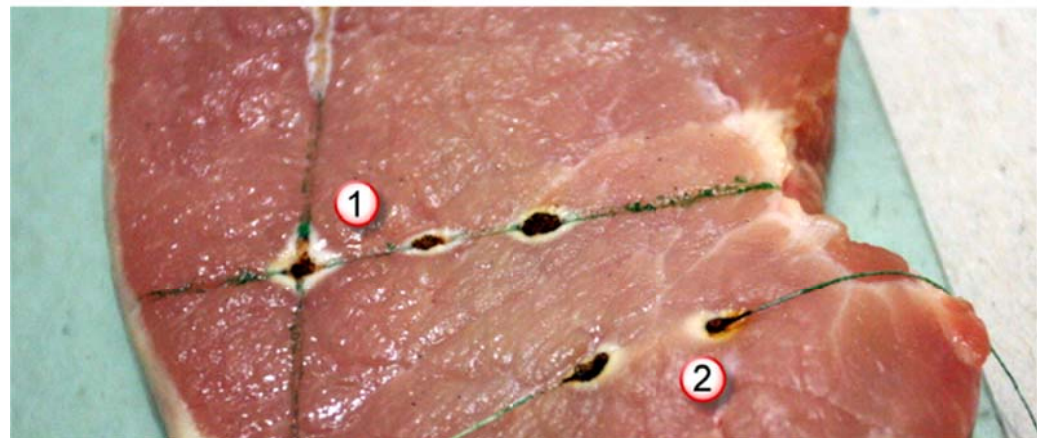


Figure 4-70. ICG lines formed by dragging soaked thread across the tissue surface (1).
ICG soaked thread implanted into tissue using a curved needle (2).

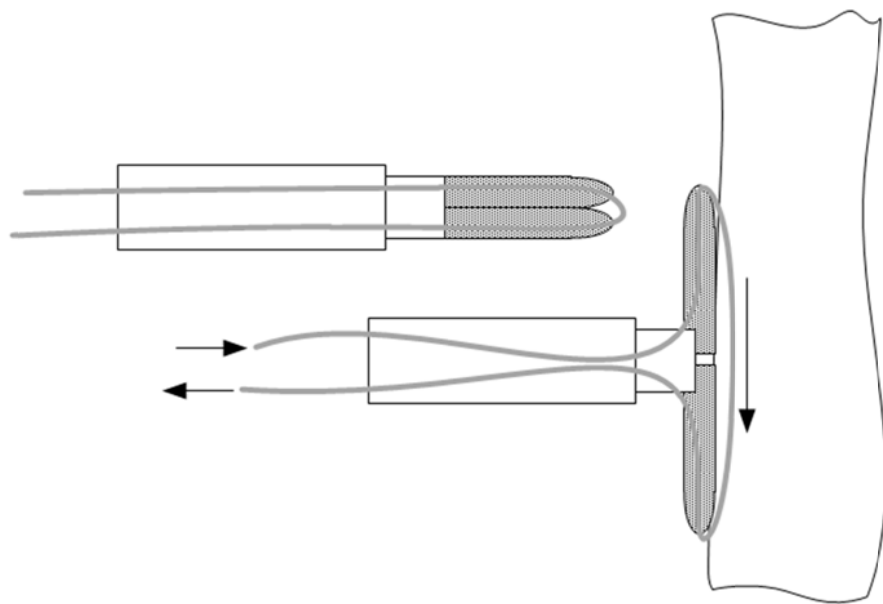


Figure 4-71. A concept “chalk”-line dye applicator. A forceps-like endoscopic device is deployed by opening the jaws to a 180° angle and placing the device in contact with tissue. Dye-saturated thread then is dragged across the tissue, guided by the jaw structure of the open forceps-like device.

On stamps and stencils

A number of different stamps and stencils made from various materials were used in attempts to improve control over where the dye was placed. In general, more problems were encountered than benefits provided by using these implements.

The main problem with the stamps was that the dye had a tendency to form droplets on the rubber stamp material rather than coat it evenly. Upon contact with the tissue, not much of the dye was transferred to the tissue.

ICG powder unmixed with water was much better at being picked up by the rubber stamp material and subsequently transferred to the tissue. However, as ICG is very expensive, using the undiluted powder form may prove to be too costly for most procedures. Perhaps some other method can be found to improve the stamping process.

With the stencils, the primary difficulty encountered was that the liquid dye had the tendency to bleed into the smallest of gaps between the stencil and the tissue.

Possible solutions included waiting for the ICG pool to dry or wiping off excess dye before removing the stencil mask. These techniques did work when tried, however drying times tended to be long, and when wiping off excess dye, typically more dye was removed than remained on the surface of the tissue.

Perhaps the stencil could be used with an atomizer that dispensed dye in a mist of tiny droplets? Maybe the ICG mixture could be made more viscous or more adherent to tissue to prevent it from being drawn into gaps?

Improvements to the ICG mixture, the stamps or the stencils could allow this method to be more viable for practical application of the dye.

Conclusions

Although a number of dye application methods have been proposed along with descriptions of anecdotal experiences with them, serious engineering and safety work needs to be done to take concepts to practical application in the clinics.

Still, these anecdotal experiences presented here do provide some evidence that fast and reliable dye application schemes can be realised for clinical use.

4.16.2. Potential methods for dye removal

To make the deconstructing dissection strategy really robust, it would be desirable for the marking task with the dye to be reversible. A number of ideas for how to achieve this were brainstormed and are described and discussed here.

Waterjet cleaning

Because diffusion of ICG into tissue happens at a very slow rate, perhaps the majority of ICG dye can be washed off of the tissue surface using a jet of water.

Care would have to be taken to prevent transfer of ICG to unwanted locations. However, this might be ameliorated by the use of large volumes of water.

Photobleaching ICG

Photobleaching of ICG with 800 nm pulsed lasers was investigated by Kumar in 1996. [335] High radiant exposure of ICG to laser radiation resulted in photodegradation of the dye, visible colour change from green to orange and a pronounced reduction of light absorption at 805 nm.

Perhaps a pulsed laser could be used for dye erasure in tandem with the cw Diomed laser used for tissue ablation?

However, the requirement of a second laser for dye erasure could reduce the value proposition offered by repurposing a relatively common diode laser for ablation, and make the idea of dye-mediated ablation less practical.

Methylene blue and its leuco form

MB-mediated laser ablation with a red laser was explored briefly in Chapter 2. MB also is very versatile in the number of ways its absorption spectrum can be changed.

Perhaps the most famous colour change involving MB is the classic “Blue Bottle” classroom experiment in which the colour of the liquid is changed from blue to clear and back. This “chemical magic” involves reversible alkaline glucose reduction of methylene blue to its colourless leuco form. [336]

However, this reaction requires the use of potassium hydroxide and sodium hydroxide, both of which are very corrosive chemicals.

MB also can be reversibly photoreduced in methylene blue sensitized gelatine (MBG) solutions and films used for holographic phase recording. [337] The bleaching effect can be maintained under constant illumination but reverses rapidly otherwise.

Unfortunately, this photobleaching effect is detrimentally affected by the presence of oxygen due to its ability to reoxidize the colourless leuco form back to MB^+ .

The potential for reversible colour change of MB exists but in laboratory conditions that are hostile to living tissue. Still, if the photobleaching effect could be made to be biologically compatible, a potentially compelling way to “erase” dyed tissue might be found.

Conclusions

Although the potential for dye erasure exists — some potential avenues of research have been presented — much work needs to be done to adapt exploitable physical phenomena to a safe and biocompatible method for dye erasure.

4.17. Chapter Conclusions

This chapter examined the concept of ICG dye-mediated laser ablation in detail.

Relevant properties of the necessary equipment and components of the laser ablation process were quantified, and the concept was tested in a live animal.

A review of the theory of laser ablation in tissue was offered followed by detailed histological examination of the aftermath of ablation. High speed videography was used to gain insight into the dye-mediated laser ablation process. A statistical model of the tissue response to ablation due to dye volume, laser irradiance and exposure time also was constructed.

Modifications were made to the standard theory to account for the dye-mediated ablation process, and this was modelled in a finite element computer model. An Arrhenius kinetic equation was used to model the self-renewing carbonisation process that is necessary for sustained ablation once the dye layer has been vaporised.

The computer model was able to predict the laser ablation rate within an order of magnitude.

Tissue damage from dye-mediated laser ablation was compared with existing dissection tools and found to be similar to some reports of coagulative necrosis caused by electrosurgery and ablation by CO₂ and Ho:YAG lasers.

Potential methods for dye application were offered and possible methods for dye removal were speculated on.

Overall, ICG-mediated laser ablation as an embodiment of the deconstructing dissection strategy potentially could deliver on the promises conferred by this strategy.

However, in its current form, there are many challenges that need to be addressed for its potential clinical benefits to outweigh its apparent drawbacks.

Ablation rates are relatively low and the thicknesses of coagulative damage zones are relatively high. But these might be improved upon with more research and experimentation.

Chapter 5:

Overall conclusions and future work

*Nothing is ever really lost, or can be lost,
No birth, identity, form — no object of the world.
Nor life, nor force, nor any visible thing;
Appearance must not foil, nor shifted sphere confuse thy brain.
Ample are time and space — ample the fields of Nature.
The body, sluggish, aged, cold — the embers left from earlier fires,
The light in the eye grown dim, shall duly flame again;
The sun now low in the west rises for mornings and for noons continual;
To frozen clods ever the spring's invisible law returns,
With grass and flowers and summer fruits and corn.*

*Walt Whitman
“Continuities” from Leaves of Grass*

5.1. Overall summary of work

What an interesting and wonderful journey we have taken.

With the backdrop of a coalition of doctors worldwide trying to reinvent minimally invasive surgery as NOTES, we started our own exploration by capturing the needs of the procedures they aspired to perform and what might be required of endoscopic cutting tools that might be used for these procedures.

We defined the white space of solution areas available for potential invention and research by reviewing the literature for existing endoscopic cutting technologies and control schemes.

We then proposed a new strategy for “deconstructing dissection” as a potential approach to address the unique manipulation challenges that exist within the context of surgery at flexible endoscopy.

A number of novel techniques embodying this strategy were conceived, explored and then evaluated. From these, one concept — dye-mediated laser ablation — was chosen as the topic to pursue for further scientific investigation.

The exploration of dye-mediated laser ablation by experimentation — including high-speed videography — revealed that ICG-mediated laser ablation is strongly dependent on the cyclic formation of carbonisation to sustain the ablation process beyond the initial lifetime of the ICG on the tissue.

An Arrhenius-based model for carbonisation was proposed, and was incorporated into a computer modelling of dye-mediated ablation, which produced reasonable results.

Finally, some qualitative experimental results and speculation on how to apply the dye and how to remove it were offered.

5.2. Main findings and conclusions

This work contributed to the body of scientific knowledge in four key areas:

1. It established the need for new control cutting tools for a new endoscopic surgical arena based on an extensive literature review of the history of surgery, the historic development of laparoscopy and current developments in NOTES.
2. It identified that white space for research and development does exist based on an extensive literature review of existing endoscopic cutting and control methods.
3. It proposed the “deconstructing dissection” strategy as a novel approach to address the unique manipulation challenges in endoscopic tissue dissection and explored numerous embodiments with specific potential benefits to the endoscopic surgeon.
4. It explored in-depth the dye-mediated laser ablation concept to better understand the governing processes. These insights might guide future work in control and optimisation of the ablation process. From this exploration, carbonisation was identified as crucial to sustained, dye-mediated laser ablation, and standard theory was modified to account for this.

Overall, this work proposed a new approach for endoscopic tissue dissection and offered evidence suggesting that the deconstructing dissection strategy is viable.

With further development, proposed concepts (in particular dye-mediated laser ablation) or other ideas implementing the deconstructing dissection strategy may provide the endoscopic surgeon with real benefits over existing methods for use in NOTES and other advanced endoscopic surgical procedures.

5.3. Recommendations for future work

With the conclusion of this work arises new opportunities for future work.

It is hoped that this work might inspire continuing research — in dye-mediated laser ablation, in deconstructing dissection, in new approaches for controlled cutting schemes, and in minimally invasive surgery in general.

Although all the proposed methods, including dye-mediated laser ablation, have substantial hurdles that need to be overcome before clinical application can be considered, they also provide or hint at control benefits that might be amplified (and drawbacks, minimised) with further research.

For dye-mediated laser ablation in particular, there are many opportunities for further research in order to cultivate it from a seedling idea to a mature clinical tool. Methods to control and optimise the process, to apply the dye and remove it, to design for compatibility with flexible endoscopy — these all can be fruitful areas for further research.

Of course, new, better concepts embodying the deconstructing dissection strategy also can be created and investigated. As can be seen with the NOTES movement, all boundaries, including the walls of the alimentary tract, can be broken.

The future (and future work) is ours to shape. Let's get to it.

5.4. Closing thoughts

Statistically speaking, very few people other than the PhD supervisor and the thesis examiners will ever read these words. But if you have made it here to the end, then well done, and thank you!

This work was started four years ago when the author left the world of large, multi-national medical companies for the quiet (but sometimes anxiety-filled) confines of a small, windowless, basement laboratory at UCLH to try to make a small but meaningful contribution to medical physics and to clinical medicine.

It is the sincere hope of the author that this work has contributed something meaningful to the world. Hopefully it also will be useful to others conducting medical research that will help people to live longer, happier and disease-free lives.

Appendix A:

Histology slide preparation techniques

Oftentimes in medical physics it is desirable to directly visualize the effects of physical processes on tissue at the cellular level. Relatively straightforward histopathological techniques can be used to make two common slide types — frozen sections and haematoxylin & eosin (H&E) stained sections.

Tissue also can be embedded in paraffin before cutting and staining, but this process is more involved and will not be described here.

As an aside, it was surprisingly difficult to find within the Department of Medical Physics and Bioengineering expertise or even protocols for cutting and making histology slides.

Many thanks go to Ms. Noreen Shaikh in the Department of Surgery for providing the author with the cryostat tissue cutting and H&E staining protocols, as well as the training and the lab space to implement them.

Also, thanks to Dr. Josephine Woodhams in the National Medical Laser Centre for sharing the LN₂ flash freezing protocol.

Flash freezing tissue with isopentane and liquid nitrogen

Flash freezing of tissue is desirable for tissue samples from which histology slides will be cut. This technique provides two benefits – (1) it freezes the state of biological tissue, and (2) it prevents damage from ice crystal formation.

Although tissue can be frozen directly with liquid nitrogen, this often is undesirable because the desired rapid thermal conduction of heat away from the tissue to the liquid nitrogen (LN2) often is impeded by an insulating nitrogen gas boundary layer that forms between the submerged tissue and the LN2.

This slows down the freezing processes and can allow damaging ice crystals to form.

A better technique involves the use of isopentane as an intermediary between the tissue and the LN2. Isopentane, C₅H₁₂, has a melting point of -159.9°C and a boiling point of 27.7°C, meaning that it can get cold enough in LN2 (-196°C) to rapidly freeze materials in a liquid bath without boiling upon contact with tissue at room temperature (25°C).

As with any procedures using LN₂, one must make sure that all safety procedures, including adequate ventilation, are followed. The liquid to gas expansion ratio of nitrogen is 1:694, so the danger of asphyxiation in confined spaces is very real.

The flash freezing protocol follows:

1. Take a long pair of forceps and a small plastic cup. Fill a small dewar with liquid nitrogen.
2. Fill the cup with isopentane, about half full.
3. Carefully immerse the cup with the forceps into the liquid nitrogen. Be careful not to let the liquid nitrogen spill into the isopentane.
4. Hold it there for about 10 seconds until it is chilled but not frozen, and then remove it from the liquid nitrogen.
5. Drop the tissue specimen into the chilled isopentane and resubmerge the cup into the liquid nitrogen.
6. Hold it there for 5 seconds.
7. Remove the plastic container from the liquid nitrogen.
8. Take out the tissue specimen and place it onto a sheet of tissue. Allow the isopentane to evaporate off by moving the specimen around.
9. Place the tissue specimen into a labelled Nunc tube.
10. Drop the tube into the liquid nitrogen.
11. You can then transfer the Nunc tube into a liquid storage dewar or a -80°C freezer.

Making frozen sections within a cryostat

Frozen sections can be cut using a microtome found within a specialized cryostat. Unfortunately, slicing samples with the microtome is a tedious and painstaking process, and the only advice the author can provide is simply to practice, practice, practice!

The sectioning protocol is as follows:

1. The metal chuck on which your sample/tissue will go should be placed in the cryostat shelf for at least 5 minutes to cool. Make sure the chuck is dry before placing it in the shelf — any wetness or condensation will freeze and you will have difficulty removing the chuck from the shelf.
2. Pour some OCT onto the chuck. Then using forceps, quickly place your tissue on top of the OCT. Spray some Cryojet sparingly over the block.

3. Add some more OCT to ensure your tissue/sample is embedded well. Be careful not to let it fall off; again use the Cryojet to quickly freeze. Place the chuck in the cryostat to equilibrate the temperature.
4. Run through the initialization procedure for your cryostat/microtome.
5. Your knife should be at an angle of 12 degrees and the screws holding the knife should be tight.
6. Place your tissue in the specimen chamber and then check the distance between the tissue and the knife. The knife should be next to your block but not touching it. Make any necessary adjustments and remember to lock the fixtures before you start cutting.
7. The wheel outside the machine (this may vary depending on your machine) moves your tissue forward towards the knife in an up and down oscillating motion.
8. Bring your knife block close to the specimen and trim the block of tissue. Trim away the embedding medium until you can see your tissue. When trimming set the cutting thickness to 15 micrometers and use the coarse cut side of the knife. (Your lab probably will allocate one half of the blade for fast, coarse cuts and the other half for cutting the actual sections. This keeps the blade sharp for cutting actual sections.)
9. Once you can see your tissue and you have an even surface, change the depth to 5-10 micrometers and clean the blade surface with a brush. Always brush away from yourself. It is important you don't brush the other way because you'll dull the blade.
10. Now move the blade to the portion allocated for cutting actual sections.
11. Cut a section at 5-10 microns to even out the surface because you have moved the blade, and then clean the surface of the blade thoroughly. This is where your section will lay. If the surface of the blade is not clean, the cut section will crinkle up giving uneven and overlapping sections.
12. Place the rotary blade (the clear block that sits on the surface of the blade) onto the blade. Ensure the rotary blade tip and the blade ends are aligned. Adjust the tension of the rotary blade — do not tighten it too much otherwise the rotary blade will not take up the section.
13. Now cut one section. Ideally it should cut in-between the rotary blade and the metal blade surfaces. If the section doesn't end up in between, remove it with your brush and adjust the rotary blade. Then try again.
14. Once you have a good section in-between the two blades, gently rotate the rotary blade away. Your section should lie flat on the surface of the metal blade.
15. Hold your pre-labelled slide, rotate the labelled surface away from yourself and place it directly onto the blade area where your section is. Be careful not to move the slide around

- otherwise the section will be destroyed. Press hard onto the surface of the slide and then remove the slide again in the same rotation.
16. Brush clean the blade surface as the section picked up will leave an imprint on the blade.
 17. You can optionally apply Geimsa Stain by pipetting a drop directly onto the section and then washing away excess stain using a gentle stream of tap water.
 18. Leave all your slides to air dry for about 2 hours. Wrap them up in foil with pairs of slides back to back with the sections facing outwards. Place them in a secure bag inside a -70°C or -80°C freezer.
 19. Clean up any shavings and leave the machine in a tidy state.

Staining with haematoxylin & eosin

The frozen sections then can be stained with haematoxylin and eosin (H&E). This is a popular staining technique in histology and is used to increase contrast to better visualize cellular structures.

Haematoxylin stains primarily cell nuclei a blue colour. Eosin is used as a counterstain that colours the cytoplasm and protein rich structures various shades of red, pink and orange.

The H&E staining protocol consists of eighteen steps in which the frozen slides are submerged in various chemicals and stains.

The staining protocol follows:

1. Dewax section in first xylene (3 minutes)
2. Dewax section in second xylene (3 minutes)
3. Place slides in 100% ethanol (1 minute)
4. 100% ethanol (1 minute)
5. 70% ethanol (1 minute)
6. Place slides under running tap water (1 minute)
7. Stain slides in Haris' haematoxylin (regressive stain) (5 minutes)
8. Wash slides in running tap water (3 minutes)
9. Differentiate in 1% acid alcohol (agitate) (6 seconds)
10. Wash in Scott's tap water until sections are blue (~5 minutes)
11. Wash briefly in tap water (< 1 minute)
12. Stain slides in 1% eosin (5 minutes)
13. Wash in running tap water (0.5-1 minute)
14. Place slide in 70% ethanol (15 seconds)

15. 100% ethanol (30 seconds)
16. 100% ethanol (30 seconds)
17. First xylene (1 minute)
18. Second xylene (1 minute)
19. Mount slide in DPX (straight from histoclear), use coverslip.

Appendix B: Alternative light transport models

In our FEM model, the simplest model of absorption-dominated light transport in tissue as a simple exponential decay following the Lambert-Bouguer Law was used for reasons described previously. However, more complicated models also can be used to model light transport.

In general, modelling light transport in turbid media such as tissue can be quite complicated. The Radiative Transfer Equation (RTE) gives the most complete description of light transport, but is very difficult to solve.

The diffusion approximation (DA) is a simplification of the RTE that is popular because assumptions are made to reduce the number of unknowns and to allow it to be solved more easily. [338] As a result, diffusion theory has been used in FEM simulations to model laser coagulation of tissue. [339][340]

However, two conditions need to be met for DA to be accurate:

1. The medium must be highly scattering, i.e. the light absorption in the medium is negligible compared to scattering ($\mu_a \ll \mu_s$).
2. The light source must be near isotropy, i.e. it is essentially diffuse.

Collimated light such as from a laser violates the second condition of near isotropy, but can be modelled by considering that it becomes highly scattered and essentially diffuse from multiple scattering events once it has reached some distance d beneath the surface of the tissue:

$$d = \frac{1}{\mu_{st}} = \frac{1}{\mu_s(1 - g)} \quad (\text{B.1})$$

Where μ_{st} is the reduced scattering coefficient, μ_s is the scattering coefficient, and g is the anisotropy factor.

However, between the surface and this characteristic distance, diffusion theory does not accurately model light transport within the tissue. However, this region encompasses our areas of interest for ICG-mediated laser ablation.

For illustrative purposes using optical coefficients for rabbit skeletal muscle at 790 nm, diffusion theory can accurately model light distribution only for tissue deeper than about 1.3 mm.

Furthermore, the first condition that the medium be scattering dominated would not hold true for our regions of interest within the ICG or carbonised tissue layers as these regions are very much absorption dominated, i.e., $\mu_a \gg \mu_s$ and absorption events greatly outnumber scattering ones.

The δ -Eddington approximation can help to improve accuracy near the surface by replacing the Eddington phase function in the RTE (used by DA) with a new phase function that is better able to cope with the forward scattering tendency of tissue. [341][342][343][344] However, this comes at the cost of greater complexity in the model.

The δ -Eddington phase function, which is composed of a Dirac delta function (to represent a forward scattering peak) and a two term phase function expansion, better agrees with the Henyey-Greenstein phase function, which is known to represent well the forward-scattering anisotropy of tissue.

Incidentally, although the Henyey-Greenstein phase function is ubiquitous in medical optics, it has its origins in astrophysics as described in Henyey and Greenstein's original 1940 paper rather than in biophotonics. [345]

Monte Carlo also can be used and is the most accurate method to model the light distribution if tissue optical coefficients are known. However, finding accurate and representative optical coefficients for tissue can be a daunting task.

The Monte Carlo algorithm explicitly models each absorption and scattering interaction as photons travel through the tissue volume. However, many, many photons are necessary to obtain a proper distribution, and as a result, this method is very computationally intensive and costly.

MCML, the open source Monte Carlo program by Wang and Jacques [346] is available for public use and probably is considered the gold standard of MC for tissue optics.

Recent work by Alerstam, Svensson and Andersson-Engels in 2009 to port execution of the MCML algorithm to modern nVidia graphics processors can take advantage of the massively parallel processing capabilities of computational and gaming GPUs.

Their open source program, CudaMCML, can speed up Monte Carlo simulations by as much as a factor of 1000 depending on how many graphics processing units one has at their disposal. [347] The program appears to scale well with the power and number of GPUs in the system, as

simulations of the wander of individual photons through the tissue are independent of each other.

Fang and Boas in 2009 also have developed an open source GPU-accelerated Monte Carlo program called MCX. [348] Unlike MCML and CudaMCML which assume a layered, axis-symmetric geometry, MCX can simulate light transport in arbitrary 3D turbid media.

However, it does not have the pedigree of independent validation by other researchers that MCML and, to a lesser extent, CudaMCML enjoy.

One weakness of the GPU accelerated code at the time the Monte Carlo method was being evaluated by the author was the limitation of GPU-based numeric computation to single precision accuracy.

However, this has been remedied as of this writing by an updated nVidia Cuda SDK and device driver supporting double precision computation in newer, higher-end nVidia GPUs.

Appendix C:

Thermal and optical coefficients

Selected optical and thermal tissue properties from the literature that were used in the FEM computer model have been reproduced here in this appendix.

Overview of coefficients used in the model

The summary tables of the coefficients used in the model in Chapter 4 are repeated here.

Table C-1. Summary of changes in thermal coefficients.

THERMAL / MECHANICAL	Undamaged (C1)	Desiccated @ 100° C (C2)	Carbonised (C3)	Vaporised @ 500° C
Specific heat, Cp [J/(kg K)]	3448 avg. pig skeletal muscle (Duck [276])	1696 pig skin (Knox et al. [333])	1390 char (Shen et al. [330])	2135 steam (NIST)
Thermal conductivity, k [W/(m K)]	0.49 avg. pig skeletal muscle (Duck [276])	0.084 biological fluids (Spells [335])	0.105 char (Shen et al. [330])	0.07 steam (NIST)
Density, ρ [kg/m³]	1041 human skeletal muscle (Duck [276])	270 25.9% not water (Duck [276])	25 10% of charcoal (McKenzie [306])	0.3 steam (NIST)

Table C-2. Summary of changes in optical coefficients.

OPTICAL	Undamaged (C1)	Coagulated (C2)	Carbonised (C3)	Vaporised @ 500° C
Absorption, μ _a [1/cm]	0.30 @ 800 nm pig skeletal muscle (Birth et al. [335])	0.63 (best guess) rat prostate (Skinner et al. [331])	1380 @ 800 nm 10% compact soot (Koylu, Faeth [336])	0.0195 @ 806 nm steam (OMLC)
ICG absorption, μ _a [1/cm]	854 @ 805 nm (measured)	854 @ 805 nm (measured)	1380 @ 800 nm 10% compact soot (Koylu, Faeth [336])	0.0195 @ 806 nm steam (OMLC)

Table C-3. Summary of how state changes are modelled.

State transition		Model
undamaged	→ coagulated	Arrhenius damage integral drives property changes.
coagulated	→ desiccated	Smooth Heaviside function for property changes. Impulse increase in heat capacity at 100° C for vaporisation.
desiccated	→ carbonised	Arrhenius integral for carbonisation drives property changes.
carbonised	→ vaporised	Smooth Heaviside function for property changes. Impulse decrease in heat capacity at 500° C from combustion.

Thermal properties

Specific heat capacity

Copyrighted material

Figure C-1. Specific heat capacity of muscle tissue [J/(g K)]. (Reproduced from Duck. [279])

Thermal conductivity

Copyrighted material

Figure C-2. Temperature and thermal conductivity of muscle tissue [W/(m K)]. (Reproduced from Duck. [279])

Tissue constituents

Copyrighted material

Figure C-3. Composition of human cardiac and skeletal muscle tissue. (Reproduced from Duck. [279])

Dependency of thermal properties on water content

$$\gamma = (6.18277 * 10 W_w + 0.938172)^{-1} \quad (C.1)$$

$$k = \gamma(1.08432 * 10 W_w + 4.15684e-4) \quad (C.2)$$

$$C_p = 0.595 W_w + 0.405 \quad (C.3)$$

W_w is the mass fraction of water (the remainder of the mass is assumed to be equal portions of protein and fat), γ is density [g/cm], k is the thermal conductivity [cal/(cm-s-C)]and C_p is the heat capacity [cal/(gm-C)] for porcine skin. (From Knox et al. [349])

Copyrighted material

Figure C-4. The thermal conductivities of biological fluids depending on water content (at near body temperatures).
(Reproduced from Spells. [350])

Optical properties

Absorption coefficient for porcine muscle
Copyrighted material

Figure C-5. Scatter and absorption coefficients for pork muscle at 632 and 800 nm.
(Reproduced from Birth et al. [351])

Normalised absorption coefficient

Copyrighted material

Figure C-6. Normalised absorption coefficient of rat prostate during coagulation.
(Reproduced from Skinner et al. [333])

Extinction coefficient of soot

Copyrighted material

Figure C-7. Extinction coefficient, k , of soot from propane combustion [$1/\mu\text{m}$].
(Reproduced from Köylü and Faeth. [336] Logarithmic grid overlay added.)

References

1. Gunn SWA. Surgeon. World journal of surgery. 1998 ;22(3):221-222.
2. Vitruvian Man - Wikipedia, the free encyclopedia [Internet]. [cited 2008 Feb 6] Available from: http://en.wikipedia.org/wiki/Vitruvian_Man
3. Birkett DH. Videoendoscopy and General Surgery: A Brief History. In: Mastery of Endoscopic and Laparoscopic Surgery. Philadelphia: Lippincott Williams & Wilkins; 2005. p. 3-5.
4. Soper NJ, Stockmann PT, Dunnegan DL, Ashley SW. Laparoscopic cholecystectomy. The new "gold standard"? Archives of surgery. 1992 ;127(8):917-921.
5. Waye JD. What is a gold standard for colon polyps? Gastroenterology. 1997 Jan ;112(1):292-4.
6. Hochberger J, Lamadé W. Transgastric surgery in the abdomen: the dawn of a new era? Gastrointestinal endoscopy. 2005 Aug ;62(2):293-6.
7. Hawes RH. Advanced Endoscopy and Endosurgical Procedures: Do We Need a New Subspecialty? Gastrointestinal endoscopy clinics of North America. 2007 ;17(3):635-639.
8. Kalloo AN, Rattner DW, Brugge WR, Gostout CJ, Hawes RH, Kantsevoy SV, et al. ASGE/SAGES working group on natural orifice transluminal endoscopic surgery [Internet]. Gastrointestinal endoscopy. 2006 ;63(2):199-203. Available from: <http://www.springerlink.com/index/P62U383145222L27.pdf>
9. Ellis H. A History of Surgery. Greenwich Medical Media; 2001.
10. Pollack SV, Carruthers A, Grekin RC. The history of electrosurgery. Dermatologic surgery : official publication for American Society for Dermatologic Surgery [et al.]. 2000 Oct ;26(10):904-8.
11. Milne JS. Surgical Instruments in Greek and Roman Times. Oxford: Clarendon Press; 1907.
12. Edmonson JM. History of the instruments for gastrointestinal endoscopy. Gastrointestinal endoscopy. 1991 ;37(2 Suppl):S27-56.
13. Hayes I. Instruments for illuminating dark cavities. Philadelphia Journal of the Medical and Physical Sciences. 1827 ;14
14. Berci G, Forde KA. History of endoscopy. Surgical endoscopy. 2000 Jan ;14(1):5-15.
15. Walk L. The history of gastroscopy. Clio medica (Amsterdam, Netherlands). 1966 ;209-222.
16. Baillie J. The endoscope. Gastrointestinal endoscopy. 2007 May ;65(6):886-93.

17. Ginsberg GG, Kochman ML, Norton ID, Gostout CJ. Clinical Gastrointestinal Endoscopy. Elsevier Saunders; 2005.
18. Kaban GK, Czerniach DR, Novitsky YW, Litwin DEM. Special Access Techniques in Laparoscopic Surgery. In: Mastery of Endoscopic and Laparoscopic Surgery. Philadelphia: Lippincott Williams & Wilkins; 2005. p. 35-45.
19. Sandor J, Ballagi F, Nagy A, Rákóczi I. A needle-puncture that helped to change the world of surgery. *Surgical endoscopy*. 2000 Feb ;14(2):201-202.
20. Laparoscopic Surgery Complications [Internet]. [cited 2008 Jun 24] Available from: http://www.danaise.com/laparoscopic_surgery_7-5.htm
21. Reavis KM, Melvin WS. Advanced endoscopic technologies. *Surgical endoscopy*. 2008 Jun ;22(6):1533-46.
22. CF-H180AL-I [Internet]. [cited 2008 May 18] Available from: http://www.olympusamerica.com/msg_section/msg_product.asp?p=3&sc=1&product=1197
23. EndoEYE Flexible Video Transnasal Esophagoscope (PEF-V) [Internet]. [cited 2008 May 27] Available from: http://www.olympusamerica.com/msg_section/msg_product.asp?p=9&sc=5&product=915
24. Boston Scientific :: Products :: SpyGlass® Direct Visualization System :: Health Care Professionals :: Overview [Internet]. [cited 2008 May 27] Available from: http://www.bostonscientific.com/Device.bsci?page=HCP_Overview&navRelId=1000.1003&method=DevDetailHCP&id=10066432&pageDisclaimer=Disclaimer.ProductPage
25. USGI Medical, Inc. [Internet]. [cited 2008 May 22] Available from: <http://www.usgimedical.com/eos/components-transport.htm>
26. Kochman ML, Swain CP. Deconstruction of the endoscope. *Gastrointestinal endoscopy*. 2007 Apr ;65(4):677-8.
27. Richards WO, Torquati A, Sekhar N, Youssef Y. The Emergence of Flexible Endoscopy as Therapy. *Laparoscopy today*. 2005 ;4(2):
28. Intuitive Surgical - da Vinci Surgical System [Internet]. [cited 2008 Jun 24] Available from: http://www.intuitivesurgical.com/products/davinci_surgicalsystem/index.aspx
29. Ishikawa N, Watanabe G, Hirano Y, Inaki N, Kawachi K, Oda M. Origami using da Vinci surgical system. *Surgical endoscopy*. 2007 ;21(7):1252-3.
30. Robot-Assisted Surgery: da Vinci [Internet]. [cited 2008 May 30] Available from: http://biomed.brown.edu/Courses/BI108/BI108_2005_Groups/04/davinci.html
31. Rothstein R, Ailinger RA, Peine W. Computer-Assisted Endoscopic Robot System for Advanced Therapeutic Procedures. *Gastrointestinal endoscopy*. 2004 ;59(5):P113.

32. Rentschler ME, Oleynikov D. Recent in vivo surgical robot and mechanism developments. *Surgical endoscopy*. 2007 Sep ;21(9):1477-81.
33. Rentschler ME, Dumpert J, Platt SR, Farritor SM, Oleynikov D. Natural orifice surgery with an endoluminal mobile robot. *Surgical endoscopy*. 2007 ;21(7):1212-5.
34. HCP: Pill Cam, Capsule Endoscopy, Esophageal Endoscopy [Internet]. [cited 2008 May 31] Available from: <http://www.givenimaging.com/en-us/HealthcareProfessionals/Pages/pageHCP.aspx>
35. Mosse CA. Devices to assist with steering colonoscopes. 2000 ;229.
36. Mosse CA, Mills TN, Appleyard MN, Kadirkamanathan SS, Swain CP. Electrical stimulation for propelling endoscopes. *Gastrointestinal endoscopy*. 2001 ;54(1):79-83.
37. Menciassi A, Quirini M, Dario P. Microrobotics for future gastrointestinal endoscopy. *Minimally invasive therapy & allied technologies : MITAT : official journal of the Society for Minimally Invasive Therapy*. 2007 Jan ;16(2):91-100.
38. Netter FH. *Atlas of Human Anatomy*. 2nd ed. East Hanover: Novartis Medical Education; 1997.
39. Gill KR, Nawaz I, Crook J, Gross SA, Ghabril MS, Jamil LH, et al. Variation in Barrett's Esophageal Wall Thickness: Is It Associated with Histology Or Segment Length? *Gastrointestinal Endoscopy*. 2008 ;67(5):2008-2008.
40. Bouma BE, Tearney GJ, Compton CC, Nishioka NS. High-resolution imaging of the human esophagus and stomach in vivo using optical coherence tomography. *Gastrointestinal Endoscopy*. 2000 ;51(4):
41. Rapaccini GL, Aliotta A, Pompili M, Grattagliano A, Anti M, Merlini B, et al. Gastric wall thickness in normal and neoplastic subjects: A prospective study performed by abdominal ultrasound [Internet]. *Gastrointestinal Radiology*. 1988 Dec ;13(1):197-199.[cited 2007 Nov 5] Available from: <http://dx.doi.org/10.1007/BF01889058>
42. Fleischer AC, Muhletaler CA, James AEJ. Sonographic assessment of the bowel wall [Internet]. *American journal of roentgenology*. 1981 May ;136(5):887-91.Available from: <http://www.ncbi.nlm.nih.gov/pubmed/6784522>
43. Marchesini R, Pignoli E, Tomatis S, Fumagalli S, Sichirillo a E, Di Palma S, et al. Ex vivo optical properties of human colon tissue. [Internet]. *Lasers in surgery and medicine*. 1994 Jan ;15(4):351-7.Available from: <http://www.ncbi.nlm.nih.gov/pubmed/7885168>
44. Greek Medicine | Hippocrates | The Oath [Internet]. [cited 2008 May 15] Available from: http://www.nlm.nih.gov/hmd/greek/greek_oath.html
45. Berguer R, Smith WD, Chung YH. Performing laparoscopic surgery is significantly more stressful for the surgeon than open surgery. *Surgical endoscopy*. 2001 Oct ;15(10):1204-7.

46. Stumpf M, Klinge U, Tittel A, Brücker C, Schumpelick V. The surgical trauma of abdominal wall incision. A comparison of laparoscopic vs open surgery with three-dimensional stereoscopy. *Surgical endoscopy*. 2001 Oct ;15(10):1147-9.
47. Novitsky YW, Litwin DEM, Callery MP. The net immunologic advantage of laparoscopic surgery. *Surgical endoscopy*. 2004 ;18(10):1411-9.
48. Peetz ME. Operative risk and cosmetic results. *Surgical endoscopy*. 2004 Nov ;18(11):1549-50.
49. Kazaryan AM, Kuznetsov NS, Shulutko AM, Beltsevich DG, Edwin B. Evaluation of endoscopic and traditional open approaches to pheochromocytoma. *Surgical endoscopy*. 2004 ;18(6):937-941.
50. Hazzan D, Shiloni E, Golijanin D, Jurim O, Gross D, Reissman P. Laparoscopic vs open adrenalectomy for benign adrenal neoplasm. *Surgical endoscopy*. 2001 ;15(11):1356-8.
51. Ignacio RC, Burke R, Spencer D, Bissell C, Dorsainvil C, Lucha PA. Laparoscopic vs open appendectomy: What is the real difference? Results of a prospective randomized double-blinded trial. *Surgical endoscopy*. 2004 Feb ;18(2):334-7.
52. Moore DE, Speroff T, Grogan E, Poulose B, Holzman MD. Cost perspectives of laparoscopic and open appendectomy. *Surgical endoscopy*. 2005 Mar ;19(3):374-8.
53. Quintana JM, Cabriada J, Aróstegui I, López De Tejada I, Bilbao A. Quality-of-life outcomes with laparoscopic vs open cholecystectomy. *Surgical endoscopy*. 2003 ;17(7):1129-34.
54. Lezoche E, Feliciotti F, Paganini AM, Guerrieri M, De Sanctis A, Minervini S, et al. Laparoscopic vs open hemicolectomy for colon cancer. *Surgical endoscopy*. 2002 Apr ;16(4):596-602.
55. Kang J-C, Chung M-H, Chao P-C, Yeh C-C, Hsiao C-W, Lee T-Y, et al. Hand-assisted laparoscopic colectomy vs open colectomy: a prospective randomized study. *Surgical endoscopy*. 2004 Apr ;18(4):577-581.
56. Pokala N, Delaney CP, Senagore AJ, Brady KM, Fazio VW. Laparoscopic vs open total colectomy: a case-matched comparative study. *Surgical endoscopy*. 2005 Apr ;19(4):531-5.
57. Polle SW, Dunker MS, Slors JFM, Sprangers MA, Cuesta MA, Gouma DJ, et al. Body image, cosmesis, quality of life, and functional outcome of hand-assisted laparoscopic versus open restorative proctocolectomy: long-term results of a randomized trial. *Surgical endoscopy*. 2007 Aug ;21(8):1301-7.
58. Jacob BP, Salky B. Laparoscopic colectomy for colon adenocarcinoma: an 11-year retrospective review with 5-year survival rates. *Surgical endoscopy*. 2005 ;19(5):643-9.
59. Gonzalez R, Smith CD, Mattar SG, Venkatesh KR, Mason E, Duncan T, et al. Laparoscopic vs open resection for the treatment of diverticular disease. *Surgical endoscopy*. 2004 Feb ;18(2):276-280.

60. Bernabe KQ, Bolton JS, Richardson WS. Laparoscopic hand-assisted versus open transhiatal esophagectomy: a case-control study. *Surgical endoscopy*. 2005 Mar ;19(3):334-7.
61. Rahden BHA von, Stein HJ, Feussner H, Siewert JR. Enucleation of submucosal tumors of the esophagus: minimally invasive versus open approach. *Surgical endoscopy*. 2004 ;18(6):924-30.
62. Reyes CD, Weber KJ, Gagner M, Divino CM. Laparoscopic vs open gastrectomy. A retrospective review. *Surgical endoscopy*. 2001 ;15(9):928-31.
63. Lee J-H, Han H-S. A prospective randomized study comparing open vs laparoscopy-assisted distal gastrectomy in early gastric cancer: early results. *Surgical endoscopy*. 2005 Feb ;19(2):168-73.
64. Vale L, Ludbrook A, Grant A. Assessing the costs and consequences of laparoscopic vs. open methods of groin hernia repair: a systematic review. *Surgical endoscopy*. 2003 Jun ;17(6):844-9.
65. Moreno-Egea A, Torralba-Martinez JA, Morales G, Fernández T, Girela E, Aguayo-Albasini JL. Open vs laparoscopic repair of secondary lumbar hernias: a prospective nonrandomized study. *Surgical endoscopy*. 2005 Feb ;19(2):184-7.
66. Kercher KW, Heniford BT, Matthews BD, Smith TI, Lincourt AE, Hayes DH, et al. Laparoscopic versus open nephrectomy in 210 consecutive patients: outcomes, cost, and changes in practice patterns. *Surgical endoscopy*. 2003 Dec ;17(12):1889-1895.
67. Chrysos E, Tsiaouassis J, Athanasakis E, Zoras O, Vassilakis JS, Xynos E. Laparoscopic vs open approach for Nissen fundoplication; A comparative study. *Surgical endoscopy*. 2002 Dec ;16(12):1679-84.
68. Matthews BD, Walsh RM, Kercher KW, Sing RF, Pratt BL, Answini GA, et al. Laparoscopic vs open resection of gastric stromal tumors. *Surgical endoscopy*. 2002 May ;16(5):803-7.
69. Feliciotti F, Guerrieri M, Paganini AM, Sanctis AD, Campagnacci R, Perretta S, et al. Long-term results of laparoscopic versus open resections for rectal cancer for 124 unselected patients. *Surgical endoscopy*. 2003 ;17(10):1530-1535.
70. Feliciotti F, Paganini AM, Guerrieri M, De Sanctis A, Campagnacci R, Lezoche E. Results of laparoscopic vs open resections for colon cancer in patients with a minimum follow-up of 3 years. *Surgical endoscopy*. 2002 Aug ;16(8):1158-61.
71. Breukink SO, Grond AJK, Pierie JPEN, Hoff C, Wiggers T, Meijerink WJHJ. Laparoscopic vs open total mesorectal excision for rectal cancer: an evaluation of the mesorectum's macroscopic quality. *Surgical endoscopy*. 2005 Mar ;19(3):307-10.
72. Nakajima J, Takamoto S, Tanaka M, Takeuchi E, Murakawa T, Fukami T. Thoracoscopic surgery and conventional open thoracotomy in metastatic lung cancer. *Surgical endoscopy*. 2001 Aug ;15(8):849-53.
73. Natural Orifice Surgery Consortium for Assessment and Research (NOSCAR) [Internet]. [cited 2008 Jun 2] Available from: <http://www.noscarr.org/index.html>

74. Image:Gallbladderop.jpg - Wikipedia, the free encyclopedia.
<http://en.wikipedia.org/wiki/Image:Gallbladderop.jpg>.
75. Trus TL, Pope GD, Finlayson SRG. National trends in utilization and outcomes of bariatric surgery. *Surgical endoscopy*. 2005 May ;19(5):616-20.
76. NHS Information Centre LS. Statistics on obesity , physical activity and diet: England, 2010. London: 2010.
77. Cohen R, Pinheiro JS, Correa JL, Schiavon C. Laparoscopic revisional bariatric surgery: myths and facts. *Surgical endoscopy*. 2005 Jun ;19(6):822-5.
78. Gentileschi P, Kini S, Catarci M, Gagner M. Evidence-based medicine: open and laparoscopic bariatric surgery. *Surgical endoscopy*. 2002 May ;16(5):736-44.
79. Stellato TA, Crouse C, Hallowell PT. Bariatric surgery: Creating new challenges for the endoscopist. *Gastrointestinal endoscopy*. 2003 Jan ;57(1):86-94.
80. Suter M, Bettschart V, Giusti V, Heraief E, Jayet A. A 3-year experience with laparoscopic gastric banding for obesity. *Surgical endoscopy*. 2000 ;14(6):532-6.
81. Cottam DR, Nguyen NT, Eid GM, Schauer PR. The impact of laparoscopy on bariatric surgery. *Surgical endoscopy*. 2005 May ;19(5):621-7.
82. Schirmer B, Watts SH. Laparoscopic bariatric surgery. *Surgical endoscopy*. 2003 ;17(12):1875-8.
83. Fernandez AZ, DeMaria EJ, Tichansky DS, Kellum JM, Wolfe LG, Meador J, et al. Experience with over 3,000 open and laparoscopic bariatric procedures. *Surgical endoscopy*. 2004 Feb ;18(2):193-7.
84. Marema RT, Perez M, Buffington CK. Comparison of the benefits and complications between laparoscopic and open Roux-en-Y gastric bypass surgeries. *Surgical endoscopy*. 2005 Apr ;19(4):525-30.
85. Lee WY, Lee W-S, Yun SH, Shin S-H, Chun H-K. Decision for salvage treatment after transanal endoscopic microsurgery. *Surgical endoscopy*. 2007 Jun ;21(6):975-9.
86. Maslekar S, Pillinger SH, Monson JRT. Transanal endoscopic microsurgery for carcinoma of the rectum. *Surgical endoscopy*. 2007 ;21(1):97-102.
87. Kinoshita T, Kanehira E, Omura K, Tomori T, Yamada H. Transanal endoscopic microsurgery in the treatment of rectal carcinoid tumor. *Surgical endoscopy*. 2007 Jun ;21(6):970-4.
88. Ishikawa K, Arita T, Shimoda K, Hagino Y, Shiraishi N, Kitano S. Usefulness of transanal endoscopic surgery for carcinoid tumor in the upper and middle rectum. *Surgical endoscopy*. 2005 Aug ;19(8):1151-4.
89. Kreissler-Haag D, Schuld J, Lindemann W, König J, Hildebrandt U, Schilling M. Complications after transanal endoscopic microsurgical resection correlate with location of rectal neoplasms. *Surgical endoscopy*. 2008 Mar ;22(3):612-6.

90. Marks JH, Marchionni C, Marks GJ. Transanal endoscopic microsurgery in the treatment of select rectal cancers or tumors suspicious for cancer. *Surgical endoscopy*. 2003 Jul ;17(7):1114-7.
91. Cocolovo C, Smith LE, Stahl T, Douglas J. Transanal endoscopic excision of rectal adenomas. *Surgical endoscopy*. 2003 Sep ;17(9):1461-3.
92. Lee W, Lee D, Choi S, Chun H. Transanal endoscopic microsurgery and radical surgery for T1 and T2 rectal cancer. *Surgical endoscopy*. 2003 Aug ;17(8):1283-7.
93. Stipa F, Burza A, Lucandri G, Ferri M, Pigazzi A, Ziparo V, et al. Outcomes for early rectal cancer managed with transanal endoscopic microsurgery: a 5-year follow-up study. *Surgical endoscopy*. 2006 ;20(4):541-5.
94. Lezoche E, Guerrieri M, Paganini AM, D'Ambrosio G, Baldarelli M, Lezoche G, et al. Transanal endoscopic versus total mesorectal laparoscopic resections of T2-N0 low rectal cancers after neoadjuvant treatment: a prospective randomized trial with a 3-years minimum follow-up period. *Surgical endoscopy*. 2005 ;19(6):751-6.
95. Paganini AM, De Sanctis A, Bartolacci S, Lezoche E, with Lezoche G, Baldarelli M, Guerrieri M, Mario. A prospective randomized study with a 5-year minimum follow-up evaluation of transanal endoscopic microsurgery versus laparoscopic total mesorectal excision after neoadjuvant therapy. *Surgical endoscopy*. 2008 ;22(2):352-8.
96. Buess G, Kipfmüller K, Hack D, Grüssner R, Heintz A, Junginger T. Technique of transanal endoscopic microsurgery. *Surgical endoscopy*. 1988 ;2(2):71-75.
97. Buess G, Kipfmüller K, Hack D, Grüssner R, Heintz A, Junginger T. Technique of transanal endoscopic microsurgery [Internet]. *Surgical endoscopy*. 1988 May ;2(2):71–75. Available from: <http://www.springerlink.com/index/G56364065210M23W.pdf>
98. Santoro E, Agresta F, Veltri S, Mulieri G, Bedin N, Mulieri M. Minilaparoscopic colorectal resection: a preliminary experience and an outcomes comparison with classical laparoscopic colon procedures. *Surgical endoscopy*. 2008 May ;22(5):1248-54.
99. Lee P-C, Lai I-R, Yu S-C. Minilaparoscopic (needlescopic) cholecystectomy: a study of 1,011 cases. *Surgical endoscopy*. 2004 Oct ;18(10):1480-4.
100. Ainslie WG, Catton JA, Davides D, Dexter S, Gibson J, Larvin M, et al. Micropuncture cholecystectomy vs conventional laparoscopic cholecystectomy: a randomized controlled trial. *Surgical endoscopy*. 2003 May ;17(5):766-72.
101. Bisgaard T, Klarskov B, Trap R, Kehlet H, J. Microlaparoscopic vs conventional laparoscopic cholecystectomy. *Surgical endoscopy*. 2002 Mar ;16(3):458-64.
102. Sarli L, Costi R, Sansebastiano G. Mini-laparoscopic cholecystectomy vs laparoscopic cholecystectomy. *Surgical endoscopy*. 2001 ;15(6):614-8.
103. Unger SW, Paramo JC, Perez M. Microlaparoscopic cholecystectomy. Less invasive gallbladder surgery. *Surgical endoscopy*. 2000 Apr ;14(4):336-9.

104. Mamazza J, Schlachta CM, Seshadri PA, Cadeddu MO, Poulin EC. Needlescopic surgery: A logical evolution from conventional laparoscopic surgery. *Surgical endoscopy*. 2001 Oct ;15(10):1208-12.
105. Leggett PL, Bissell CD, Churchman-Winn R, Ahn C. Three-port microlaparoscopic cholecystectomy in 159 patients. *Surgical endoscopy*. 2001 Mar ;15(3):293-6.
106. Mori T, Ikeda Y, Okamoto K, Sakata K, Ideguchi K, Nakagawa K, et al. A new technique for two-trocar laparoscopic cholecystectomy. *Surgical endoscopy*. 2002 Apr ;16(4):589-91.
107. Ghezzi F, Raio L, Mueller MD, Gyr T, Buttarelli M, Franchi M. Vaginal extraction of pelvic masses following operative laparoscopy. *Surgical endoscopy*. 2002 ;16(12):1691-1696.
108. Zanetti-Dällenbach R, Bartley J, Müller C, Schneider A, Köhler C. Combined vaginal-laparoscopic-abdominal approach for the surgical treatment of rectovaginal endometriosis with bowel resection: a comparison of this new technique with various established approaches by laparoscopy and laparotomy. *Surgical endoscopy*. 2008 ;22(4):995-1001.
109. Scharday HM, Schopf S, Kammal M, Barone M, Rudert W, Hernandez-Richter T, et al. Invisible scar endoscopic thyroidectomy by the dorsal approach: experimental development of a new technique with human cadavers and preliminary clinical results. *Surgical endoscopy*. 2008 Apr ;22(4):813-20.
110. Cuesta MA, Berends F, Veenhof AAFA. The "invisible cholecystectomy": A transumbilical laparoscopic operation without a scar. *Surgical endoscopy*. 2008 May ;22(5):1211-3.
111. Yamaner S, Bilsel Y, Bulut T, Bugra D, Buyukuncu Y, Akyuz A, et al. Endoscopic diagnosis and management of complications following surgery for gallstones. *Surgical endoscopy*. 2002 ;16(12):1685-90.
112. Champion JK, Hunt T, DeLisle N. Role of routine intraoperative endoscopy in laparoscopic bariatric surgery. *Surgical endoscopy*. 2002 Dec ;16(12):1663-5.
113. Kalimi R, Cosgrove JM, Marini C, Stark B, Gecelter GR. Combined intraoperative laparoscopic cholecystectomy and endoscopic retrograde cholangiopancreatography: Lessons from 29 cases. *Surgical endoscopy*. 2000 Mar ;14(3):232-234.
114. Morino M, Rebecchi F, Giaccone C, Taraglio S, Sidoli L, Ferraris R. Endoscopic ablation of Barrett's esophagus using argon plasma coagulation (APC) following surgical laparoscopic fundoplication. *Surgical endoscopy*. 2003 ;17(4):539-42.
115. Saccomani G, Durante V, Magnolia MR, Ghezzo L, Lombezzi R, Esercizio L, et al. Combined endoscopic treatment for cholelithiasis associated with choledocholithiasis. *Surgical endoscopy*. 2005 Jul ;19(7):910-4.
116. Somogyi L, Chuttani R, Croffie J, Disario J, Liu J, Mishkin D, et al. Guidewires for use in GI endoscopy. *Gastrointestinal endoscopy*. 2007 Apr ;65(4):571-6.
117. DiSario J, Chuttani R, Croffie J, Liu J, Mishkin D, Shah R, et al. Biliary and pancreatic lithotripsy devices. *Gastrointestinal endoscopy*. 2007 ;65(6):750-756.

118. Cook Medical | Endoscopy | Billroth II Sphincterotome [Internet]. [cited 2008 Jun 25] Available from: <http://www.cookmedical.com/esc/dataSheet.do?id=1121>
119. Sivak MVJ. Polypectomy: looking back. *Gastrointestinal endoscopy*. 2004 Dec ;60(6):977-82.
120. Baron TH. Snare, knives, and scissors. *Techniques in gastrointestinal endoscopy*. 2006 Jan ;8(1):22-27.
121. Frimberger E, Delius S von, Feussner H, Henke J, Roesch T, Prinz C, et al. Submucosal endoscopy - a novel approach to en bloc endoscopic mucosal resection. *Gastrointestinal endoscopy*. 2006 ;63(5):AB80.
122. Farrell JJ. Submucosal fluid cushion and EMR: who rules the roost? *Gastrointestinal endoscopy*. 2008 May ;67(6):840-2.
123. Gotoda T, Kaltenbach T, Soetikno R. Is en bloc resection essential for endoscopic resection of GI neoplasia? *Gastrointestinal endoscopy*. 2008 May ;67(6):805-7.
124. Fleischer D. Endoscopic mucosal resection: (not) made in the USA (so commonly). A dissection of the definition, technique, use, and controversies. *Gastrointestinal endoscopy*. 2000 Sep ;52(3):440-4.
125. Pouw RE, Gondrie JJ, Alvarez Herrero L, Van Vilsteren FG, Peters F, Rosmolen W, et al. A Randomized Prospective Trial Comparing the Cap-Technique and Multi-Band Mucosectomy Technique for Piecemeal Endoscopic Resection in Barrett's Esophagus. *Gastrointestinal endoscopy*. 2008 ;67(5):AB75.
126. Rajan E, Gostout CJ, Feitoza AB, Leontovich ON, Herman LJ, Burgart LJ, et al. Widespread EMR: a new technique for removal of large areas of mucosa. *Gastrointestinal endoscopy*. 2004 ;60(4):623-627.
127. Kondo H, Gotoda T, Ono H, Oda I, Kozu T, Fujishiro M, et al. Percutaneous traction-assisted EMR by using an insulation-tipped electrosurgical knife for early stage gastric cancer. *Gastrointestinal endoscopy*. 2004 Feb ;59(2):284-8.
128. Oka S, Tanaka S, Kaneko I, Mouri R, Hirata M, Kawamura T, et al. Advantage of endoscopic submucosal dissection compared with EMR for early gastric cancer. *Gastrointestinal endoscopy*. 2006 Dec ;64(6):877-83.
129. Carpenter S, Petersen BT, Chuttani R, Croffie J, DiSario J, Liu J, et al. Polypectomy devices. *Gastrointestinal endoscopy*. 2007 May ;65(6):741-9.
130. Yoshinaga S, Gotoda T, Kusano C, Oda I, Nakamura K, Takayanagi R. Clinical impact of endoscopic submucosal dissection for superficial adenocarcinoma located at the esophagogastric junction. *Gastrointestinal endoscopy*. 2008 Feb ;67(2):202-9.
131. Saito Y, Takisawa H, Suzuki H, Takizawa K, Yokoi C, Nonaka S, et al. Endoscopic submucosal dissection of recurrent or residual superficial esophageal cancer after chemoradiotherapy. *Gastrointestinal endoscopy*. 2008 Feb ;67(2):355-9.

132. Shimizu Y, Yamamoto J, Kato M, Yoshida T, Hirota J, Ono Y, et al. Endoscopic submucosal dissection for treatment of early stage hypopharyngeal carcinoma. *Gastrointestinal endoscopy*. 2006 Aug ;64(2):255-9; discussion 260-2.
133. Chung IK, Kim HJ, Lee S-H, Tae LH, Cho JY, Hwang BY, et al. Therapeutic outcome in 1000 cases of endoscopic submucosal dissection (ESD) for early gastric neoplasms; Korean ESD Study Group (KESG) multi-center study. *Gastrointestinal endoscopy*. 2008 ;67(5):2008-2008.
134. Takenaka R, Kawahara Y, Okada H, Tsuzuki T, Yagi S, Kato J, et al. Endoscopic submucosal dissection for cancers of the remnant stomach after distal gastrectomy. *Gastrointestinal endoscopy*. 2008 Feb ;67(2):359-63.
135. Takeuchi Y, Uedo N, Iishi H, Yamamoto S, Yamamoto S, Yamada T, et al. Endoscopic submucosal dissection with insulated-tip knife for large mucosal early gastric cancer: a feasibility study (with videos). *Gastrointestinal endoscopy*. 2007 Jul ;66(1):186-93.
136. Tanaka S, Oka S, Kaneko I, Hirata M, Mouri R, Kanao H, et al. Endoscopic submucosal dissection for colorectal neoplasia: possibility of standardization. *Gastrointestinal endoscopy*. 2007 Jul ;66(1):100-7.
137. Antillon MR, Bartalos CR, Miller ML, Diaz-Arias AA, Ibdah JA, Marshall JB. En bloc endoscopic submucosal dissection of a 14-cm laterally spreading adenoma of the rectum with involvement to the anal canal: expanding the frontiers of endoscopic surgery (with video). *Gastrointestinal endoscopy*. 2008 Feb ;67(2):332-7.
138. Fujishiro M, Yahagi N, Kakushima N, Kodashima S, Ichinose M, Omata M. Successful endoscopic en bloc resection of a large laterally spreading tumor in the rectosigmoid junction by endoscopic submucosal dissection. *Gastrointestinal endoscopy*. 2006 ;63(1):178-183.
139. Chiu PWY, Chan KF, Lee YT, Sung JJY, Lau JYW, Ng EKW. Endoscopic submucosal dissection used for treating early neoplasia of the foregut using a combination of knives. *Surgical endoscopy*. 2008 Mar ;22(3):777-83.
140. Kodashima S, Fujishiro M, Yahagi N, Kakushima N, Omata M. Endoscopic submucosal dissection using flexknife. *Journal of clinical gastroenterology*. 2006 ;40(5):378-84.
141. Yamamoto H, Sekine Y, Higashizawa T, Kihira K, Kaneko Y, Hosoya Y, et al. Successful en bloc resection of a large superficial gastric cancer by using sodium hyaluronate and electrocautery incision forceps. *Gastrointestinal endoscopy*. 2001 ;54(5):629-632.
142. Brooker J, Saunders B, Suzuki N, Sibbons P. Twin-endoscope scissors resection (T-ESR). *Surgical endoscopy*. 2001 ;15(12):1463-1466.
143. Pearl JP, Marks JM. Endolumenal therapies for gastroesophageal reflux disease: are they dead? *Surgical endoscopy*. 2007 Jan ;21(1):1-4.
144. Swain P, Park P-O, Mills T. Bard EndoCinch: the device, the technique, and pre-clinical studies. *Gastrointestinal endoscopy clinics of North America*. 2003 ;13(1):75-88.

145. Pleskow D, Rothstein R, Kozarek R, Haber G, Gostout C, Lo S, et al. Endoscopic full-thickness plication for the treatment of GERD: Five-year long-term multicenter results. *Surgical endoscopy*. 2008 ;22(2):326-32.
146. Feretis C, Benakis P, Dimopoulos C, Dailianas A, Filalithis P, Stamou KM, et al. Endoscopic implantation of Plexiglas (PMMA) microspheres for the treatment of GERD. *Gastrointestinal endoscopy*. 2001 ;53(4):423-426.
147. Cipolletta L, Rotondano G, Dughera L, Repici A, Bianco MA, De Angelis C, et al. Delivery of radiofrequency energy to the gastroesophageal junction (Stretta procedure) for the treatment of gastroesophageal reflux disease. *Surgical endoscopy*. 2005 Jun ;19(6):849-53.
148. Houston H, Khaitan L, Holzman M, Richards WO. First year experience of patients undergoing the Stretta procedure. *Surgical endoscopy*. 2003 Mar ;17(3):401-4.
149. Lutfi RE, Torquati A, Kaiser J, Holzman M, Richards WO. Three year's experience with the Stretta procedure: Did it really make a difference? *Surgical endoscopy*. 2005 Feb ;19(2):289-95.
150. Fritscher-Ravens A, Mosse CA, Mukherjee D, Yazaki E, Park P-O, Mills T, et al. Transgastric gastropexy and hiatal hernia repair for GERD under EUS control: a porcine. *Gastrointestinal endoscopy*. 2004 ;59(1):89-95.
151. Torquati A, Richards WO. Endoluminal GERD treatments: critical appraisal of current literature with evidence-based medicine instruments. *Surgical endoscopy*. 2007 May ;21(5):697-706.
152. Mellinger JD. Endoluminal GERD therapy: inside, outside, upside, downside. *Surgical endoscopy*. 2007 May ;21(5):695-6.
153. Erickson RA. EUS-guided FNA. *Gastrointestinal endoscopy*. 2004 ;60(2):267-279.
154. Sawhney MS, Kratzke RA, Lederle FA, Holmstrom AM, Nelson DB, Kelly RF. EUS-guided FNA for the diagnosis of advanced lung cancer. *Gastrointestinal endoscopy*. 2006 Jun ;63(7):959-65.
155. Giovannini M. Concentration-dependent ablation of pancreatic tissue by EUS-guided ethanol injection. *Gastrointestinal endoscopy*. 2007 Feb ;65(2):278-80.
156. Matthes K, Mino-Kenudson M, Sahani DV, Holalkere N, Brugge WR. Concentration-dependent ablation of pancreatic tissue by EUS-guided ethanol injection. *Gastrointestinal endoscopy*. 2007 Feb ;65(2):272-7.
157. Micames CG, Gress FG. Local EUS-guided injection of chemotherapeutic agents as adjuvant to systemic treatment: the first steps are made. *Gastrointestinal endoscopy*. 2007 Mar ;65(3):454-6.
158. Magno P, Ko C-W, Buscaglia JM, Giday SA, Jagannath SB, Clarke JO, et al. EUS-guided angiography: a novel approach to diagnostic and therapeutic interventions in the vascular system. *Gastrointestinal endoscopy*. 2007 Sep ;66(3):587-91.

159. Swain CP, Mills TN. Anastomosis at flexible endoscopy: an experimental study of compression button gastrojejunostomy. *Gastrointestinal endoscopy*. 1991 ;37(6):628-31.
160. Seifert H, Wehrmann T, Schmitt T, Zeuzem S, Caspary WF. Retroperitoneal endoscopic debridement for infected peripancreatic necrosis. *The Lancet*. 2000 ;356:653-655.
161. Kalloo AN, Singh VK, B S, Niiyama H, Hill SL, Kantsevoy SV. Flexible transgastric peritoneoscopy: a novel approach to diagnostic and therapeutic interventions in the peritoneal cavity. *World journal of surgery*. 2004 ;60(1):114-117.
162. Jagannath SB, Kantsevoy SV, Vaughn CA, Chung SSC, Cotton PB, Gostout CJ, et al. Peroral transgastric endoscopic ligation of fallopian tubes with long-term survival in a porcine model. *Gastrointestinal endoscopy*. 2005 Mar ;61(3):449-53.
163. Kantsevoy SV, Jagannath SB, Niiyama H, Chung SSC, Cotton PB, Gostout CJ, et al. Endoscopic gastrojejunostomy with survival in a porcine model. *Gastrointestinal endoscopy*. 2005 Aug ;62(2):287-292.
164. Park P-O, Bergstrom M, Ikeda K, Fritscher-Ravens A, Swain P. Experimental studies of transgastric gallbladder surgery: cholecystectomy and cholecystogastric anastomosis (videos). *Gastrointestinal endoscopy*. 2005 ;61(4):601-6.
165. Bergström M, Ikeda K, Swain P, Park P-O. Transgastric anastomosis by using flexible endoscopy in a porcine model (with video). *Gastrointestinal endoscopy*. 2006 ;63(2):307-12.
166. Wagh MS, Merrifield BF, Thompson CC. Survival studies after endoscopic transgastric oophorectomy and tubectomy in a porcine model. *Gastrointestinal endoscopy*. 2006 ;63(3):473-478.
167. Fong DG, Pai RD, Fishman DS, Ryou M, Thompson CC. Transcolonic hepatic wedge resection in a porcine model. *Gastrointestinal endoscopy*. 2006 ;63(5):AB102.
168. Merrifield BF, Wagh MS, Thompson CC. Peroral transgastric organ resection: a feasibility study in pigs. *Gastrointestinal endoscopy*. 2006 Apr ;63(4):693-7.
169. Rao GV, Reddy DN. Transgastric appendectomy in humans. 2006 ;
170. Sumiyama K, Gostout CJ, Rajan E, Bakken TA, Deters JL, Knipschild MA, et al. Pilot study of the porcine uterine horn as an in vivo appendicitis model for development of endoscopic transgastric appendectomy. *Gastrointestinal endoscopy*. 2006 Nov ;64(5):808-12.
171. Kantsevoy SV, Jagannath SB, Niiyama H, Isakovich NV, Chung SSC, Cotton PB, et al. A novel safe approach to the peritoneal cavity for per-oral transgastric endoscopic procedures. *Gastrointestinal endoscopy*. 2007 ;65(3):497-500.
172. Sumiyama K, Gostout CJ, Rajan E, Bakken TA, Knipschild MA. Transesophageal mediastinoscopy by submucosal endoscopy with mucosal flap safety valve technique. *Gastrointestinal endoscopy*. 2007 Apr ;65(4):679-83.

173. Meireles O, Kantsevoy SV, Kalloo AN, Jagannath SB, Giday SA, Magno P, et al. Comparison of intraabdominal pressures using the gastroscope and laparoscope for transgastric surgery. *Surgical endoscopy*. 2007 ;21(6):998-1001.
174. Sumiyama K, Gostout CJ, Rajan E, Bakken TA, Knipschild MA, Chung S, et al. Transgastric cholecystectomy: transgastric accessibility to the gallbladder improved with the SEMF method and a novel multibending therapeutic endoscope. *Gastrointestinal endoscopy*. 2007 Jun ;65(7):1028-34.
175. Park P-O, Bergström M, Ikeda K, Fritscher-Ravens A, Mosse S, Kochman M, et al. Endoscopic pyloroplasty with full-thickness transgastric and transduodenal myotomy with sutured closure. *Gastrointestinal endoscopy*. 2007 Jul ;66(1):116-20.
176. Matthes K, Yusuf TE, Willingham FF, Mino-Kenudson M, Rattner DW, Brugge WR. Feasibility of endoscopic transgastric distal pancreatectomy in a porcine animal model. *Gastrointestinal endoscopy*. 2007 Oct ;66(4):762-6.
177. Shih SP, Kantsevoy SV, Kalloo AN, Magno P, Giday SA, Ko C-W, et al. Hybrid minimally invasive surgery--a bridge between laparoscopic and translumenal surgery. *Surgical endoscopy*. 2007 Aug ;21(8):1450-3.
178. Hondo FY, Giordano-Nappi JH, Maluf-Filho F, Matuguma SE, Sakai P, Poggetti R, et al. Transgastric access by balloon overtube for intraperitoneal surgery. *Surgical endoscopy*. 2007 Oct ;21(10):1867-9.
179. Zhu JF. Scarless endoscopic surgery: NOTES or TUES. *Surgical endoscopy*. 2007 ;21(10):1898-9.
180. Rolanda C, Lima E, Pêgo JM, Henriques-Coelho T, Silva D, Moreira I, et al. Third-generation cholecystectomy by natural orifices: transgastric and transvesical combined approach (with video). *Gastrointestinal endoscopy*. 2007 Jan ;65(1):111-7.
181. Bessler M, Stevens PD, Milone L, Parikh M, Fowler D. Transvaginal laparoscopically assisted endoscopic cholecystectomy: a hybrid approach to natural orifice surgery. *Gastrointestinal endoscopy*. 2007 Dec ;66(6):1243-5.
182. McGee MF, Rosen MJ, Marks J, Chak A, Onders R, Faulx A, et al. A reliable method for monitoring intraabdominal pressure during natural orifice transluminal endoscopic surgery. *Surgical endoscopy*. 2007 ;21(4):672-6.
183. Ryou M, Pai R, Sauer J, Rattner D, Thompson C. Evaluating an optimal gastric closure method for transgastric surgery. *Surgical endoscopy*. 2007 ;21(4):677-80.
184. Kantsevoy SV, Hu B, Jagannath SB, Isakovich NV, Chung SSC, Cotton PB, et al. Technical feasibility of endoscopic gastric reduction: a pilot study in a porcine model. *Gastrointestinal endoscopy*. 2007 Mar ;65(3):510-513.
185. Filho AJB, Noda RW, Kondo W, Kawahara N, Rangel M, Branco AW. Initial experience with hybrid transvaginal cholecystectomy. *Gastrointestinal endoscopy*. 2007 Dec ;66(6):1245-8.

186. Scott DJ, Tang S-jiang, Fernandez R, Bergs R, Goova MT, Zeltser I, et al. Completely transvaginal NOTES cholecystectomy using magnetically anchored instruments. *Surgical endoscopy*. 2007 ;21(12):2308-16.
187. Lima E, Henriques-Coelho T, Rolanda C, Pêgo JM, Silva D, Carvalho JL, et al. Transvesical thoracoscopy: a natural orifice transluminal endoscopic approach for thoracic surgery. *Surgical endoscopy*. 2007 Jun ;21(6):854-8.
188. Whiteford MH, Denk PM, Swanström LL. Feasibility of radical sigmoid colectomy performed as natural orifice transluminal endoscopic surgery (NOTES) using transanal endoscopic microsurgery. *Surgical endoscopy*. 2007 Oct ;21(10):1870-4.
189. Fong DG, Pai RD, Thompson CC. Transcolonic endoscopic abdominal exploration: a NOTES survival study in a porcine model. *Gastrointestinal endoscopy*. 2007 ;65(2):312-318.
190. Hazey JW, Narula VK, Renton DB, Reavis KM, Paul CM, Hinshaw KE, et al. Natural-orifice transgastric endoscopic peritoneoscopy in humans: Initial clinical trial. *Surgical endoscopy*. 2008 Jan ;22(1):16-20.
191. Perretta S, Dallemande B, Coumaros D, Marescaux J. Natural orifice transluminal endoscopic surgery: transgastric cholecystectomy in a survival porcine model. *Surgical endoscopy*. 2008 ;22(4):1126-30.
192. Deviere J, Valdes GO, Herrera LC, Closset J, Le Moine O, Eisendrath P, et al. Safety, feasibility and weight loss after transoral gastroplasty: First human multicenter study. *Surgical endoscopy*. 2008 ;22(3):589-598.
193. Zornig C, Mofid H, Emmermann A, Alm M, Waldenfels H-A von, Felixmüller C. Scarless cholecystectomy with combined transvaginal and transumbilical approach in a series of 20 patients. *Surgical endoscopy*. 2008 Jun ;22(6):1427-1429.
194. Palanivelu C, Rajan PS, Rangarajan M, Parthasarathi R, Senthilnathan P, Prasad M. Transvaginal endoscopic appendectomy in humans: a unique approach to NOTES--world's first report. *Surgical endoscopy*. 2008 ;22(5):1343-7.
195. Zorron R, Maggioni LC, Pombo L, Oliveira AL, Carvalho GL, Filgueiras M. NOTES transvaginal cholecystectomy: preliminary clinical application. *Surgical endoscopy*. 2008 Feb ;22(2):542-7.
196. Sumiyama K, Gostout CJ, Rajan E, Bakken TA, Knipschild MA, Chung S, et al. Pilot study of transesophageal endoscopic epicardial coagulation by submucosal endoscopy with the mucosal flap safety valve technique (with videos). *Gastrointestinal endoscopy*. 2008 Mar ;67(3):497-501.
197. Willingham FF, Gee DW, Lauwers GY, Brugge WR, Rattner DW. Natural orifice transesophageal mediastinoscopy and thoracoscopy. *Surgical endoscopy*. 2008 Apr ;22(4):1042-7.
198. Swain P. A justification for NOTES--natural orifice transluminal endosurgery. *Gastrointestinal endoscopy*. 2007 ;65(3):514-6.

199. Valdivieso E, Saenz R, Claudio N. Natural orifice transluminal endoscopic surgery: putting together minimally invasive techniques for a new era. *Gastrointestinal endoscopy*. 2007 Aug ;66(2):340-2.
200. Buess G, Cuschieri A. Raising our heads above the parapet: ES not NOTES. *Surgical endoscopy*. 2007 Jun ;21(6):835-7.
201. Agarwal BB, Agarwal S. Surgical pilgrimage - the need to avoid navigation through drains, medicine or “medisin”: our notes on NOTES. *Surgical endoscopy*. 2008 Jan ;22(1):271-2.
202. Pomp A. Notes on NOTES: The emperor is not wearing any clothes. *Surgical endoscopy*. 2008 ;22(2):283-4.
203. Swanström LL. Beyond endoluminal therapeutic endoscopy. *Gastrointestinal endoscopy*. 2007 Jul ;66(1):121-2.
204. Swanström LL, Whiteford MH, Khajanchee Y. Developing essential tools to enable transgastric surgery. *Surgical endoscopy*. 2008 ;22(3):600-4.
205. Nakao NL. Deconstruction of the endoscope: completing my wish list. *Gastrointestinal endoscopy*. 2007 Nov ;66(5):997-1000.
206. Inui K. Natural orifice transluminal endoscopic surgery: a step toward clinical implementation? *Gastrointestinal endoscopy*. 2007 Apr ;65(4):694-5.
207. Rattner DW. Laying the foundation for NOTES: another brick in the wall. [Internet]. *Gastrointestinal endoscopy*. 2010 Apr ;71(4):842-3. Available from: <http://www.ncbi.nlm.nih.gov/pubmed/20363427>
208. Denk PM, Swanström LL, Whiteford MH. Transanal endoscopic microsurgical platform for natural orifice surgery [Internet]. *Gastrointestinal endoscopy*. 2008 Nov ;68(5):954-9. Available from: <http://www.ncbi.nlm.nih.gov/pubmed/18984102>
209. Salinas G, Saavedra L, Agurto H, Quispe R, Ramírez E, Grande J, et al. Early experience in human hybrid transgastric and transvaginal endoscopic cholecystectomy. [Internet]. *Surgical endoscopy*. 2010 May ;24(5):1092-8. Available from: <http://www.ncbi.nlm.nih.gov/pubmed/19997754>
210. Romanelli JR, Earle DB. Single-port laparoscopic surgery: an overview. [Internet]. *Surgical endoscopy*. 2009 Jul ;23(7):1419-27. Available from: <http://www.ncbi.nlm.nih.gov/pubmed/19347400>
211. Pryor AD, Tushar JR, DiBernardo LR. Single-port cholecystectomy with the TransEnterix SPIDER: simple and safe. [Internet]. *Surgical endoscopy*. 2010 Apr ;24(4):917-23. Available from: <http://www.ncbi.nlm.nih.gov/pubmed/19760329>
212. Akahoshi K, Honda K, Akahane H, Akiba H, Matsui N, Motomura Y, et al. Endoscopic submucosal dissection by using a grasping-type scissors forceps: a preliminary clinical study (with video). [Internet]. *Gastrointestinal endoscopy*. 2008 Jun ;67(7):1128-33. Available from: <http://www.ncbi.nlm.nih.gov/pubmed/18355820>

213. Moran EA, Gostout CJ, Bingener J. Preliminary performance of a flexible cap and catheter-based endoscopic suturing system. [Internet]. *Gastrointestinal endoscopy*. 2009 Jun ;69(7):1375-83. Available from: <http://www.ncbi.nlm.nih.gov/pubmed/19481658>
214. Park P-O, Long GL, Bergström M, Cunningham C, Vakharia OJ, Bakos GJ, et al. A randomized comparison of a new flexible bipolar hemostasis forceps designed principally for NOTES versus a conventional surgical laparoscopic bipolar forceps for intra-abdominal vessel sealing in a porcine model. [Internet]. *Gastrointestinal endoscopy*. 2010 Apr ;71(4):835-41. Available from: <http://www.ncbi.nlm.nih.gov/pubmed/19942215>
215. Mullady DK, Lautz DB, Thompson CC. Treatment of weight regain after gastric bypass surgery when using a new endoscopic platform: initial experience and early outcomes (with video). [Internet]. *Gastrointestinal endoscopy*. 2009 Sep ;70(3):440-4. Available from: <http://www.ncbi.nlm.nih.gov/pubmed/19555944>
216. Thompson CC, Ryou M, Soper NJ, Hungess ES, Rothstein RI, Swanstrom LL. Evaluation of a manually driven, multitasking platform for complex endoluminal and natural orifice transluminal endoscopic surgery applications (with video). [Internet]. *Gastrointestinal endoscopy*. 2009 Jul ;70(1):121-5. Available from: <http://www.ncbi.nlm.nih.gov/pubmed/19394008>
217. Charles S. Techniques and tools for dissection of epiretinal membranes. Graefe's archive for clinical and experimental ophthalmology = Albrecht von Graefes Archiv für klinische und experimentelle Ophthalmologie. 2003 ;241(5):347-52.
218. Sakaguchi H, Ohji M, Gomi F, Sawa M, Oshima Y, Ikuno Y, et al. New micro vertical scissors for the surgical ablation of retinal angiomatic proliferation. *American journal of ophthalmology*. 2005 Feb ;139(2):377-80.
219. Mintz Y, Horgan S, Cullen J, Falor E, Talamini MA. Dual-lumen natural orifice transluminal endoscopic surgery (NOTES): a new method for performing a safe anastomosis. *Surgical endoscopy*. 2008 ;22(2):348-51.
220. Evans JA, Rosato FE, Ginsberg GG. Gastrostomy port assisted full-thickness gastric resection by using the peroral SurgASSIST introduced via an oroesophageal overtube in a porcine model. *Gastrointestinal endoscopy*. 2007 ;65(4):684-687.
221. Kaehler GFBA, Langner C, Suchan KL, Freudenberg S, Post S. Endoscopic full-thickness resection of the stomach: an experimental approach. *Surgical endoscopy*. 2006 ;20(3):519-21.
222. Rajan E, Gostout CJ, Burgart LJ, Leontovich ON, Knipschild MA, Herman LJ, et al. First endoluminal system for transmural resection of colorectal tissue with a prototype full-thickness resection device in a porcine model. *Gastrointestinal endoscopy*. 2002 Jun ;55(7):915-920.
223. Becker DG, Cook TA, Wang TD, Park SS, Kreit JD, Tardy Jr ME, et al. A 3-year multi-institutional experience with the liposhaver. *Archives of facial plastic surgery : official publication for the American Academy of Facial Plastic and Reconstructive Surgery, Inc. and the International Federation of Facial Plastic Surgery Societies*. 1999 ;1(3):171-6.

224. Miyashita M, Tajiri T, Maruyama H, Makino H, Nomura T, Sasajima K, et al. Endoscopic mucosal resection scissors for the treatment of early gastric cancer. *Endoscopy*. 2003 Jul ;35(7):611-2.
225. Olympus EndoTherapy - Categories [Internet]. [cited 2008 Jun 23] Available from: http://www.olympusamerica.com/msg_section/et/et_category.asp?id=10
226. Beilstein MC, Kochman ML. Endoscopic incision of a refractory esophageal stricture: novel management with an endoscopic scissors. *Gastrointestinal endoscopy*. 2005 Apr ;61(4):623-5.
227. Boorder T de, Kruger AB, Klaessens J, Grimbergen M, Verdaasdonk RM. Comparing different treatment modalities for partial nephrectomies without ischemic period: laser, Hydro-Jet and RF. In: Proceedings of SPIE. 2008.
228. Piek J, Wille C, Warzok R, Gaab M-R. Waterjet dissection of the brain: experimental and first clinical results. Technical note. *Journal of neurosurgery*. 1998 Nov ;89(5):861-4.
229. Shekarriz H, Shekarriz B, Upadhyay J, Bürk C, Wood DP, Bruch H-P. Hydro-jet assisted laparoscopic partial nephrectomy: initial experience in a porcine model. *The Journal of urology*. 2000 Mar ;163(3):1005-8.
230. Granick MS, Posnett J, Jacoby M, Noruthun S, Ganchi PA, Datiashvili RO. Efficacy and cost-effectiveness of a high-powered parallel waterjet for wound debridement. *Wound repair and regeneration : official publication of the Wound Healing Society [and] the European Tissue Repair Society*. 2006 ;14(4):394-7.
231. Sold MG, Grobholz R, Post S, Enderle MD, Kaehler GFBA. Submucosal cushioning with water jet before endoscopic mucosal resection : Which fluids are effective? *Surgical endoscopy*. 2008 ;22(2):443-7.
232. Eversole LR, Rizoou I, Kimmel AI. Pupal response to cavity preparation by an erbium chromium:YSGG laser-powered hydrokinetic system. *Journal of the American Dental Association (1939)*. 1997 ;128(8):1099-1106.
233. Nakagawa A, Hirano T, Komatsu M, Sato M, Uenohara H, Ohyama H, et al. Holmium: YAG laser-induced liquid jet knife: possible novel method for dissection. *Lasers in surgery and medicine*. 2002 Jan ;31(2):129-35.
234. Hirano T, Nakagawa A, Uenohara H, Ohyama H, Jokura H, Takayama K, et al. Pulsed liquid jet dissector using holmium:YAG laser-a novel neurosurgical device for brain incision without impairing vessels. *Acta neurochirurgica*. 2003 May ;145(5):401-6.
235. Ohki T, Nakagawa A, Hirano T, Hashimoto T, Menezes V, Jokura H, et al. Experimental application of pulsed Ho:YAG laser-induced liquid jet as a novel rigid neuroendoscopic dissection device. *Lasers in surgery and medicine*. 2004 Jan ;34(3):227-34.
236. Fletcher D, Palanker D. Pulsed liquid microjet for microsurgery. *Applied physics letters*. 2001 ;78(13):1933-5.

237. Sumiyama K, Gostout CJ, Rajan E, Bakken TA, Knipschild MA, Marler RJ. Submucosal endoscopy with mucosal flap safety valve. *Gastrointestinal endoscopy*. 2007 ;65(4):688-94.
238. Fante RG, Fante RL. The Physical Basis of Surgical Electrodisssection. *Ophthalmic Plastic and Reconstructive Surgery*. 2003 ;19(2):145-148.
239. Low / Medium Power Electrosurgery Review 2002. London: 2002.
240. Ramsay JWA, Shepherd NA, Butler M, Gosling PT, Miller RA, Wallace DMA, et al. A comparison of bipolar and monopolar diathermy probes in experimental animals. *Urological Research*. 1985 ;13(2):99-102.
241. Goulet CJ, Disario JA, Emerson L, Hilden K, Holubkov R, Fang JC. In vivo evaluation of argon plasma coagulation in a porcine model. *Gastrointestinal endoscopy*. 2007 Mar ;65(3):457-62.
242. PEAK Surgical - PlasmaBlade [Internet]. [cited 2008 Sep 2] Available from: <http://www.peaksurgical.com/products/plasmablades/>
243. Botto H, Lebret T, Barre P, Orsoni J, JM. Electrovaporization of the prostate with the Gyrus device. *Journal of endourology*. 2001 Apr ;15(3):313-6.
244. Abouljoud MS, Arenas J, Yoshida A, Kim D. New application of the bipolar vapor plasma coagulation system for laparoscopic major liver resections. *Surgical endoscopy*. 2008 Feb ;22(2):426-9.
245. LigaSure - The Science of Vessel Sealing [Internet]. [cited 2008 Sep 2] Available from: <http://www.ligasure.com/pages/intro.htm>
246. Kim FJ, Chammas MF, Gewehr E, Morihisa M, Caldas F, Hayacibara E, et al. Temperature safety profile of laparoscopic devices: Harmonic ACE (ACE), Ligasure V (LV), and plasma trisector (PT). *Surgical endoscopy*. 2008 ;22(6):1464-9.
247. Cuschieri A. Technology for minimal access surgery. *British Medical Journal*. 1999 ;319(1304):1-6.
248. JOHNSON & JOHNSON GATEWAY® [Internet]. [cited 2008 Sep 2] Available from: <http://www.jnj.se/home.jhtml?contentId=09008b9880a2ba17&loc=USENG&page=viewContent>
249. File:Commercial laser lines.svg - Wikipedia, the free encyclopedia [Internet]. Available from: http://en.wikipedia.org/wiki/File:Commercial_laser_lines.svg
250. Brannon JH, Lankard JR, Baise a I, Burns F, Kaufman J. Excimer laser etching of polyimide [Internet]. *Journal of Applied Physics*. 1985 ;58(5):2036. Available from: <http://link.aip.org/link/JAPIAU/v58/i5/p2036/s1&Agg=doi>
251. Deckelbaum LI, Natarajan MK, Bittl JA, Rohlf K, Scott J, Chisholm R, et al. Effect of intracoronary saline infusion on dissection during excimer laser coronary angioplasty: A randomized trial. *Journal of the American College of Cardiology*. 1995 Nov ;26(5):1264-1269.

252. Chan KF, Vassar GJ, Pfefer J, Teichman JMH, Glickman RD, Weintraub ST, et al. Holmium:YAG laser lithotripsy: A dominant photothermal ablative mechanism with chemical decomposition of urinary calculi. *Lasers in surgery and medicine*. 1999 ;25(1):22-37.
253. Teichman JMH, Schwesinger WH, Lackner J, Cossman RM. Holmium: YAG laser lithotripsy for gallstones; A preliminary report. *Surgical endoscopy*. 2001 Sep ;15(9):1034-7.
254. Deppe H, Horch H-H. Laser applications in oral surgery and implant dentistry. *Lasers in medical science*. 2007 ;22(4):217-21.
255. Raanani E, Aravot D, Abramov D, Erez E, Sandbank J, Giler S, et al. Fiberoptic-guided CO₂ laser for harvesting of the internal mammary artery. *European journal of cardio-thoracic surgery : official journal of the European Association for Cardio-thoracic Surgery*. 1997 Jun ;11(6):1093-6.
256. Temelkuran B, Hart SD, Benoit G, Joannopoulos JD, Fink Y. Wavelength-scalable hollow optical fibres with large photonic bandgaps for CO₂ laser transmission. *Nature*. 2002 Dec ;420(6916):650-3.
257. Price TT, Sharma A, Montgomery PQ. How we do it: vocal cord Nd-YAG laser surgery, under local anaesthetic, using a flexible trans-nasal laryngo-oesophagoscope. *Lasers in medical science*. 2007 ;22(3):127-30.
258. Sato S, Ogura M, Ishihara M, Kawauchi S, Arai T, Matsui T, et al. Nanosecond, high-intensity pulsed laser ablation of myocardium tissue at the ultraviolet, visible, and near-infrared wavelengths: in-vitro study. *Lasers in surgery and medicine*. 2001 Jan ;29(5):464-73.
259. Saito T, Honda N, Saito H. Advantage and disadvantage of KTP-532 laser tonsillectomy compared with conventional method. *Auris, nasus, larynx*. 1999 Oct ;26(4):447-52.
260. Sumiyama K, Gostout CJ, Rajan E, Bakken TA, Knipschild MA. Chemically assisted endoscopic mechanical submucosal dissection by using mesna. *Gastrointestinal endoscopy*. 2008 Mar ;67(3):534-8.
261. Chen WR, Adams RL, Higgins AK, Bartels KE, Nordquist RE. Photothermal effects on murine mammary tumors using indocyanine green and an 808-nm diode laser: an in vivo efficacy study. *Cancer Letters*. 1996 ;98:169-173.
262. Hino S, Kakutani H, Ikeda K, Yasue H, Sumiyama K, Uchiyama Y, et al. Low power diode laser treatment using indocyanine green for eradication of esophageal varices. *Endoscopy*. 2001 Oct ;33(10):873-5.
263. Hayashi T, Arai T, Tokonabe S, Itoh H, Kikuchi M. Diode-laser ablation therapy for submucosal gastric cancer using indocyanine-green solution injection to the submucosa. *Proceedings of SPIE*. 1997 ;2975:408-414.
264. Arai T, Hayashi T, Nakamura N, Hino S, Kikuchi M, Miura S, et al. Indocyanine green enhanced diode laser ablation for porcine gastric wall with ablation depth monitoring using scattering light. In: *Proceedings of the 20th Annual International Conference of*

- the IEEE Engineering in Medicine and Biology Society. Vol.20 Biomedical Engineering Towards the Year 2000 and Beyond (Cat. No.98CH36286). IEEE; 1998. p. 1900-1901.
265. Hayashi T, Arai T, Nakamura N, Tajiri H, Miura S, Kikuchi M. Endoscopic mucosal incision by diode laser for the early cancer treatment in alimentary tract: effect of submucosal indocyanine-green-solution injection. Proceedings of SPIE. 1999 ;3590(January):425-430.
 266. Sato M, Ishihara M, Arai T, Asazuma T, Kikuchi T, Hayashi T, et al. Use of a new ICG-dye-enhanced diode laser for percutaneous laser disc decompression. Lasers in surgery and medicine. 2001 Jan ;29(3):282-7.
 267. Yamashita Y, Sakai T, Watanabe K, Maekawa T, Shirakusa T. Dye-enhanced selective laser ablation for surgical mucosectomy. Surgical laparoscopy, endoscopy & percutaneous techniques. 1999 Dec ;9(6):387-91.
 268. Lu I, Nobis RH. Medical instrument handle and medical instrument having a handle. 2007 ;1-18.
 269. Lu I, Nobis RH. Medical cannula and medical cannula system. 2007 ;1-8.
 270. Lu I, Nobis RH. Medical instrument having an articulatable end effector. 2007 ;1-18.
 271. Lu I, Nobis RH. Medical instrument having a medical needle-knife. 2007 ;1-10.
 272. Nobis RH, Lu I, Vakharia O. Medical instrument handle and medical instrument having same. 2007 ;1-14.
 273. Nobis RH, Lu I. Medical tubular assembly. 2007 ;1-9.
 274. Nobis RH, Lu I. Medical instrument having a medical snare. 2007 ;1-10.
 275. Prahl S. Optical absorption of indocyanine green (ICG) [Internet]. Available from: <http://omlc.ogi.edu/spectra/icg/index.html>
 276. Prahl S. Optical absorption of methylene blue [Internet]. Available from: <http://omlc.ogi.edu/spectra/mb/index.html>
 277. Prahl S. tabulated molar extinction coefficient for hemoglobin in water [Internet]. Available from: <http://omlc.ogi.edu/spectra/hemoglobin/summary.html>
 278. Du H, Fuh RCA, Li J, Corkan LA, Lindsey JS. PhotochemCAD‡: A Computer-Aided Design and Research Tool in Photochemistry [Internet]. Photochemistry and Photobiology. 2008 ;68(2):141–142. Available from: <http://www3.interscience.wiley.com/journal/119940664/abstract>
 279. Duck FA. Physical Properties of Tissue: A Comprehensive Reference Book. Academic Press; 1990.
 280. Bown SG, Salmon PR, Kelly DF, Calder BM, Pearson H, Weaver BM, et al. Argon laser photocoagulation in the dog stomach. [Internet]. Gut. 1979 Aug ;20(8):680-687. [cited 2011 Jan 25] Available from: <http://gut.bmjjournals.org/cgi/doi/10.1136/gut.20.8.680>

281. Publishing BMJ, Society B, Gut G, To N. The British Society of Gastroenterology [Internet]. Gut. 1979 May ;20(5):A433-A462.[cited 2011 Jan 25] Available from: <http://gut.bmjjournals.org/cgi/doi/10.1136/gut.20.5.A433>
282. Bown SG, Salmon PR, Storey DW, Calder BM, Kelly DF, Adams N, et al. NdYAG laser photocoagulation in the dog stomach. [Internet]. Gut. 1980 Oct ;21(10):818-825.[cited 2011 Jan 25] Available from: <http://gut.bmjjournals.org/cgi/doi/10.1136/gut.21.10.818>
283. Kelly DF, Bown SG, Salmon PR, Calder BM, Pearson H, Weaver BM. Nature and extent of histological changes induced by argon laser photocoagulation in canine gastric mucosa. [Internet]. Gut. 1980 Dec ;21(12):1047-1055.[cited 2011 Jan 25] Available from: <http://gut.bmjjournals.org/cgi/doi/10.1136/gut.21.12.1047>
284. Mahvash M, Voo LM, Kim D, Jeung K, Wainer J, Okamura AM. Modeling the forces of cutting with scissors. [Internet]. IEEE transactions on bio-medical engineering. 2008 Mar ;55(3):848-56.Available from: <http://www.ncbi.nlm.nih.gov/pmc/articles/PMC2709828/>
285. Ahearne M, Siamantouras E, Yang Y, Liu K-K. Mechanical characterization of biomimetic membranes by micro-shaft poking. [Internet]. Journal of the Royal Society, Interface / the Royal Society. 2009 May ;6(34):471-8.Available from: <http://www.ncbi.nlm.nih.gov/pmc/articles/PMC2659696/>
286. Overview of materials for Cyanoacrylate Adhesive [Internet]. [cited 2010 May 15] Available from: <http://www.matweb.com/search/DataSheet.aspx?MatGUID=d0d7dbec7666421caf8aa08724b634c5&ckck=1>
287. Wood J, Morrill S. Toughened cyanoacrylate adhesives containing alkene-acrylate copolymers and method for production. 2004 ;1-20.
288. Yoo KH, Lee S-J, Jeon SH. Simple renal cyst sclerotherapy with acetic acid: our 10-year experience. [Internet]. Journal of endourology / Endourological Society. 2008 Nov ;22(11):2559-63.[cited 2011 Jan 27] Available from: <http://www.ncbi.nlm.nih.gov/pubmed/18928389>
289. Suba EJ, Raab SS. Cervical cancer screening by simple visual inspection after acetic acid. [Internet]. Obstetrics and gynecology. 2002 Mar ;99(3):517-8.Available from: <http://www.ncbi.nlm.nih.gov/pmc/articles/PMC11864690/>
290. Conio M, Rajan E, Sorbi D, Norton I, Herman LJ, Filiberti R, et al. Comparative performance in the porcine esophagus of different solutions used for submucosal injection. Gastrointestinal endoscopy. 2002 Oct ;56(4):513-6.
291. Uraoka T, Fujii T, Saito Y, Sumiyoshi T, Emura F, Bhandari P, et al. Effectiveness of glycerol as a submucosal injection for EMR. Gastrointestinal endoscopy. 2005 May ;61(6):736-40.
292. Yamamoto H, Kawata H, Sunada K, Satoh K, Kaneko Y, Ido K, et al. Success rate of curative endoscopic mucosal resection with circumferential mucosal incision assisted by

- submucosal injection of sodium hyaluronate. *Gastrointestinal endoscopy*. 2002 Oct ;56(4):507-12.
293. Feitoza AB, Gostout CJ, Burgart LJ, Burkert A, Herman LJ, Rajan E. Hydroxypropyl methylcellulose: A better submucosal fluid cushion for endoscopic mucosal resection. *Gastrointestinal endoscopy*. 2003 ;57(1):41-47.
294. Lee S-H, Park J-H, Park DH, Chung I-K, Kim H-S, Park S-H, et al. Clinical efficacy of EMR with submucosal injection of a fibrinogen mixture: a prospective randomized trial. *Gastrointestinal endoscopy*. 2006 Nov ;64(5):691-6.
295. Lee YS, Wetzel ED, Egres RGJ, Wagner NJ. Advanced body armor utilizing shear thickening fluids. In: 23rd Army Science Conference. Orlando, FL: 2002. p. 1-6.
296. Wetzel ED, Wagner NJ, Lee YS, Egres R, Kirkwood K, Kirkwood J, et al. Novel flexible body armor utilizing shear thickening fluid (STF) composites [Internet]. In: Composite Materials. San Diego: 2003. p. 1-19. Available from: http://d.wanfangdata.com.cn/NSTLHY_NSTL_HY718418.aspx
297. Kawara M, Tanahashi MM. Motor Driven Oscillating Razor. 1991 ;14.
298. Davey MG. Oscillating blade razor [Internet]. US Patent 5,794,342. 1998 Aug ;11. Available from: <http://www.google.com/patents?hl=en&lr=&vid=USPAT5794342&id=nrsgAAAAEBAJ&oi=fnd&dq=Oscillating+Blade+Razor&printsec=abstract>
299. Gangi a, Dietemann JL, Guth S, Vinclair L, Sibilia J, Mortazavi R, et al. Percutaneous laser photocoagulation of spinal osteoid osteomas under CT guidance. [Internet]. *AJR*. American journal of neuroradiology. 1998 ;19(10):1955-8. Available from: <http://www.ncbi.nlm.nih.gov/pubmed/9874556>
300. Amin Z, Lees WR, Bown SG. Technical note: interstitial laser photocoagulation for the treatment of prostatic cancer. [Internet]. *The British journal of radiology*. 1993 Nov ;66(791):1044-7. Available from: <http://www.ncbi.nlm.nih.gov/pubmed/8281381>
301. Amin Z, Bown SG, Lees WR. Local treatment of colorectal liver metastases: a comparison of interstitial laser photocoagulation (ILP) and percutaneous alcohol injection (PAI). [Internet]. *Clinical radiology*. 1993 Sep ;48(3):166-71. Available from: <http://www.ncbi.nlm.nih.gov/pubmed/8403761>
302. Taylor DL, Schafer S a, Nordquist R, Payton ME, Dickey DT, Bartels KE. Comparison of a high power diode laser with the Nd:YAG laser using in situ wound strength analysis of healing cutaneous incisions. [Internet]. *Lasers in surgery and medicine*. 1997 Jan ;21(3):248-54. Available from: <http://www.ncbi.nlm.nih.gov/pubmed/9291081>
303. Devoisselle JM, Mordon S, Desmettre T. Fluorescence properties and metabolic features of indocyanine green (ICG) as related to angiography. *Surv Ophthalmol*. 2000 ;45(1):15-27.
304. Fox IJ, Wood EH. Indocyanine green: physical and physiologic properties. [Internet]. In: Proceedings of the staff meetings. Mayo Clinic. 1960. p. 732. Available from: <http://www.ncbi.nlm.nih.gov/pubmed/13701100>

305. Landsman MLJ, Kwant G, Mook GA, Zijlstra WG. Light-absorbing properties, stability, and spectral stabilization of indocyanine green. *Journal of applied physiology*. 1976 Apr ;40(4):575-83.
306. Haritoglou C, Gandorfer A, Schaumberger M, Tadayoni R, Gandorfer A, Kampik A. Light-Absorbing Properties and Osmolarity of Indocyanine-Green Depending on Concentration and Solvent Medium. *Investigative ophthalmology & visual science*. 2003 Jun ;44(6):2722-2729.
307. Elfbaum SG, Laden K. The Effect of Dimethyl Sulfoxide on Percutaneous Absorption : A Mechanistic Study , Part I. *Journal Of The Society Of Cosmetic Chemists*. 1968 ;127(6):119-127.
308. Elfbaum SG, D P, Laden K. The Effect of Dimethyl Sulfoxide on Percutaneous Absorption : A Mechanistic Study . Part II. *Journal Of The Society Of Cosmetic Chemists*. 1968 ;172163-172.
309. Abramoff M, Magelhaes P, Ram S. Image processing with ImageJ [Internet]. *Biophotonics Int*. 2004 ;11(7):36 - 42.[cited 2010 Jul 2] Available from: <http://www.citeulike.org/user/christofseiler/article/2853779>
310. McKenzie AL. How far does thermal damage extend beneath the surface of CO₂ laser incisions? *Physics in medicine and biology*. 1983 Aug ;28(8):905-12.
311. Welch AJ. The thermal response of laser irradiated tissue. *IEEE Journal of quantum electronics*. 1984 ;20(12):1471-81.
312. Welch a J, Valvano JW, Pearce J a, Hayes LJ, Motamedi M. Effect of laser radiation on tissue during laser angioplasty. [Internet]. *Lasers in surgery and medicine*. 1985 Jan ;5(3):251-64.Available from: <http://www.ncbi.nlm.nih.gov/pubmed/2525659>
313. Gemert MJ van, Schets G a, Stassen EG, Bonnier JJ. Modeling of (coronary) laser-angioplasty. [Internet]. *Lasers in surgery and medicine*. 1985 Jan ;5(3):219-34.Available from: <http://www.ncbi.nlm.nih.gov/pubmed/4010433>
314. Jacques SL, Prahl SA. Modeling optical and thermal distributions in tissue during laser irradiation. *Lasers in surgery and medicine*. 1987 ;6494-503.
315. McKenzie AL. A three-zone model of soft-tissue damage by a CO₂ laser. *Physics in medicine and biology*. 1986 ;31(9):967-983.
316. McKenzie AL. An extension of the three-zone model to predict depth of tissue damage beneath Er:YAG and Ho:YAG laser excisions. *Physics in medicine and biology*. 1989 ;34(1):107-114.
317. McKenzie AL. Physics of thermal processes in laser-tissue interaction. *Physics in medicine and biology*. 1990 Sep ;35(9):1175-209.
318. Zhang JZ, Shen YG, Zhang XX. A dynamic photo-thermal model of carbon dioxide laser tissue ablation. *Lasers in medical science*. 2009 May ;24(3):329-38.

319. Verdaasdonk RM, Borst C, Gemert MJ van. Explosive onset of continuous wave laser tissue ablation. *Physics in medicine and biology*. 1990 Aug ;35(8):1129-44.
320. Jacques SL. Role of tissue optics and pulse duration on tissue effects during high-power laser irradiation. *Applied Optics*. 1993 ;32(13):2447-2454.
321. Trout GR. Variation in Myoglobin Denaturation and Color of Cooked Beef, Pork, and Turkey Meat as Influenced by pH, Sodium Chloride, Sodium Tripolyphosphate, and Cooking Temperature [Internet]. *Journal of Food Science*. 1989 May ;54(3):536-540. Available from: <http://www.blackwell-synergy.com/doi/abs/10.1111/j.1365-2621.1989.tb04644.x>
322. Hodge J. Dehydrated foods, chemistry of browning reactions in model systems [Internet]. *Journal of Agricultural and Food Chemistry*. 1953 ;1(15):928-943. [cited 2010 Jul 29] Available from: <http://pubs.acs.org/doi/abs/10.1021/jf60015a004>
323. Mckenzie AL, Byrne PO. Can photography be used to measure isodose distributions of space irradiance for laser photodynamic therapy? *Phys Med Biol*. 1988 ;33(1):113-31.
324. Hill WJ, Hunter WG. A Review of Response Surface Methodology: A Literature Survey [Internet]. *Technometrics*. 1966 ;8(4):571 - 590. [cited 2010 Jul 17] Available from: <http://www.jstor.org/stable/1266632>
325. Engel E, Schraml R, Maisch T, Kobuch K, König B, Szeimies R-M, et al. Light-induced decomposition of indocyanine green. [Internet]. *Investigative ophthalmology & visual science*. 2008 May ;49(5):1777-83. [cited 2010 Aug 23] Available from: <http://www.ncbi.nlm.nih.gov/pubmed/18436812>
326. Guo J. Pyrolysis of wood powder and gasification of wood-derived char. *Shock*. 2004 ;1-170.
327. Wissler EH. Pennes' 1948 paper revisited [Internet]. *Journal of Applied Physiology*. 1998 ;85(1):35. Available from: <http://jap.physiology.org/cgi/content/abstract/85/1/35>
328. Jr FH. The predictability and the significance of thermally induced rate processes leading to irreversible epidermal injury [Internet]. *Am J Path*. 1948 ;[cited 2010 Jul 30] Available from: http://scholar.google.com/scholar?hl=en&q=henriques+thermally+induced+rate+processes+leading+to+irreversible&btnG=Search&as_sdt=2000&as_ylo=&as_vis=0#0
329. Thurner F, Mann U. Kinetic investigation of wood pyrolysis [Internet]. *Industrial & Engineering Chemistry Process Design and Development*. 1981 Jul ;20(3):482-488. Available from: <http://pubs.acs.org/doi/abs/10.1021/i200014a015>
330. Shen DK, Fang MX, Luo ZY, Cen KF. Modeling pyrolysis of wet wood under external heat flux. *Fire Safety J*. 2007 ;42:210-217.
331. Skinner M, Everts S, Reid A, Vitkin I. Changes in optical properties of ex vivo rat prostate due to heating [Internet]. *Physics in Medicine*. 2000 ;13:75 [cited 2010 Sep 8] Available from: <http://iopscience.iop.org/0031-9155/45/5/319>

332. Morosolli ARC, Veeck EB, Niccoli-Filho W, Gomes MF, Graças V Goulart M das. Healing process after surgical treatment with scalpel, electrocautery and laser radiation: histomorphologic and histomorphometric analysis. [Internet]. Lasers in medical science. 2010 Jan ;25(1):93-100. Available from: <http://www.ncbi.nlm.nih.gov/pubmed/19408037>
333. Molgat YM, Pollack SV, Hurwitz JJ, Bunas SJ, Manning T, McCormack KM, et al. Comparative study of wound healing in porcine skin with CO₂ laser and other surgical modalities: preliminary findings. [Internet]. International journal of dermatology. 1995 Jan ;34(1):42-7. Available from: <http://www.ncbi.nlm.nih.gov/pubmed/7896488>
334. Blomberg BME von, Sietses C, Cuesta MA, Eijsbouts QAJ. Ultrasonic energy vs monopolar electrosurgery in laparoscopic cholecystectomy [Internet]. Surgical Endoscopy. 2001 Jan ;15(1):69-71. [cited 2008 May 12] Available from: <http://dx.doi.org/10.1007/s004640010061>
335. Kumar KS. Spectroscopy of Indocyanine Green Photodegradation. 1996 ;(October):76.
336. Vandaveer WR, Mosher M. The blue bottle revisited [Internet]. Journal of Chemical Education. 1997 Apr ;74(4):402. Available from: <http://pubs.acs.org/doi/abs/10.1021/ed074p402>
337. Carré C, Lougnot DJ, Capolla N, Lessard RA. Studies of the photoreduction of methylene blue in gelatin solutions and films with a view to improving the holographic recording process at 633 nm. Applied Physics B: Lasers and Optics. 1991 ;52(5):326-330.
338. Schweiger M, Arridge SR, Hiraoka M, Delpy DT. The finite element method for the propagation of light in scattering media: Boundary and source conditions [Internet]. Medical Physics. 1995 Nov ;22(11):1779-1792. Available from: <http://link.aip.org/link/?MPH/22/1779/1>
339. Mohammed Y, Verhey JF. A finite element method model to simulate laser interstitial thermo therapy in anatomical inhomogeneous regions. BioMedical Engineering OnLine. 2005 ;4(2):1-16.
340. Zhang R, Verkruyse W, Aguilar G, Nelson JS. Comparison of diffusion approximation and Monte Carlo based finite element models for simulating thermal responses to laser irradiation in discrete vessels. [Internet]. Physics in medicine and biology. 2005 ;50(17):4075-86. Available from: <http://www.ncbi.nlm.nih.gov/pubmed/16177531>
341. Cox BT, Arridge SR, Beard PC. Light transport for photoacoustic image inversion: a diffusion-based, 2D FE model including the -Eddington phase function. London: 2008.
342. Spott T, Svaasand LO. Collimated light sources in the diffusion approximation. Applied optics. 2000 Dec ;39(34):6453-65.
343. Prahl SA. Light transport in tissue. 1988 ;
344. Joseph JH, Wiscombe WJ, Weinman JA. The delta-Eddington approximation for radiative flux transfer [Internet]. Journal of the Atmospheric Sciences. 1976 ;33(12):2452–2459. Available from: http://iacweb.ethz.ch/staff/aroesch/Delta_Eddington_Approximation.pdf

345. Greenstein JL, Henyey LG. Diffuse radiation in the galaxy. 1940.
346. Wang L, Jacques SL. Monte Carlo modeling of light transport in multi-layered tissues in standard C [Internet]. University of Texas MD Anderson Cancer Center. 1995 ;10(2):1-183. Available from:
<http://citeserx.ist.psu.edu/viewdoc/download?doi=10.1.1.127.837&rep=rep1&type=pdf>
347. Alerstam E, Svensson T, Andersson-Engels S. Parallel computing with graphics processing units for high-speed Monte Carlo simulation of photon migration. [Internet]. Journal of biomedical optics. 2009 ;13(6):060504. Available from:
<http://www.ncbi.nlm.nih.gov/pubmed/19123645>
348. Fang Q, Boas DA. Monte Carlo Simulation of Photon Migration in 3D Turbid Media Accelerated by Graphics Processing Units. Optics Express. 2009 ;17(22):20178-20190.
349. Knox FS, Wachtel TL, McCahan GR, Knapp SC. Thermal properties calculated from measured water content as a function of depth in porcine skin [Internet]. Burns. 1986 Dec ;12(8):556-62. Available from: <http://www.ncbi.nlm.nih.gov/pubmed/3454688>
350. Spells KE. The thermal conductivities of some biological fluids [Internet]. Physics in Medicine and Biology. 1960 ;5139. Available from:
<http://www.iop.org/EJ/abstract/0031-9155/5/2/304>
351. Birth G, Davis C, Townsend W. The scatter coefficient as a measure of pork quality [Internet]. Journal of Animal Science. 1978 ;46(3):639-645. [cited 2010 Sep 8] Available from: <http://jas.fass.org/cgi/content/abstract/46/3/639>